Design and Development of Non-Woven Nanofibers as Drug Delivery System

by

Patel Pratikshkumar Rameshbhai
10BB15J26033

A thesis submitted to the
Academy of Scientific & Innovative Research
for the award of the degree of
DOCTOR OF PHILOSOPHY
in
SCIENCE

Under the supervision of
Dr. GVN Rathna

CSIR- National Chemical Laboratory, Pune

Academy of Scientific and Innovative Research
AcSIR Headquarters, CSIR-HRDC campus
Sector 19, Kamla Nehru Nagar,
Ghaziabad, U.P. – 201 002, India

March, 2022

Certificate

This is to certify that the work incorporated in this Ph.D. thesis entitled, *"Design and Development of Non-Woven Nanofibers as Drug Delivery System"*, submitted by *Patel Pratikshkumar Rameshbhai* to the Academy of Scientific and Innovative Research (AcSIR) in partial fulfillment of the requirements for the award of the Degree of *Doctor of Philosophy in Science*, embodies original research work carried-out by the student. We, further certify that this work has not been submitted to any other University or Institution in part or full for the award of any degree or diploma. Research material(s) obtained from other source(s) and used in this research work has/have been duly acknowledged in the thesis. Image(s), illustration(s), figure(s), table(s) etc., used in the thesis from other source(s), have also been duly cited and acknowledged.

Mr. Patel Pratikshkumar Rameshbhai

Research Scholar

Date: 04/03/2022

Dr. GVN Rathna

Research Supervisor

Date: 04/03/2022

STATEMENTS OF ACADEMIC INTEGRITY

I Patel Pratikshkumar Rameshbhai, a Ph.D. student of the Academy of Scientific and Innovative Research (AcSIR) with Registration No. 10BB15J26033 hereby undertake that, the thesis entitled *"Design and Development of Non-Woven Nanofibers as Drug Delivery System"* has been prepared by me and that the document reports original work carried out by me and is free of any plagiarism in compliance with the UGC Regulations on *"Promotion of Academic Integrity and Prevention of Plagiarism in Higher Educational Institutions (2018)"* and the CSIR Guidelines for *"Ethics in Research and in Governance (2020)"*.

Signature of the Student
Date: 04/03/2022
Place: P u n e

It is hereby certified that the work done by the student, under my/our supervision, is plagiarism-free in accordance with the UGC Regulations on *"Promotion of Academic Integrity and Prevention of Plagiarism in Higher Educational Institutions (2018)"* and the CSIR Guidelines for *"Ethics in Research and in Governance (2020)"*.

Signature of the Supervisor
Name: Dr. GVN Rathna
Date: 04/03/2022
Place: P u n e

ACKNOWLEDGEMENTS

Pratikshkumar Patel R.

Pratikshkumar Patel R.

must nevertheless go to *Amarnath,* for being my friend and confidant during my entire Ph.D. tenure and for constantly providing support, motivation and inspiration to further my work, in regards to Ph.D. and more. With all my lab mates I attended many conferences and I will always cherish those moments. I thank my closest friends Dr. Rajan Pandya, Dr. Arun Dadwal, Dr. Abhishek Balmik, Rashid Dr. Pravin Dwievdi, Dr. Vineeta Soni, who were life savers and always ready to help and support me in my difficult time. Besides, I extend my thanks to my other close friends like Dr.Ragini, Monika and Sourosree. With all these close groups of friends, I have made many outdoor trips, parties, seen movies, and created memories. I will always remember late-night discussions and chitchats with Amarnath, Mahendra and Arun over chai shai. I thank you all for your company, love, and care. It is very difficult to find friends like Dr. Brijesh Sharma, Dr. Sanjeev Kheria, and Dr. Yachita Sharma who match my mindset and frequency, particularly when you got the honesty, daring, and truthfulness to the level of sickness.

I stayed in the hostel from the first year and over these years I have made so many friends. I extend many thanks to my NCL seniors and friends Dr. Nidhi, Dr. Negi, Dr. Varchaswal, Sanjukta, Praveen Singh, Govid Porwal, Dr. Pravin Shinde, Dr. Arun Nikam, Dr. Abhijit, Rahul, Dr. Santigopal, Dr. Sayan, Dr. Gaurav, Dr. Ramireddy, Dr. Chaitanya, Dr. Trinadh, Dr. Sagar, for being a valuable part of my life at NCL. How can I forget my Cricket group, Dr. Deepak Kumar, Shahebaaz, Dr. Yashpal, Dr. Manojkumar, Dr. Prahant Patil, Dr. Mahendra Pawar, Dr. Shakeel. Dr. Sudhakar, Dr. Deepak Chand, Prashant Yadav, Manish, Vikas, Mahendra Wagh, Gopal, Himanshu, Anupam, Shrikanth, Sandy, Dr. Aashish, Nirsad, Ravi, Gopal, Ajith, Sonu, Sidharth, Narugopal, Santosh, Shubam, Umasaran, Dharmendra, Priyam, Inderjeet, Dhananjay, Rohit (Jr. and Sr.), Anirban, Shibin, Prem, Dr. Anup, Sumanta, Golu, Dinesh, Kailash Pandare, Kailash (baba), Bharath, Rajesh, Vinayak, Kundan, Nittan, Rakesh, Pratiksha, Kranti, Priyanka, Shikha, and Pavan. I would like to say special thanks to our CSIR-NCL team with whom I played SBBLT namely, S. Mane, A. Phadake, Prashant, Balmiki, Ravi Kute, Karanjkar, Saini, Sanjay, Dr.Vinod, Mahendra Jagtap, Sachin, Sanjay Jadav and Sunil Patel.

I would also like to thank my M.Pharm friends Dr. Nishita Mistry, Preeti Patel, Karan Samyani, Jigar Rathod, Nirav Patel, Bharath Senta, Dushyant, Bhumik Patel, Jigar Thanki, Virender, and Dr. Dipesh Baradiya, my hometown brothers Umesh, Manish, Vipul, Nimesh, Hardik, Bitu, Abhinav, Akshay, Mayank, Suraj, and Nitin who have constantly been in touch

Pratikshkumar Patel R.

with me all these years and asked about my wellbeing. Despite only a few meetings past these years, the bond we share is remarkable. I would like to say special thanks to Pinka for his continuous presence and his effort and never give up attitude helped me to go through all ups and downs.

I would like to express my heartfelt gratefulness to my parents, Mrs. Niruben Patel & Mr. Rameshbhai Patel, who provide me unconditional love and support. Their contribution is immense and cannot be stated in words, it is because of them I have come this far in life. Thank you for believing and keeping patience with me. I would also like to express my gratitude to all my relatives, Mukesh (mama), Shubhash (mama), Hitesh (mama), Swati (mami) and Harshita (Mami). I would to take opportunity to thanks my beloved grandparents, Devliben (wai), Raniyamaster (dada), Daili (wai), Hirabhai (dada) and Paliben (wai). Lastly, I would like to say thank you from the depth of my heart to Dr. Dipti Gawai for her continuous support, guidance, love and care in my difficult times, without her it wouldn't not possible for me to come this far. It gives me immense pleasure to thank everyone who helped me write my thesis successfully (kindly excuse me if I forgot to mention anyone).

Finally, acknowledgment would not be completed without thanking God, for giving me the strength and the determination to overcome the hardship faced in my life.

Pratikshkumar Patel

Pratikshkumar Patel R.
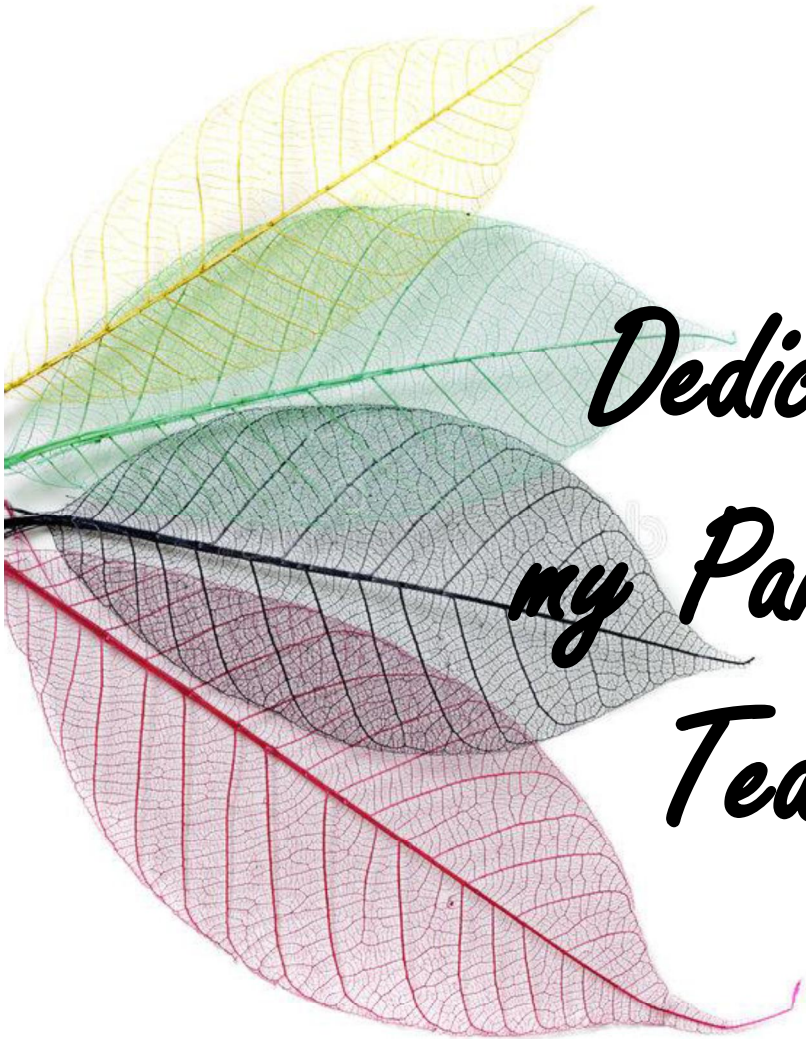
Dedicated to
my Parents and
Teachers

Abbreviations and symbols

DDS	Drug delivery system
NF	Nanofibers
PK	Pharmacokinetics
FDA	Food and drug administration
SEM	Scanning electron microscope
FE-SEM	Field emission scanning electron microscope
TEM	Transmission electron microscope
HRTEM	High resolution transmission electron microscope
FTIR	Fourier transform infrared spectroscopy
UV-Vis	Ultra violet visible spectrophotometry
DSC	Differential scanning calorimetry
TGA	Thermogravimetric analysis
MTT	3-(4,5-Dimethylthiazol-2-yl)-2,5-diphenyltetrazolium bromide
RT	Room temperature
HP	Hemolytic percentage
PP	Polypropylene
PS	Polystyrene
PVC	Polyvinyl chloride
PET	Polyethylene terephthalate
PE	Polyethylene
Cur	Curcumin
PLA	Polylactic acid
PET	Polyethylene terephthalate
PMMA	Polymethyl methacrylate
PEO	Polyethylene oxide
CMC	Carboxymethyl cellulose
LiCl	Lithium Chloride
NaCl	Sodium Chloride
DAPI	4′,6-diamidino-2-phenylindole

HTAB	Hexadecyl trimethyl ammonium Bromide
PS	Polystyrene
PAN	Polyacetonitrle
PVDF	Poly(vinylidene fluoride)
PHBV	Poly (3-hydroxybutyrate-co-3- hydroxyvalerate)
PLGA	poly lactic glycolic acid
SF	Silk fibroin
AV	Aloe vera
DI	Deionized water
PBS	Phosphate buffer saline
EtOH	Ethanol
EGFR	Epithelial growth factor receptor
THF	Tetrahydrofuran
BSA	Bovine serum albumin
NHS	N-hydroxysulfosuccinimide
HDF	human dermal fibroblast
MNP	magnetic nanoparticles
PTX	paclitaxel
BCC	Basal cell carcinoma
SCC	Squamous cell carcinoma
AK	Actinic keratosis
HPMCP	Dehydroxypropyl methylcellulose phthalate
CA	Cellulose acetate
PVA	Polyvinyl alcohol
PU	Polyurethane
PVP	Polyvinyl pyrrolidone
CDF	3, 4- difluorobenzylidene curcumin
MRI	Magnetic resonance imaging
EA	Egg albumin
BSA	Bovine serum albumin
HSA	Human serum albumin

MTz	Metronidazole
NM	Nanofibers mats
XRD	X-ray diffraction
CD	Circular dichroism
EDTA	Ethylenediaminetetraacetic acid
SLN	Solid lipid nanoparticles
HA	Hyaluronic acid
DHFR	Dihydrofolate reductase
S. aureus	Staphylococcus aureus
E.coli	Escherichia coli
ZnO	Zinc oxide
AT	Amoxicillin trihydrate
CH	Chlorohexidine digluconate
API	Active pharmaceutical ingredient
WHO	World health organization
NPEA	Neem oil polyesteramide
RBCs	Red blood cells
SMN	Stearic coated magnetic nanoparticles
SQUID	Superconducting quantum interference device
FU	Fluorouracil

Table of contents

Chapter 2. Objective and scope of work

Chapter 3. Development of hydrophilic PLA/PCL/EA nanofiber mat as a drug delivery system and study its properties for tissue regeneration

Chapter 4. Bioinspired Hyaluronic Acid Based Nanofibers Immobilized with 3, 4-Difluorobenzylidene Curcumin for Treating Bacterial Infections

Chapter 5.   **Blends of oil based polyesteramide as nanofiber mat for dual drug delivery for wound healing application**

Chapter 6. Blend of neem oil based polyesteramide as magnetic nanofiber mat for efficient cancer therapy

Chapter 7. Conclusion and Future Prospects

Abstract

Poster, oral presentations and Conferences attended

List of publications

List of Figures

[Chapter 4](#)

List of tables

CHAPTER 1

Introduction and literature survey

Chapter 1

This chapter discusses the properties of nanofibers, the background of the electrospinning technique, and its emergence in chronological order. Also, this chapter covers the types of electrospinning methods and their mechanism. Further, elaborated the reported factors affecting the properties of nanofibers, characterization methods and applications in tissue engineering, drug delivery, nanofibers as biosensor, skin cancer treatment, and magnetic nanofibers.

1. Introduction

Nanotechnology is evolving rapidly, and it is widely studied in various fields for different applications. In the biomedical stream, nanotechnology has gained enormous importance due to the favourable physicochemical properties, which were more suitable when compared to the bulk technology. The nanomaterials have a high surface-to-volume ratio, hence permeable through various channels and membranes showing high efficacy and more preferred for targeted drug delivery. Accordingly, nanotechnology has thus enabled researchers to develop diverse biomedical biomaterials such as nanorods[1-3], nanoplates[4, 5], nanogels[6, 7], nanoparticles[8, 9], nanoemulsion[10], and nanofibers[7, 11]. Nevertheless, nanofibers got much attention in the last two decades due to their straightforward production, distinctive properties, ease of reproduction, and therefore, studied for diverse applications like tissue engineering, scaffolds, drug delivery, implants, wound material, biosensor, vitamins etc. Though there are various techniques utilized for the fabrication of nanofibers, such as melt-spinning[12], melt blowing[13], solution spinning[14], templating [15, 16], phase separation[17, 18], and self-assembly[18-20], the electrospinning method is considered idler, as it is simple, easy, and economical to develop on a lab and industrial scale.

Fabrication of nanofibers by electrospinning can be possible only when a material has high molecular weight, has suitable viscoelastic property, and is blended with one or materials that also should have a decent molecular weight. Chiefly polymers were adapted for the fabrication of electrospun nanofibers. The polymer was

conventionally divided into three primary forms: natural, synthetic, and semisynthetic. Natural polymers are obtained from nature and can be extracted such as keratin, collagen, hyaluronic acid, silk, wool, proteins etc. Synthetic polymers are human-made such polymers are primarily obtained from petroleum oil products examples are polypropylene (PP), polyvinyl chloride (PVC), Polystyrene (PS), nylon etc. Lastly, semisynthetic polymers were developed using natural polymers by modifying or making acceptable changes into the particular polymers like cellulose derivatives were made cellulose acetate, cellulose nitrate etc. Polymers can be classified in terms of their degradation nature, like biodegradable and non-biodegradable polymers.

Further, nanofibers have a remarkable property in the biomedical field because they can maintain moisture around the wound, inhibit scar formation, enhance the growth of cells, and can mimic extracellular matrix. Due to these properties, nanofibers are extensively used in wound healing, tissue engineering, drug delivery, bone engineering, implants, blood vessel engineering, cartilage engineering and as anti-bacterial mats, etc. Such properties are unoffered by bulk materials as many bioactive molecules are required compared to nanofibers. The surface to volume area ratio of bulk is much lesser than nanofibers, due to which the multiplication of cells is also lesser when compared to nanofibers. Hence nanofibers are preferred over bulk materials **(Fig.1.1).** Accordingly, many articles are being published every year, and this number is increasing exponentially. **Fig.1.2** shows a few of the illustrations where the nanofibers are being used for biomedical applications. The information is taken from the Web of Science.

Figure 1.1 Application of nanofibers in the biomedical field
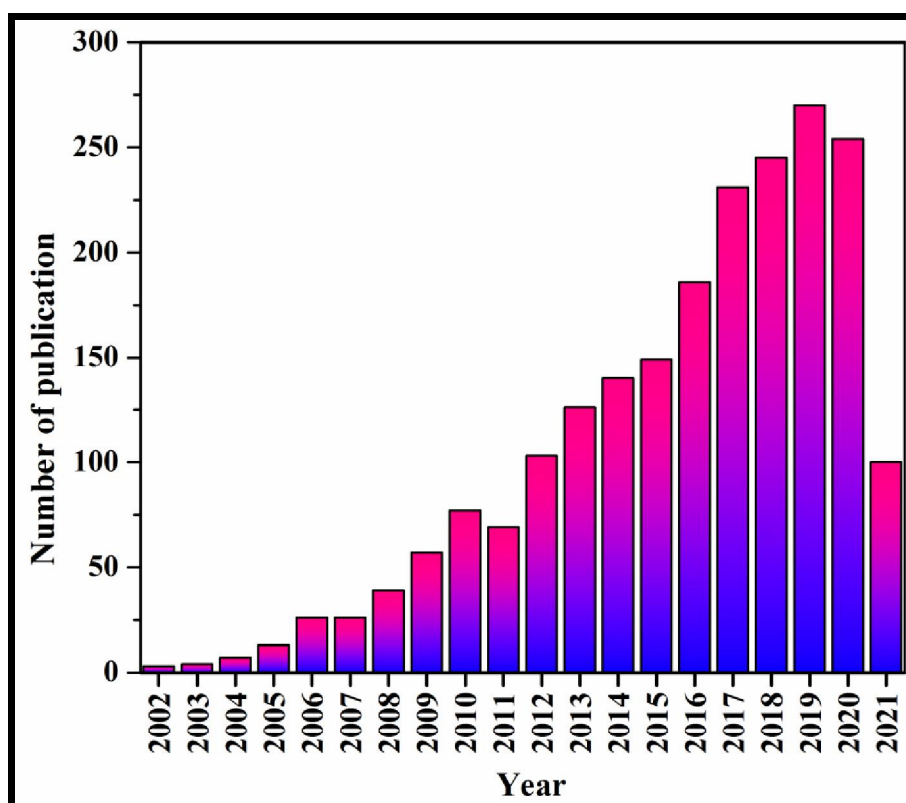
Figure 1.2 Year-wise articles published on nanofibers in the area of biomedical applications

There are mainly two types of fibers available, 1) natural fibers existing since 4000 years ago and 2) preparation of man-made fibers, which started since 100 years ago. Initially, fibers were developed by conventional methods from artificial silk The production of synthetic fibers is increasing significantly due to their high functionality and high performance, which plays a crucial role in various applications. Du Pont Company was foremost to produce the synthetic fibers that were finer than spider thread, stronger than steel and aesthetic in appearance compared to silk or nylon. However, electrospinning came into existence in 1544-1603, which was documented by William gilbert. In his experiment, the English physicist William Gilbert applied a high voltage under which a drop of water warped into a cone-shaped when it was held below an electrically charged amber[21] due to electrostatic attraction between liquids. This deformation is later known as the Taylor cone[22]. In 1882, English physicist Lord Rayleigh (1842-1919) analysed the unsteady states of liquid droplets that were electrically charged and recognized that the liquid was ejected in tiny jets when equilibrium was formed between the surface tension and electrostatic force[23]. In 1887, British physicist Charles Vernon Boys (1855-1944) reported nanofiber development and production[24]. In 1902 and 1903, Cooley and Morton patented the 1st device to spray the liquids under the influence of electrical charge, and the fabrication of artificial silk was undertaken by Kiyohito et al. in 1929[25]. Between 1934 and 1944, Anton Formhals attempted the production of nanofibers and published the first patent describing the experimental output of nanofibers[26]. Later, in 1966, Harold Simons published a patent for a device that could produce thin and light nanofiber fabrics with diverse themes.

Electrospun nanofibers have become more popular than nanoparticles in the biomedical field because the technique used for fabrication is quite simple, secure, cost-effective, highly reproducible, and can be reproduced in small and large quantities. Moreover, unlike nanoparticles, electrospun nanofibers are easy to maintain desirable size, involve less solvent and simple and easy to fabricate, and involve minimum wastage, with excellent stability and better properties. The other advantages include high porosity and permeability with improved efficacy.

1.1   Fabrication of Electrospun nanofibers

The production of electrospun nanofibers is done by applying an electric field using a high voltage to a polymer solution. During the electrospinning process, the charged droplet of polymer solution ejecting from the needle creates a repulsive force on the droplet's surface by exceeding the surface tension and gradually forms a jet with an increase in the voltage. As a result, the entangled polymer chains create a whipping motion and elongates, followed by solvent evaporation and solidification, and get collected on the oppositely charged collector in the form of a nanofibers network. Figure 1 shows the electrospinning unit, which is an assembly of (1) a high voltage electric system, (2) a syringe pump, (3) a syringe with a needle of predetermined pore diameter, and (4) a metal collector.

1) **High voltage electric system** (Positive current) is attached to a needle syringe. Generally, a high voltage system in the range of 0 to 50 kV with the production of 0.5 amp of electric current is in practice. When subjected to increased voltage, a droplet of the polymer solution transforms into a Tailor cone at critical voltage elongates to form polymeric fibers and gets deposited on the collector as solid fibers (micron to nanometer in diameter). On the other hand, nanofibers with bulbs would be formed if the voltage increases beyond the critical voltage. Hence the electric charge plays a vital role in the fabrication of nanofibers.

2) **Syringe pump** unit helps in holding the syringe with the needle and drives the polymer solution at a predetermined flow rate as designed for a given instrument. The syringe pump has a facility to hold single, double or multiple syringes to function simultaneously or individually. In addition, the rate of solution flow can be regulated as a function time.

   Types of syringe with varying diameters of the needle affect the morphology of nanofibers. There are different **types of syringe needle** systems available like coaxial, tri-axial, multi-needle, magnetic field-assisted, conjugate, centrifugal electrospun for different kinds of applications, and they can be used to increase the production of nanofibers in less time and to make hollow, porous, core-sheath nanofibers (**Fig.1.3**). The various **diameter of needles**

were used to get the desired size; the smaller the diameter of the needle the smaller the diameter size of nanofibers obtained; similarly, larger the diameter larger will be the size of nanofibers[27].
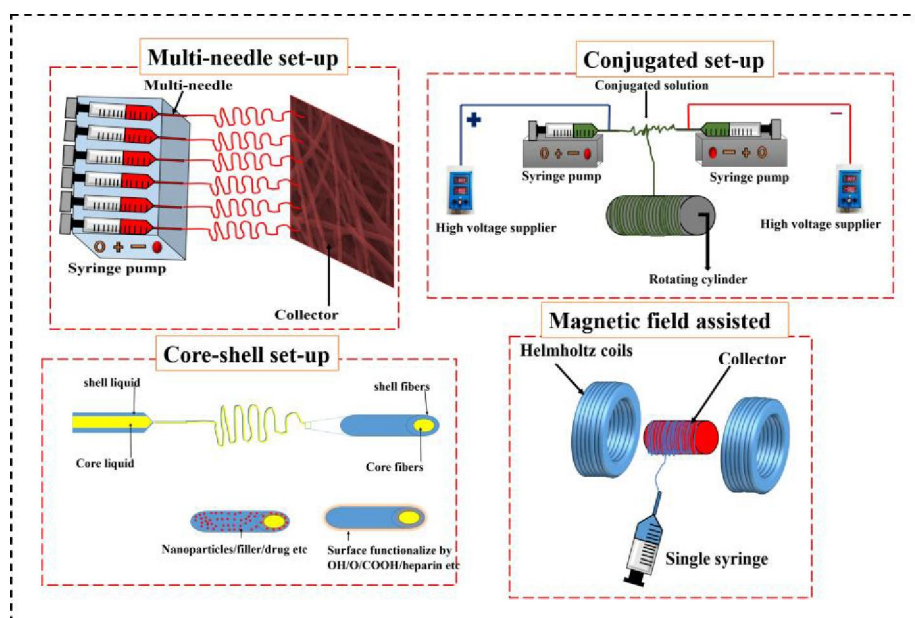
Figure 1.3 Different type's syringes used in the electrospinning method

3) **Collecting system** (negatively charged): The collecting system in the electrospinning unit is used for collecting the nanofibers. The fibres ejecting from the positive source are driven to attract the negative source. Accordingly, nanofibers get deposited on the collector. (**Fig.1.4**). There are various kinds of collectors available for the collection of nanofibers. The morphology of nanofibers changes completely when the collector system is changed. Here we have shown the collectors and their morphology of nanofibers, as shown in **Fig. 1.4**. There are mainly six different kinds of collectors in practice: solid plate collector, guide wires collector, rotating drum/mandrel, rotating wire drum, rotating disk, and liquid bath collector.
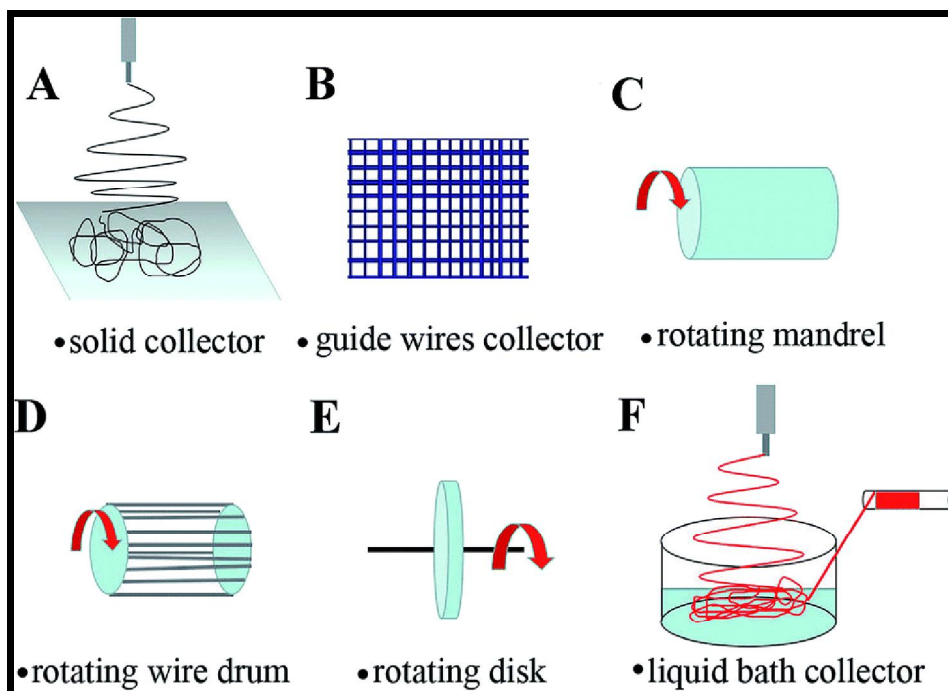
Figure 1.4 Different types of collector used in electrospinning method

The electrospinning unit can be horizontal or vertical. In horizontal, electric force is the only source to pull the fibers from needle to collector. In vertical, two forces which pull the fibers from needle to collector are electric force and gravitational force, which narrows down the size of nanofibers[28]. Modifications can be done in the basic instrumentation like needleless assembly, multiple needle assembly, etc. Based on the requirement, various types of collectors are used like (a) drum collector, (b) plate collector, (c) liquid bath collector, etc.

1.2 Types of electrospinning

There are mainly two different electrospinning methods in practice for the production of fibers. The property of nanofibers depends on the method we choose for fabricating. The methods are as follows;

1) Melt-electrospinning
2) Solution electrospinning

1.2.1 Melt-electrospinning of nanofibers

The melt electrospinning process is considered safe with high output. It is one of the best methods because various types of polymeric materials can be used for fabrication, wherein energy consumption is less. It is reported that the fibres produced using these methods were superior in mechanical, optical and electrical properties[29]. This method is preferred and recommended over the solution electrospinning method because it is cost-effective as no solvent is used for application and for recovery, which is an asset for the environment and healthy living. Further, the time involved for the dissolution of polymers is saved[30]. Usually, the average diameter of the nanofibers obtained using the melt electrospinning unit ranges from 10 to 50 μm. **Fig. 1.5** depicts the schematic representation of the melt electrospinning unit. Polymers like polyethylene terephthalate (PET), polypropylene and polyethylene (PE) are being studied using melt electrospinning techniques[31-33]. The list of polymers used for fabricating the fibres using melt-electrospinning was presented in **(Table 1.1).**

Although melt-electrospinning has distinct advantages over solution electrospinning, very little work has been done due to its limitations. The limitations are that the electric discharge problem is associated with the equipment due to the intrinsic difficulties related to the polymer, such as low electrical conductivity and high viscosity. The schematic diagram of melt electrospinning is shown in **Fig.1.5.**
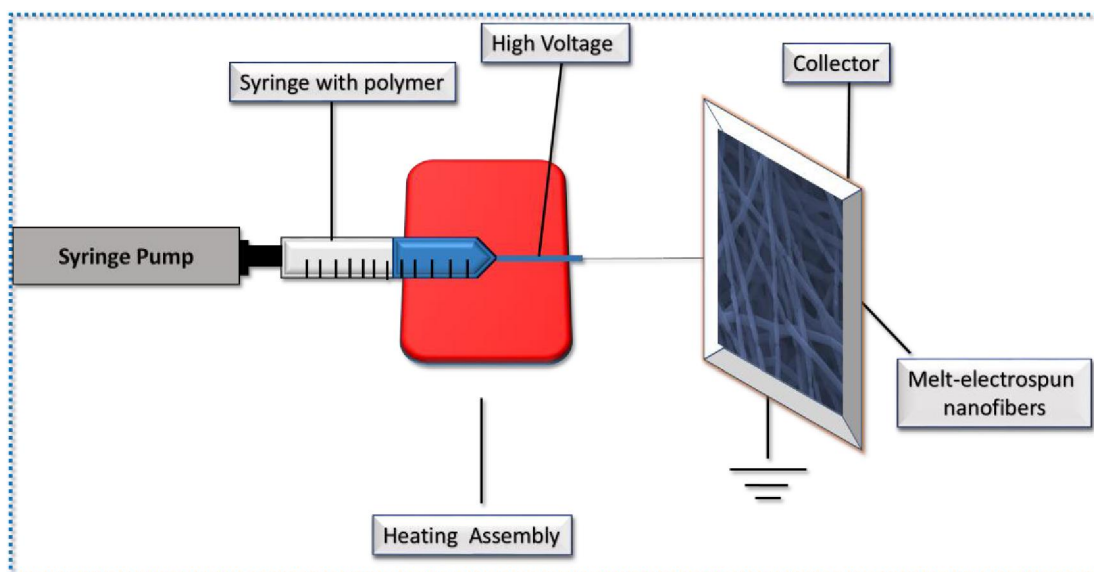
Figure 1.5 Melt-electrospinning apparatus

Table 1.1 Examples of polymeric fibers developed using melt electrospinning

Sr.no	Polymer	Temp	Reference
1	PLA (polylactic acid)	200 °C	[34]
2	PE (Polyethylene)	200-220 °C	[31]
3	PP (Polypropylene)	280-290 °C	[32]
4	Polyethylene terephthalate (PET)	260 °C	[33]
5	Nylon-6	270–280°C	[35]
6	Polyalirate	330°C	[33]
7	Polymethyl methacrylate (PMMA)	45°C	[36]
8	20% PEG5000- block PCL5000 + 80% PCL	90°C	[37]

1.2.2   Solution electrospinning of nanofibers

As discussed in the earlier section (**1.1**), in the 1990s, the pioneering work of Doshi and R. Eneker (1995) re-investigated the interest in electrospinning and established it as an effective way to produce nanofibers for different applications[38]. Solution electrospinning is relatively easy and convenient as no additional assembly is required, like heating assembly in melt electrospinning. Solution electrospinning provides a wide range of nanofibers where the diameter of the nanofibers ranges from less than 100 nm to 1000 nm. The solution electrospinning method is preferable to fabricate nanofibers for the thermally unstable polymers and degrade during the melting process[29]. The schematic representation of solution electrospinning is shown in **Fig.1.6**.
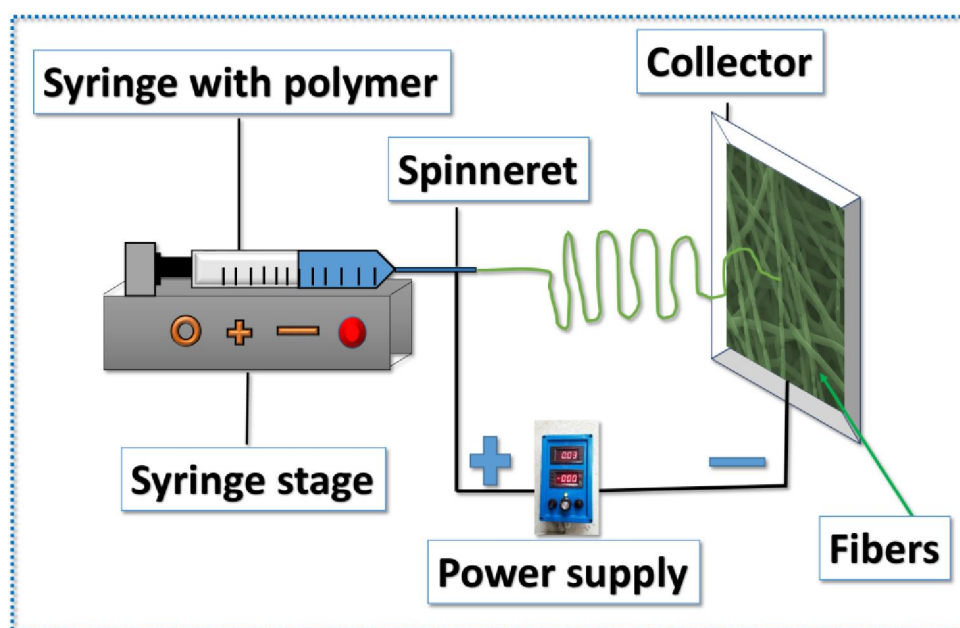
Figure 1.6 Solution electrospinning apparatus

1.3   Factor affecting nanofibers morphology

In the solution electrospinning process, the morphology of the nanofibers depends on three essential parameters: solution properties, electrospinning process parameters, and environmental parameters. Therefore, it is necessary to understand the influence

of these parameters on the fabrication of nanofibers, which was well documented in the reported literature.

1.3.1 Electrospinning process parameters

1.3.1.1 Applied voltage

In the electrospinning process, a high voltage unit is an essential component to regulate the voltage under which the solution ejects at a fixed flow rate of the polymer solution. As mentioned in the above section (**1.1**), generally, a high voltage system in the range of 0 to 50 kV with the production of 0.5 amp of electric current is usually in practice. When high voltage is applied, a droplet of the polymeric solution transforms into a tailor cone, which at critical voltage elongates to form fibers, solidifying before being deposited on the collector. The diameter size of the fibers may range from a micron to ~50 nanometer [39]. The change in voltage will impact the polymers to spin (depends on the physical properties); hence voltage may not be the same for all polymers. Likewise, the diameter of the nanofiber also depends on the applied voltage. If the voltage is increased beyond the critical voltage, nanofibers with bulbs/beads will be formed[39]. For example, beads were formed with an increase in the applied voltage for polyethylene oxide (PEO)/water[40]. Some groups have reported that when the applied voltage is higher, the diameter of the nanofiber is also increased[41]. Therefore, based on the published literature and our experimental data, we infer that high voltage plays a crucial role in the fabrication of nanofibers.

1.3.1.2 Flow rate

Flow rate is one of the vital parameters to obtain smooth nanofibers. To attain a desirable diameter of the nanofibers without beads, it is crucial to optimize the flow rate of the solution that can easily dispense from the metallic needle. The flow rate of the solution of the respective polymer may vary depending upon the solution properties. Usually, with the increase in the flow rate, the chances of bead formation are more because the polymer solution will not get enough time to evaporate (evaporation depends on the volatility of the solvent) before being settled on the collector. For instance, Megelski et al., 2002 studied nanofiber development using a

polystyrene solution, which recorded beads' formation when the flow rate was at 0.10 mL/min. However, when the flow rate was decreased to 0.07 mL/min, smooth and bead free nanofibers were obtained[39]. It is therefore suggested that the retarded flow rate helps to obtain smooth and fine nanofibers.

Further, it also suggests that with the increase in flow rate, the diameter size of the nanofiber was increased[39]. Nanofibers with uniform diameter will be achieved at a minimal flow rate because a stable jet cone is formed, inhibiting bead formation. It is reported that a discontinuous jet cone leads to the formation of nanofibers with a wide range of diameters and beads. In many cases, due to this phenomenon, ribbon-like structures were formed[39].

1.3.1.3 Distance between the tip of needle and collector

To fabricate the nanofibers in various diameters, the distance between the tip of the needle and the collector plays an essential role. For instance, if the distance between the tip and collector increases, the nanofiber diameter decreases because of an increase in the distance, which enables more time for the polymer/s chains to elongate and evaporate the solvent before being collected on the collector. However, when the distance is less, the residency period of the solvent is longer as the time to evaporate the solvent is less, and therefore the diameter of the nanofibers is large or else beaded[42]. Therefore, to obtain nanofibers' smooth and desired size, the distance between the tip of the needle and collector should be optimized. The morphology of the nanofibers changes though the distance is maintained because of the variations in polymeric concentration and blend composition. Studies on the development of nanofibers as a function of distance were reported by Baumgarten et al. 1971, Matabola and Moutloali et al.; 2013 and Wang and Kumar et al. 2006. From their observations, it is concluded that the distance between the needle tip and collector plays a crucial role in manipulating the morphology of nanofibers[42-44] and therefore, it is essential to fix the distance according to polymer properties.

1.3.2   Effect of solution parameters on nanofiber morphology

After learning the significance of the electrospinning process parameters in defining the morphology, it is also important to know the importance of the solution properties to achieve smooth and bead free nanofibers. The various solution parameters that are involved in producing smooth and refined nanofibers are the molecular weight of polymer (relative molecular mass), solution concentration, viscosity, conductivity, surface tension, and the type of solvent used to prepare solution[29, 45].

1.3.2.1 Viscosity and concentration of the polymeric solution

Polymers of natural or synthetic origin are widely used for fabricating nanofibers by electrospinning method either by melt or solution process. In the solution electrospinning method, a desirable viscosity of the polymeric solution is required to develop nanofibers. The viscosity of the polymeric solution depends on the type of the polymer, the solvent, temperature, molecular weight of the polymer and interaction between solvent and polymer. Depending on the structure and functionality of the polymer, the viscosity of the solution may be increased or decreased. Usually, the viscosity of the polymeric solution increases with an increase in the molar concentration of a polymer or an increase in the molecular weight of a polymer. Generally, a decrease in temperature increases the viscosity; however, it may again depend on the structure and functionality of the polymer. Several reports in the literature related to desirable polymer viscosity for producing nanofibers. For example, polyethene oxide (PEO) of different concentrations with different viscosities were electrospun. The results showed viscosity range of 1 to 20 poise was desirable for producing nanofibers. Similar studies were also done with other polymers, for example, cellulose acetate in different concentrations, where the desirable viscosity for spinning nanofibers was from 1- 10.5 poise. It is clear from the above two examples that for the formation of nanofibers, a required viscosity is critical, and it is dependent on the type of polymer and its concentration. Below and above these viscosities, the polymer solution is either sprayed or forms fragment of fibers with or without bulbs on the nanofibers. In case the viscosity of the solution is very high, the flow of solution is interrupted, and solvent dries; as a result, the polymer clogs the

pore of the needle.[46, 47]. Viscosity is always proportional to polymer concentration. Therefore the diameter of the nanofiber will increase with the increase in the polymer concentration[48].

1.3.2.2 Surface tension

The surface tension is another important parameter that influences nanofibers' fabrication by electrospinning method. To enable the fiber formation, the electrostatic repellent force on the surface of the charged polymer solution must be greater than the surface tension of the polymer solution. For the production of smooth and bead free nanofibers, the surface tension of the solution should be low. Generally, the surface tension of the solution can be reduced by increasing the concentration of solution, which can help fabricate smooth and fine nanofibers.

Another possibility to reduce the surface tension of the solution is to keep the concentration constant and vary the composition of solvent or add ionic salts or surfactants to the polymeric solution. Ahmed Abutaleb and co-author showed the effect of surfactant on surface tension by polyetherimide fibers using four different surfactants Lithium Chloride (LiCl), Sodium Chloride (NaCl), Triton X-100 and Hexadecyl trimethyl ammonium Bromide (HTAB)[49].

1.3.2.3 Conductivity of solution

In the electrospinning process, the conductivity of the polymer depends on the ability of the electrifying property. The conductivity of the polymeric solution increases with an increase in the electric conducting quantity and the morphology of the nanofibers is directly proportional to the strength of the conductivity[50]. The conductivity depends on the type of polymer and solvent used. For example, Chi-Wang et al. studied five different polymers such as polyhydroxybutyrate (PHB), polystyrene (PS), polyacetonitrle (PAN), and poly-D-L-lactic acid with different conductivity to analyze the morphology. The conductivity of the polymer solution can be improved by the addition of salt. To decrease the diameter of nanofiber, the addition of a desired quantity of salt to the polymer solution before electrospinning is advisable[51].To manipulate the conductivity of a polymer solution, the salts used are nickel acetate,

cobalt acetate, KH$_2$PO$_4$, NaCl, etc[51, 52]. It was observed that natural polymers are more conductive than synthetic polymers. A moderate conductivity of the polymer solution will enable the production of nanofibers. For example, blends of natural polymeric solution chitosan and sodium alginate are highly conductive; still, they cannot form nanofibers as it is low in molecular. However, when this polymer blended with other synthetic polymers, it attained the desired conductivity to produce fine nanofibers of in a range of 200 to 300 nm[53, 54]. The reported literature shows that the conductivity of solution and polymers should be sustainable to produce smooth and refined nanofibers. Each polymer has different conductivity, so there is always a need to study the conductivity of the respective polymer and their blends to attain suitable conductivity for electrospinning. Also, it should be noted that the conductivity depends on the polymer, solvent and doping agents to improve conductivity.

1.3.2.4 Effect of solvent on nanofibers morphology

The solvent is another essential factor, which plays a significant role in producing nanofibers. Solvent properties like conductivity, the solubility of polymers and volatility influences the electrospinning process and affect the morphology of nanofibers. It is reported that to fabricate nylon-4, 6 nanofibers, the conductivity of the solvent plays a vital role. Wherein the diameter of the nanofiber mat decreased with an increase in conductivity of the solvent[51]. From the earlier studies, it is evident that to attain good nanofibers, the dissolution of polymer should be 100% and the solvent should be reasonably volatile with low to medium boiling point so that during the spinning process, the nanofibers will solidify and deposit on the collector. In case the solvent's boiling point is high, the time taken to evaporate the solvent from the nanofiber will be slow, and therefore, there is a possibility of beaded nanofiber formation with an enlarged diameter[55] . If the volatility of the solvent is very high the solvent gets evaporated before it is being spun and clogs at the nozzle of the needle[13]. A mixture of solvents with a marked difference in volatility will create pores on the nanofiber, where the porosity can be manipulated as desirable[46, 56]. Therefore, as reported, selecting a suitable solvent for electrospinning is crucial to obtaining smooth nanofibers.

1.3.2.5 Molecular weight of the polymer

As explained in the above section, the viscosity of the solution depends on polymer concentration and a suitable solvent; however, we should also refer here the viscosity depends on the molecular weight of the polymer. High molecular weight polymers of the same concentration are more viscous than the same concentration of the polymer with low molecular weight. Since desired viscosity is one of the essential parameters to electrospun, there is a need to manipulate the concentration of the polymer to spin the nanofibers. Further, it also reported that the mechanical strength of the nanofibers increases with the increase in polymer molecular weight. For instance, if a polymer is of low molecular weight, the possibility to form beaded nanofibers will be more and results in electrospray forming nanoparticles[47]. So generally, the polymer with high molecular weight is always preferred for electrospinning purposes to obtain smooth and uniform nanofibers[48]. Further, increase in the molecular weight of the polymer results in ribbon-like structure instead of thin fibers. For instance, polystyrene (PS), poly(ether imide) and Poly(vinylidene fluoride) (PVDF)[57] are few of them which reported ribbon like nanofibers. Hence it is important to note that molecular weight of the polymer is also an essential parameter in controlling the formation of nanofibers.

1.3.3   Environmental parameters

1.3.3.1 Effect of temperature and humidity

In addition to solution electrospinning parameters, the environmental parameters such as temperature, humidity, and the pressure created by air affect the morphology and diameter of the nanofibers[58, 59]. *Temperature:* To attain uniform nanofibers, it is crucial to maintain constant ambient temperature because the viscosity of the polymer is not only dependent on the concentration and solvent, it also dependents on the temperature. If the temperature is changed, the viscosity of the solution can either decrease or increase depending on the polymer property. The decrease in solution viscosity with the increase in temperature is attributed to an increase in the mobility of solution molecules. Further, the change in viscosity is also dependent on the boiling point of the solvent and the rate at which it evaporates during the preparation of solution. An increase in the rate of evaporation with the rising temperature increases

the viscosity and the morphology varies, which is again depends on the type of polymer. De Vrieze et al. 2009 studied the fabrication of nanofibers using cellulose acetate and PVP with the temperature variation, results showed a decrease in the diameter of the nanofibers with the increase in temperature[55]. ***Humidity****:* Generally, the electrospinning unit is maintained in a closed chamber. So, any change in the humidity in the chamber can change the morphology of the nanofibers. In the presence of humidity the volatility of the solvent is reduced hence the rate of evaporation of solvent will be reduced which may increase or decrease the diameter of the nanofiber. In case the hydrophobic polymers are being electrospun, the presence of humidity can create pores on the nanofibers due to the change in the evaporation rate of organic solvents[60]. For example, the diameter size of PVA nanofibers decreased from 667 to 161 nm, and for PEO, it also decreased from 252 to 75 nm when the humidity was changed from 4 to 60 %. Similarly, the diameter of the nanofibers of the blend of PVA/hyaluronic acid was decreased from 231 to 46 nm when humidity was changed from 4 to 50 %[60, 61]. ***Air pressure****:* Generally, the electrospinning is done under atmospheric pressure under a closed chamber. However, if the atmospheric pressure is changed, the volatility of the solvents will change, which may interfere with the fiber formation and also the precision of the fiber deposition. It is always necessary to maintain constant pressure so as to sustain the stability of the jet, otherwise the nanofibers may break during deposition[61]. Finally, we conclude that, to fabricate smooth and fine nanofibers, the above parameters (process parameters, solution properties and environmental parameters) are needed to be considered and should be tuned accordingly to sustain the reproducibility of nanofibers production.

1.4   Characterization of nanofibers

Characterization of nanofibers is an essential aspect for determining the geometrical, chemical, physical and mechanical changes exhibited after nanofibers' fabrication. These studies determine the fate of the nanofibers developed for the said application. As these nanofibers are being used for diverse applications, the properties required will also change. We are currently focusing on nanofibers for biomedical applications, so the following characterisations will be explained accordingly. For any nanofiber

network developed the first and foremost study is to determine the geometry of nanofibers. The size and appearance of the nanofibers will be analysed, which is done by SEM, FESEM and TEM. But most extensively used is SEM and FESEM for finding the geometry of the nanofibers. Also, the porosity and pore diameter is analysed by BET, capillary flow porometer or mercury porosimeter. Currently BET is being used extensively for determining the pore diameter and its surface area. FTIR does chemical analysis and NMR.to understand the functional changes or molecular structure of the polymers used and any changes after blending and also to identify the presence of the polymers, drug, fillers used in the nanofiber mat by identifying their chemical nature. The structural morphology by XRD to know the crystalline or amorphous nature of the polymers before and after fabrication of nanofibers. Physical properties, include hydrophilicity, thermal, biodegradation of the nanofiber network. The permeation of gases can be analysed based on the porosity and hydrophilicity can be determined by contact angle measurements and swelling the cross-linked or stable nanofibers in their respective solvent media to analyse their ability to absorb the solvent. The thermal stability using DSC to understand the glass transition, crystalline and melting temperatures of the polymers and filler used in the nanofiber network. The decomposition temperature of the nanofiber mat is analysed using thermogravimetric analysis. Decomposition temperature may increase or decrease of the polymers depending upon the changes that occur before and after the fabrication of nanofibers. Biodegradation studies are done to understand the ability of the nanofibers to degrade before and after the fabrication of nanofibers. This information provides biosafety of the nanofiber mat after application. Mechanical properties of the nanofibers are studied using DMA or UTM (universal tensile machine) for determining the mechanical strength of the nanofiber network. Nanofibers being randomly woven; it may be challenging to analyse the Tensile property. However, the aligned nanofiber networks it is feasible to determine.

The nanofibers used for biomedical application should be biocompatible with the living systems, so cell culture studies, are done using various cell lines as per the requirement (*in vitro*). After learning the per cent of cell viability the *in vivo* studies can be done using the animal models as per the requirement. The drug release from

the nanofiber mat depends on the swelling ratio of the nanofiber mat when in contact with the media. The higher the swelling in media, the faster the rate of drug release from the nanofibers. So, based on the requirement, the swelling ratio can be manipulated by selective screening of the polymers. Generally, rate of swelling and percent of swelling are determined to understand the mechanism of release studies.

1.5 Applications of electrospun nanofibers in the biomedical field

1.5.1 Nanofibers in tissue engineering

Organ failure and loss of tissue is a common problem in the health care sector. Injuries resulting from accidents, drowning, falls or burns and violence from assault, self-inflicted violence or acts of war, kills more than 5 million people worldwide annually. A large proportion of people face injuries with temporary or either permanent disabilities. Based on the US statistics in 2019, about 113,000 patients are waiting for organ transplantation in their country. However, only 36,528 transplants were performed on each day, leaving at least 20 people to die while waiting for organ transplantation (Organ statics). Hence, tissue engineering is in demand to produce organs by in vitro methods to save the lives of the needy. As studied in the above sections, nano-scaffolds are considered unique and are more promising than bulk scaffold for the development scaffolds for regeneration of the organs. Three ways can do tissue engineering- autologous (cells obtained from the same individual), allogeneic (cells obtained from the same species) and xenogeneic (cells obtained from different species). Nanofibers scaffolds in tissue engineering can act like extracellular cellular matrix, providing advantages like better cell adhesion, no scar formation, having a high surface area to volume ratio, etc., hence can be used in tissue regeneration. For tissue engineering, mostly biodegradable and biocompatible polymers were used, and such polymer are biocompatible. Polymers that are biodegradable under the influence of enzymatic and hydrolytic activities have better cellular and cell proliferation environment, and spaces or holes created by the degraded fibers allow ECM (extracellular matrix) to infiltrate and provide nutrition for the proliferating cells[62]. Therefore, biodegradable and biocompatible polymers were utilized in tissue engineering [63, 64]. To fabricate nanofibers, biodegradable and biocompatible polymers of natural and synthetic origin are used, including

collagen, silk, gelatin, hyaluronic acid, PHBV Poly (3-hydroxybutyrate-co-3-hydroxyvalerate), PCL, PLA, etc. Polycaprolactone (PCL), with and without a coating of chitosan nanofibers has been studied for cartilage tissue engineering using peritoneal cells[65]. Scaffold of poly lactic-glycolic acid (PLGA)/gelatin randomly oriented nanofibers indicated that it can benefit bone regeneration [66]. Carbon nanotubes have been incorporated in multi-layered cellulose acetate nanofibers for tissue engineering to increase mechanical strength, fibroblast cells spreading, and proliferation compared with CS/ALG multilayer-assembled fibrous scaffolds[67]. Cardiac tissue regeneration can be done by using poly (L-lactic acid)-co-poly (ε-caprolactone) (PLACL), silk fibroin (SF) and aloe vera (AV). Cardiac expression of proteins myosin and connexin 43 was analyzed in the confocal microscope, and it was observed that PLACL/SF/AV is having better expression than PLACL nanofibers[68]. Surface functionalization of nanofibers can provide a better and more efficient system for tissue regeneration by increasing the mechanical, chemical and biological properties. Gelatin was functionalized by tyrosine protein and 1, 2, 3-triazole ring for cartilage regeneration. As gelatin is water soluble, gelatin nanofibers was cross-linked by glutaraldehyde and 1-ethyl-3-(3-dimethylaminopropyl) carbodiimide (EDC)/N-hydroxysulfosuccinimide (NHS). Gelatin functionalized nanofibers showed good cell viability in chondrocytes cell and *in-vitro* studies also showed the nanofibers provided better cell growth and attachment. The results showed that cross-linked gelatin has potential for use in cartilage engineering[69]. Amin sadeghi and co-author also prepared gelatin, PVA and chondroitin sulfate nanofibers for skin tissue engineering. They prepared nanofibers by using water as a solvent. They have studied the influence of chondroitin sulfate on mechanical, physical and biological properties. Cell proliferation and MTT assay confirmed that the chondronitin sulfate help to attach human dermal fibroblast (HDF) cells and cell proliferation on the nanofibers[70].The process of tissue engineering is shown in (Fig.4).
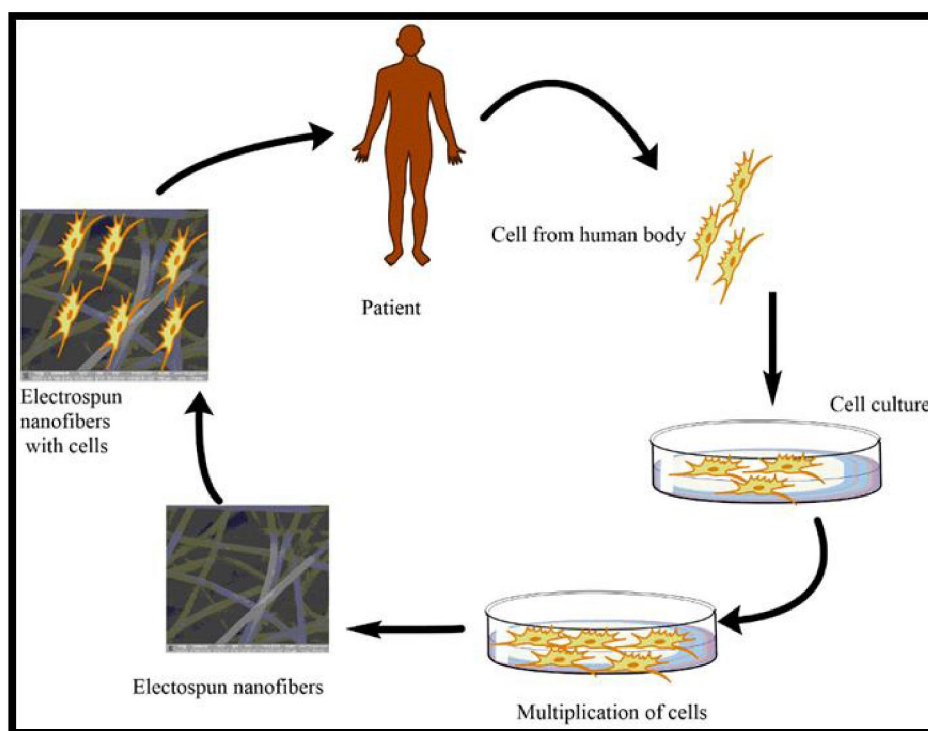
Figure 1.7 Tissue engineering process

1.5.2 Nanofibers as a drug delivery system

In the biomedical field, encapsulation of drug in a polymeric matrix to achieve the highest efficiency is a big task for the investigators working in drug delivery. Nanotechnology is being used for minimizing the drug concentration. Accordingly, there are several nanomaterials developed for drug delivery applications, such as nanoparticles, nanorods, carbon nanotubes, inorganic magnetic nanoparticles, micelles, nanoemulsions, dendrimers and nanofibers. Currently, the nanofibers developed by the electrospinning method are being well studied for drug delivery application, as this method is simple, easy and economically viable to produce in large quantities with drugs for suitable application[62]. Therefore, the pharmaceutical sector is now looking towards nanofibers as an advanced drug delivery system for various applications in the biomedical field. Nanofibers can carry both the hydrophilic and hydrophobic drugs that can be loaded on nanofibers by physical and chemical methods. Nanofibers have been used to deliver drugs through oral, buccal, or transdermal[71-73]. Traditional cancer treatment requires excessive use of drugs which causes toxicity to healthy cells, so nanofibers may be considered as an

excellent medium for delivering the drug because the production is cost-effective, being nano, the loading efficiency will be more and more functional at low concentrations with higher efficacy. For instance, Mohammad Norouz et. al. (2019) fabricated PLGA nanofbers containing salinomycin, an antibiotic drug, but they had demonstrated as an anti-cancer drug. The biodegradable PLGA nanofibers showed a sustained release of the salinomycin for at least 14 days. Cytotoxicity of the PLGA loaded salinomycin was evaluated on human glioblastoma U-251 cells, and more than 50% of the treated cells showed apoptosis in 48 h[74]. Recently, Eri Niiyama et al. (2018) developed a smart system to kill the lung adenocarcinoma cells using nanofibers containing both magnetic nanoparticles (MNP) as well as paclitaxel (PTX). Nanofibers loaded with magnetic nanoparticles were activated by exposure to the magnetic field. There *in-vitro* anti-tumour studies demonstrated that both MNP- and PTX-loaded nanofibers killed about 66% of cells, whereas only PTX-loaded nanofibers killed about 43% of cells[75]. **Table 1.2** shows the nanofibers developed from various polymers to deliver drugs for various applications.

Table 1.2. Nanofibers as drug delivery system

Sr.no	Polymer	Active molecule	Applications	Reference
1	PCL/PEO	Doxycycline	Tetracycline antibiotic	[76]
2	Eudragit L100-55,	Methylprednisolone	Corticosteroid	[77]
3	Polyvinylpyrrolidone (PVP) K90 or Polycaprolactone (PCL)	Quercetin or tamoxifen citrate	Breast cancer	[78]
4	PCL	Metronidazole and ciprofloxacin hydrochloride	Periodontal diseases	[79]
5	Polyethylene oxide and carboxymethyl cellulose	Progesterone	Preventing preterm birth	[80]
6	PLGA	Vaccinia virus	Colon cancer	[81]
7	PCL	, Plant polyphenol	Human cancer	[82]

8	(PVA/CS) hybrid nanofibers	Gold nanorods /DOX	Ovary cancer cells/Cell imaging	[83]
9	PEO/PDLLA	Rapamycin	Glioblastoma	[84]
10	Polycaprolactone	Resveratrol	Periodontal disease	[85]

1.5.3   Nanofibers for skin cancer treatment

Skin cancer is the most common malignancy in humans, with over a million cases detected every year. It was expected that around 2 to 3 million non-melanoma skin cancers and 132,000 melanoma skin cancers occur globally every year[86]. The global market for non-melanoma and melanoma skin cancer treatment is projected to grow by $ 705 million and $12.4 billion, respectively, by 2025. Among skin carcinomas, two types are identified; (i) basal cell carcinoma (BCC), whose malignity remains strictly local, and (ii) squamous cell carcinoma (SCC), is a result of uncontrolled growth of abnormal cells in the skin and has potential to metastasize to the other parts of the body. It is also known that SCC is typically developed from pre-cancerous lesions, such as actinic keratosis (AK), and *in situ* carcinoma caused by damage from UV rays, showing focal areas of abnormal keratinocyte proliferation and differentiation combined with stromal alterations [87]. If SCC is left untreated, up to 10 % of AKs develop into SCC, and in rare cases, AKs may also turn into BCC. AK and SCC are usually treated by invasive approaches (e.g. surgical curettage, electrodesiccation, Mohs surgery, cryosurgery), but radiotherapy and photodynamic therapy (71-87 %) are mostly employed. Imiquimod (82-90 %), an acute pro-inflammatory agent with serious side effects, is usually employed as a topical cream (5-fluorouracil is available around 80 %), in particular when surgery is not recommended [88]. Nanomaterials being more efficient over bulk materials, Malathi Sampath et al. (2014) fabricated biodegradable PLGA copolymer loaded with curcumin by melt polycondensation method. PLGA-curcumin nanofibers demonstrated the efficacy on skin cancer (A431) cell line and showed the capability of releasing the drug for a prolonged period of time[89].

Similarly, Gayatri Patel et al. (2019) developed nanofibers by blending chitosan with PVA loaded with 5-fluorouracil. The developed nanofibers showed a decrease in

cell viability of cancer cells by 50 % within 24 h. Results suggested that such a system can be a promising drug delivery system for BCC skin cancer[90]. Molybdenum nanoparticles embedded on PCL nanofibers were considered good candidates for targeted skin cancer treatment because these nanofibers, when experimented with zebrafish, showed reduced progression by cancer cells within 14 days[91]. Hence, the literature suggests that nanofiber can be a promising tool for skin cancer treatment.

1.5.4 Nanofibers as biosensor

The device which is used for detecting biological samples like biomolecule, a biological or a microorganism is known as a biosensor. Biosensor work by three significant parts; first a component that helps to find an analyte and produce a signal, second a signal transducer and third a reader device[92]. The development of new horizons as opened for biosensors after nanotechnology came in existence as it's enhanced the specificity, sensitivity detection time and low cost. The biosensor development in nanostructure may vary in size from 1 nm to 100nm; the shape may also vary depending on systems like nanoparticles, nanotubes, nanowires, nanorods, nanosheets, nanofibers, etc. There is growing interest in nanofibers from all of this nanostructure system from the past many decades. The electrospinning techniques that have been utilised in the production of nanofibers have been vigorously used in the production of nanofibers due to its structural characteristic like large surface to area, high surface modification, high reactivity can be done, increase the biocompatibility of biosensor as biocompatible polymer were used. The development of a biosensor with high sensitivity is necessary to enhance the detection of signals. The surface modification of nanofibers can be done by ways such as adsorption, entrapment in a membrane, cross-linking, and covalent bonding. However, mostly adsorption method is preferred due to ease and versatility for surface modification, but leakage is still an significant issue hence covalent strategies were used for avoiding leaching issues. Jing yun huang et al. 2014 reported that ZnO loaded nanofibers were prepared by immobilizing the glucose oxidase for biosensing glucose. The glucose oxidase loaded nanofibers have a high sensitivity (69 $\mu A/mMcm^{-2}$), fast response (3s) and low detection limit (10 μM).They reported that

the prepared system could be produced repeatedly and in a controlled manner for glucose estimation[93]. Noora Isoaho et al. 2018 have fabricated Pt-grown carbon nanofiber to detect enzymatic glutamate biosensors and reported its biocompatibility[94]. A significant amount of growth has been observed in nanofibers for biosensing applications but still a long way to go. The improvement is needed to control the diameter of nanofibers, transducer, and immobilization of biomolecule[95].

1.5.5   Magnetic nanofibers as drug delivery system

The magnetic nanoparticles were initially being used for drug delivery in the 1980s, but only in the last several decades are the research on magnetic nanoparticles catching popularity and becoming popular due to their attractive properties in cancer therapy and imaging. In the pharmaceutical industry, stimulating and controlling the release of bioactive agents to specific sites of action is a significant priority. This is something that the magnetic component can handle. Superparamagnetic nanoparticles are incorporated in polymeric nanoparticles, functionalized with drug carriers, embedded in hydrogel gels, nanofibers, films, liposomes, and protein macromolecules to explore such biomedical systems application. Because of the significance of magnetic nanomaterial, this is widely employed in cancer diagnosis and therapy, as well as cardiovascular illnesses. Many studies have found that adding magnetic nanoparticles has triggered release to enhance the *in vitro* drug release rate or behaviour. The introduction of an external magnetic field can push magnetic nanoparticles to a specific action region (**Figs. 1.8 and 1.9**) because it offers non-invasive methods and regulates the release of drugs with the application of an external magnetic field. Additionally, magnetic nanoparticles are simple to suspend in organic solvents and to load in polymers, thus, it can lead to a significant advancement in disease therapy.

Polymeric nanofibers are well known for a wide range of biological applications, such as wound healing, tissue engineering, and drug delivery. Many reports have been published based nanofibers immobilized with magnetic nanoparticles for controlled and targeted delivery of drugs. For example, in a recently published article, the magnetic nanoparticles were incorporated in two cellulose

derivatives, dehydroxypropyl methylcellulose phthalate (HPMCP) and cellulose acetate (CA), in which they have used indomethacin and aspirin as model drugs. They studied drug release in intestinal media and controlled drug release under the guidance of an external magnetic field[96]. In another study, citric acid-coated magnetic nanoparticles were mixed into polyvinyl alcohol (PVA) and subjected to infusion gyration to produce composite fibres with 100 to 300 nm diameters. Under the influence of an external magnetic field, the bioactive agent acetaminophen, that was immobilised in magnetic nanofibers was studied for controlled release[97].
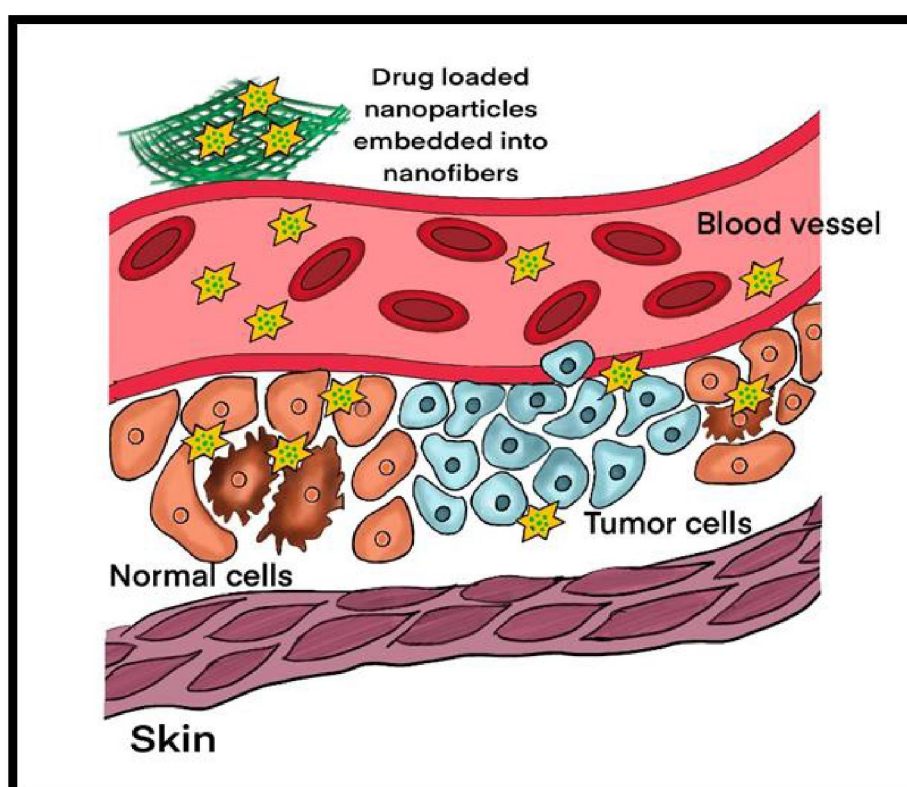
Figure 1.8 Effect of drug loaded nanofibers on normal cells and cancer cells
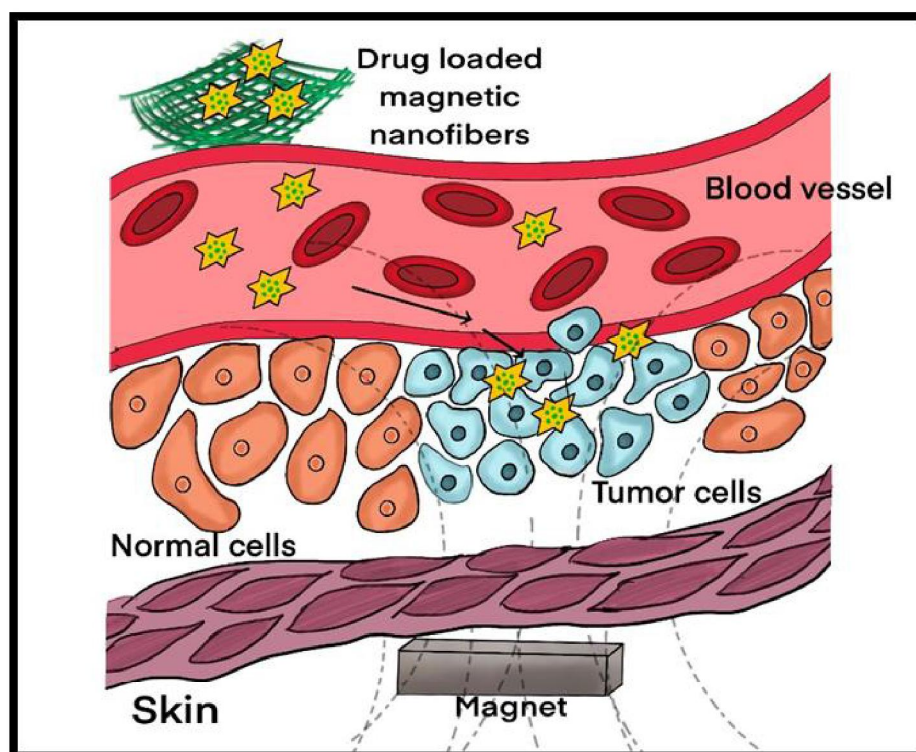
Figure 1.9 Effect of magnetic drug-loaded nanofibers on normal cells and cancer cells

1.6   Conclusion and future perspective

The electrospinning method in the biomedical field has evolved due to its ease of use, adaptability, and flexibility in controlling the fiber diameter, high porosity and high surface-area-to-volume ratio, high mechanical properties. Electrospun nanofibers are considered prominent materials in biomedical fields as they are biocompatible and biodegradable. The features of nanofibers like high surface-to-volume ratio, high mechanical strength, and enhanced porosity make them ideal for tissue engineering applications, scaffolds, controlled drug delivery, etc.

Producing the nanofibers at a lab scale is easy, but if we think about commercial or industrial scale, still there is a long way to go. First of all, we have to build a robust method capable of producing high-quality nanofibers on a large scale. We are still fabricating the nanofibers by establishing methods. The current electrospinning method suffers from various drawbacks: low throughput, specialized instrumentation, high voltage power supply, etc. Moreover, the process is time-consuming, needs

conducting targets, and obtaining uniform nanofibers is still a challenge. The reported nanofibers still face drawbacks like low mechanical strength due to their low crystallinity and random orientation. So it is essential to overcome such drawbacks of current electrospinning fabrication methods. The throughput of nanofibers can be increased by multi-needle and needless electrospinning, which can be further developed. Increasing the throughput of nanofibers will reduce the time to get the desired quantity. Secondly, the desired mechanical strength of nanofibers can be attained or can be manipulated by changing or selecting suitable raw materials or can be coupled with two or more materials. There are various methods that can be used to increase nanofibers' physicochemical properties, like vapor pressure of solvent (wielding the cross area of nanofibers), heat treatment, plasma treatment, chemical grafting, and by controlling the arrangement of nanofibers. Although many researchers have investigated the nanofibers in an animal model and cell cultures, most of the studies are still limited to qualitative proof-of-concept investigations of the cytocompatibility of the nanofibrous scaffolds in terms of cellular adhesion, proliferation, and differentiation. To make them suitable for human use, *in vivo* studies in animal models, if possible on human and clinical trials, will prove useful for evaluating the effect and significance of the nanofiber system in healthcare applications.

Finally, in conclusion, nanofibers technology can significantly impact biomedical applications. Nanofibers technology can further be improved for commercial applications, and in the future, we hope that nanofibers can be fabricated on a large scale.

1.7 References

[1] M.E. Pearce, J.B. Melanko, A.K. Salem, Multifunctional nanorods for biomedical applications, Pharmaceutical research 24(12) (2007) 2335-2352.

[2] R. Gopikrishnan, K. Zhang, P. Ravichandran, S. Baluchamy, V. Ramesh, S. Biradar, P. Ramesh, J. Pradhan, J.C. Hall, A.K. Pradhan, Synthesis, characterization and biocompatibility studies of zinc oxide (ZnO) nanorods for biomedical application, Nano-Micro Letters 2(1) (2010) 31-36.

[3] Z. Ma, H. Xia, Y. Liu, B. Liu, W. Chen, Y. Zhao, Applications of gold nanorods in biomedical imaging and related fields, Chinese Science Bulletin 58(21) (2013) 2530-2536.

[4] V.K. Mishra, B.N. Bhattacharjee, O. Parkash, D. Kumar, S.B. Rai, Mg-doped hydroxyapatite nanoplates for biomedical applications: a surfactant assisted microwave synthesis and spectroscopic investigations, Journal of Alloys and Compounds 614 (2014) 283-288.

[5] A. Ray, R. Kopelman, B. Chon, K. Briggman, J. Hwang, Scattering based hyperspectral imaging of plasmonic nanoplate clusters towards biomedical applications, Journal of biophotonics 9(7) (2016) 721-729.

[6] M. Asadian-Birjand, A. Sousa-Herves, D. Steinhilber, J.C. Cuggino, M. Calderon, Functional nanogels for biomedical applications, Current medicinal chemistry 19(29) (2012) 5029-5043.

[7] N.S. Rejinold, A. Nair, M. Sabitha, K.P. Chennazhi, H. Tamura, S.V. Nair, R. Jayakumar, Synthesis, characterization and in vitro cytocompatibility studies of chitin nanogels for biomedical applications, Carbohydrate polymers 87(1) (2012) 943-949.

[8] A.K. Gupta, M. Gupta, Synthesis and surface engineering of iron oxide nanoparticles for biomedical applications, biomaterials 26(18) (2005) 3995-4021.

[9] Z. Li, J.C. Barnes, A. Bosoy, J.F. Stoddart, J.I. Zink, Mesoporous silica nanoparticles in biomedical applications, Chemical Society Reviews 41(7) (2012) 2590-2605.

[10] D.K. Sarker, Engineering of nanoemulsions for drug delivery, Current drug delivery 2(4) (2005) 297-310.

[11] R. Jayakumar, M. Prabaharan, S.V. Nair, H. Tamura, Novel chitin and chitosan nanofibers in biomedical applications, Biotechnology advances 28(1) (2010) 142-150.

[12] K. Morikawa, M. Green, M. Naraghi, A Novel Approach for Melt Electrospinning of Polymer Fibers, Procedia Manufacturing 26 (2018) 205-208.

[13] H. Zhang, Q. Zhen, Y. Liu, R. Liu, Y. Zhang, One-step melt blowing process for PP/PEG micro-nanofiber filters with branch networks, Results in Physics 12 (2019) 1421-1428.

[14] C. Drosou, M. Krokida, C.G. Biliaderis, Composite pullulan-whey protein nanofibers made by electrospinning: Impact of process parameters on fiber morphology and physical properties, Food Hydrocolloids 77 (2018) 726-735.

[15] H. Li, Y. Ke, Y. Hu, Polymer nanofibers prepared by template melt extrusion, Journal of applied polymer science 99(3) (2006) 1018-1023.

[16] M. Ikegame, K. Tajima, T. Aida, Template synthesis of polypyrrole nanofibers insulated within one-dimensional silicate channels: hexagonal versus lamellar for recombination of polarons into bipolarons, Angewandte Chemie International Edition 42(19) (2003) 2154-2157.

[17] P.X. Ma, R. Zhang, Synthetic nano-scale fibrous extracellular matrix, Journal of Biomedical Materials Research: An Official Journal of The Society for Biomaterials, The Japanese Society for Biomaterials, and The Australian Society for Biomaterials 46(1) (1999) 60-72.

[18] Z. Yang, B. Xu, Supramolecular hydrogels based on biofunctional nanofibers of self-assembled small molecules, Journal of Materials Chemistry 17(23) (2007) 2385-2393.

[19] X. Feng, G. Yang, Q. Xu, W. Hou, J.J. Zhu, Self-Assembly of Polyaniline/Au Composites: From Nanotubes to Nanofibers, Macromolecular rapid communications 27(1) (2006) 31-36.

[20] Y. Hong, R.L. Legge, S. Zhang, P. Chen, Effect of amino acid sequence and pH on nanofiber formation of self-assembling peptides EAK16-II and EAK16-IV, Biomacromolecules 4(5) (2003) 1433-1442.

[21] W. Gilbert, E. Wright, De magnete, magneticisque corporibus, et de magno magnete tellure: physiologia noua, plurimis & argumentis, & experimentis demonstrata, excudebat Short1967.

[22] G.I. Taylor, Disintegration of water drops in an electric field, Proceedings of the Royal Society of London. Series A. Mathematical and Physical Sciences 280(1382) (1964) 383-397.

[23] L. Rayleigh, XX. On the equilibrium of liquid conducting masses charged with electricity, The London, Edinburgh, and Dublin Philosophical Magazine and Journal of Science 14(87) (1882) 184-186.

[24] C.V. Boys, On the production, properties, and some suggested uses of the finest threads, Proceedings of the Physical Society of London 9(1) (1887) 8.

[25] K. Ishida, T. Nishizawa, Effect of alloying elements on stability of epsilon iron, Transactions of the Japan Institute of Metals 15(3) (1974) 225-231.

[26] N. Tucker, J.J. Stanger, M.P. Staiger, H. Razzaq, K. Hofman, The history of the science and technology of electrospinning from 1600 to 1995, Journal of engineered fibers and fabrics 7(2_suppl) (2012) 155892501200702S10.

[27] B.M. Abunahel, N.Z.N. Azman, M. Jamil, Effect of Needle Diameter on the Morphological Structure of Electrospun n-Bi2O3/Epoxy-PVA Nanofiber Mats, International Journal of Chemical and Materials Engineering 12(6) (2018) 296-299.

[28] S. Thenmozhi, N. Dharmaraj, K. Kadirvelu, H.Y. Kim, Electrospun nanofibers: new generation materials for advanced applications, Materials Science and Engineering: B 217 (2017) 36-48.

[29] R. Bhattarai, R. Bachu, S. Boddu, S. Bhaduri, Biomedical applications of electrospun nanofibers: Drug and nanoparticle delivery, Pharmaceutics 11(1) (2019) 5.

[30] R. Nayak, R. Padhye, L. Arnold, 2 - Melt-electrospinning of nanofibers, in: M. Afshari (Ed.), Electrospun Nanofibers, Woodhead Publishing2017, pp. 11-40.

[31] L. Larrondo, R. St. John Manley, Electrostatic fiber spinning from polymer melts. I. Experimental observations on fiber formation and properties, Journal of Polymer Science: Polymer Physics Edition 19(6) (1981) 909-920.

[32] S. Lee, S. Kay Obendorf, Developing protective textile materials as barriers to liquid penetration using melt-electrospinning, Journal of Applied Polymer Science 102(4) (2006) 3430-3437.

[33] N. Ogata, N. Shimada, S. Yamaguchi, K. Nakane, T. Ogihara, Melt-electrospinning of poly (ethylene terephthalate) and polyalirate, Journal of Applied Polymer Science 105(3) (2007) 1127-1132.

[34] H. Zhou, T.B. Green, Y.L. Joo, The thermal effects on electrospinning of polylactic acid melts, Polymer 47(21) (2006) 7497-7505.

[35] D. Cho, E. Zhmayev, Y.L. Joo, Structural studies of electrospun nylon 6 fibers from solution and melt, Polymer 52(20) (2011) 4600-4609.

[36] F. Li, Y. Zhao, S. Wang, D. Han, L. Jiang, Y. Song, Thermochromic core–shell nanofibers fabricated by melt coaxial electrospinning, Journal of applied polymer science 112(1) (2009) 269-274.

[37] N. Detta, T.D. Brown, F.K. Edin, K. Albrecht, F. Chiellini, E. Chiellini, P.D. Dalton, D.W. Hutmacher, Melt electrospinning of polycaprolactone and its blends with poly (ethylene glycol), Polymer international 59(11) (2010) 1558-1562.

[38] J. Doshi, D.H. Reneker, Electrospinning process and applications of electrospun fibers, Journal of electrostatics 35(2-3) (1995) 151-160.

[39] S. Megelski, J.S. Stephens, D.B. Chase, J.F. Rabolt, Micro-and nanostructured surface morphology on electrospun polymer fibers, Macromolecules 35(22) (2002) 8456-8466.

[40] J.M. Deitzel, J.D. Kleinmeyer, J.K. Hirvonen, N.C.B. Tan, Controlled deposition of electrospun poly (ethylene oxide) fibers, Polymer 42(19) (2001) 8163-8170.

[41] C. Zhang, X. Yuan, L. Wu, Y. Han, J. Sheng, Study on morphology of electrospun poly (vinyl alcohol) mats, European polymer journal 41(3) (2005) 423-432.

[42] K.P. Matabola, R.M. Moutloali, The influence of electrospinning parameters on the morphology and diameter of poly (vinyledene fluoride) nanofibers-effect of sodium chloride, Journal of Materials Science 48(16) (2013) 5475-5482.

[43] P.K. Baumgarten, Electrostatic spinning of acrylic microfibers, Journal of colloid and interface science 36(1) (1971) 71-79.

[44] T. Wang, S. Kumar, Electrospinning of polyacrylonitrile nanofibers, Journal of applied polymer science 102(2) (2006) 1023-1029.

[45] N. Okutan, P. Terzi, F. Altay, Affecting parameters on electrospinning process and characterization of electrospun gelatin nanofibers, Food Hydrocolloids 39 (2014) 19-26.

[46] V. Pillay, C. Dott, Y.E. Choonara, C. Tyagi, L. Tomar, P. Kumar, L.C. du Toit, V.M.K. Ndesendo, A review of the effect of processing variables on the fabrication of electrospun nanofibers for drug delivery applications, Journal of Nanomaterials 2013 (2013).

[47] S.S. Ojha, M. Afshari, R. Kotek, R.E. Gorga, Morphology of electrospun nylon-6 nanofibers as a function of molecular weight and processing parameters, Journal of applied polymer science 108(1) (2008) 308-319.

[48] S.-H. Tan, R. Inai, M. Kotaki, S. Ramakrishna, Systematic parameter study for ultra-fine fiber fabrication via electrospinning process, Polymer 46(16) (2005) 6128-6134.

[49] A. Abutaleb, D. Lolla, A. Aljuhani, H. Shin, J. Rajala, G. Chase, Effects of surfactants on the morphology and properties of electrospun polyetherimide fibers, Fibers 5(3) (2017) 33.

[50] J.-Y. Zheng, M.-F. Zhuang, Z.-J. Yu, G.-F. Zheng, Y. Zhao, H. Wang, D.-H. Sun, The effect of surfactants on the diameter and morphology of electrospun ultrafine nanofiber, Journal of Nanomaterials 2014 (2014) 8.

[51] N.A.M. Barakat, M.A. Kanjwal, F.A. Sheikh, H.Y. Kim, Spider-net within the N6, PVA and PU electrospun nanofiber mats using salt addition: Novel strategy in the electrospinning process, Polymer 50(18) (2009) 4389-4396.

[52] M. El-Newehy, Electrospinning; Historical Background, Fabrication and Applications, (2017).

[53] D.P. Bhattarai, L.E. Aguilar, C.H. Park, C.S. Kim, A review on properties of natural and synthetic based electrospun fibrous materials for bone tissue engineering, Membranes 8(3) (2018) 62.

[54] A. Haider, S. Haider, I.-K. Kang, A comprehensive review summarizing the effect of electrospinning parameters and potential applications of nanofibers in biomedical and biotechnology, Arabian Journal of Chemistry 11(8) (2018) 1165-1188.

[55] S. De Vrieze, T. Van Camp, A. Nelvig, B. Hagström, P. Westbroek, K. De Clerck, The effect of temperature and humidity on electrospinning, Journal of materials science 44(5) (2009) 1357-1362.

[56] R. Fryczkowski, M. Gorczowska, B. Fryczkowska, J. Janicki, The effect of solvent on the properties of nanofibres obtained by electrospinning from a mixture of poly (3-hydroxybutyrate) and polyaniline, Synthetic Metals 166 (2013) 14-21.

[57] S. Koombhongse, W. Liu, D.H. Reneker, Flat polymer ribbons and other shapes by electrospinning, Journal of Polymer Science Part B: Polymer Physics 39(21) (2001) 2598-2606.

[58] Y. Cheng, H. Cheng, C. Jiang, X. Qiu, K. Wang, W. Huan, A. Yuan, J. Wu, Y. Hu, Perfluorocarbon nanoparticles enhance reactive oxygen levels and tumour growth inhibition in photodynamic therapy, Nature communications 6 (2015) 8785.

[59] R. RoÅ¡ic, P. Kocbek, J. Pelipenko, J. Kristl, S.a. Baumgartner, Nanofibers and their biomedical use, Acta pharmaceutica 63(3) 295-304.

[60] J. Pelipenko, J. Kristl, B. Janković, S. Baumgartner, P. Kocbek, The impact of relative humidity during electrospinning on the morphology and mechanical properties of nanofibers, International journal of pharmaceutics 456(1) (2013) 125-134.

[61] J.H. Park, M.R. Karim, I.K. Kim, I.W. Cheong, J.W. Kim, D.G. Bae, J.W. Cho, J.H. Yeum, Electrospinning fabrication and characterization of poly (vinyl alcohol)/montmorillonite/silver hybrid nanofibers for antibacterial applications, Colloid and Polymer Science 288(1) (2010) 115.

[62] N. Khan, Applications of electrospun nanofibers in the biomedical field, SURG Journal 5(2) (2012) 63-73.

[63] W.-J. Li, J.A. Cooper Jr, R.L. Mauck, R.S. Tuan, Fabrication and characterization of six electrospun poly (α-hydroxy ester)-based fibrous scaffolds for tissue engineering applications, Acta biomaterialia 2(4) (2006) 377-385.

[64] P.A. Walker, K.R. Aroom, F. Jimenez, S.K. Shah, M.T. Harting, B.S. Gill, C.S. Cox, Advances in progenitor cell therapy using scaffolding constructs for central nervous system injury, Stem Cell Reviews and Reports 5(3) (2009) 283-300.

[65] S.H. Ku, C.B. Park, Human endothelial cell growth on mussel-inspired nanofiber scaffold for vascular tissue engineering, Biomaterials 31(36) (2010) 9431-9437.

[66] Z.X. Meng, Y.S. Wang, C. Ma, W. Zheng, L. Li, Y.F. Zheng, Electrospinning of PLGA/gelatin randomly-oriented and aligned nanofibers as potential scaffold in tissue engineering, Materials Science and Engineering: C 30(8) (2010) 1204-1210.

[67] Y. Luo, S. Wang, M. Shen, R. Qi, Y. Fang, R. Guo, H. Cai, X. Cao, H. Tomás, M. Zhu, Carbon nanotube-incorporated multilayered cellulose acetate nanofibers for tissue engineering applications, Carbohydrate polymers 91(1) (2013) 419-427.

[68] V. Bhaarathy, J. Venugopal, C. Gandhimathi, N. Ponpandian, D. Mangalaraj, S. Ramakrishna, Biologically improved nanofibrous scaffolds for cardiac tissue engineering, Materials Science and Engineering: C 44 (2014) 268-277.

[69] M. Agheb, M. Dinari, M. Rafienia, H. Salehi, Novel electrospun nanofibers of modified gelatin-tyrosine in cartilage tissue engineering, Materials Science and Engineering: C 71 (2017) 240-251.

[70] A. Sadeghi, M. Zandi, M. Pezeshki-Modaress, S. Rajabi, Tough, hybrid chondroitin sulfate nanofibers as a promising scaffold for skin tissue engineering, International Journal of Biological Macromolecules (2019).

[71] H.S. Sofi, A. Abdal-Hay, S. Ivanovski, Y.S. Zhang, F.A. Sheikh, Electrospun nanofibers for the delivery of active drugs through nasal, oral and vaginal mucosa: Current status and future perspectives, Materials Science and Engineering: C 111 (2020) 110756.

[72] P.H.L. Tran, W. Duan, T.T.D. Tran, Recent developments of nanoparticle-delivered dosage forms for buccal delivery, International journal of pharmaceutics 571 (2019) 118697.

[73] M. Joshi, B.S. Butola, K. Saha, Advances in topical drug delivery system: Micro to nanofibrous structures, Journal of Nanoscience and Nanotechnology 14(1) (2014) 853-867.

[74] M. Norouzi, Z. Abdali, S. Liu, D.W. Miller, Salinomycin-loaded Nanofibers for Glioblastoma Therapy, Scientific reports 8(1) (2018) 9377.

[75] E. Niiyama, K. Uto, C. Lee, K. Sakura, M. Ebara, Alternating magnetic field-triggered switchable nanofiber mesh for cancer thermo-chemotherapy, Polymers 10(9) (2018) 1018.

[76] Ş.M. Eskitoros-Togay, Y.E. Bulbul, S. Tort, F.D. Korkmaz, F. Acartürk, N. Dilsiz, Fabrication of doxycycline-loaded electrospun PCL/PEO membranes for a potential drug delivery system, International journal of pharmaceutics (2019).

[77] Y. Turanlı, S. Tort, F. Acartürk, Development and characterization of methylprednisolone loaded delayed release nanofibers, Journal of Drug Delivery Science and Technology 49 (2019) 58-65.

[78] J.-J. Li, Y.-Y. Yang, D.-G. Yu, Q. Du, X.-L. Yang, Fast dissolving drug delivery membrane based on the ultra-thin shell of electrospun core-shell nanofibers, European Journal of Pharmaceutical Sciences 122 (2018) 195-204.

[79] Š. Zupančič, L. Preem, J. Kristl, M. Putrinš, T. Tenson, P. Kocbek, K. Kogermann, Impact of PCL nanofiber mat structural properties on hydrophilic drug release and antibacterial activity on periodontal pathogens, European Journal of Pharmaceutical Sciences 122 (2018) 347-358.

[80] F. Brako, B.T. Raimi-Abraham, S. Mahalingam, D.Q.M. Craig, M. Edirisinghe, The development of progesterone-loaded nanofibers using pressurized gyration: A novel approach to vaginal delivery for the prevention of pre-term birth, International journal of pharmaceutics 540(1-2) (2018) 31-39.

[81] N. Badrinath, Y.I. Jeong, H.Y. Woo, S.Y. Bang, C. Kim, J. Heo, D.H. Kang, S.Y. Yoo, Local delivery of a cancer-favoring oncolytic vaccinia virus via poly (lactic-co-glycolic acid) nanofiber for theranostic purposes, International journal of pharmaceutics 552(1-2) (2018) 437-442.

[82] Y.-J. Kim, M.R. Park, M.S. Kim, O.H. Kwon, Polyphenol-loaded polycaprolactone nanofibers for effective growth inhibition of human cancer cells, Materials Chemistry and Physics 133(2-3) (2012) 674-680.

[83] E. Yan, M. Cao, Y. Wang, X. Hao, S. Pei, J. Gao, Y. Wang, Z. Zhang, D. Zhang, Gold nanorods contained polyvinyl alcohol/chitosan nanofiber matrix for cell imaging and drug delivery, Materials Science and Engineering: C 58 (2016) 1090-1097.

[84] B. Wang, H. Li, Q. Yao, Y. Zhang, X. Zhu, T. Xia, J. Wang, G. Li, X. Li, S. Ni, Local in vitro delivery of rapamycin from electrospun PEO/PDLLA nanofibers for glioblastoma treatment, Biomedicine & Pharmacotherapy 83 (2016) 1345-1352.

[85] Š. Zupančič, S. Baumgartner, Z. Lavrič, M. Petelin, J. Kristl, Local delivery of resveratrol using polycaprolactone nanofibers for treatment of periodontal disease, Journal of drug delivery science and technology 30 (2015) 408-416.

[86] Cancer Facts & Figures

2018, American Cancer Society (2018).

[87] M.C.F. SimÃµes, J.J.S. Sousa, A. Pais, Skin cancer and new treatment perspectives: A review, Cancer letters 357(1) 8-42.

[88] E. Stockfleth, H. Kerl, T. Zwingers, C. Willers, Lowâ€dose 5â€fluorouracil in combination with salicylic acid as a new lesionâ€• directed option to treat topically

actinic keratoses: histological and clinical study results, British Journal of Dermatology 165(5) 1101-1108.

[89] M. Sampath, R. Lakra, P. Korrapati, B. Sengottuvelan, Curcumin loaded poly (lactic-co-glycolic) acid nanofiber for the treatment of carcinoma, Colloids and Surfaces B: Biointerfaces 117 (2014) 128-134.

[90] G. Patel, B.K.N. Yadav, Formulation, Characterization and In Vitro Cytotoxicity of 5-Fluorouracil Loaded Polymeric Electrospun Nanofibers for The Treatment of Skin Cancer, Recent patents on nanotechnology (2019).

[91] I. Janani, R. Lakra, M.S. Kiran, P.S. Korrapati, Selectivity and sensitivity of molybdenum oxide-polycaprolactone nanofiber composites on skin cancer: Preliminary in-vitro and in-vivo implications, Journal of Trace Elements in Medicine and Biology 49 (2018) 60-71.

[92] H. Stevenson, A. Bacon, K.M. Joseph, W.R.W. Gwandaru, A. Bhide, D. Sankhala, V.N. Dhamu, S. Prasad, A Rapid Response Electrochemical Biosensor for Detecting Thc In Saliva, Scientific reports 9(1) (2019) 1-11.

[93] J.Y. Huang, M.G. Zhao, Z.Z. Ye, Electrospun porous ZnO nanofibers for glucose biosensors, Trans Tech Publ, pp. 3-6.

[94] N. Isoaho, E. Peltola, S. Sainio, J. Koskinen, T. Laurila, Pt-grown carbon nanofibers for enzymatic glutamate biosensors and assessment of their biocompatibility, RSC advances 8(62) (2018) 35802-35812.

[95] E. Sapountzi, M. Braiek, J.-F. Chateaux, N. Jaffrezic-Renault, F. Lagarde, Recent advances in electrospun nanofiber interfaces for biosensing devices, Sensors 17(8) (2017) 1887.

[96] L. Wang, M. Wang, P.D. Topham, Y. Huang, Fabrication of magnetic drug-loaded polymeric composite nanofibres and their drug release characteristics, Rsc Advances 2(6) (2012) 2433-2438.

[97] A.S. Perera, S. Zhang, S. Homer-Vanniasinkam, M.-O. Coppens, M. Edirisinghe, Polymer–magnetic composite fibers for remote-controlled drug release, ACS applied materials & interfaces 10(18) (2018) 15524-15531.

CHAPTER 2

Objective and scope of work

Chapter 2

This chapter has enclosed the objectives and hypothesis of the four working chapters of the thesis.

2.1 Objective and scope of work

Nanofibers have emerged as a promising choice for drug delivery and tissue engineering in recent years due to their small size, ease of replication, capacity to resemble ECM (extracellular matrix), ease in loading bioactive agents, ability to permeate air, and biocompatibility[1, 2]. Self-assembly, phase separation, melt-blown technology, airbus spray, template synthesis, and electrospinning are some of the technologies that are being used for fabricating nanofibers[3-5]. Out of which, electrospinning is the preferred technology as it is simple and easy to use and has the capacity to produce continuous nanofibers in large quantities. Further, it is convenient to blend and manipulate polymers and active molecules as desired for the application. Electrospinning technology is used to fabricate nanofibers from synthetic and natural polymers[6, 7]. Natural polymers like gelatin, hyaluronic acid, chitosan, silk fibroin, and collagen and synthetic polymers like PLA (poly (lactic acid), PCL (polycaprolactone), PVP (polyvinyl pyrrolidone), PU (polyurethane), and many more are used to make nanofibers for biomedical applications[8-11]. PLA and PCL have recently gained popularity because they are mechanically strong, biocompatible, and biodegradability[12]. Nevertheless, they lack hydrophilicity, as both polymers are hydrophobic and as a result, cell interactions and proliferation is minimized[13]. Several attempts were made to improve the hydrophilicity of these polymers utilizing proteins like human serum albumin and bovine serum albumin[14-16]. In the present thesis, chapter 1, a new protein, egg albumen (EA) was investigated to improve hydrophilicity. Accordingly, we have fabricated and characterized electrospun PLA/PCL nanofibers with EA and studied its drug release property, cell proliferation and interactions so as to find its potential for tissue engineering applications.

For several decades, critical healthcare-acquired bacterial infections have been a problem, and a significant variety of synthetic antibacterial medications, either in

huge dosages or in combination with other treatments, are used to treat it. However, traditional natural bioactive molecules (curcumin, piperine, cumin, neem etc.) are also used for treating bacterial infection. Curcumin, a bioactive component of turmeric has been used in pharmaceutics and as well in food applications over the past two decades due to its antibacterial, anticancer, anti-inflammatory, antifungal, and antioxidant properties. Curcumin is hydrophobic in nature, so it is less bioavailable therefore, the properties are not well experienced for therapy. For this purpose, it is being derivatized or complexed for enhancing its bioavailability and efficacy. Accordingly, the derivatized curcumin, CDF (3, 4- difluorobenzylidene curcumin) which was developed and explored for anticancer study, however, the antibacterial property of the CDF was not studied[17]. It is imperative to study the antibacterial property of CDF to prove that the antibacterial property is sustained after derivatization of Cur so that the synergy of the CDF is sustained and efficacy to treat cancer shall improve. Accordingly, novel nanofiber formulations with and without CDF were designed and studied for their antibacterial and drug release properties to find their significance in treating infected tumours or wounds.

Advanced nanotechnology has long been seen as a potential drug delivery technique for cancer therapy. Numerous drug delivery systems have been investigated, including nanogels, nanoparticles, micelles, emulsions, nanofibers, and so on. However, there is always a need for advanced DDS (drug delivery system) to treat cancer more effectively. It is known that we are deficient in DDS with precise dose and controlled drug release regime that can bypass healthy cells and concentrate at the targeted site for improved therapy. To minimize the side-effects of anti-cancer drug, various targeted materials have been explored, including folic acid, biotin, interferon, magnetic nanoparticles, etc. Magnetic nanoparticles are widely inspected for targeted drug delivery, purification of cells, tissue engineering, MRI (magnetic resonance imaging), sensors etc., as magnetic nanoparticles can be driven to a desirable location under the influence of an external magnetic field for it to function. In this context, the development and evaluation of drug release kinetics of new nanofiber formulations immobilized with magnetic nanoparticles and cancer drugs under the influence of

magnetic-filed shall provide the knowledge to consider those for localized cancer therapy.

Chronic and traumatic wounds also contribute to significant challenges in drug delivery applications due to the emergence of antimicrobial resistance. To combat this obstacle, several formulations such as cream, bandages, lotion, ointment, and others have been employed to accelerate wound healing. Multiple drugs are added to the formulation to intensify the recovery and eliminate bacterial resistance. However, these formulations have certain drawbacks, such as improper dosage, repeated installation, scar formation, and time consumption. Hence, it is important to develop a cutting-edge system that allows quick healing, minimum scarring, and minimal application with maximum bacterial receptivity. As a possible solution, we have developed a novel blend of polymeric nanofiber that can accelerate wound closure, reduce scar formation, and overcome bacterial resistance by incorporating a dual drug within the nanofibers.

Hence, the present research was carried out with the following objectives:

- To design and develop various polymeric blends using environment-friendly synthetic and natural polymers.
- To fabricate non-woven nanofibers immobilized with bioactive agents as drug delivery systems
- To evaluate the physicochemical properties of the developed non-woven nanofibers by different characterization techniques,
- To demonstrate *in vitro* and *in vivo* studies such as drug release, anti-microbial, *in vitro* cytotoxicity and tissue regeneration studies.

2.2 References

[1] I. Behere, G. Ingavle, In vitro and in vivo advancement of multifunctional electrospun nanofiber scaffolds in wound healing applications: Innovative nanofiber designs, stem cell approaches, and future perspectives, Journal of Biomedical Materials Research Part A 110(2) (2022) 443-461.

[2] P. Kamble, B. Sadarani, A. Majumdar, S. Bhullar, Nanofiber based drug delivery systems for skin: A promising therapeutic approach, Journal of Drug Delivery Science and Technology 41 (2017) 124-133.

[3] T. Maruyama, W.K. Restu, Intracellular self-assembly of supramolecular gelators to selectively kill cells of interest, Polymer Journal 52(8) (2020) 883-889.

[4] A. Eatemadi, H. Daraee, N. Zarghami, H. Melat Yar, A. Akbarzadeh, Nanofiber: Synthesis and biomedical applications, Artificial cells, nanomedicine, and biotechnology 44(1) (2016) 111-121.

[5] A. Morie, T. Garg, A.K. Goyal, G. Rath, Nanofibers as novel drug carrier–an overview, Artificial cells, nanomedicine, and biotechnology 44(1) (2016) 135-143.

[6] M. Keshvardoostchokami, S.S. Majidi, P. Huo, R. Ramachandran, M. Chen, B. Liu, Electrospun nanofibers of natural and synthetic polymers as artificial extracellular matrix for tissue engineering, Nanomaterials 11(1) (2021) 21.

[7] M.S. Islam, B.C. Ang, A. Andriyana, A.M. Afifi, A review on fabrication of nanofibers via electrospinning and their applications, SN Applied Sciences 1(10) (2019) 1-16.

[8] A. Arun, P. Malrautu, A. Laha, S. Ramakrishna, Gelatin Nanofibers in Drug Delivery Systems and Tissue Engineering, Engineered Science 16 (2021) 71-81.

[9] K.C. Castro, M.G.N. Campos, L.H.I. Mei, Hyaluronic acid electrospinning: Challenges, applications in wound dressings and new perspectives, International Journal of Biological Macromolecules 173 (2021) 251-266.

[10] B. Banimohamad-Shotorbani, A. Rahmani Del Bakhshayesh, A. Mehdipour, S. Jarolmasjed, H. Shafaei, The efficiency of PCL/HAp electrospun nanofibers in bone regeneration: A review, Journal of medical engineering & technology 45(7) (2021) 511-531.

[11] M.J. Mochane, T.S. Motsoeneng, E.R. Sadiku, T.C. Mokhena, J.S. Sefadi, Morphology and properties of electrospun PCL and its composites for medical applications: A mini review, Applied Sciences 9(11) (2019) 2205.

[12] X. Gao, S. Han, R. Zhang, G. Liu, J. Wu, Progress in electrospun composite nanofibers: composition, performance and applications for tissue engineering, Journal of Materials Chemistry B 7(45) (2019) 7075-7089.

[13] O. Suwantong, Biomedical applications of electrospun polycaprolactone fiber mats, Polymers for Advanced Technologies 27(10) (2016) 1264-1273.

[14] R. Fang, E. Zhang, L. Xu, S. Wei, Electrospun PCL/PLA/HA based nanofibers as scaffold for osteoblast-like cells, Journal of nanoscience and nanotechnology 10(11) 7747-7751.

[15] N. Killi, R.A. Dhakare, A. Singam, M. Lokanadham, H. Chitikeshi, R.V.N. Gundloori, Design and fabrication of mechanically strong nano-matrices of linseed oil based polyesteramide blends, MedChemComm 7(12) 2299-2308.

[16] J. Hu, M.P. Prabhakaran, X. Ding, S. Ramakrishna, Emulsion electrospinning of polycaprolactone: influence of surfactant type towards the scaffold properties, Journal of Biomaterials Science, polymer edition 26(1) (2015) 57-75.

[17] P. Kesharwani, S. Banerjee, S. Padhye, F.H. Sarkar, A.K. Iyer, Hyaluronic acid engineered nanomicelles loaded with 3, 4-difluorobenzylidene curcumin for targeted killing of CD44+ stem-like pancreatic cancer cells, Biomacromolecules 16(9) (2015) 3042-3053.

CHAPTER 3

Development of hydrophilic PLA/PCL/EA nanofiber mat as a drug delivery system and study its properties for tissue regeneration
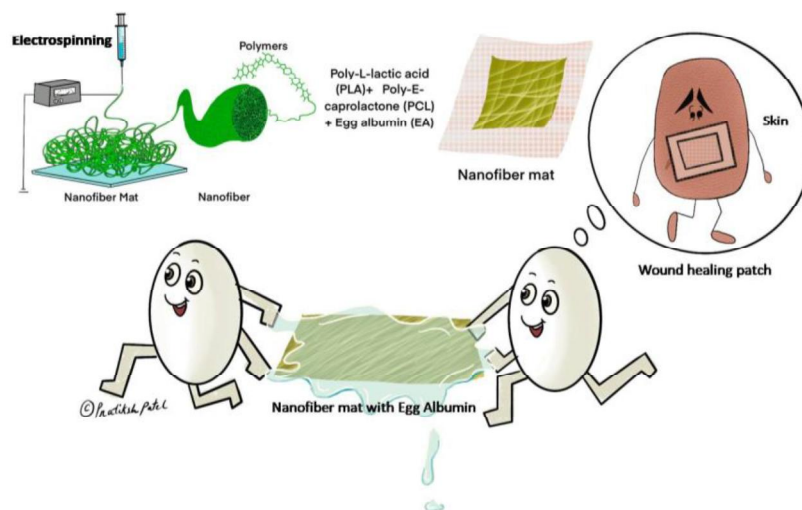
❖ **Chapter 3 has been published in the research article**

Chapter 3

In this chapter, we prepared non-woven nanofibers using the combination of hydrophobic polymers (PLA and PCL) and hydrophilic protein (Egg albumin) to enhance the rate of drug release and studied the cell interactions and proliferation to understand its applicability in tissue engineering.

3.1 Introduction

Hydrophobic polymers like poly-ε-caprolactone (PCL) and poly-L-lactic acid (PLA) can form good nanofibers by electrospinning techniques[1-7]. It is reported that the blends of PCL and PLA are being used for various biomedical applications such as scaffolds for bone, tissue regeneration, implants and sutures as they are biodegradable and biocompatible[8-18]. Several studies have reported that the blends of PCL and PLA complement each other[19, 20]. PLA is a highly stiff and rigid polymer with a high glass transition temperature. As a result, it was considered to be brittle and less favourable for biomedical applications. On the other end, PCL, being a soft and ductile polymer, with a low melting temperature and glass transition temperature. Hence, PCL was chosen to blend with PLA to improve the practical application[21]. However, their hydrophobic nature is considered a limiting factor in modulating desirable biological functions and cell interactions. Accordingly, it is evident that in biomedical applications, a hydrophilic polymer (natural or synthetic origin) with biocompatible properties is considered to be more favorable to interact with cells [22-24]. Hence, blending the PLA and PCL with the hydrophilic polymers of either natural or synthetic origin offers enhanced hydrophilicity without being modified chemically. Consequently, a wide variety of blends in the combination of PCL and PLA with hydrophilic polymers were explored for biomedical applications. For instance, the different kinds of polymers such as PEO (polyethylene oxide), poly(2-hydroxyethyl methacrylate), gelatin, collagen, bovine serum albumin (BSA) and, human serum albumin (HSA), etc were investigated by designing in various forms such as films, gels, nanomaterials to evaluate their potential for tissue engineering[25-27]. Recently, for tissue engineering application, mimic of extra cellular matrix (ECM) is being researched, comprising versatile non-woven nanofibrous structures

that support cell adhesion and bioactivity. The reported studies showed that the natural polymers, for example; proteins are inherently bioactive with better cell interacting domains (functional groups), facilitating cell adhesion, proliferation and cell differentiation. In line with these findings, protein blends with PCL, PLGA and PLA were fabricated in the form of nanofibers to mimic ECM[28-35]. However, the animal proteins such as collagen, gelatin, BSA, and HSA require to pass the stringent regulatory clearances and further, the cost to renew those in their pure form is exorbitant. Further, for the stability of these proteins, chemical cross-linkers may be required, which may lead to cell toxicity. Therefore, protein such as egg albumen (GRAS) is being explored as it is non-toxic, hydrophilic, easy to renew, cost-effective and forms a stable structure through physical crosslinks due to the presence of enough sulfhydryl groups to form disulfide linkages. In our earlier studies, we have developed biomaterials in bulk and nanoform using egg albumen blends[36]. The studies were encouraging, so the nano-biomaterials of PCL and PLA blends, which have limited biomedical application due to their hydrophobicity are being studied to improve hydrophilicity. Blending PCL and PLA with EA is anticipated to increase the hydrophilicity of the nano-biomaterial, and as explained above, the EA being a protein is inherently bioactive and is suggested to favour cell viability, cell adhesion and proliferation.

The electrospinning technique is a versatile method for the fabrication of nanofibers. It is the most preferred system because it is easy, simple, economical to use, and can manipulate the diameter of fibers by changing the needle pore diameter as desirable[37-39]. Currently, the electrospinning technique is being extensively studied for biomedical applications, especially in tissue regeneration, because they mimic extracellular matrix and provide better cell interactions[40-44]. The significance of those nanofibers can be further enhanced by immobilizing drugs for controlled release. For instance, immobilization of metronidazole (MTz) in nanofibers can help in preventing the infection from a pathogenic microorganism which is a matter of concern in the healthcare system. MTz belongs to the nitroimidazole class and is soluble in aqueous media. The melting temperature is ~163°C. It has antibiotic, antifungal and antiprotozoal activity with a half-life of 8 h. The growth of the

microbes is inhibited due to the formation of nitroso radicals, which helps in inhibiting nucleic acid synthesis. As a result, DNA of microbial cells is disrupted. MTz is more active in anaerobic bacteria (primarily Gram-negative bacteria) and protozoans when compared to aerobic bacteria[45, 46]. **Fig. 3.1** shows the structure of the MTz.

In this study, we aimed to develop a blend of PCL, and PLA with the hydrophilic EA in the form of nanofiber mats (NM) to enhance the stability and hydrophilicity for cell compatibility and evaluate their potential for tissue regeneration application. Accordingly, EA/PCL/PLA blends of various compositions with the increasing EA content were developed and fabricated NM of various compositions. The surface morphology of the NM was analyzed. The physical and chemical properties of NM were studied using different techniques, the influence of hydrophilicity in cell viability and proliferation were evaluated. Further, the *in vitro* release of MTz, antibacterial property and interaction of MTz with EA were studied.

3.2 Materials and Methods
3.2.1 Materials

Metronidazole PLA (Mw~60,000 Da) (PLA) and PCL (Mw~68000 Da) (PCL) were purchased from Sigma-Aldrich Co., St. Louis, USA. Egg albumen (EA) was acquired from Otto Biochemika Reagent, Mumbai, India. Chloroform and formic acid were of analytical reagent grade, procured from Rankem, Thane, India. Phosphate buffered saline (PBS) 3-(4, 5-Dimethylthiazol-2-yl)-5 diphenyl tetrazolium bromide (MTT), fetal bovine serum (FBS), dulbecco's modified eagle's medium (DMEM), and trypsin were acquired from Sigma-Aldrich Co., St. Louis, USA. Antibiotics, glucose, 4′, 6-diamidino-2-phenylindole (DAPI), Eosin, and ethylenediaminetetraacetic acid (EDTA) were procured from Hi-Media Laboratories Ltd., Mumbai, India. Propanol, acetone, and dimethyl sulfoxide (DMSO) were bought from Merck Ltd., Mumbai, India. The 3T3L1 (mouse embryonic fibroblast- adipose like cell line) cell line was procured from the National Centre for Cell Sciences (NCCS), Pune, India. All reagents, solvents, and media for antibacterial studies and components of buffer for drug release studies were of analytical grade and were obtained from the local chemical companies in India.

3.2.2   Preparation of solutions for electrospinning

Individual polymer solutions of EA, PCL, PLA and their blends with and without MTz were prepared in various compositions, as given in **Table 3.1**. Chloroform was used as a solvent for the dissolution of PLA and PCL polymers, whereas EA was dissolved in formic acid. The polymers dissolved in respective solvents were mixed and vortexed to obtain homogenous solutions to attain the desired composition of blends. The polymeric blend composition, which can form a good NM, was selected and incorporated with the drug (MTz) at various concentrations of 10, 20 and 30%, respectively to attain drug-loaded polymer blend solutions and fabricated as NM. The 10, 20 and 30% was calculated based on the total polymer concentration. For example, 10% of metronidazole is 10 g loaded in 100 g of polymer (w/w). Accordingly, the maximum loading was 30%. The various compositions prepared are specified in **Table 3.1**. PLA and PCL at 4% each were blended to fabricate nanofiber without EA, which is used as a control (PCE0). Later to this EA was added in different concentrations to PCE0. The concentration of EA was ranged from 1 to 4% (Table 3.1). The suitable composition, PCE2 with 2% EA was chosen to immobilize the drug, MTz in various concentrations, as shown in **Table 3.1**. Chemical structure of polymers and drug are shown in **Fig. 3.1**.

Table 3.1 Compositions used for fabricating NM

Sr. No	PLA (w/v %)	PCL (w/v %)	EA (w/v %)	Drug (w/w % w.r.t. to total polymer)
PCE0	4	4	0	0
PCE1	4	4	1	0
PCE2	4	4	2	0
PCE3	4	4	3	0
PCE4	4	4	4	0
PCE2 D10	4	4	2	10

PCE2 D20	4	4	2	20
PCE2 D30	4	4	2	30
PC D20	4	4	0	20

* Weight/weight % with respect to total polymer weight (w/w% w.r.t to total polymer). *P= PLA, C= PCL, E= EA and D= MTz.
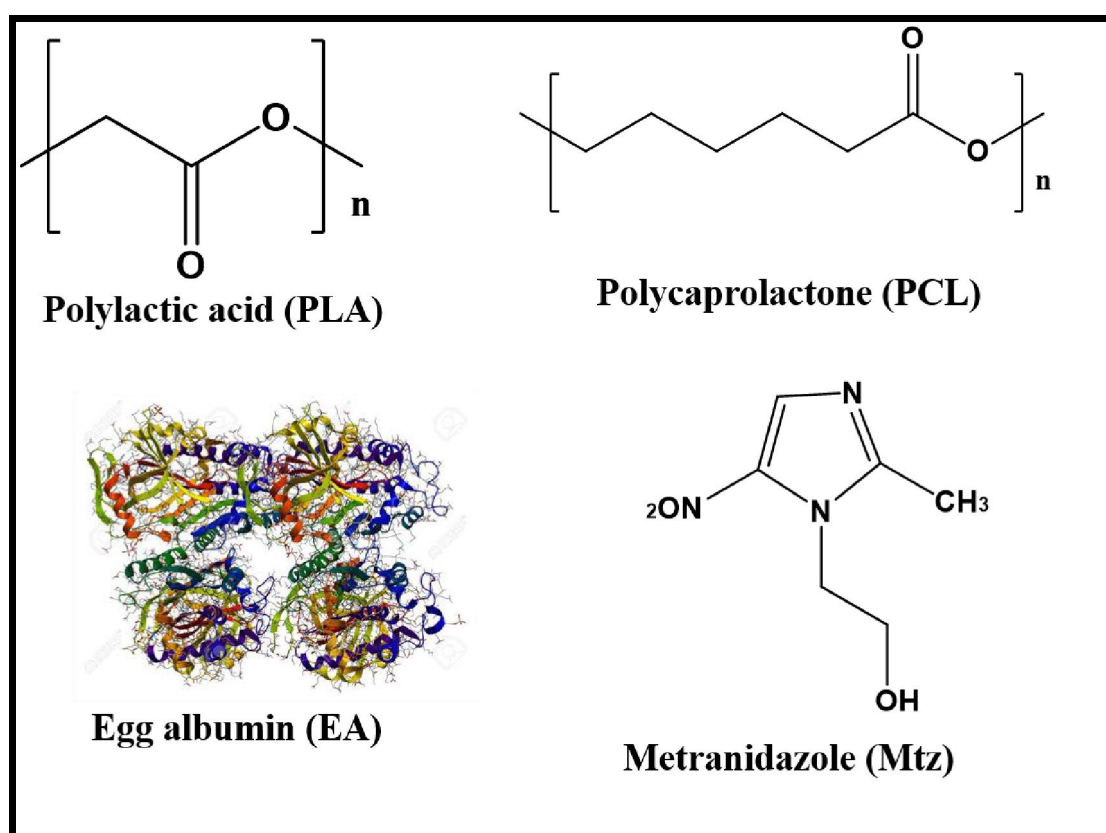
Figure 3. 1 Chemical structures of PLA, PCL, EA and MTz

3.2.3 Fabrication of nanofibers of blend solutions by electrospinning method

Polymeric solutions were electrospun using a 10 mL syringe, equipped with a stainless-steel hypodermic needle with the desired pore diameter as a nozzle for spinning the polymer solution. The syringe filled with a polymeric solution was mounted on a syringe pump with a controller to control the flow rate of the solution.

The syringe needle was connected to a high-voltage generator operated in positive DC mode. An aluminium plate was set in a closed chamber to collect NM. The electrospinning experiments were done at room temperature. The parameters were fixed like the distance between the tip of the needle and the collector was 10 cm; the flow rate and the applied voltage were 0.50 mL/h and 15 kV, respectively. Typically, most of the polymers were electrospun at the above parameters to attain NM; therefore, all compositions with and without MTz were electrospun at those parameters. The developed NM was crosslinked by annealing at 60 °C for 2 h in the oven [47].

3.3   Characterization of developed nanofibers

The developed nanofibers with and without MTz were analyzed using various techniques to understand the physical properties of the various nanofibers developed. The morphology and diameter of nanofibers were analyzed by SEM (EDAX, Micro Analysis System, and Model Quanta 200 3D Dual-beam SEM). The sample used for SEM observations was prepared by mounting a small portion of the non-woven NM on a stub. Later, the mounted stubs were sputtered with gold/palladium using a coating unit, FEI, USA and tungsten filament (W) was used as an electron source, and the resolution was 3 nm. The functional characteristics of polymers and electrospun nanofibers were recorded using FTIR [Perkins Elmer, spectrometer I, FTIR diffused reflectance (DRIFT) mode, USA]. The recording of the spectrum was done in the wavelength range from 4000 to 500 cm^{-1} with a resolution of 4 cm^{-1}. Each spectrum is composed of an average of 8 scans.

The crystallinity of MTz polymers and various nanofibers were evaluated using wide-angle X-ray diffraction (WXRD) containing a P-Analytical X-ray diffractometer model X-PERT PRO (Amelo, The Netherlands) with Cu Kα_1 radiation (40 kV, 100 mA, $\lambda = 0.154$). The samples were scanned in the 2θ range of 2- 35° to investigate the change in crystal structure before and after the formation of nanofibers with and without MTz. The glass transition temperature (T$_g$), crystallization temperature (T$_c$) and melting temperature (T$_m$) were determined for MTz, pure polymers and NM with and without MTz using the DSC instrument (Model Q10 DSC, TA Instrument, USA).

About 5 to 6 mg of the sample (polymer/NM) was loaded in a DSC pan, and the pan was sealed by applying pressure. In the first cycle, the sample was equilibrated to -70 °C for 2 min and later heated to 100 ºC at a rate of 10 ºC/min. In the second cycle, the sample was heated -70 °C to 200 °C at a rate of 10 °C/min. The thermogram was run under the nitrogen atmosphere at a flushing rate, 50 mL/min. The hydrophilicity of the NM was studied using contact angle measurements. Fabricated NM were cut (0.5 x 0.5 cm) and placed on the sample holder. The contact angle was measured by the drop-casting method. A red dye (Rhodamine B, 1 mg in 10 mL of water) was utilized to measure the angle to visualize the water drop. The NM were placed on a glass slide, and a droplet of water was dropped on NM using a pipette. To ensure consistency, the volume of a water droplet at each dispensing was maintained at 30 μL by controlling the speed of the drop and each measurement was taken after 5 seconds of dispensing. For each sample, the contact angle θ, was measured using J image software. Three measurements were taken and averaged at different spots to attain the contact angle.

3.3.1 Swelling and weight loss studies

The amount of water absorbed by the NM determines the strength of its hydrophilicity. Swelling studies were done at ambient temperature using 10 mg of NM in duplicates. The respective NM were transferred into a beaker containing 10 mL of distilled water that was maintained at ambient temperature. At successive intervals of time, the swollen weights of NM were taken after removing the surface water gently using the tissue paper. The total amount of water absorbed was calculated using equation 1.

$$SW = \frac{M - M_i}{M_i} \times 100$$
<div align="right">Equation 1</div>

Where, SW is swelling weight in percent, M is the swollen weight of NM in water, Mi is the initial weight of NM.

To study NM weight loss, the respective NM of various compositions of 1 cm^2 were immersed in a pH 7.4 of PBS solution for 24 h. After 24 h, the NM were removed and dried at room temperature (25°C). Equation 2 was used for calculating the weight loss. All the calculations were done in duplicates.

$$\text{Weight loss\%} = \frac{\text{Final weight} - \text{Initial weight}}{\text{Initial weight}} \times 100 \qquad \text{Equation 2}$$

The % of weight loss with the dissolution of polymer or protein from NM, Final weight is the weight of NM sample after drying, Initial weight of NM before immersing in PBS.

3.3.2 Interaction studies of EA with MTz

The physical interactions between EA and MTz were studied using circular dichroism (CD) and fluorescence spectroscopy. To investigate the changes in the secondary structure of EA in the presence of MTz, the CD was used. CD measurements were carried out in the range of 200-250 nm at an interval of 1 nm and the CD spectra were collected with the scan speed of 20 nm/min. An average of 10 scans was done to collect the CD spectrum.

Fluorescence measurements were performed with an LS50B spectrofluorometer (Perkin Elmer, USA). The excitation and emission slits' width was set at 0.625 nm. Fluorescence emission spectra were recorded in the range of 260 to 600 nm wavelengths using an excitation wavelength of 275 nm. The concentration of 3 µM of EA is kept constant, and the respective concentrations of MTz (3, 6, 9, 12, 15, 18 and 21 µM) were added to the EA solution to analyse the interactions between EA and EA MTz by CD and fluorescence spectrofluorometric.

3.3.3 *In-vitro* drug release studies

The respective NM of 5 mg of with and without MTz were placed in a wide-mouth glass bottle containing 2 mL of phosphate buffer saline (PBS) of pH 7.4. The release of MTz was monitored at regular intervals by placing the respective container with NM in a temperature-regulated shaker bath of 50 rpm maintained at 37 °C. At each

interval of time, 1 mL of buffer solution was removed from the sample bottle for the estimation of MTz and replaced with 1 mL of fresh buffer. The MTz containing sample buffer was analyzed by UV visible spectrophotometry (Shimadzu UV-1601PC) at a wavelength of 320 nm to determine the amount released at each interval and extrapolated the quantity using a standard calibration curve of MTz. The respective NM without MTz was used as a control. The release studies were done in duplicate and all the samples were analyzed twice for reproducibility. The results were presented in terms of cumulative percent release as a function of release time. Equation 3, shows the method for obtaining the cumulative percent of MTz released.

$$Cumulative\ amount\ of\ MTz\ released\ (\%) \frac{Mt}{M\infty} \times 100 \qquad \text{Equation 3}$$

Where, M_t is the amount of MTz released at time t, M_∞ is the amount of MTz loaded in NM prior to electrospinning of the respective solution.

3.3.4 *In-vitro* antibacterial study

The bactericidal activity of the nanofibers containing MTz was tested using growth inhibition studies against Gram-positive bacteria *S. aureus* and Gram-negative bacteria *E. coli* which are more often found in the wounds[48, 49]. For the antibacterial assay, the bacterial strains were first grown on a solid nutrient agar medium and from the agar plates, fresh colonies were inoculated into 100 mL of nutrient broth medium. Growth was monitored at every 3 h by UV–visible spectrophotometer (Shimadzu, UV-1601) until the optical density (OD) reached 1 at 600 nm (OD of 1 corresponded to a concentration of 10^8 CFU/mL of medium) [50]. Subsequently, 1 mL from the above preparation was further added to 100 mL of freshly prepared nutrient broth medium supplemented with the test sample (1cm x 1cm). The test samples include NM with and without MTz at concentrations of 10, 20, and 30%, respectively. The test samples were compared with the control, where the broth solution (supplemented with bacteria) without NM was used as a control. All the flasks were incubated at 37 °C in a rotary shaker at 150 rpm. The growth rates and the bactericidal concentrations were monitored by measuring the OD at 600 nm by UV spectrophotometer at an interval of 0, 1, 2 and 5 h.

3.3.5   Evaluation of percent of hemolytic activity (HP)

Blood was obtained from human volunteers from National Chemical Laboratory, Health center, Pune, India. The blood sample was stabilized using EDTA. Red blood cells (RBCs) were isolated from whole blood using density gradient centrifugation. The whole blood of 5 mL was slowly added on top of 5 mL of PBS saline solution and then centrifuged at 2000 rpm for 30 min. The supernatant was discarded, and collected the RBCs which were washed thrice with phosphate buffer saline of pH 7.4 and centrifuged at 2000 rpm for 30 min. A stock solution of the washed RBCs was prepared without serum at 2% (v/v) using a phosphate buffer of pH 7.4. Later, 2 mL of the diluted RBCs suspension was transferred to each of the 2 mL eppendrof tubes containing 10 mg of NM of different compositions of PCE0, PCE1, PCE2, PCE3 and PCE4. Similarly, the negative and positive blood samples were prepared without NM in phosphate buffer and de-ionized water, respectively. The respective eppendrof tubes were then incubated for 2 h at 37 °C. During the incubation, at every 30 min the samples were shaken gently to re-suspend the precipitated RBCs and centrifuged at 1500 g for 10 min at room temperature. The supernatant was then placed in another 96-well microtiter plate, and hemoglobin (Hb) release was measured spectrophotometrically by reading the OD at 541 nm using a micro-titer plate reader (Tecan) in PBS. The percentage of RBC lysis was calculated based on the assumption that 100% RBC lysis resulted by mixing blood with distilled water at a 1:1 (v/v) ratio. Equation 4 was used for calculating the percent (%) of HP.

$$HP\ (\%) = \frac{Dt - Dnc}{Dpc - Dnc} \times 100 \hspace{4cm} \text{Equation 4}$$

Where, Dt is the absorbance of the test samples, Dpc and Dnc are the absorbance's of the positive and negative controls, respectively.

3.3.6   Cytotoxicity study

The monolayer cell culture was trypsinized and the cell count was adjusted to 1.0 x 10^5 cells/mL using DMEM containing 10% FBS. To each well of the 96 well

microtiter plate, 0.1 mL of the diluted cell suspension (approximately 10,000 cells) was added. After 24 h, when a partial monolayer was formed, the supernatant was flicked off, and the monolayer was washed once with the medium. 100 μL of the respective sample concentrations of polymer samples (EA, PCL, PLA, and NM of PCE2) were added to the partial monolayer of microtiter plates. The plates were then incubated at 37 °C for 3 days in 5% CO_2 atmosphere, and microscopic examination was carried out, and observations were noted after every 24 h interval. After 72 h, the sample solutions in the wells were discarded and 50 μL of MTT in PBS was added to each well. The plates were gently shaken and incubated for 3 h at 37 °C in 5% CO_2 atmosphere. The supernatant was removed, and 100 μL of propanol was added, and the plates were gently shaken to solubilize the formed formazan. The absorbance was measured using a microplate reader at a wavelength of 540 nm. The percentage growth inhibition was calculated, and the concentration of test drug needed to inhibit cell growth by 50% (CTC50) values were generated from the dose-response curves for each cell line[51]. MTT assay was repeated for consistency. Further, to understand the influence of hydrophilicity on cell proliferation, cell culture studies were performed and analyzed by fluorescence microscopy. Briefly, the polymeric blend solutions were prepared in different concentrations, which are shown in Table 1 (PCE0, PCE1, PCE2, PCE3 and PCE4). The prepared solutions were subjected to electrospinning for 10 min to coat a thin layer of NM on the respective glass coverslips. Later on, the individual NM (coverslip) was crosslinked by annealing at 60 °C for 2 h. The above-mentioned samples were sterilized by UV irradiation and cultured using HeLa cervical cancer cells. Briefly, cells were seeded at 5000 per well (hemocytometer) on glass coverslips, coated with and without NM. The cells were incubated at 37 °C for 24 h in the presence of CO_2 atmosphere and DMEM supplemented with 10% FBS. After the incubation for 24 h, the cells were fixed using 4% paraformaldehyde and washed with PBS. Later, the cells were stained by DAPI (0.5 mg/mL), and eosin (1.0 mg/mL) and then these cells were observed under a fluorescence microscope to understand the cell growth on the NM (Carl Zeiss (Model: Axio Observer.Z1, Oil emersion objective, 20X, Germany). Images of the cells were captured under green and indigo filters.

3.4 Results and Discussion

Though there are several reports on improving hydrophilicity of the PLA and PCL-based materials, blending these polymers with the economically viable EA to improve stability, compatibility and hydrophilicity was demonstrated for the first time so as to exploit EA for the application in tissue engineering. As mentioned in **section 3.1**, EAis easy to renew at a lower cost, and the structural and functional properties are similar to the FDA-approved human serum albumin (HSA). Further EA being a protein, it is suggested to be inherently bioactive and favour cell viability, adhesion, and proliferation. Therefore, NM with said properties and hydrophilicity are considered advanced materials, which mimic extracellular matrix for biomedical applications. Therefore, we developed hydrophilic PCL/PLA/EA nanofibers of various compositions (**Table 3.1**) and examined hydrophilicity, physicochemical properties and biocompatibility for analyzing their potential as nano-biomaterial for tissue regeneration.

3.4.1   Scanning electron microscope (SEM)

The various compositions, as shown in **Table 3.1** were subjected to electrospinning, where the processing parameters were fixed and the concentrations of the polymers and blend compositions were manipulated to produce the NM. The respective pure PLA and PCL solutions of different concentrations were initially tried to optimize the desired concentration to obtain smooth nanofibers. Later, various compositions with EA were developed. Our earlier investigations showed that pure EA could not produce nanofibers at any given concentration because it is less viscoelastic than poly (vinyl alcohol). Therefore EA alone nanofibers were not reported [52]. **Fig. 3.2** shows the nanofiber morphology of PLA and PCL with increasing EA concentrations (PCE0, PCE1, PCE2, PCE3 and PCE4). It was observed that the diameter of the NM increased with an increase in EA concentration in the blend composition, from 250 to 400 nm. The diameter of nanofibers was increased with the increasing polymer concentration due to the increased viscoelastic force in the nanofiber jet, which resisted stretching repulsive forces of charges. Therefore the diameter of the nanofiber was increased[53]. Among the various compositions, PCE2 was chosen for MTz

loading as PCE2 recorded a higher percent of swelling (more hydrophilic) when compared to other formulations (**section 3.4.5.2**). Accordingly, MTz was immobilized in PCE2 at various concentrations (10, 20, and 30% of MTz with respect to total polymer concentration) and fabricated in the form of nanofibers, which were designated as PCE2 D10, PCE2 D20 and PCE2 D30. The surface morphology of the nanofibers is shown in **Fig.3.2** and **Fig. 3.3** (size distribution of NM). The nanofibers appeared to be smooth, and the change in nanofiber diameter was insignificant with the increase in the drug concentration ranging from 10 to 30%. Later, the developed nanofibers mats were stabilized by annealing at 60 °C for 2 h to get crosslinked NM, where the sulfhydryl groups of EA were formed as disulfide linkages at 60 °C [52].
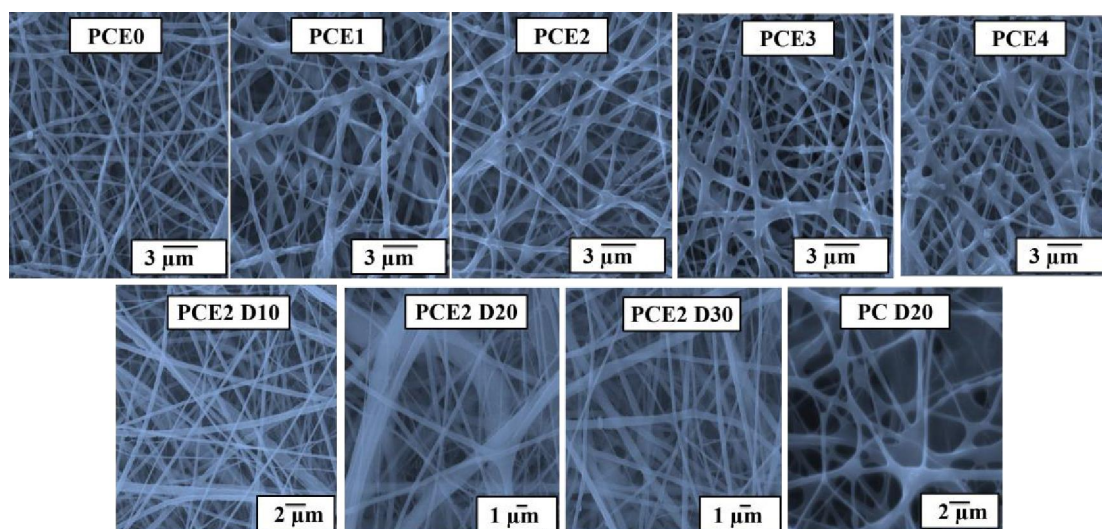
Figure 3. 2 SEM image of PCE0, PCE1, PCE2, PCE3, PCE4, PCE2 D10, PCE2 D20, PCE2 D30 and PC D20.
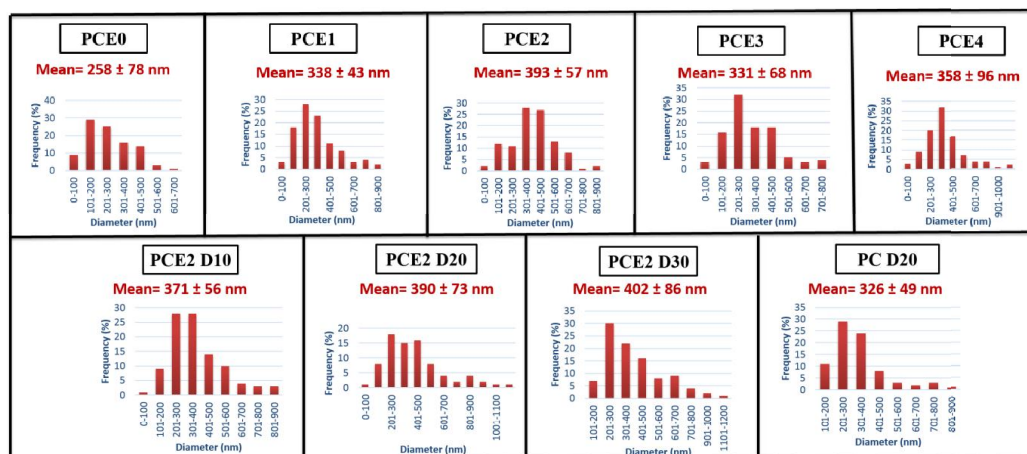
Figure 3. 3 Average nanofiber diameter (nm) were analyse by Image J software of PCE0, PCE1, PCE2, PCE3, PCE4, PCE2 D10, PCE2 D20, PCE2 D30 and PC D20.

3.4.2   Fourier transform infrared spectroscopy (FTIR)

The infrared absorption spectra for the pure polymers (EA, PCL and PLA), MTz, and NM of polymeric blends of EA/PCL/PLA with and without MTz (**Fig. 3.4**). IR spectrum of pure EA showed characteristic peaks at 3298 cm^{-1}, indicating the presence of –NH stretching of the secondary amide, –C=O stretching at 1650 cm^{-1} (amide-I) and –NH bending at 1542 cm^{-1} (amide II), a weak band at 2880 cm^{-1} due to –SH stretching, –CH stretching at 2965 cm^{-1} and a peak at 1397 cm^{-1} was observed due to plane wagging. Pure PCL showed a characteristic band at 2943 cm^{-1} due to asymmetric stretching of aliphatic –CH$_2$, a peak at 2864 cm−1 for symmetric –CH$_2$ stretching and a peak at 1725 cm^{-1} for –C=O stretching. A prominent and sharp peak was recorded at 1186 cm^{-1}, corresponding to carbonyl stretching of the ester bond (–COOC–). IR spectrum of PLA showed a band at 2995 cm^{-1} is due to C–H stretching, 1752 cm^{-1} was recoded due to –C=O, and a band at 1088 cm^{-1} is due to ether C–O–C. The spectrum of the pure MTz showed a broad absorption band at 3233 cm^{-1} due to –OH stretching, 3098 cm^{-1} band due to –CH$_2$ stretching, a band at 1545 cm^{-1} is due to NO$_2$ a band at 1184 cm^{-1} is due to –C–N. The IR spectra of the NM of PCE2 D20 and PCE3 showed the characteristic peaks of all the polymers and MTz, indicating their presence. However, some of the peaks were either merged or shifted to a higher frequency because the corresponding bands of polymers and drugs were very close to each other. For example, the carbonyl, amine and hydroxyl groups. The shifting of

bands indicated hydrogen ion interactions between the polymers and MTz (for example the shift of bands from 3248 to 3289 cm^{-1}, 2945 to 2951 cm^{-1}, 1758 to 1763 cm^{-1}, 1656 to 1654 cm^{-1}, 1184 to 1185 cm^{-1}, and, 1095 to 1088 cm^{-1}).
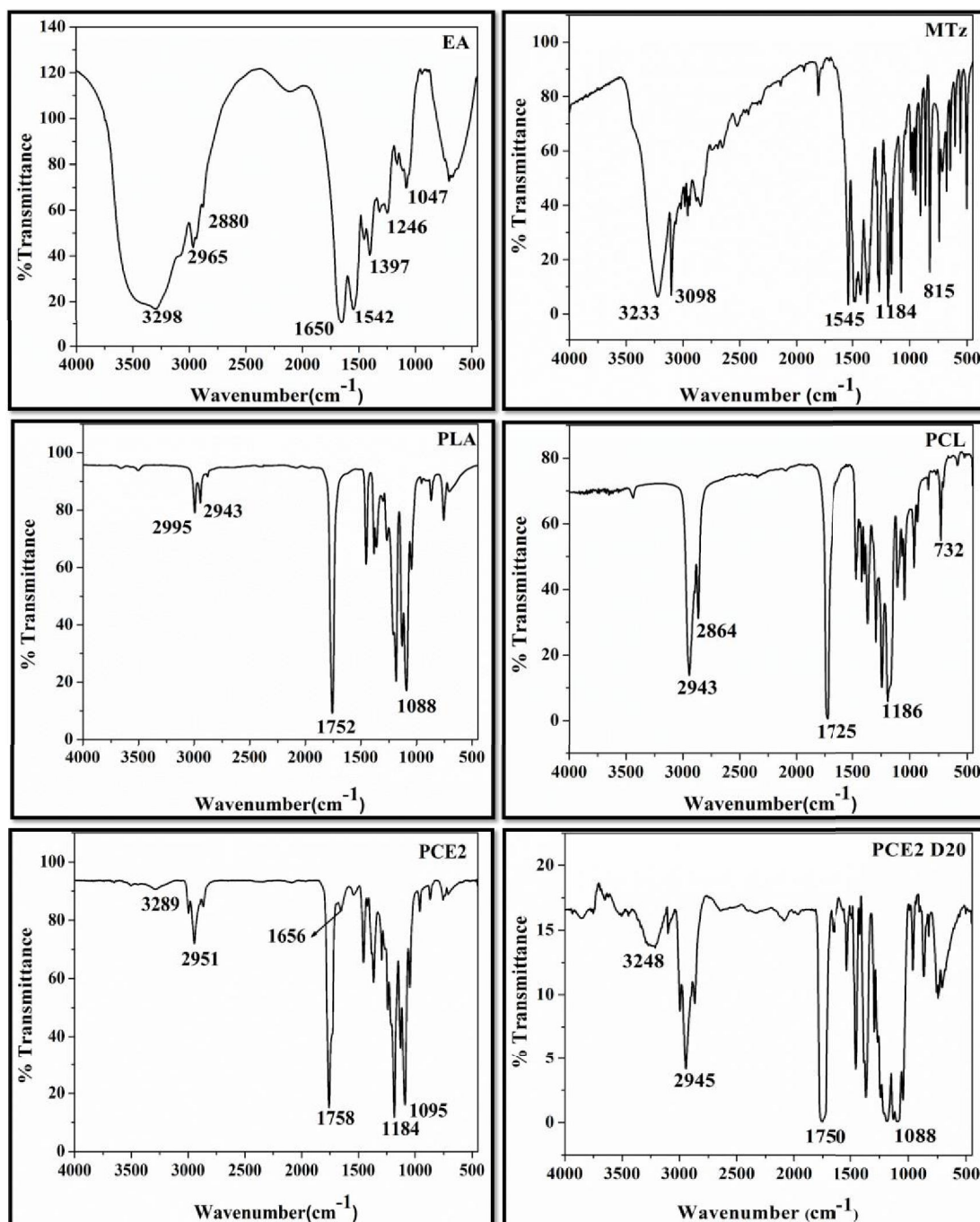
Figure 3. 4 FTIR spectra of EA, PCL, PLA, MTz, PCE2 and PCE2 D20

3.4.3 Wide-angle X-ray diffraction (WXRD)

Fig. 3.5 shows the X-ray diffraction patterns for the pure EA, MTz, the respective nanofibers of pure PCL and PLA, and their blends with EA and MTz. These XRD studies were done to investigate the degree of crystallinity in the polymers before and after the fabrication of nanofibers. As reported, the pure PLA being semi crystalline recorded two peaks at 2Θ of 16º and 19º. Similarly, pure PCL also showed two peaks at 2Θ of 21º and 24º. Pure EA did not show any crystalline peaks as it is amorphous in nature. MTz is a crystalline material, and its XRD patterns showed a characteristic peak at 12º [54]. MTz became amorphous after immobilizing in NM due to interactions between polymers and MTZ. The XRD of the blend PCE2 NM showed low intense crystalline peaks, at 16º, 21º and 23º indicating the presence of PCL and PLA. The decrease in the intensity of crystalline peaks of PLA and PCL was due to the blending of the polymers and the formation of hydrogen ion interactions between the polymers (PCL/PLA/EA). It may also be understood that the decrease in intensity of the peaks was due to the limited time of reorientation of polymer chains during the electrospinning process[55]. Further, in **Fig. 3.5**, it was observed that due to the addition of MTz (crystalline drug) in NM, the intensity of the crystalline peak of PLA reduced. However, the crystallinity of PCL was unaltered. From these observations it is evident that the crystalline MTz was well miscible with PLA and EA (fluorescence studies) than PCL, as a result MTz transformed to an amorphous form, and the crystalline peak of PLA was reduced.
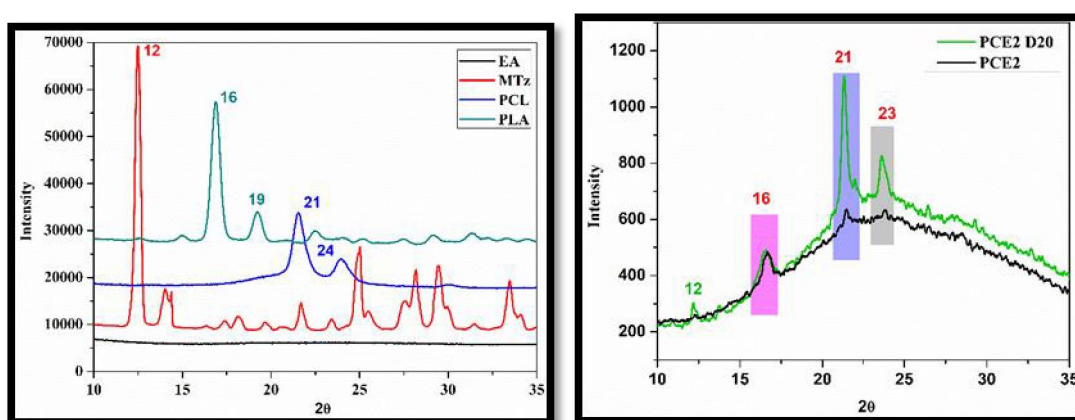
Figure 3. 5 XRD patterns of EA, MTz, PCL, PLA, PCE2 and PCE2 D20

3.4.4 Differential scanning calorimetry (DSC)

Fig. 3.6 showed the thermogram of pure polymers, MTz and NM of PCE2 and PCE2 20. Pure EA did not record any glass transition temperature (T_g) or melting temperature (T_m) as it is a natural protein. PCL being crystalline in nature, the thermogram of pure PCL recorded T_g at -65 °C and the T_m at 55 °C[56]. The (T_g) of pure PLA was recorded at 55 °C while T_m was recorded at 177 °C, and crystalline temperature (T_c) of pure PLA was observed at 104 °C[57]. The pure MTz depicted an endothermic peak due to T_m at 160 °C, which is similar to the reported literature[58]. The nanofibers blend of PCE2 showed T_m of both PLA and PCL at 179 °C and 54 °C, respectively. However, a new T_g was recorded at 6 °C. This T_g appeared between the T_g of PCL and PLA, which indicates a homogenous blending of polymers. Further, the increase in T_m of PLA was due to the incorporation of PCL as PCL promoted the crystallization of PLA[21] as a result of interactions between them. The MTz loaded nanofibers of PCE2 D20 blend represented all the peaks of the polymers except the T_m of MTz, because it had lost its crystallinity due to the interactions between functional molecules of polymers and MTz. The XRD patterns of PCE2 D20 also indicated the same (**Fig. 3.5**). The T_g increased with the immobilization of MTZ in PCE2, indicating interactions of MTZ with polymers and hence NM of PCE2 D20 is considered to be rigid.
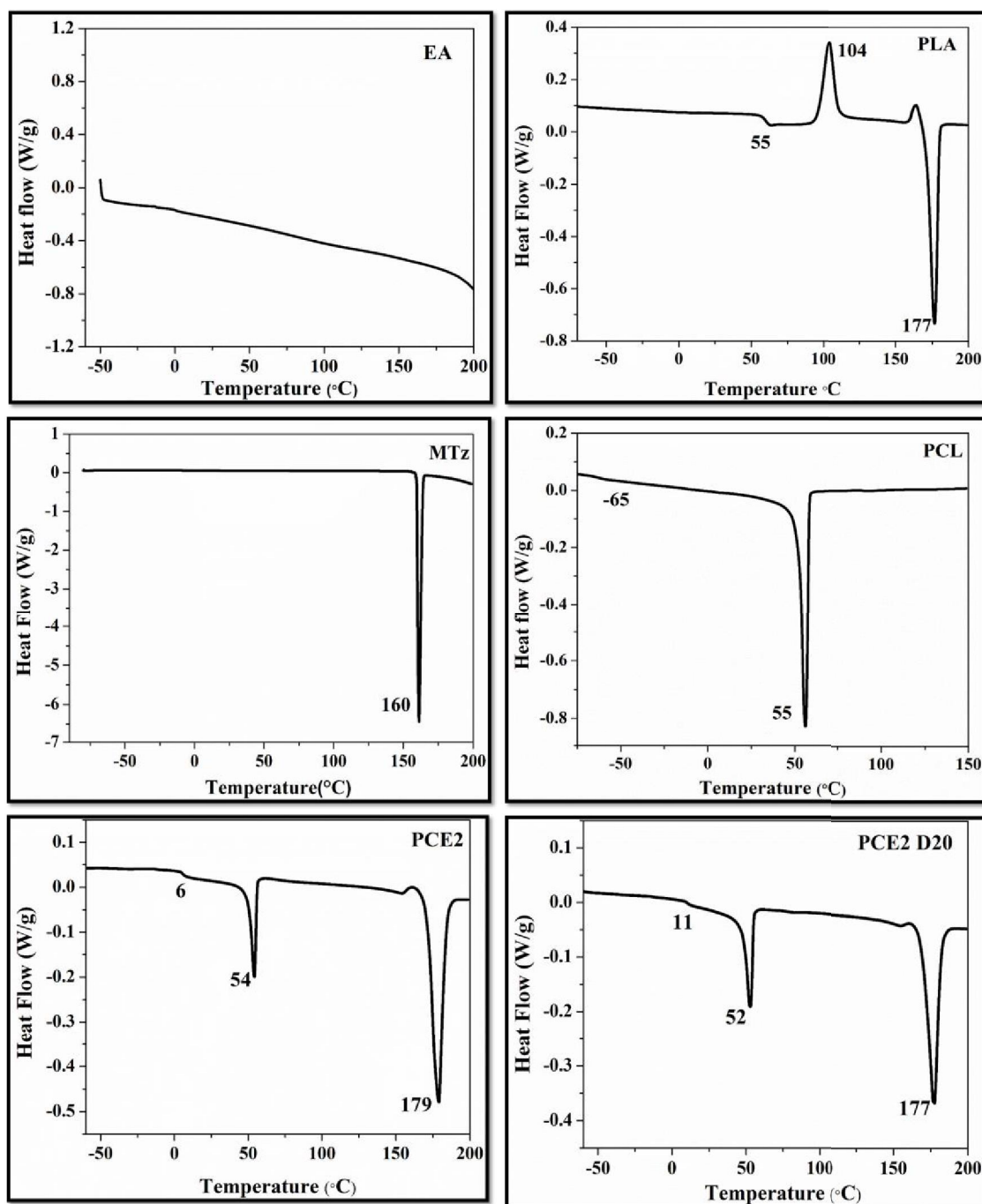
Figure 3. 6 DSC thermogram of EA, PCL, PLA, MTz, PCE3 and PCE2 D20

3.4.5 Measurements of hydrophilicity

Hydrophilicity is one of the important aspects for the biomaterials to be used in tissue regeneration because it was well understood that the materials with hydrophilicity show better cell interactions than the materials that are hydrophobic[59]. In these

investigations, the hydrophilicity of the NM was determined by qualitative and quantitative methods such as contact angle measurements and swelling behaviour.

3.4.5.1 Contact angle

The contact angle was defined as the angle formed by the intersection of two tangent lines to the liquid and solid surfaces at the perimeter of contact between the two phases and the third surrounding phase. It is understood that the water contact angle will decrease with increasing surface hydrophilicity. In these studies, to understand the water contact angle, the concentration of PLA and PCL were kept constant, and the concentration of EA was changed from 1 to 4%. The contact angles of NM were recorded for PCE0 (80.8^{o}), PCE1 (62.7^{o}), PCE2 (57.3^{o}), PCE3 (51.9^{o}) and PCE4 (45.0^{o}). The decrease in contact angle from 80.87^{o} to 45.0^{o} indicated an increase in hydrophilicity of NM, which is due to an increase in EA concentration in NM (**Fig. 3.7**).

Figure 3. 7 Contact angle measurement of PCE0, PCE1, PCE2, PCE3 and PCE4

3.4.5.2 Swelling and weight loss studies

The hydrophilicity of NM was also determined by the quantitative method in aqueous media following equation 1. **Fig. 3.8** shows the swelling behaviour of NM of various compositions at different time intervals, such as 5, 15 and 60 min. It was observed

that there was a marginal increase in swelling for the NM composition of PCE0 because PCL and PLA are hydrophobic. In the case of PCE1, the swelling of the NM was higher when compared to PCE0 due to the presence of EA. Likewise, there was a gradual increase in swelling with the increase in the concentration of EA in the blend compositions PCE2. However, a decrease in swelling was observed for the compositions PCE3 and PCE4, which attributes due to an increase in crosslinking density with an increase in the concentration of EA. PEC2 being ideal for drug release studies, MTz was loaded in PEC2. It was noticed that the percent of swelling for the MTz loaded PCE2 was insignificant because of the increased interactions between EA and MTz (**Fig. 3.8**).

Figure 3. 8 Percent of swelling for PCE0, PCE1, PCE2, PCE3, PCE4, PCE2 D10 and PCE2 D20 NM.

The weight loss of PCE0, PCE1, PCE2, PCE3 and PCE4 was investigated in the pH 7.4 of PBS solution for 24 h and the results are depicted in **Fig. 3.9**. The PCE0 composition did not record weight loss as PCL and PLA are hydrophobic in nature. The hydrophilic compositions, PCE1 and PCE2 had not shown any weight loss, which indicated that EA at 1 and 2 % resulted in homogenous blending with PLA-

PCL and, therefore, was well entrapped and crosslinked. In contrast, 3% and 4% of EA were excess and were present on the nanofiber mat's surface, hence prone for easy dissolution and therefore recorded weight loss, which was 2.08% and 2.87% for PCE3 and PCE4, respectively.
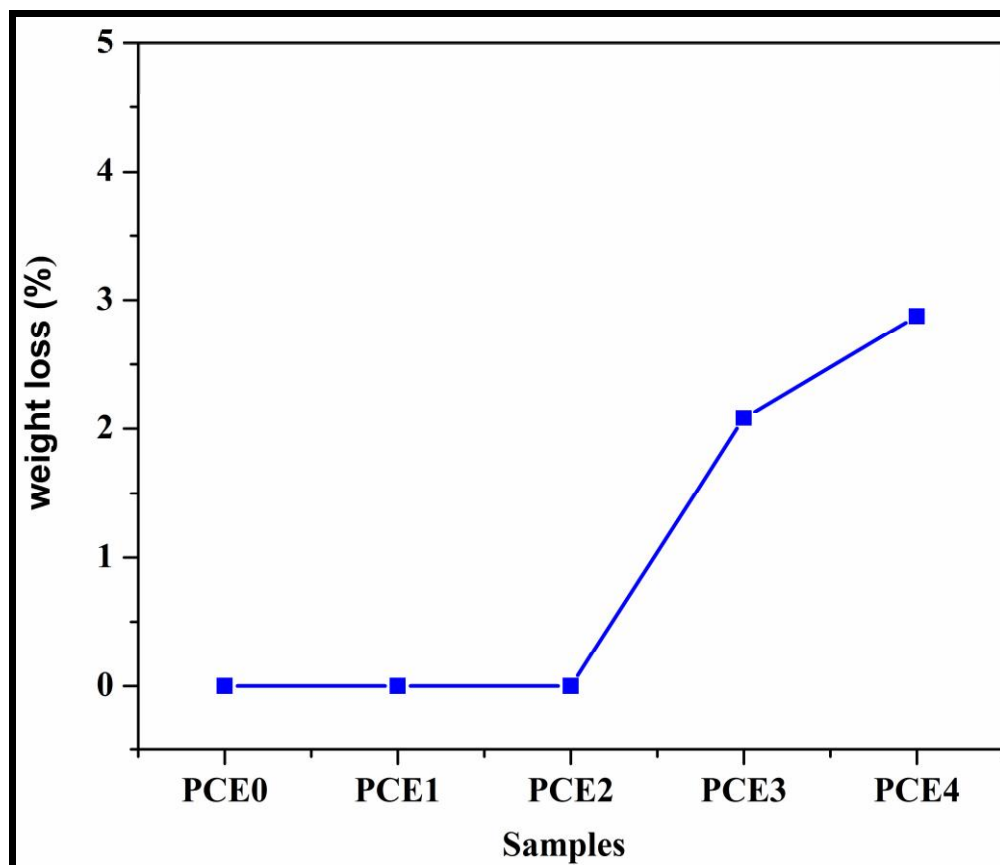
Figure 3. 9 Weight loss study of PCE0, PCE1, PCE2, PCE3 and PCE4 in pH 7.4 PBS for 24 h.

3.4.6 Interaction study of EA and MTz

The binding interaction of EA and MTz was studied by fluorescence spectroscopy and CD method. The studies were done by keeping the concentration of EA constant and varying MTz. The native tryptophan of EA (3 µM) was excited at 285 nm, and emission was seen at 331 nm. Quenching of EA increased as the concentration of MTz increased from 3 µM to 21 µM. Quenching was observed due to the interactions between EA and MTz. The increase in quenching shows the substantial binding property of MTz with EA. MTz does not show any peak in fluorescence spectroscopy.

Further, there was no shift of emission peak with the addition of MTz in EA, **Fig. 3.10** depicts an increase in quenching intensity with an increase in MTz concentration.
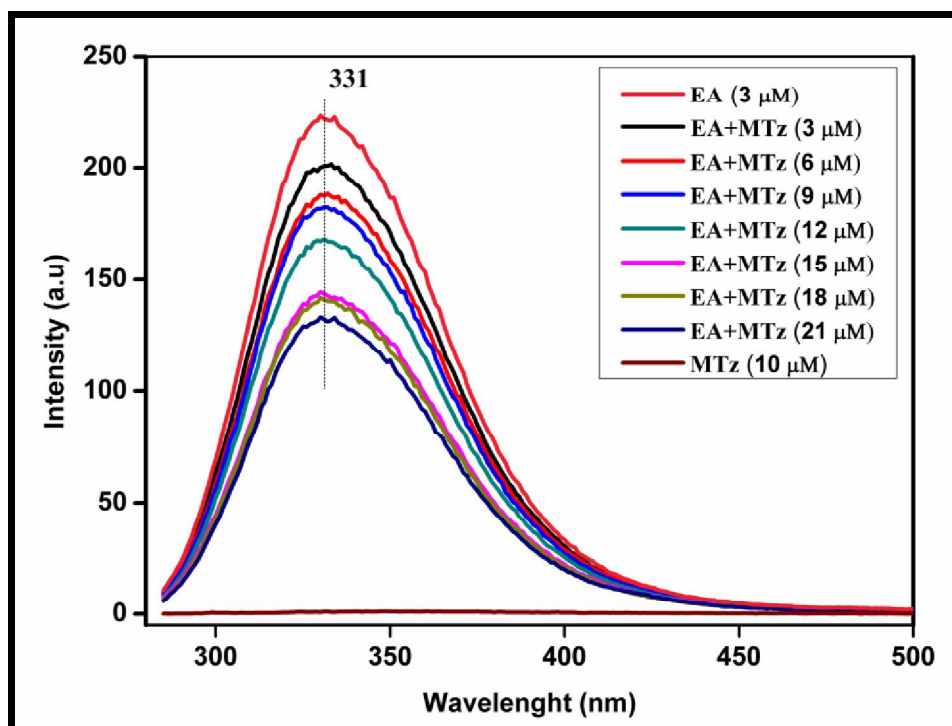
Figure 3. 10 Fluorescence spectroscopy of EA and MTz (3 to 21 μM).

CD is one of the efficient and reliable methods to determine the changes in the secondary structure of the protein. CD was used to verify changes in the secondary structure of EA in the presence of MTz. CD plot of EA showed two-bands at 208 and 222 nm, which is a characteristic property of α- helix of protein. Our studies observed that there was no change in the secondary structure even after increasing the concentration of MTz from 3 μM to 21 μM. This indicated that the interactions are physical (**Fig. 3.11**).
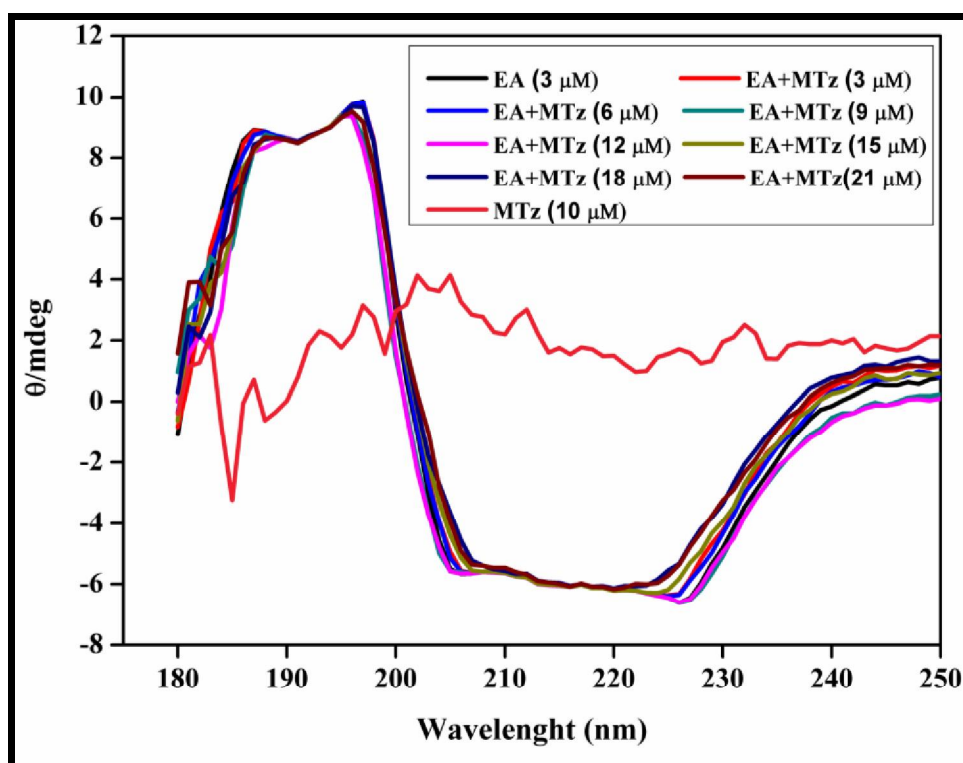
Figure 3. 11 Circular dichorism of EA and MTz (3 to 21 µM).

3.4.7 Drug release study

To understand the release profile of MTz loaded nanofibers, *in-vitro* release studies were done for the NM of PCE2 D10, PCE2 D20 and PCE2 D30 in phosphate buffer of pH 7.4 at 37±0.5 ºC in a water bath shaker as a function of time. The obtained release data was compared with the MTz loaded NM of PC D20 to understand the rate and extent of MTz released in the presence and absence of the hydrophilic component, EA. **Fig. 3.12**, depicts the release profiles of all the compositions. It was observed that 52% of the drug was released in 3 h for the NM loaded with 30% of MTz, wherein burst release followed by slow and sustained release was recorded up to 79 h, where a total of 85% of MTz was released. While in 20% MTz loaded NM, 42% of the drug was released in 3 h, and later 28% of MTz was released in 79 h, indicating slow and sustained release. In 10% of MTz loaded NM, 74% was released in 79 h. More percent of drug was released in case of 30% drug loaded NM than 20% because of the excess of the drug present on the surface of the nanofibers. The overall results showed that initial burst release followed by slow and sustained release was recorded for all the compositions. Also, the amount and the rate of the MTz released

increased as the concentration of the MTz increased in the NM because of the concentration gradient of MTz and the process of dissolution and diffusion of MTz[60]. Further, as expected, the NM of PC D20 (without EA) recorded only 40% of MTz after 79 h of release studies, which practically indicated that in the absence of hydrophilic component (EA), the rate and the extent of release was significantly less than the NM with EA. Similar, observations were reported for the nanofibers of poly (lactic acid) (PLA), poly (ethylene-co-vinyl acetate) (PEVA), or a blend of the two polymers, which was loaded tetracycline hydrochloride[61].
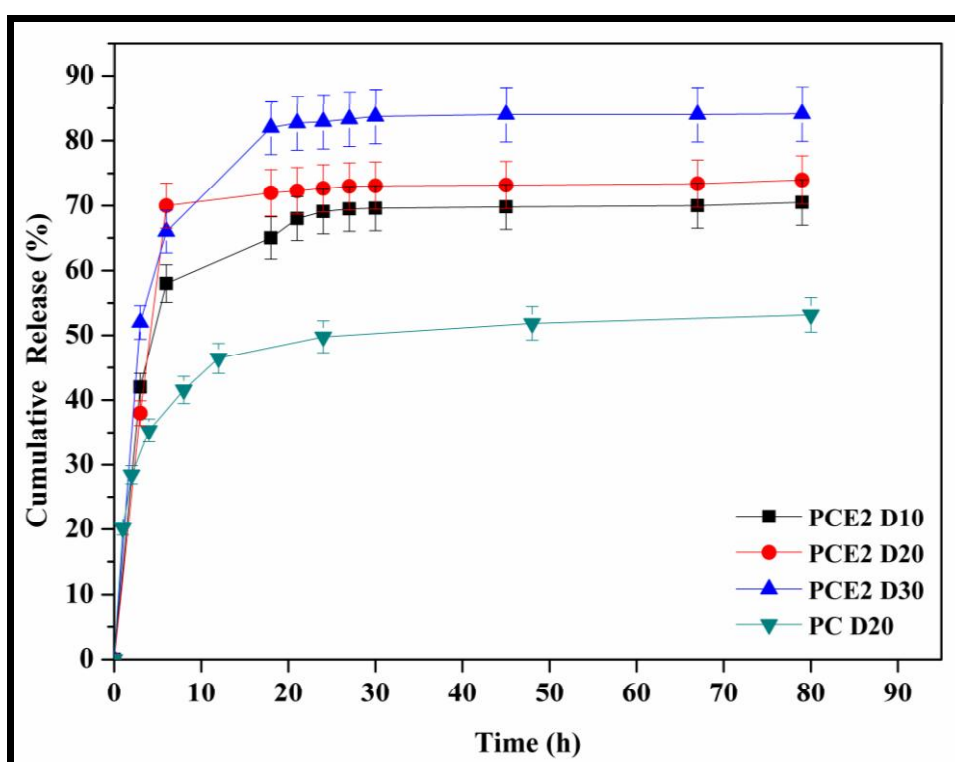
Figure 3. 12 Release studies of MTz from NM in pH 7.4 phosphate buffer solution.

3.4.8 Antibacterial study

The optical density method was used to determine the antibacterial activity of NM with and without MTz at different concentrations on the growth of *S. aureus and E. coli.* The bacterial medium without NM was used as a control. *S. aureus and E. coli* were used to study antibacterial activity because mostly Gram-positive and Gram-negative bacteria are found in the wounds. The optical density (OD) was measured at 600 nm at regular intervals from 0 to 5 h to determine the number of bacteria present

in the medium. It was evident that as the OD is greater, the lesser the antibacterial activity. From **Fig. 3.13** it was observed that the OD was maximum for both control and the NM of PCE2, as there was no bacterial inhibition. However, OD decreased with the increasing MTz concentration in NM (PCE2 D10, PCE2 D20, and PCE2 D30) as it had inhibited *S. aureus and E. coli*. Accordingly, NM with 30% drug loaded (PCE2 D30) showed maximum antibacterial activity. Similar studies were reported, which confirmed that MTz is effective against *S. aureus* and *E. coli* bacterial strain[62, 63].
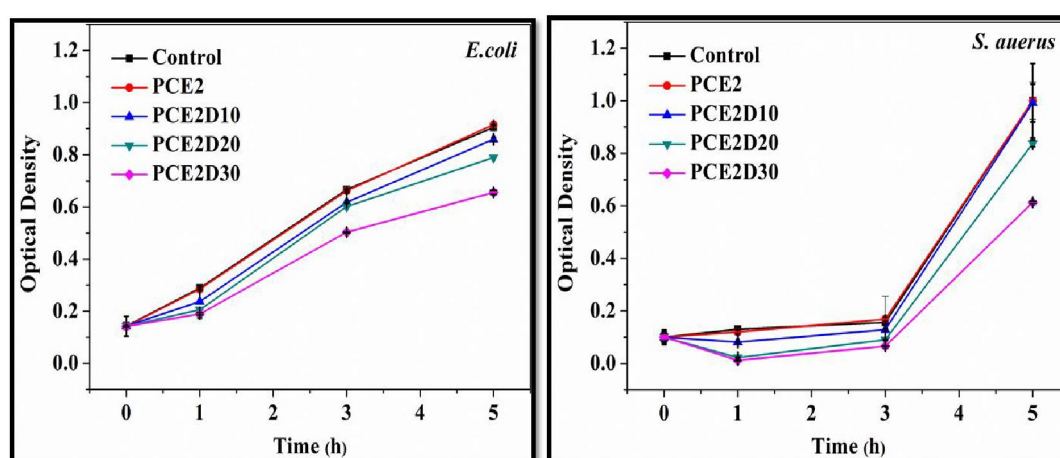
Figure 3. 13 Antibacterial studies were done in *E. Coli* and *S. aureus* of PCE2, PCE2 D10, PCE2 D20, and PCE2 D30.

3.4.9   Hemolysis Assay

In order to study the compatibility of the developed material with human blood, hemolysis studies are considered one of the most reliable methods. For our studies, we collected blood samples from the volunteers of CSIR-National Chemical Laboratory, at NCL-dispensary, Pune, after obtaining ethical clearance. As described in the experimental section (**3.3.5**), the negative and positive control and compositions of PCE0, PCE1, PCE2, PCE3 and PCE3 were subjected to hemolysis test (**Fig. 3.14**). The results showed 0% hemolytic activity for the negative control (phosphate buffer, pH 7.4), whereas the positive control (de-ionized water) showed 100% hemolytic activity. The nanofibers without EA PCE0 showed 0.69% of hemolytic activity, the nanofibers with EA, at various compositions recorded less than 0.3% (PCE1 (0.08%), PCE2 (0.17%), PCE3 (0.17%) and PCE4 (0.27%)). According to the reported

literature[64], the materials that showed hemolytic activity below 5% are considered safe for drug delivery by an invasive method. Our studies observed that NM of all the compositions showed hemolytic activity less than 5%; therefore, these can be used for biomedical applications.
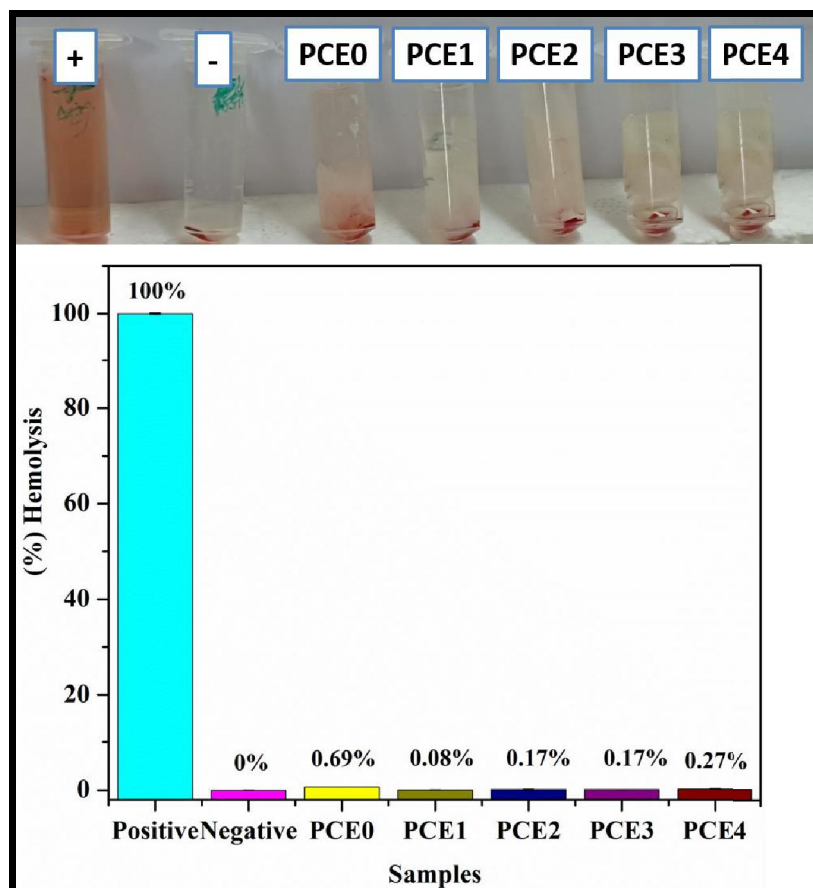
Figure 3. 14 Hemolysis assay of PCE0, PCE1, PCE2, PCE3 and PCE4.

3.4.10 Cytotoxicity Studies

Cell viability studies were done using MTT assay for the test samples of pure polymers such as EA, PCL, PLA, and the nanofibers of PCE2. The percent of cytotoxicity of pure polymer and nanofibers were studied on cells of 3T3-L1. **Fig. 3.15** represents the relative cell viability of the pure polymers of EA, PCL, PLA, and NM of PCE2 at a concentration of 1000 µg/mL. Earlier studies reported that the pure PCL and PLA are biocompatible and FDA approved and EA, an edible protein, is generally recognized as safe (GRAS). In our studies, the respective cell viability of EA, PCL, PLA and PCE2 was recorded at 80, 78, 80, and 84%, respectively. So, it

was considered that all these polymers showed cell viability at ~80 to 85%. PCE2 showed maximum cell viability because of increased hydrophilicity, indicating that hydrophilicity enhances cell interactions, favouring cell viability. The remaining 15 to 20% of cytotoxicity could be due to the extensive period of cell culture for 72 h instead of 24 to 48 h because of which, the cells might have got exhausted. Similar observations were reported in earlier studies[65]. Hence, we concluded that pure polymers and the fabricated nanofibers are non-toxic and compatible with 3T3-L1. Therefore, we consider that these will be suitable as a scaffold for tissue regeneration.
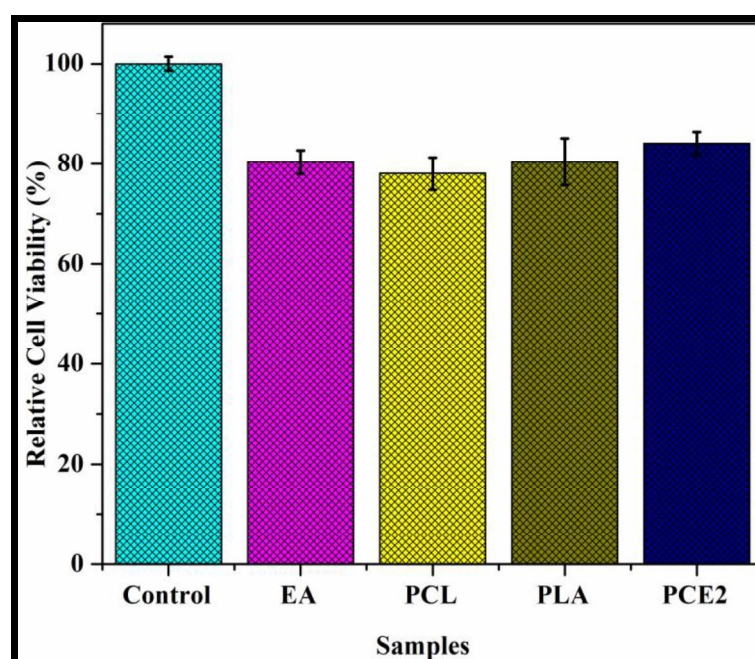
Figure 3. 15 MTT assay using 3T3-L1 cell line for 72 h.

Further, the effect of hydrophilicity on cell growth was studied by fluorescence microscopy for NM with and without EA (PCE0, PCE1, PCE2, PCE3 and PCE4) against HeLa cells by culturing these samples for 24 h. **Fig. 3.16** show the fluorescence images of the tested sample (control (A), PCE0 (B), PCE1 (C), PCE2 (D), PCE3 (E) and PCE4 (F)), where image A was used as a control (glass coverslips which are without nanofibers). Images from B to F showed a gradual increase in the number of cells due to an increase in hydrophilicity with the increase in the concentration of EA in the NM. The low density of cells was observed in images A and B as compared to the images of C, D, E and F because EA is absent in samples A and B. Further, the density of the cells was ploddingly enhanced in images C, D, E

and F as the concentration of EA was increasing. The **Fig. 3.16** suggested that EA has a significant effect on the growth of cells without EA. From this data, we concluded that EA can be utilized in tissue engineering or drug delivery system as it is more favorable for cells to multiply and hence anticipate better patient compliance with the application.

The overall results of the various analysis suggested that hydrophilicity is considered one of the main factors for better interactions with the cells to promote cell division and cell proliferation.
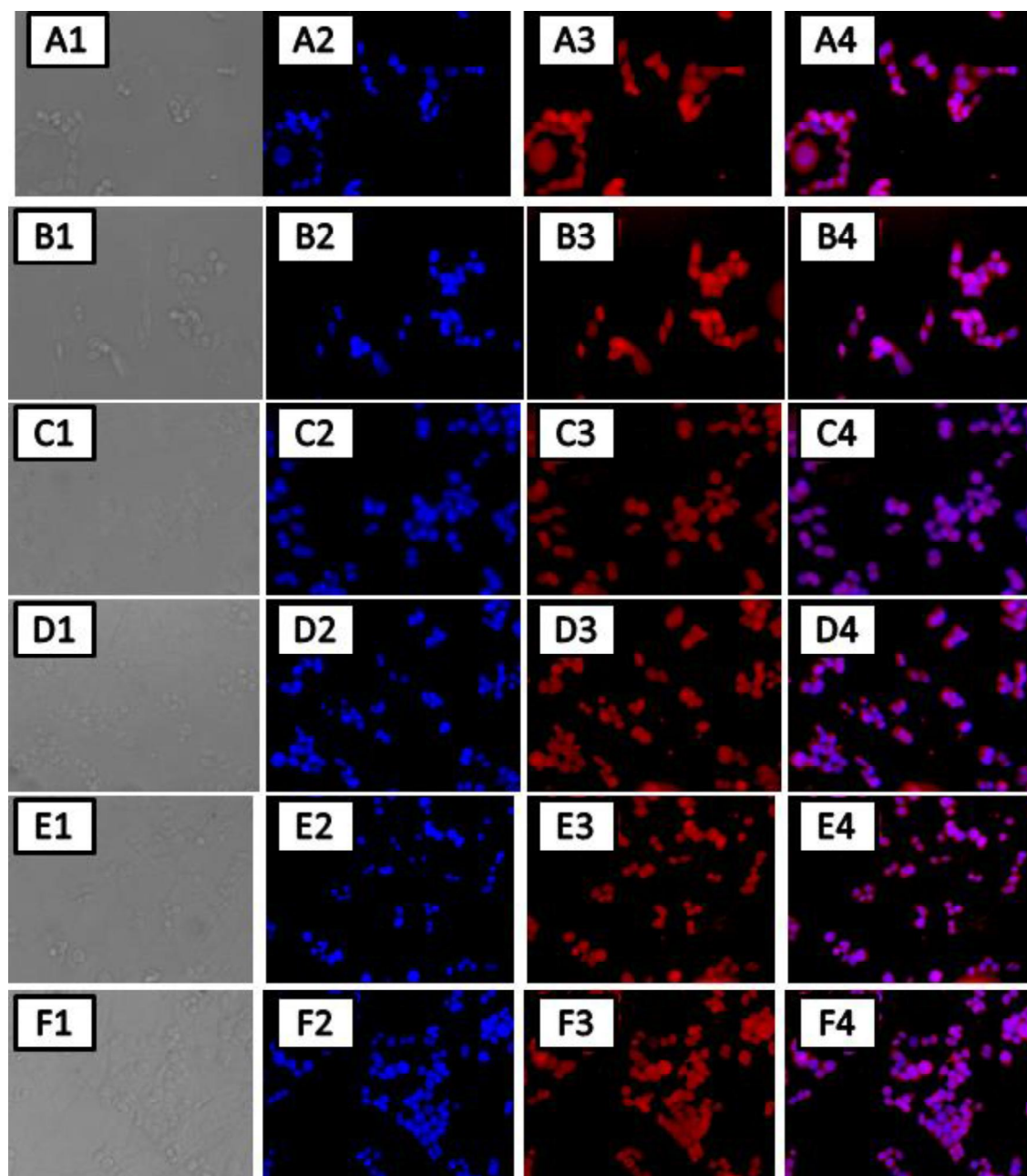
Figure 3. 16 Fluorescence microscope images of A) control, B) PCE0, C) PCE1, D) PCE2, E) PCE3, F) PCE4, and 1) Bright field, 2) DAPI, 3) Eosin, 4) Merged.

3.5   Conclusion

In this study, we developed NM using hydrophobic polymers PCL, PLA blended with hydrophilic natural protein, EA as it is less exploited for biomedical application though the properties are similar to that of FDA approved HSA. This study aims to replace the very expensive proteins with the affordable EA as it would be cost-effective in renewing and application. The developed nanomaterials with EA showed

an increase in hydrophilicity with the increasing in EA concentration, which was confirmed by the swelling and contact angle studies. Physicochemical properties such as FTIR, DSC, XRD, and fluorescence studies were analyzed to understand the hydrogen and functional interactions between the polymers and the MTz. After fabrication of NM with MTz, the crystalline peak of MTz disappeared, indicating strong functional interactions between EA and MTz and hence became amorphous after fabrication. The drug release studies showed the release of MTz was proportional to the concentration of MTz and hydrophilicity of the NM. As anticipated, the positive results of the MTT assay, cell proliferation, hemolysis, and *in vitro* antibacterial studies revealed that the developed NM with EA are suitable for tissue regeneration and therefore recommended for next level studies for the application.

3.6 References

[1] H. Li, C. Zhu, J. Xue, Q. Ke, Y. Xia, Enhancing the mechanical properties of electrospun nanofiber mats through controllable welding at the cross points, Macromolecular rapid communications 38(9) 1600723.

[2] S.K. Bhullar, D. Rana, H. Lekesiz, A.C. Bedeloglu, J. Ko, Y. Cho, Z. Aytac, T. Uyar, M. Jun, M. Ramalingam, Design and fabrication of auxetic PCL nanofiber membranes for biomedical applications, Materials Science and Engineering: C 81 334-340.

[3] R.P. Shadamarshan, H. Balaji, H.S. Rao, K. Balagangadharan, S.V. Chandran, N. Selvamurugan, Fabrication of PCL/PVP electrospun fibers loaded with trans-anethole for bone regeneration in vitro, Colloids and Surfaces B: Biointerfaces 171 (2018) 698-706.

[4] S. Mohandesnezhad, E. Alizadeh, Y. Pilehvar-Soltanahmadi, S. Davaran, A. Goodarzi, M. Khatamian, N. Zarghami, M. Samiei, M. Aghazadeh, In vitro evaluation of novel Zeolite-hydroxyapatite blended scaffold for dental tissue engineering, (2020).

[5] N. Eselini, S. Tirkes, A.O. Akar, U. Tayfun, Production and characterization of poly (lactic acid)-based biocomposites filled with basalt fiber and flax fiber hybrid, Journal of Elastomers & Plastics 52(8) (2020) 701-716.

[6] L. Huang, J. Tan, W. Li, L. Zhou, Z. Liu, B. Luo, L. Lu, C. Zhou, Functional polyhedral oligomeric silsesquioxane reinforced poly (lactic acid) nanocomposites for

biomedical applications, Journal of the mechanical behavior of biomedical materials 90 (2019) 604-614.

[7] S. Afshar, S. Rashedi, H. Nazockdast, M. Ghazalian, Preparation and characterization of electrospun poly (lactic acid)-chitosan core-shell nanofibers with a new solvent system, International journal of biological macromolecules 138 (2019) 1130-1137.

[8] S. Pisani, R. Dorati, B. Conti, T. Modena, G. Bruni, I. Genta, Design of copolymer PLA-PCL electrospun matrix for biomedical applications, Reactive and Functional Polymers 124 77-89.

[9] S.F. Hashemi, M. Mehrabi, A. Ehterami, A.M. Gharravi, F.S. Bitaraf, M. Salehi, In-vitro and in-vivo studies of PLA/PCL/gelatin composite scaffold containing ascorbic acid for bone regeneration, Journal of Drug Delivery Science and Technology 61 (2021) 102077.

[10] F.S. Fattahi, A. Khoddami, O. Avinc, Poly (lactic acid)(PLA) nanofibers for bone tissue engineering, J. Text. Polym 7 (2019) 47.

[11] T.V. Shah, D.V. Vasava, A glimpse of biodegradable polymers and their biomedical applications, e-Polymers 19(1) (2019) 385-410.

[12] S. Liu, Y.-Y. Xie, B. Wang, Role and prospects of regenerative biomaterials in the repair of spinal cord injury, Neural regeneration research 14(8) (2019) 1352.

[13] M. Ojaghi, F. Soleimanifar, A. Kazemi, M. Ghollasi, M. Soleimani, N. Nasoohi, S.E. Enderami, Electrospun poly-l-lactic acid/polyvinyl alcohol nanofibers improved insulin-producing cell differentiation potential of human adipose-derived mesenchymal stem cells, Journal of cellular biochemistry 120(6) (2019) 9917-9926.

[14] M. Salehi, A. Ai, A. Ehterami, M. Einabadi, A. Taslimi, A. Ai, H. Akbarzadeh, G.J. Ameli, S. Farzamfar, S. Shirian, In vitro and In vivo Investigation of poly (lactic acid)/hydroxyapatite nanoparticle scaffold containing nandrolone decanoate for the regeneration of critical-sized bone defects, Nanomedicine Journal 7(2) (2020) 115-123.

[15] W. Nie, Y. Gao, D.J. McCoul, G.J. Gillispie, Y. Zhang, L. Liang, C. He, Rapid mineralization of hierarchical poly (l-lactic acid)/poly (ε-caprolactone) nanofibrous scaffolds by electrodeposition for bone regeneration, International journal of nanomedicine 14 (2019) 3929.

[16] M. Nofar, D. Sacligil, P.J. Carreau, M.R. Kamal, M.-C. Heuzey, Poly (lactic acid) blends: Processing, properties and applications, International journal of biological macromolecules 125 (2019) 307-360.

[17] T. Xu, J.M. Miszuk, Q. Yao, Z. Liang, H. Sun, H. Fong, Electrospun three-dimensional nanofibrous scaffolds based on polycaprolactone for stem cells

differentiation and bone regeneration, Electrospun Polymers and Composites, Elsevier2021, pp. 179-215.

[18] S.M. Espinoza, H.I. Patil, E. San Martin Martinez, R. Casañas Pimentel, P.P. Ige, Poly-ε-caprolactone (PCL), a promising polymer for pharmaceutical and biomedical applications: Focus on nanomedicine in cancer, International Journal of Polymeric Materials and Polymeric Biomaterials 69(2) (2020) 85-126.

[19] K.K. Sankaran, U.M. Krishnan, S. Sethuraman, Axially aligned 3D nanofibrous grafts of PLA–PCL for small diameter cardiovascular applications, Journal of Biomaterials Science, Polymer Edition 25(16) (2014) 1791-1812.

[20] H.J. Haroosh, Y. Dong, D.S. Chaudhary, G.D. Ingram, S.-i. Yusa, Electrospun PLA: PCL composites embedded with unmodified and 3-aminopropyltriethoxysilane (ASP) modified halloysite nanotubes (HNT), Applied Physics A 110(2) (2013) 433-442.

[21] R.T. Zhu, M.H. Tan, P. Zhang, L. Zhang, X.M. Chen, F.W. Yang, Morphological Structure and Thermal Property of PLA/PCL Nanofiber by Electrospinning, Trans Tech Publ, pp. 418-422.

[22] A. Sadeghi, F. Moztarzadeh, J.A. Mohandesi, Investigating the effect of chitosan on hydrophilicity and bioactivity of conductive electrospun composite scaffold for neural tissue engineering, International journal of biological macromolecules 121 (2019) 625-632.

[23] G.K. Arbade, J. Srivastava, V. Tripathi, N. Lenka, T.U. Patro, Enhancement of hydrophilicity, biocompatibility and biodegradability of poly (ε-caprolactone) electrospun nanofiber scaffolds using poly (ethylene glycol) and poly (L-lactide-co-ε-caprolactone-co-glycolide) as additives for soft tissue engineering, Journal of Biomaterials Science, Polymer Edition 31(13) (2020) 1648-1670.

[24] C. Lei, H. Zhu, J. Li, J. Li, X. Feng, J. Chen, Preparation and characterization of polyhydroxybutyrate-co-hydroxyvalerate/silk fibroin nanofibrous scaffolds for skin tissue engineering, Polymer Engineering & Science 55(4) (2015) 907-916.

[25] H.-J. Jin, J. Park, R. Valluzzi, P. Cebe, D.L. Kaplan, Biomaterial films of Bombyx M ori silk Fibroin with Poly (ethylene oxide), Biomacromolecules 5(3) (2004) 711-717.

[26] J.B. Rose, S. Pacelli, A.J.E. Haj, H.S. Dua, A. Hopkinson, L.J. White, F.R.A.J. Rose, Gelatin-based materials in ocular tissue engineering, Materials 7(4) (2014) 3106-3135.

[27] Z. Gün Gök, M. İnal, O. Bozkaya, M. Yiğitoğlu, İ. Vargel, Production of 2-hydroxyethyl methacrylate-g-poly (ethylene terephthalate) nanofibers by electrospinning and evaluation of the properties of the obtained nanofibers, Journal of Applied Polymer Science 137(41) (2020) 49257.

[28] T. Li, L. Wang, Y. Huang, B. Xin, S. Liu, BSA loaded bead-on-string nanofiber scaffold with core-shell structure applied in tissue engineering, Journal of Biomaterials Science, Polymer Edition 31(9) (2020) 1223-1236.

[29] A. Prabhath, V.N. Vernekar, V. Vasu, M. Badon, J.E. Avochinou, A.D. Asandei, S.G. Kumbar, E. Weber, C.T. Laurencin, Kinetic degradation and biocompatibility evaluation of polycaprolactone-based biologics delivery matrices for regenerative engineering of the rotator cuff, Journal of Biomedical Materials Research Part A (2021).

[30] J. Hu, M.P. Prabhakaran, X. Ding, S. Ramakrishna, Emulsion electrospinning of polycaprolactone: influence of surfactant type towards the scaffold properties, Journal of Biomaterials Science, polymer edition 26(1) (2015) 57-75.

[31] C. Martins, F. Sousa, F. Araujo, B. Sarmento, Functionalizing PLGA and PLGA derivatives for drug delivery and tissue regeneration applications, Advanced healthcare materials 7(1) (2018) 1701035.

[32] M. İnal, Z. Gün Gök, G. Elif Kartal, N. Banu Verim, S. Murat, T. Apaydın, M. Yiğitoğlu, The Fabrication of Poly (Σ-caprolactone)–Poly (ethylene oxide) Sandwich Type Nanofibers Containing Sericin-Capped Silver Nanoparticles as an Antibacterial Wound Dressing, Journal of Nanoscience and Nanotechnology 21(5) (2021) 3041-3049.

[33] Y. Zheng, D. Su, J. Yuan, L. Zha, Y. Xiao, J. Che, Electrospun Poly (ε-Caprolactone)/Silk Fibroin Coaxial Core-Sheath Nanofibers Applied to Scaffolds and Drug Carriers, Polymer Engineering & Science 60(4) (2020) 802-809.

[34] W. Kalaithong, R. Molloy, T. Theerathanagorn, W. Janvikul, Novel poly (l-lactide-co-caprolactone)/gelatin porous scaffolds for use in articular cartilage tissue engineering: Comparison of electrospinning and wet spinning processing methods, Polymer Engineering & Science 57(8) (2017) 875-882.

[35] V. Švachová, V. Khunová, D. Pavliňák, Z. Fohlerová, L. Vojtová, The Effect of halloysite on structure and properties of polycaprolactone/gelatin nanofibers, Polymer Engineering & Science 57(6) (2017) 506-512.

[36] G.V.N. Rathna, J.P. Jog, A.B. Gaikwad, Development of non-woven nanofibers of egg albumen-poly (vinyl alcohol) blends: influence of solution properties on morphology of nanofibers, Polymer journal 43(7) (2011) 654-661.

[37] X. Xie, Y. Chen, X. Wang, X. Xu, Y. Shen, A. Aldalbahi, A.E. Fetz, G.L. Bowlin, M. El-Newehy, X. Mo, Electrospinning nanofiber scaffolds for soft and hard tissue regeneration, Journal of Materials Science & Technology (2020).

[38] J. Wang, J.A. Jansen, F. Yang, Electrospraying: possibilities and challenges of engineering carriers for biomedical applications—a mini review, Frontiers in chemistry 7 (2019) 258.

[39] S. Nagam Hanumantharao, S. Rao, Multi-functional electrospun nanofibers from polymer blends for scaffold tissue engineering, Fibers 7(7) (2019) 66.

[40] Z. Bao, C. Xian, Q. Yuan, G. Liu, J. Wu, Natural Polymer-Based Hydrogels with Enhanced Mechanical Performances: Preparation, Structure, and Property, Advanced healthcare materials 8(17) (2019) 1900670.

[41] H.S. Sofi, R. Ashraf, A.H. Khan, M.A. Beigh, S. Majeed, F.A. Sheikh, Reconstructing nanofibers from natural polymers using surface functionalization approaches for applications in tissue engineering, drug delivery and biosensing devices, Materials Science and Engineering: C 94 (2019) 1102-1124.

[42] A. Haider, S. Haider, M.R. Kummara, T. Kamal, A.-A.A. Alghyamah, F.J. Iftikhar, B. Bano, N. Khan, M.A. Afridi, S.S. Han, Advances in the scaffolds fabrication techniques using biocompatible polymers and their biomedical application: A technical and statistical review, Journal of Saudi chemical society 24(2) (2020) 186-215.

[43] I.R. Calori, G. Braga, P.d.C.C. de Jesus, H. Bi, A.C. Tedesco, Polymer scaffolds as drug delivery systems, European Polymer Journal 129 (2020) 109621.

[44] F. Tuğcu-Demiröz, S. Saar, S. Tort, F. Acartürk, Electrospun metronidazole-loaded nanofibers for vaginal drug delivery, Drug development and industrial pharmacy 46(6) (2020) 1015-1025.

[45] F. Cd, K. Ne, K.C. Lamp, Metronidazole. A therapeutic review and update, Drugs 54(5) (1997) 679-708.

[46] N. Dione, S. Khelaifia, J.-C. Lagier, D. Raoult, The aerobic activity of metronidazole against anaerobic bacteria, International journal of antimicrobial agents 45(5) (2015) 537-540.

[47] G.V.N. Rathna, J.P. Jog, A.B. Gaikwad, Development of non-woven nanofibers of egg albumen-poly (vinyl alcohol) blends: influence of solution properties on morphology of nanofibers, Polymer journal 43(7) 654-661.

[48] E. Fulkerson, C.J. Della Valle, B. Wise, M. Walsh, C. Preston, P.E. Di Cesare, Antibiotic susceptibility of bacteria infecting total joint arthroplasty sites, J Bone Joint Surg Am 88(6) (2006) 1231-1237.

[49] T. Amna, M.S. Hassan, N.A.M. Barakat, D.R. Pandeya, S.T. Hong, M.-S. Khil, H.Y. Kim, Antibacterial activity and interaction mechanism of electrospun zinc-doped titania nanofibers, Applied microbiology and biotechnology 93(2) 743-751.

[50] F.P. Tally, B.R. Goldin, N. Sullivan, J. Johnston, S.L. Gorbach, Antimicrobial activity of metronidazole in anaerobic bacteria, Antimicrobial agents and chemotherapy 13(3) (1978) 460-465.

[51] J.A. Obaleye, A. Lawal, Synthesis, characterization and antifungal studies of some metronidazole complexes, (2009).

[52] G.V.N. Rathna, J.P. Jog, A.B. Gaikwad, Development of non-woven nanofibers of egg albumen-poly (vinyl alcohol) blends: influence of solution properties on morphology of nanofibers, Polymer journal 43(7) 654.

[53] B. Tarus, N. Fadel, A. Al-Oufy, M. El-Messiry, Effect of polymer concentration on the morphology and mechanical characteristics of electrospun cellulose acetate and poly (vinyl chloride) nanofiber mats, Alexandria Engineering Journal 55(3) (2016) 2975-2984.

[54] M. Budai-Szűcs, A. Léber, L. Cui, M. Józó, P. Vályi, K. Burián, B. Kirschweng, E. Csányi, B. Pukánszky, Electrospun PLA Fibers Containing Metronidazole for Periodontal Disease, Drug Design, Development and Therapy 14 (2020) 233.

[55] D.W. Hutmacher, T. Schantz, I. Zein, K.W. Ng, S.H. Teoh, K.C. Tan, Mechanical properties and cell cultural response of polycaprolactone scaffolds designed and fabricated via fused deposition modeling, Journal of Biomedical Materials Research Part A 55(2) (2001) 203-216.

[56] M. Ceylan, S.-Y. Yang, R. Asmatulu, Effects of gentamicin-loaded PCL nanofibers on growth of Gram positive and Gram negative bacteria, (2017).

[57] A.K. Matta, R.U. Rao, K.N.S. Suman, V. Rambabu, Preparation and characterization of biodegradable PLA/PCL polymeric blends, Procedia materials science 6 (2014) 1266-1270.

[58] U. Hani, R.S. Bhat, H.G. Shivakumar, Formulation design and evaluation of metronidazole microspheres in a bioadhesive gel for local therapy of vaginal candidiasis, Lat Am J Pharm 30(1) (2011) 161-7.

[59] W. Wang, G. Caetano, W.S. Ambler, J.J. Blaker, M.A. Frade, P. Mandal, C. Diver, P. BÃ¡rtolo, Enhancing the hydrophilicity and cell attachment of 3D printed pcl/graphene scaffolds for bone tissue engineering, Materials 9(12) 992.

[60] Y.L. Patel, P. Sher, A.P. Pawar, The effect of drug concentration and curing time on processing and properties of calcium alginate beads containing metronidazole by response surface methodology, AAPS PharmSciTech 7(4) (2006) E24-E30.

[61] E.-R. Kenawy, G.L. Bowlin, K. Mansfield, J. Layman, D.G. Simpson, E.H. Sanders, G.E. Wnek, Release of tetracycline hydrochloride from electrospun poly (ethylene-co-vinylacetate), poly (lactic acid), and a blend, Journal of controlled release 81(1-2) (2002) 57-64.

[62] N. Killi, R.A. Dhakare, A. Singam, M. Lokanadham, H. Chitikeshi, R.V.N. Gundloori, Design and fabrication of mechanically strong nano-matrices of linseed oil based polyesteramide blends, MedChemComm 7(12) (2016) 2299-2308.

[63] M.H. El-Newehy, S.S. Al-Deyab, E.-R. Kenawy, A. Abdel-Megeed, Fabrication of electrospun antimicrobial nanofibers containing metronidazole using nanospider technology, Fibers and Polymers 13(6) (2012) 709-717.

[64] A.A. Shitole, P.W. Raut, N. Sharma, P. Giram, A.P. Khandwekar, B. Garnaik, Electrospun polycaprolactone/hydroxyapatite/ZnO nanofibers as potential biomaterials for bone tissue regeneration, Journal of Materials Science: Materials in Medicine 30(5) (2019) 1-17.

[65] S. Agrawal, P.R. Patel, R.V.N. Gundloori, Proteins as Nanocarriers To Regulate Parenteral Delivery of Tramadol, ACS Omega 4(4) (2019) 6301-6310.

CHAPTER 4

Bioinspired Hyaluronic Acid Based Nanofibers Immobilized with 3, 4-Difluorobenzylidene Curcumin for Treating Bacterial Infections
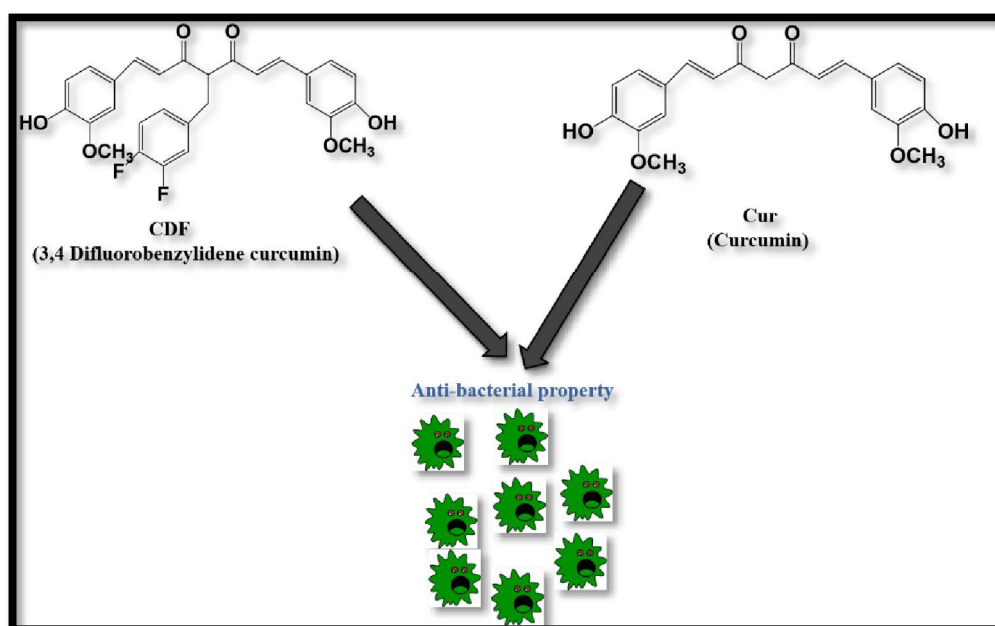
Chapter 4

This chapter deals with the fabrication of hyaluronic acid nanofibers by blending PHBV and PEO with immobilized Curcumin or 3, 4- difluorobenzylidene curcumin to evaluate its antibacterial property. Later, these nanofibers were also studied for *in vitro* drug release cell proliferation compared with immobilized curcumin blends.

4.1 Introduction

Critical bacterial infection has been an issue for the past several decades and a large number of synthetic antibacterial drugs, either in large doses or in combination with several drugs are being experimented[1-4]. With the advent of these new drugs, the traditional treatment using natural bioactive molecules (curcumin, piperine, cumin, neem etc.) has lost its significance in treating those bacterial infections. However, the natural bioactive molecules being multifaceted, its significance surfaced in treating a wide range of infections with a single molecule and therefore is being prioritised. For the past two decades, Cur (curcumin), which is an active ingredient of turmeric, is being exploited in pharmaceutics in addition to food applications due to its antimicrobial, anticancer, anti-inflammatory antifungal, and antioxidant properties. Cur being hydrophobic in nature is being derivatized or complexed with other bioactive molecules to enhance the bioavailability for better therapy[5-9]. The development of active Cur derivatives in different forms to improve bioavailability is well documented to treat various ailments[10, 11]. For example; nano-lioposme[12], SLN (solid lipid nanoparticles)[13], polymeric nanoparticles[14, 15], nanofibers, peptide and protein carriers[16, 17] etc.

As noted above, the development of natural Cur based therapeutics has shown high potential however, it has faced limitations due to its poor bioavailability and stability *in vivo*. In this regard, the synthetic analog, CDF (3, 4- Difluorobenzylidene Curcumin) has demonstrated a 16-fold improvement in stability and remarkable anticancer potency compared to its natural derivative, Cur[18-20]. Recently Iyer et al. have derivatized Cur to CDF and immobilized CDF in micelles of HA (hyaluronic acid) conjugated co-poly (styrene maleic acid) to treat pancreatic cancers, which exhibited superior anti-cancer properties[21]. Ever since Cur is widely used as an

antibacterial agent, nevertheless, derivatizing Cur may alter the pharmaceutical properties, so sustaining its property after functionalization is critical for effective treatment of cancer patients as they are immunosuppressed and are prone to bacterial infections. Therefore, it is pivotal to study the antibacterial properties of CDF; accordingly, we aimed at developing CDF immobilized nanomaterial to demonstrate the antibacterial response of CDF in treating infected wounds.

Nanotechnology is being considered as the advanced technology for drug delivery applications. The multifunctional nanomaterials immobilized with drugs such as nanoparticle, nanogels, nanofibers, dendrimers and micelles are being investigated to improve the therapeutic efficiency in patients[21-25]. For the past two decades, the research to design and development of nanofibers using natural and synthetic polymers has been progressing rapidly for a wide range of applications due to its unique properties[26-28]. Nanofibers for biomedical application is largely documented and even commercialized for various applications[29-32]. Nanofibers developed by electrospinning technique is becoming popular as developing those is easy, simple and cost effective. Further, the properties of nanofibers can be tailored conveniently using various polymers with bioactive agents. In our lab, we have developed and studied bioactive nanomaterials for tissue engineering applications [33]. The surface-to-volume ratio being large, the availability of the drug is always more for better therapy. Further, the nanofiber mats are highly porous, and aids in permeation of gases and also the network structure of the nanofibers mimics the extracellular matrix. Therefore, the nanofibers with antimicrobial drugs would be favourable for transdermal and tissue regeneration applications [34].In this study, we chose HA as one of the constituents to prepare nanofiber mat because it is a highly water soluble polysaccharide, which is an integral part of our body system. This is mostly embedded in connective, epithelial, nerval tissues and synovial fluids. So, developing a nanofiber mat using HA will undoubtedly mimic the tissue as it is hydrophilic, biocompatible, biodegradable, non-immunogenic and efficient to accommodate the exudates of the wound. The HA based bulk and nanomaterials are already reported for wound healing applications with good wound healing properties [35, 36]. HA being soft, mechanically weak and highly hydrophilic, there is a need for

HA to be blended with suitable polymers to balance the properties for end application. Therefore, it is being blended with various mechanically strong polymers[37-39]. For instance, we chose poly (3-hydroxybutyrate-co-hydroxyvalerate) (PHBV) and poly (ethylene oxide) (PEO) polymers to blend with HA. PHBV is polyester produced by bacteria, it is hydrophobic, biodegradable, non-toxic and non-immunogenic with mechanical strength that is comparable to polyethylenes[40]. Therefore, for the past two decades, PHBV has been explored for wound treatment, in orthopaedic systems and as controlled drug delivery systems[41]. PEO is an amphiphilic and inert polymer, which is non-toxic, resistant to protein adhesion, non-immunogenic and has the ability to solubilize the drug molecule; therefore, it is extensively used in pharmaceutical applications.

The main objective of this research findings is to immobilize CDF in the nanofiber mat of the blend of HA, PHBV and PEO and study the sustainability of the antibacterial property after derivatizing Cur to CDF. Accordingly, the various blends of HA/PHBV/PEO with and without CDF were prepared and fabricated nanofibers. Further, the surface morphology, physical and chemical properties of those were analysed. The antibacterial studies were done using *S. aureus* and the molecular docking studies of CDF and Cur were performed on dihydrofolate reductase (DHFR) enzyme of *S. aureus* bacteria, by using Autodock vina 4.0 version. Further *in vitro* drug release kinetics, cell viability, cell proliferation, haemolysis and scratch assay were done to understand the suitability of the nanofiber formulation for inhibition of bacterial growth.

4.2 Materials and methods

4.2.1 Materials

HA (Average Mw 10 kDa) was purchased from Life core Biomedical (Chaska, MN). Poly (3-hydroxybutyrate-co-3-hydroxyvalerate) (PHBV) was obtained from Good Fellow, Huntingdon, England. Polyethylene oxide (PEO) purchased from Alfa Aesar, (Mw 300,000). Cur was purchased from SD Fine. CDF was synthesized as described earlier[42]. Phosphate buffered saline (PBS), 3-(4,5-Dimethylthiazol-2-yl)-5 diphenyl tetrazolium bromide (MTT), fetal bovine serum (FBS), dulbecco's modified eagle's

medium (DMEM), zein, and trypsin were acquired from Sigma-Aldrich Co., St. Louis, USA. Antibiotics, glucose, 4′,6-diamidino-2-phenylindole (DAPI), Eosin and EDTA (ethylene diamine tetra acetic acid) were procured from Hi-Media Laboratories Ltd. Mumbai, India. Propanol, acetone and dimethyl sulfoxide (DMSO) were bought from Merck Ltd. Mumbai, India. The 3T3L1 (mouse embryonic fibroblast- adipose like cell line) cell line was procured from the National Centre for Cell Sciences (NCCS), Pune, India. All reagents, solvents, and media for antibacterial studies and components of buffer for drug release studies were of analytical grade and were obtained from local chemical companies in India.

4.2.2   Fabrication and crosslinking of nanofibers

Nanofibers were prepared by solution electrospinning. Solution A was prepared by dissolving PEO (0.5% w/v) in water at 50 ºC to this solution 3% (w/v) of HA was added and kept on a roller mixer for 24 h for uniform mixing. Solution B was prepared by dissolving PHBV (6.5% w/v) in TFE (2,2,2-Trifluoroethanol) and ethanol (100 µL:900 µL), after 30 min of vortex the solution was left on a roller mixer for 24 h (B). The homogenous solutions, A and B (A total of 10% of polymer concentration was formed) were mixed and kept in a roller mixer for at least 12 h to achieve a uniform solution mixture. The solution mixture was taken in a 5 mL plastic syringe fitted with a needle diameter of 0.90 × 38 mm, which was placed on a syringe pump for pumping the solution mixture. The flow rate of the solution was set to 0.5 mL/h and applied at 20 kV voltage of by connecting a positive electrode to the needle. The negative electrode was connected to a metal collector to collect nanofibers, and the distance between the needle tip and plate collector was set at 15 cm. The tailored nanofibers were then peeled off from aluminium foil and dried in a vacuum oven at 40 ºC for 4 h to remove any residue of solvents. To load, the drug was added in solution B; three different concentrations of drug were prepared at 5, 10 and 15% w/w of the total polymer weight. Different concentrations of hyaluronic acid nanofiber, with and without drug, were fabricated, as shown in **Table 4.1**.

Table 4. 1 Different concentrations of blends of hyaluronic acid with and without drug for fabrication of nanofibers

Formulation	PHBV (% w/v)	PEO (% w/v)	Hyaluronic acid (% w/v)	Drug w.r.t total polymer weight (% w/w)	
				Cur	CDF
HA 1	9	-	1		
HA 2	6.5	0.5	3		
HA 3	6.5	0.5	3	5	
HA 4	6.5	0.5	3	10	
HA 5	6.5	0.5	3	15	
HA 6	6.5	0.5	3		5
HA 7	6.5	0.5	3		10
HA 8	6.5	0.5	3		15

To crosslink the nanofibers, 5% of $CaCl_2$ was prepared in distilled water. Fabricated HA nanofibers were immersed in 5% of $CaCl_2$ solution for 24 h. After 24 h crosslinking, an excess amount of $CaCl_2$ was washed off by immersing the nanofibers in distilled water. The nanofibers were later characterized by a field emission scanning electron microscope (FE-SEM) to analyse their morphology and size.

4.3   Characterization of materials

The surface morphology and diameter of the fabricated nanofibers of HA with and without Cur and CDF were analysed using field emission scanning electron microscope (FE-SEM), HITACHI S-4800. Before imaging, the sample used for FE-SEM observations were prepared by mounting a small portion of a non-woven nanofiber mat on a stub. Later, the mounted stubs were sputtered with gold using a Coating Unit (FEI, USA), and Tungsten filament -(W) was used as an electron source with a resolution of 3 nm. Image J software was used to analyse the average diameter of nanofibers, The glass transition temperature (T_g) and melting temperature (T_m) were determined for crude form of Cur, CDF, PHBV, PEO and fabricated electrospun nanofibers using the DSC instrument (Model Q10 DSC, TA Instrument, USA). About 5 to 6 mg of the sample (polymer/NM) was loaded in a DSC pan, and the pan was

sealed by applying pressure. In the first cycle, the sample was equilibrated to -70 °C for 2 min and later heated to 100 ºC at a rate of 10 ºC/min. In the second cycle, the sample was heated -70 °C to 250 °C at a rate of 10 °C/min. The thermogram was run under the nitrogen atmosphere at a flushing rate, 50 mL/min. ATR-FTIR spectroscopy was performed for Cur, CDF, PHBV, PEO and blends of electrospun nanofibers using Perkins Elmer, Spectrometer 1, FTIR diffuse reflectance (DRIFT, mode, USA). Spectra were collected between 400 and 4000 cm^{-1}, each spectrum was an average of 16 scans.

4.3.1 Drug release studies

The drug release study of Cur (15%) and CDF (15%) loaded nanofibers was done in an Equation 3 shaking incubator for a period of 240 h. Briefly, in a sample vial, 10 mg of drug loaded nanofibers were placed in 5 mL of phosphate buffer (pH 7.4), which contained 20% of methanol. The shaking incubator was set at 50 rpm, at 37 ± 2 °C. At each interval of time, 1 mL of buffer solution was removed from the sample bottle for the estimation of MTz and replaced with 1 mL of fresh buffer. The CDF and Cur containing sample buffer were analyzed by UV visible spectrophotometry (Shimadzu UV-1601PC) at a wavelength of 420 nm to determine the amount released at each interval and extrapolated the quantity using a standard calibration curve of CDF and Cur. The release studies were done in duplicates, and all the samples were analyzed twice for reproducibility. The results were presented in terms of cumulative percent release as a function of release time. Equation 1 shows the method for obtaining the cumulative percent of CDF and Cur released.

$$\text{Cumulative amount of drug released } (\%) = \frac{Mt}{M\infty} \times 100 \hspace{2cm} \text{Equation 1}$$

Where, M_t is the amount of CDF and Cur released at time t, M_∞ is the amount of CDF and Cur loaded in NM prior to electrospinning of the respective solution.

4.3.2 Antibacterial studies

The antibacterial activity of Cur and CDF raw was estimated and Cur and CDF loaded nanofiber mats was investigated against *Staphylococcus aureus* (*S. aureus,* ATCC

25923) by optical density method. Briefly, the bacterial strain was inoculated in 15 mL of nutrient broth for 12 h at 37 °C on a rotator shaker. The bacterial growth was monitored using an Ultraspec 10 cell density meter (BIOCHROM LTD, Cambridge, England, UK). The OD of the bacterial solution was recorded 1 at 620 nm, which corresponds to the concentration of 10^8 CFU mL^{-1}. From this solution, 40 μL was added to a freshly prepared 10 mL nutrient broth solution as a control. Similarly, the test samples were prepared (with and without Cur, CDF nanofiber mat of 1 cm^2) and incubated at 37 °C in a rotary shaker at 150 rpm. The growth rates were monitored by measuring the OD of the test samples with respect to time at regular intervals up to 12 h.

4.3.3 Molecular docking

In order to compare the binding affinity of Cur and CDF molecules with the dihydrofolate reductase (DHFR) enzyme receptor of *S.auerus*, docking studies were performed. Dihydrofolate reductase (DHFR) enzyme is an important protein of *S.auerus* that helps in the reduction of dihydrofolate to tetrahydrofolate through NADPH, which is the main pathway for the production of intracellular purines (adenine and guanine). The replication of DNA can be terminated by inhibition of DFHR enzyme leading to bacterial cell death[43]. The ligand and receptor 3D structures were energy-minimized using Swiss-pdb viewer 4.1.00 (Swiss institute of bioinformatics). Then, a conformational analysis of both the ligands, i.e. Cur and CDF were performed in order to select its global minimum, using Open Babel version 2.3.2. Docking studies were performed using AutoDock Vina (Scripps Research, La Jolla, CA, USA), a program designed for the prediction of the binding among small molecules and the receptor with a known 3D structure[44]. Auto Dock Tools 4.0 were used to prepare the ligands and the macromolecule, i.e. DHFR, which was obtained from Protein Data Bank with PBD entry 3FRB. Both ligand and receptor were prepared by removing all the water molecules. Kollman charges were added to the receptor molecule. Similarly, Gasteiger charges and polar hydrogen were added to the ligands and non-polar hydrogens were merged.

Molecular docking was performed using Lamarckian Genetic Algorithm (LGA)[45], keeping the receptor molecule rigid throughout the docking simulation, and the rest of the docking parameters were set to default values. AutoDock Tools, PyMOL[46, 47] and Discovery Studio Visualizer version 20.1.0.19295 were used for post docking analysis to compare the binding energy and interacting residues between DHRF and Cur and DHRF and CDF.

4.3.4 Hemolysis assay

Blood was acquired from human volunteers from National Chemical Laboratory Health Centre, Pune, India and the blood sample was stabilized using EDTA. Red blood cells (RBCs) were isolated from whole blood using density gradient centrifugation. Briefly, 5 mL blood was slowly added in 5 mL of PBS saline solution and then centrifuged at 2000 rpm for 30 min. The supernatant was discarded, and red blood cells (RBCs) were collected. Further, the RBCs were washed thrice with phosphate buffer saline of pH 7.4 and centrifuged at 2000 rpm for 30 min. A stock solution of RBCs was prepared without serum at 2% (v/v) using phosphate buffer of pH 7.4. Later, 2 mL of the diluted RBCs suspension was transferred to each of the 2 mL eppendrof tubes containing 10 mg of nanofibers loaded with 5, 10, and 15% of Cur and CDF and also nanofibers without the drugs. The negative and positive blood samples were prepared in a similar manner without nanofibers in phosphate buffer, and de-ionized water, respectively and all the tubes were then incubated for 2 h at 37 °C. After every 30 min during the incubation, the samples were shaken gently to re-suspend the precipitated RBCs and centrifuged at 1500 g for 10 min at room temperature. The supernatant was then placed in another 96-well microtiter plate, and the released haemoglobin (Hb) was measured spectrophotometrically at 541 nm using a microtiter plate reader (Tecan) in PBS. The percentage of RBC lysis was calculated based on the assumption that 100% RBC lysis resulted by mixing blood with distilled water at 1:1 (v/v) ratio.

The hemolytic percentage was calculated using Equation 2 as:

$$HP(\%) = \frac{Dt - Dnc}{Dpc - DNC} \times 100 \qquad \text{Equation 2}$$

Where, Dt is the absorbance of the test samples, Dpc and Dnc are the absorbance's of the positive and negative controls, respectively.

4.3.5 Cell proliferation study

L929 mouse fibroblast cells were cultured in DMEM, Low Glucose, Pyruvate, HEPES supplemented with 10% FBS and maintained at 37 °C in 5% CO_2 humidified atmosphere. Cellular growth on the fabricated nanofibers was studied by seeding L929 cells onto sterilized nanofibers. Briefly, disc-shaped nanofibers of 5 mm diameter were cut and sterilized by dry autoclave and by UV exposure for 30 min. Triplicates of HA 2-HA 8 discs were inserted in each well of a non-treated, non-adherent, sterile 96 well plate. A confluent 25 cm^2 flask of L929 was trypsinized after discarding media and washing with sterile phosphate buffer saline (PBS). Cells were harvested and counted with the aid of a hemocytometer, 1 x 10^4/100 μL cells were seeded in each well with the sample. Post incubation for 48 h at 37 °C in 5% CO_2 atmosphere, the media in the wells was siphoned out, and the nanofibers in the wells were washed thrice with sterile PBS. 300 μL of 5% paraformaldehyde solution was added in each well and incubated at RT for 15 min. After incubation, paraformaldehyde was flicked off, and the nanofibers were washed with PBS. From the DAPI dye stock (1 mg/mL) 0.5 μL/5 mL PBS was prepared, 300 μL was added to the wells and incubated for 15 min at RT in the dark. Finally, PBS wash was given and the nanofibers were observed under an epifluorescent microscope.

4.3.6 Scratch assay

In vitro wound healing is generally done following the migration assay method. Accordingly, L929 cells were seeded in 96 well culture plates at a density of 1×10^5 cells/mL and incubated for 16 h at 37 °C in 5% CO_2 atmosphere in order to achieve a monolayer. Using a 200 μL micropipette tip, the monolayer was scratched in a straight line manually to create a scratch. The detached cell debris were removed and the well was washed with 300 μL of the growth medium. The respective nanofiber mats containing Cur and CDF were carefully placed in the wells and supplemented with the growth medium. Upon incubation, the closure of gaps by cell migration and growth was observed using an inverted microscope after 24 and 48 h.

4.3.7   MTT assay

Cytotoxicity studies of fabricated nanofibers were estimated by MTT assay in L929 cells. The monolayer of cells was grown in DMEM containing 10% FBS was trypsinized and the cell count was adjusted to 1.0×10^5 cells/mL. To each well of the 96 well microplates, 0.1 mL of the diluted cell suspension (approximately 10,000 cells/100 µL) was added. After 24 h, when a monolayer was formed, the media was flicked off and the monolayer was washed with sterile PBS and UV sterilized raw materials PHBV, PEO, HA, HA 1 and HA 2 were added to the wells. The plates were then incubated at 37 ºC for 48 h under 5% of CO_2 humidified atmosphere. After 24 h, the media in the wells was substituted with 110 µL of DMEM containing 10% v/v MTT reagent (5 mg/mL stock in PBS) and again incubated for 4h in the dark. After 4h, the supernatant in the wells was removed and 100 µL of DMSO was added and the plates were gently shaken to solubilize the formazan thus formed. The absorbance was measured using a microplate reader at a wavelength of 550 nm, and the relative percentage of cell viability was calculated.

4.3.8 Cell adhesion

Cellular adhesion on the nanofibers was studied by seeding L929 cells onto sterilized nanofibers. As explained in section **4.3.7**, sterilized triplicates of H1-H8 discs were inserted in each well of a non-treated, non-adherent sterile 96 well plate. Cells were harvested from a confluent L929 flask, and 10,000 cells/100 µL were seeded in each well with the sample. Negative control was also prepared in triplicates by seeding cells without the sample in a treated 96 well plate. The plates were incubated at 37 °C under humidified 5% CO_2 atmosphere for 48 h. Post incubation, the media in the wells was siphoned out, and the nanofibers in the wells were washed with sterile PBS. Later added 50 µL of trypsin to the plates and incubated for 6-8 min at 37 °C in 5% CO_2 atmosphere. Subsequently, added 50 µL of DMEM-FBS to both the plates and properly mixed the contents of the well with the aid of a micropipette. Using a hemocytometer the cell number was counted, and relative cell adherence was calculated using the cell count in the control plate as a reference.

4.4   Results and Discussion

4.4.1   Morphology of nanofibers by FE-SEM

The surface morphology and diameter of the nanofibers of various compositions as listed in **Table 4.1** were evaluated by FE-SEM. After optimizing, the spinning parameters were fixed for all the compositions. HA is a highly hydrophilic and viscous polymer, so beyond 3% the HA was not suitable for blending. It is reported that HA alone cannot form nanofibers, so we prepared the blends of HA using PEO and PHBV. The total polymer weight of the blend was maintained at 10% and varied the concentration of HA while keeping the PEO and PHBV 0.5 and 6.5%. It was observed that the morphology of fabricated nanofiber was mainly influenced by the concentration of PHBV. PEO being amphiphilic, favoured cell interactions and assisted in the formation of smooth nanofibers. Two different compositions of blend nanofibers (HA 1, HA 2) were prepared and subjected to electrospinning. Out of these compositions, HA 1 and HA 2 compositions produced nanofibers that were randomly oriented, smooth and bead free. The average diameter of nanofibers ranged from 300 to 400 nm (**Fig. 4.1** and **Fig. 4.2**). HA 2 was selected for loading the Cur and CDF because the HA 1 nanofibers were brittle due to the high amount of PHBV (9%) content in nanofibers. The HA nanofibers were crosslinked with $CaCl_2$ to sustain stability. Ca^{2+} ions being positively charged, they interacted with the negatively charged carboxyl group of the glucuronic acid residue of HA[48, 49], thereby providing stability of the nanofibers.
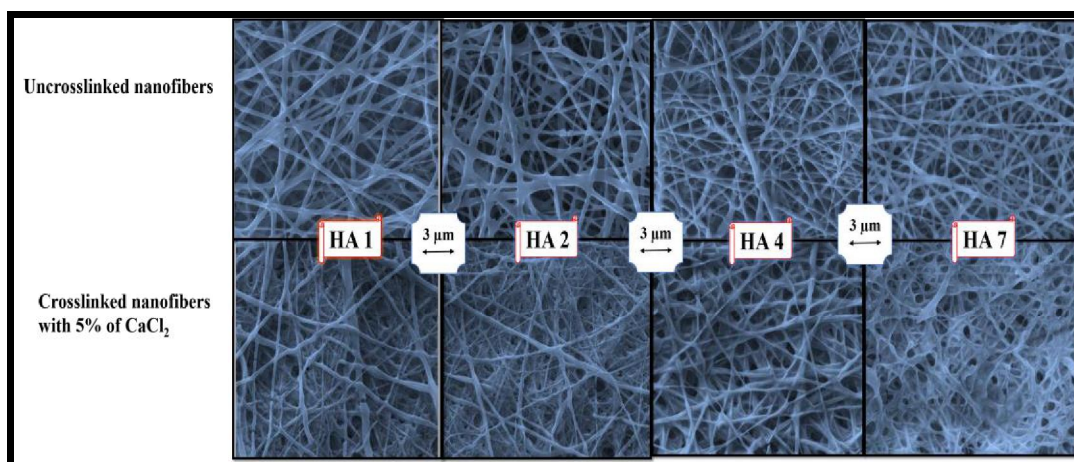
Figure 4. 1 FESEM micrographs at 15000x revealed the surface morphology of electrospun nanofibers of HA 1, HA 2, HA 4, and HA 7 without and with crosslinking of 5 % CaCl₂ respectively.
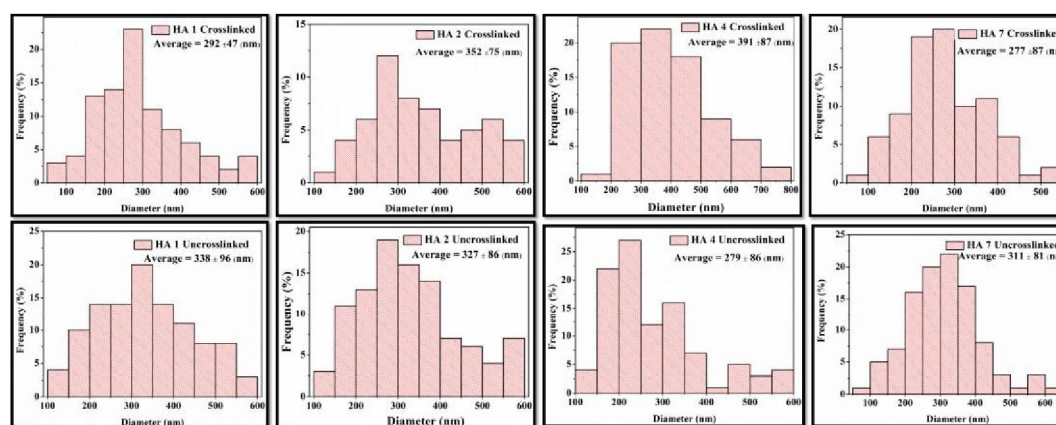
Figure 4. 2 Size distribution was estimated by Image J software for electrospun nanofibers of HA 1, HA 2, HA 4, and HA 7 without and with crosslinking of 5 % CaCl2 respectively.

4.4.2 FTIR

The complexation of HA with PHBV, PEO, CDF and Cur in nanofibers were determined by FTIR, as shown in **Fig. 4.3**. The raw HA showed a fingerprint peak of phenolic N–H stretching at 3408 cm⁻¹, whereas C=O stretching and N–H bending peaks were observed at 1609 cm⁻¹. At 1408 cm⁻¹ C–H₂ bending was observed[50]. For neat PHBV, characteristic peaks were detected at 2978 cm⁻¹ and 2931 cm⁻¹, which were symmetric and asymmetric stretching of CH₃ group and at 1726 cm⁻¹ due to

carbonyl stretching[51]. PEO spectrum showed O–H stretching vibration at 3500 cm^{-1}, whereas C–H stretching was observed at 2896 cm^{-1} and 1478 cm^{-1}. A peak at 1105 cm^{-1} was due to O–H stretching vibration of the alcoholic and C–O–C ether linkage [52]. For Cur, a characteristic peak was observed at 3508 cm^{-1} which was due to phenolic O–H stretching vibration. At $1633 cm^{-1}$ and 1614 cm^{-1} C=O stretching and phenolic ring stretching vibrations were observed, respectively. At 1428 cm^{-1} peak of C–H bending vibration, 1278 cm^{-1} peak of C–O stretching, 1024 cm^{-1} peak of C–O–C stretching vibrations were recorded[53]. CDF showed a peak 3295 cm^{-1} which was due to phenolic O–H group and at 1570 cm^{-1} showed C–H bending vibration, 1421 cm^{-1} showed a C–O stretching. And 980 cm^{-1} peak depicted C–O–C stretching vibrations[54]. HA 2 recorded a broad peak at 3444 cm^{-1} due to N-H stretching of HA and O–H stretching vibration of PEO was observed, but the broad peak got subdued. The peak at 2978 and 2931 cm^{-1} is due to the CH_3 group of PHBV; another carbonyl stretching peak of PHBV was observed at 1708 cm^{-1}. PEO was further confirmed when the peak was observed at 1376 cm^{-1} and 1125 cm^{-1}. In HA 5 and HA 8, peak of C–O–C stretching vibrations were observed at 1046 cm^{-1}, at 1268 cm^{-1} peak of C–O stretching and downshift of C–H showed peak from 1512 cm^{-1} to 1428 cm^{-1} which ascertained the presence of Cur and CDF.
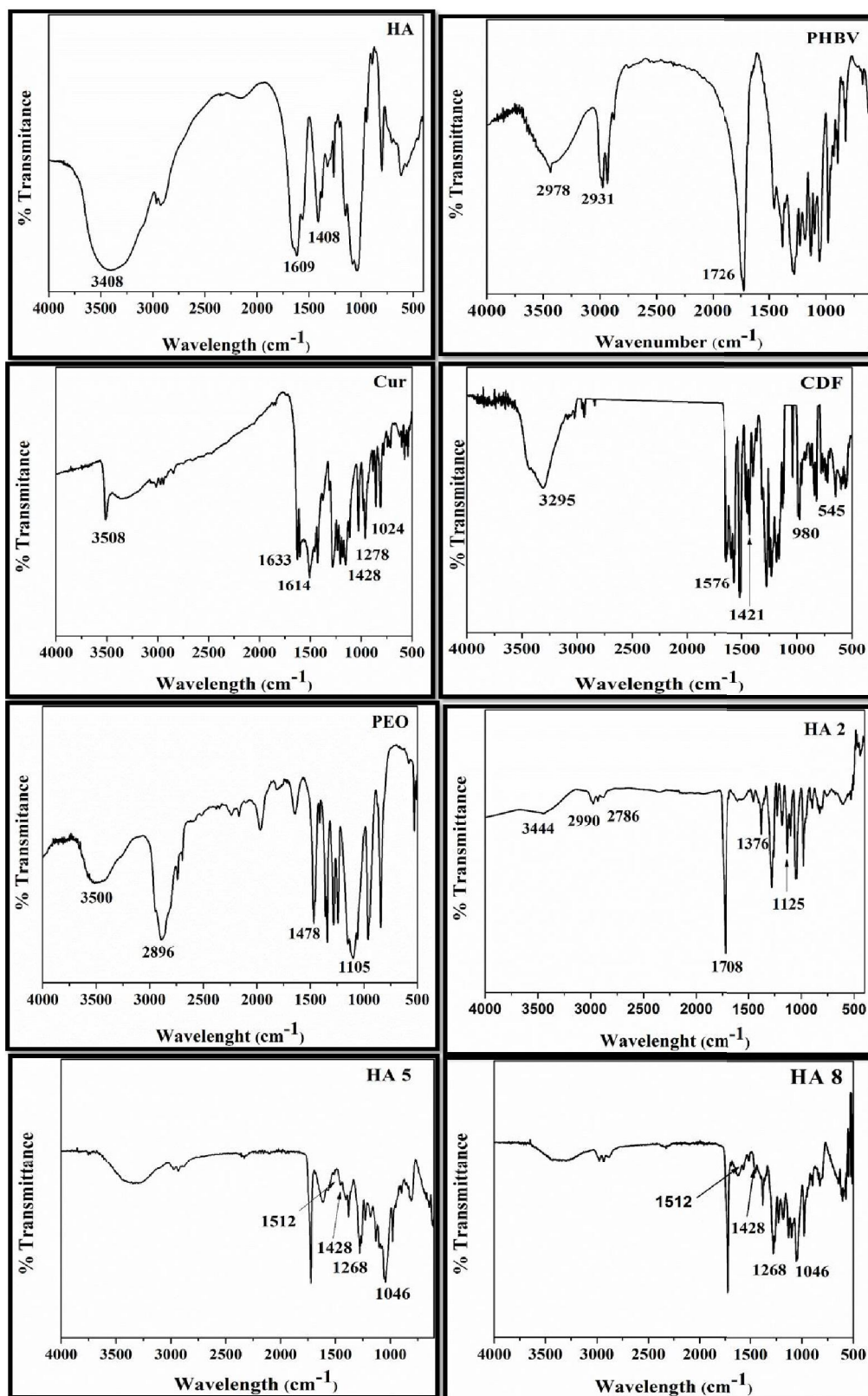
Figure 4. 3 FTIR spectra of developed nanofibers HA 2, HA 5 and HA 8 and raw

material, Cur, PEO, HA, HA, Cur, and CDF

4.4.3 DSC

The thermal properties of electrospun nanofibers and polymers were studied by DSC (**Fig. 4.1**). PHBV being semi-crystalline polymer, and endothermic peak due to the melting temperature (T_m) of PHBV was recorded at 158 °C, which was similar to that of the reported value.[55]. PEO is a semi crystalline polymer hence showed a sharp endothermic peak at T_m 66°C and T_g at -60[56, 57]. The sharp endothermic peak of CDF and Cur showed the melting temperature at 218 °C and 178 °C, respectively[54, 58]. The T_g of PEO was shifted from -60 to -44 °C in HA 2, HA 4 and HA 7 which suggested the prepared polymers were well blended. Further, two endothermic peaks were observed for fabricated nanofibers from that HA 2 showed a peak at 67 °C, which is due to PEO. The slight increase in T_m may be due to crosslinking of nanofibers with Ca^{2+}, and for HA 4 (55 °C) and HA 7 (56 °C) the decrease in T_m might be because of the electrospinning process, and this also attributed to the entanglements between the HA and PEO molecular chains, which led to the confined crystallization of PEO which was also reported in the literature[59]. In the blends, the T_m of PHBV (158 °C) did not vary much for example; T_m was158 °C for HA 2, 157 °C for HA 4 and 159 °C for HA 7 nanofiber mats. The melting peak of Cur and CDF disappeared after immobilization and fabrication of nanofibers. This indicated that the drugs interacted with the polymers and became amorphous during the process of fabrication of nanofibers. Similar studies were reported in our earlier investigation[33].
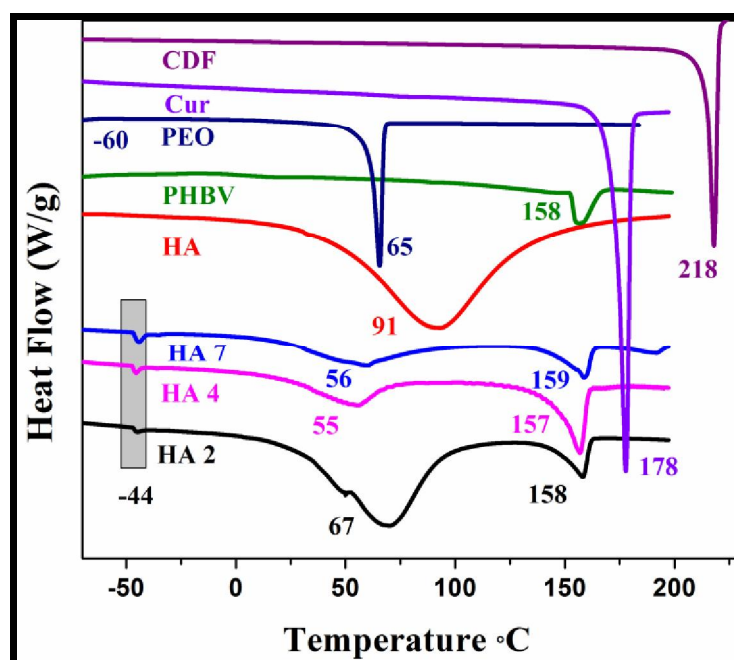
Figure 4. 4 DSC thermal analysis was studied under dry nitrogen of different compositions PHBV, PEO, HA, CDF, Cur, HA 2, HA 4, and HA 7.

4.4.4 Drug release

The *in vitro* drug release studies were carried out by maintaining physiological pH 7.4 and temperature 37 ± 1 ºC in a bath sonicator. The release of CDF and Cur from the respective nanofiber mats are shown in **Fig. 4.5**. *In vitro* release studies showed a significant difference in the release of both CDF and Cur from the respective nanofibers. In the first hour of the release study, Cur and CDF recorded a release of 4 and 1.4%, respectively. After 240 h, 37 and 25% of Cur and CDF were released from the respective nanofiber mats. In both cases, a slow and sustained release was observed. CDF being more hydrophobic in nature, the release rate was slow as compared to Cur. Hence, the exhaustion rate of CDF from nanofiber mat being slow, the benefit of application for wound healing is considered to be more effective than the nanofiber loaded with Cur.
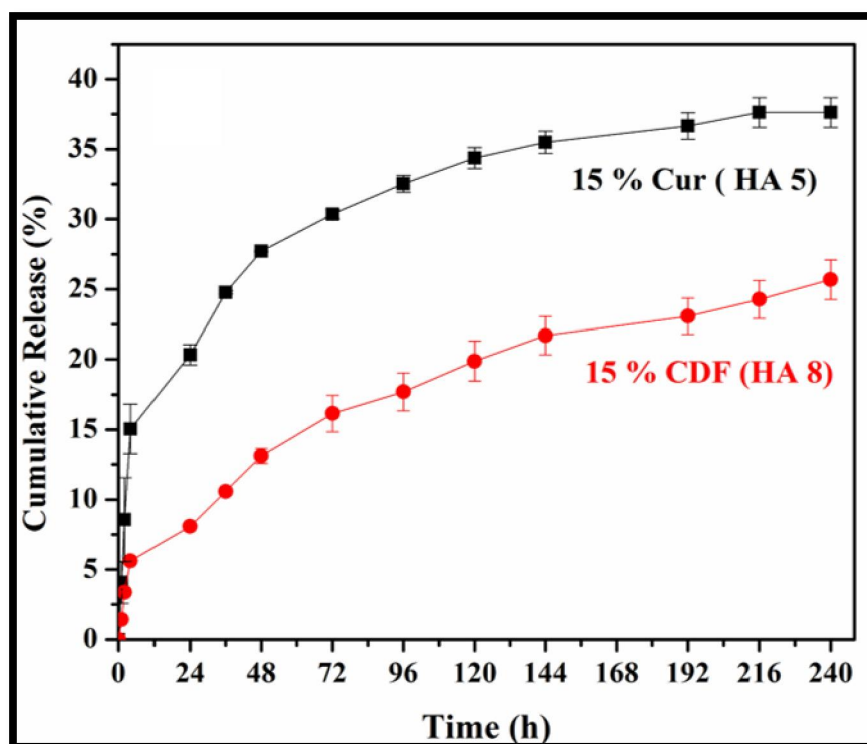
Figure 4. 5 Drug release studies in pH 7.4 at 37 ºC of HA 5 and HA 8 nanofibers in phosphate buffer solution pH.7.4.

4.4.5   Antibacterial studies

The study of the antibacterial property of electrospun nanofibers with Cur (5, 10 and 15%) and CDF (5, 10 and 15%) and alone CDF and CUR was evaluated using Gram-positive bacteria, *S.auerus* (**Fig.4.6**). As mentioned in the experimental section, optical density method was used for testing. The OD was measured at 620 nm at different intervals of time up to a period of 12 h. It was observed that with increase in the concentration of CDF and Cur in nanofibers, bacterial growth decreased (**Fig. 4A** and **Fig. 4B**). The OD measurements of pure CDF and Cur at the concentration of 2 mg mL^{-1} was also studied to understand the difference in the antibacterial property in their native form to confirm the antibacterial property before and after modification of Cur. From **Fig. 4C** it was observed that both Cur and CDF showed similar antibacterial properties against *S. aureus*. Finally, we conclude that CDF and Cur loaded nanofibers and alone CDF and Cur have almost the same bactericidal activity in *S.auerus*.
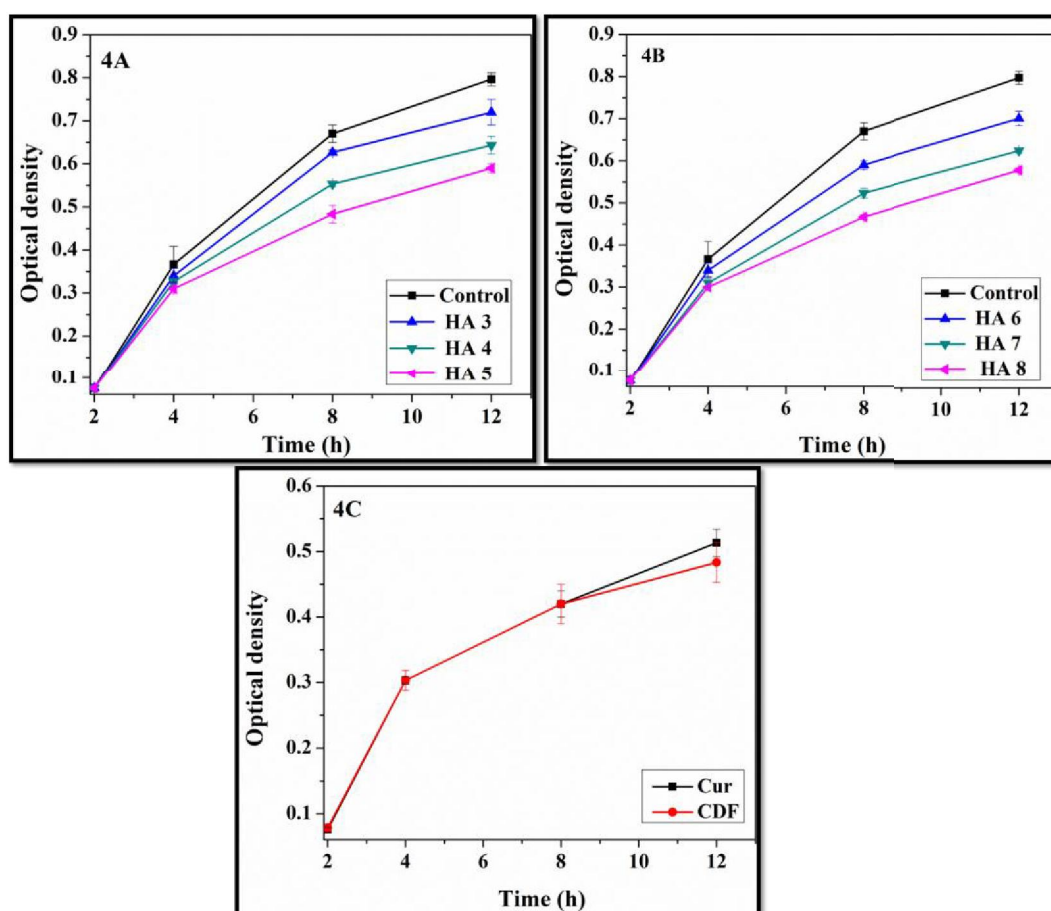
Figure 4. 6 Antibacterial studies were studied of alone Cur drug loaded nanofibers HA 3, 4, 5 (**Fig. 4A**). Antibacterial studies were studied of control (without drug loaded nanofibers) alone CDF drug loaded nanofibers HA 6, 7, 8 (**Fig. 4B**). And in **Fig. 4C** depicted the anti-bacterial studies of raw CDF and Cur. All studies were done by using *S.aureus* (Gram-positive) bacteria.

4.4.6 Molecular docking

The comparative docking studies of the ligands, Cur and CDF with the DHFR receptor (3FRB from Protein Data Bank) were performed, using AutoDock Vina, to see their mode of interaction. The obtained binding energies of both the ligands against DHFR are presented in Table 1S. The main residues of DHFR that have shown a more significant interaction was either by hydrogen bonding or electrostatic interactions with the curcumin like Ala58, Thr455, Phe895, Ile494, Val50, Leu191 and Lys442 (**Fig. 4A**). Cur shows interaction by conventional hydrogen bonding with OH group of phenol ring at THR455 active residue of enzyme and through C=O

ketone with ALA58. Van der Waals contacted on the active side residues of enzymes. One of the phenyl ring of Cur shows interaction by Pi-Pi stacked and Pi-sigma on the active side of residue of PHE895 and ILE494, respectively. Further, a carbon-hydrogen bond is formed at residue VAL50, whereas Leu191and Lys442 show interaction through pi-alkyl or alkyl bonds. The docking studies suggest that Cur is predominantly interacted with DHFR protein by hydrogen-bonding, Pi sigma, P=Pi stacked and electrostatic bonds.

For CDF, the active site residue of DHFR has well interacted with CDF on phenolic ring of OH group by conventional hydrogen bond at Gln179. The ligand-receptor show numerous interacting residues forming Alkyl and Pi- Alkyl bonds at Lys442, Ile494, Phe895, Tyr947, Val50, and Ile132 and Pi-Sigma bonding Leu191 as demonstrated in **Fig. 4B**. In conclusion, from the binding energies obtained (Table 1S), we can say that CDF showed almost similar affinity like Cur towards DHFR. CDF's affinity towards DHFR suggests its possible mechanism against *S.aureus* as even after modification, it has not lost its property hence can be used for better therapeutics against the bacteria.

Table 4. 2 Binding energies obtained from docking studies.

Binding Energy (kcal/mol)		
	Cur	**CDF**
DHFR	-8.3	-10.5
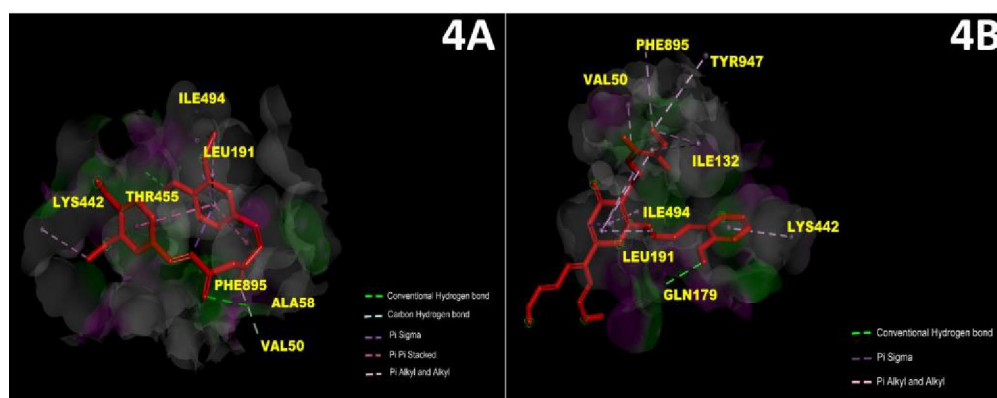
Figure 4. 7 Dihydrofolate reductase (DHFR) enzyme of *S. aureus* complexed with Cur (3FRB from Protein Data Bank). DHFR is docked with Cur was visualized in 3D structure (Discovery Studio Visualizer version 20.1.0.19295). Cur interacted with active site residue of was due to conventional hydrogen bond (Green dashed line), carbon hydrogen bond (Light blue dashed line), Pi sigma (Purple dashed line), Pi Pi stacked (Pink dashed line) and Pi alkyl, alkyl (light pink dashed line) and Van der Waals forces (**Fig. 4A**). Dihydrofolate reductase (DHFR) enzyme of *S. aureus* complexed with CDF (3FRB from Protein Data Bank). DHFR is docked with CDF was visualized in 3D structure (Discovery Studio Visualizer version 20.1.0.19295). CDF interacted with active site residue of was due to conventional hydrogen bond (Green dashed line), Pi sigma (Purple dashed line), Pi alkyl, alkyl (light pink dashed line) and Van der Waals forces (**Fig. 4B**).

4.4.7 Hemolysis

Evaluating the biocompatibility of developed material is an essential part for biomedical application. Accordingly, we performed hemolysis assay as per our earlier reported literature.[60] As explained in the experimental section, the negative and positive control and the various compositions from HA 1 to HA 8 were subjected to hemolysis test (**Fig. 4.8**). The results showed 0% hemolysis activity for the negative control (phosphate buffer saline, pH 7.4), whereas 100% hemolysis activity was seen in the positive control (de-ionized water) (**Fig. 4.9**). The nanofibers with and without CDF and Cur (HA 1 to HA 8) demonstrated less than 0.5% hemolysis. According to the reported literature, materials that show hemolysis activity below 5% are considered to be safe for drug delivery application by invasive method[61]. From our

studies we observed that nanofibers for all compositions showed haemolytic activity less than 5% and therefore these can be utilized for potential biomedical applications.
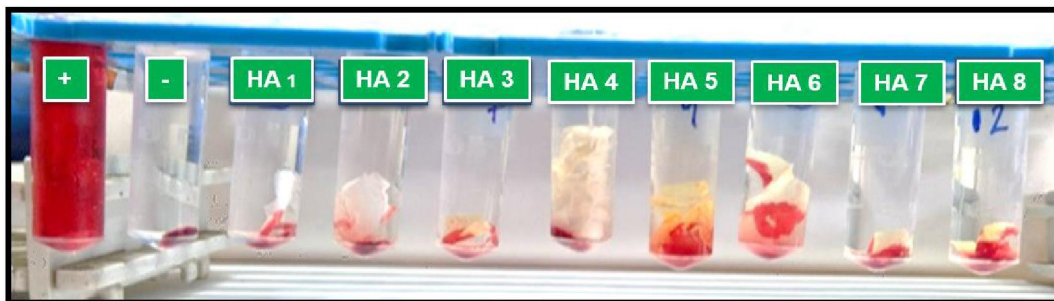
Figure 4. 8 Hemolysis assay in human blood sample of HA 1 to HA 8 formulation
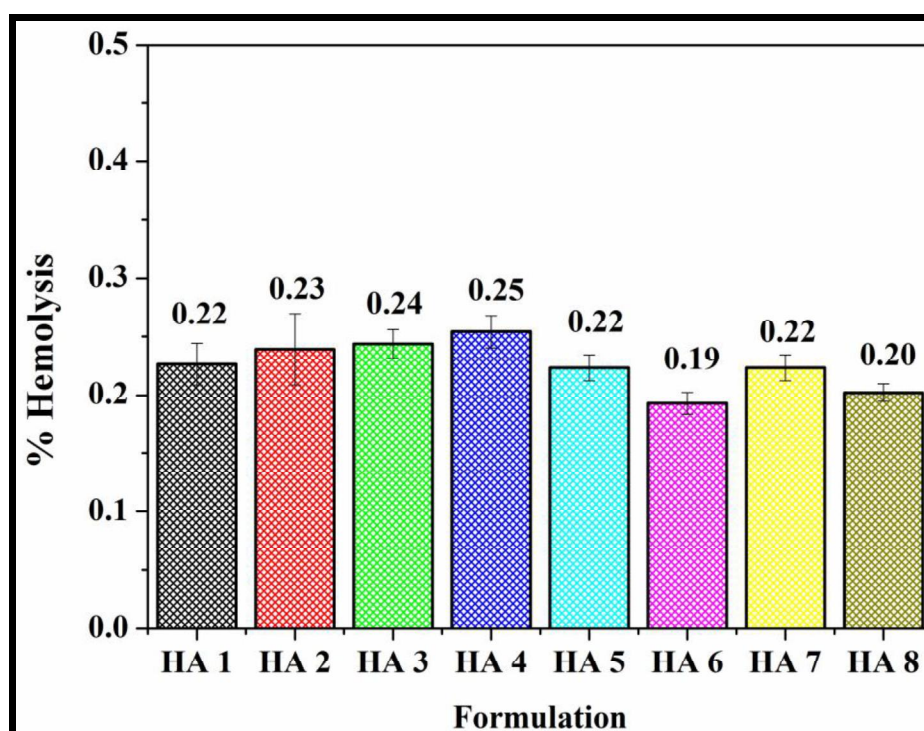
Figure 4. 9 Hemolysis assay in human blood sample of HA 1 to HA 8 formulation in bar diagram.

4.4.8 Cell proliferation study

Cellular proliferation and growth on the electrospun nanofibers are important factors for their applicability in the wound healing process. Upon seeding the mouse fibroblast L929 cells on various compositions of the nanofiber mats (HA 2 was kept

as control and HA 3 to HA 8 with Cur and CDF) were incubated for 24 h at standard cell incubation conditions, it was noticed that the cells were adhering to the developed mats (HA 2 to HA 8). The growth of cells was observed due to the presence of HA and PEO molecules as they gave an environment to facilitate the cell growth[39, 62]. The mats emitted green fluorescence because of Cur content which has autofluorescence capacity. The nuclei of L929 cells stained with DAPI (Blue colour) were observed on the mats, and we observed that the increasing concentration of Cur and CDF had a little detrimental effect on cell adhesion, which is shown in **Fig. 4.10**. However, in HA 5 and HA 8 nanofibers, the density of cell decreased as compared to HA 2, HA 3, HA 4, HA 6, and HA 7. The reason behind the decrease in the population of cells was due to an increase in the hydrophobicity and noxious effect of CDF and Cur in nanofibers. Further, cells were well proliferated in HA 2, HA 3, HA 4, HA 6 and HA 7 because of the hydrophilicity of nanofibers which made them susceptible to cell growth. Therefore, fibroblast L929 cells utilize the biocompatible nanofibrous matrix to bind and grow, thus accelerating the process of wound healing. Hence, cell proliferation studies revealed that the growth and proliferation of cell is much dependent on the hydrophilicity of nanofibers.
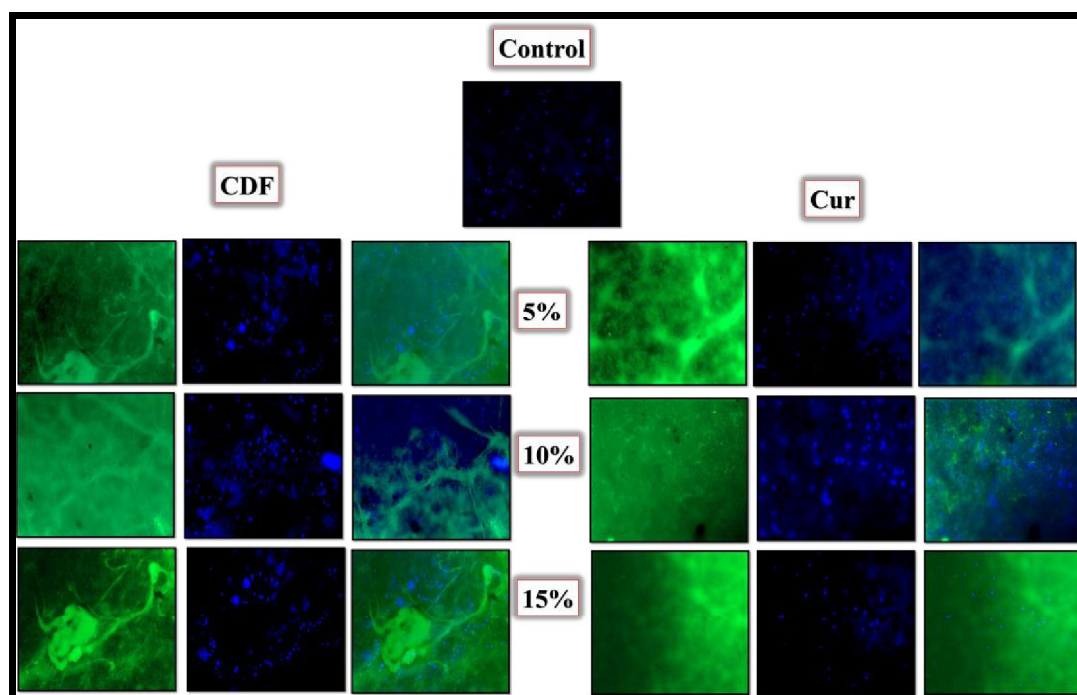
Figure 4. 10 Cell proliferation of CDF and Cur loaded nanofibers (HA 3 to HA 8) were studied by L929 mouse fibroblast cell lines by keeping control as HA 2.

4.4.9 Scratch assay

Cellular migration and re-epithelialization are vital for wound healing and are facilitated by the migration of skin cells from the wound margins towards the centre of the wound. In control, we observed that the gap's width remained the same, which means cells did not migrate or occupy the gap area. Whereas, in HA nanofibers (HA 3 to HA 8) loaded with Cur and CDF, it was observed that the gap was being filled by the cells after 24 to 48 h. HA 2 demonstrated the maximum cellular migration. As a result, gap closure and increase in cell density were observed, in NF with Cur and CDF it was observed that with increasing concentration of drug the efficiency of gap filling slightly decreased and cell were not densely packed as HA 2 nanofibers. The NF's with high drug concentrations of 10 and 15% were found to be slower than 5% (HA 3 and HA 6) in assisting the cellular migration, as shown in **Fig. 4.11**. The slower and less densely packed cells resulted due to high concentration of CDF and Cur (HA 4, HA 5 HA 7 and HA 8) might have produced a toxic effect on cell and in addition high concentration of CDF and Cur as increase the hydrophobic

concentration in nanofiber which hampered the cell growth in comparison HA 2, HA 3 and HA6. Hence, the nanofibers are efficient and provide the environment to the cells to attach as an extracellular matrix, promote cell division and fill the wounded gap in cell plate. Whereas in the control sample, the cells were unable to fill the gap as there was no extracellular matrix. Therefore, the scratch assay confirmed that regulated hydrophilicity and hydrophobicity significantly impacted cell growth and promoted cell division for better wound healing.
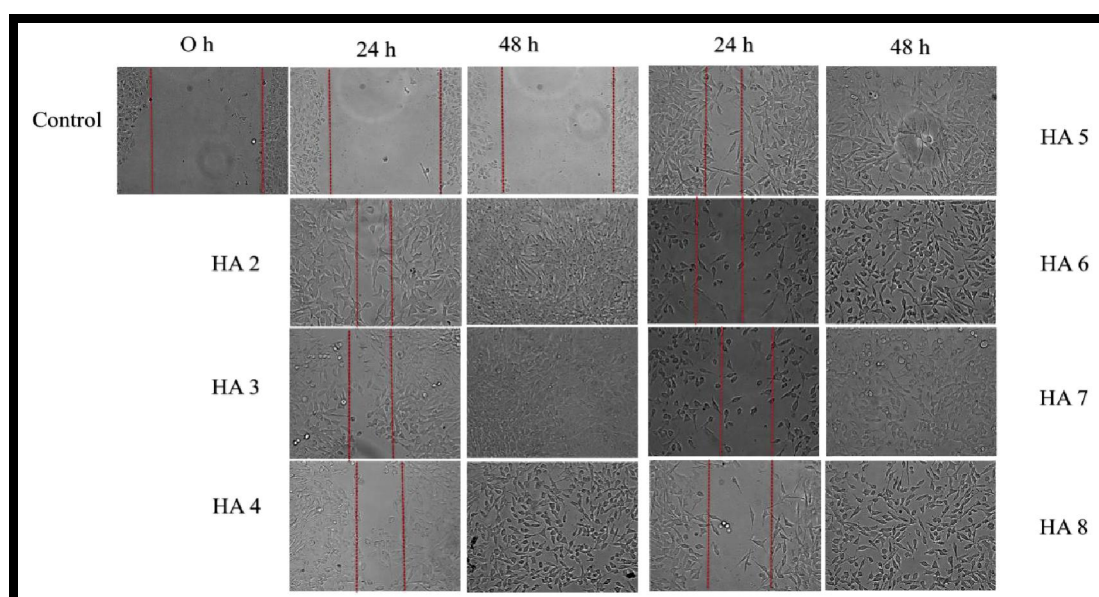
Figure 4. 11 Scratch assay was done using L929 mouse fibroblast cell line on HA 2 to HA 8 formulations for 48 h.

4.4.10 MTT assay

The cytotoxicity for PHBV, PEO HA and HA 1 and HA 2 nanofiber mats was observed by MTT assay in L929 fibroblast cells for 48 h. The cell viability was performed in the presence of HA 1 and HA 2 nanofibers was on par with FDA approved HA, PEO and PHBV as shown in **Fig. 4.12**. The pure HA, PEO and PHBV showed more than 80% cell viability, indicating those as safe materials for wound healing application. Further, the HA 2 and HA 3 nanofibers also showed 80% cell viability, suggesting that fabricated mats have non-toxic and high cell viability towards L929 fibroblast cells. Therefore, developed nanofibers are considered to be

non-toxic, safe, and are cell compatibility and as a result these nanomaterials can be the promising materials for biomedical applications.
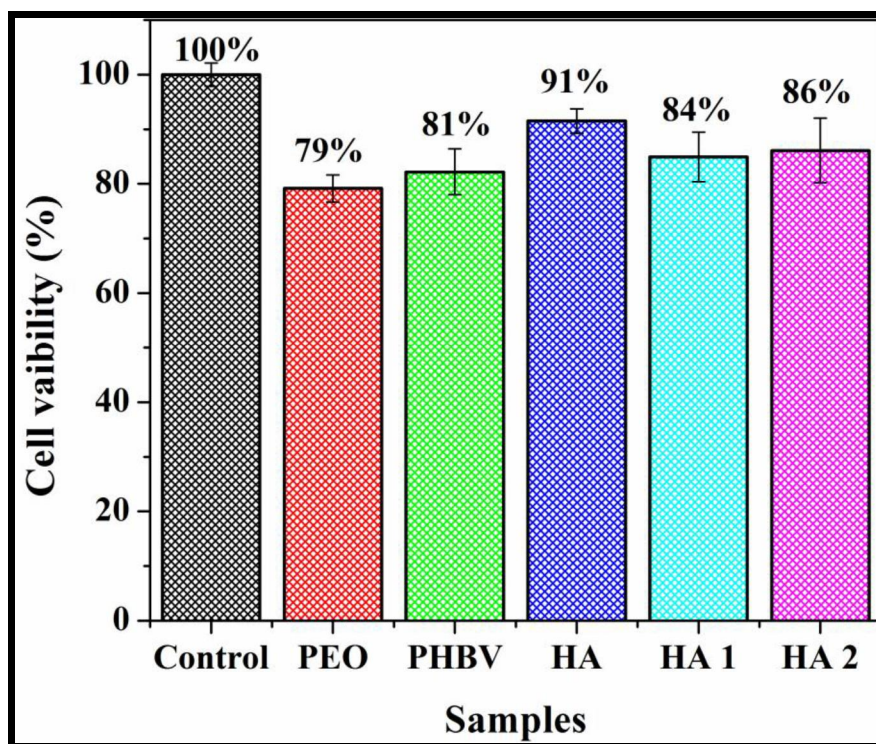
Figure 4. 12 Cell viability was studied on L929 fibroblast cell line for 24 h on PEO, PHBV, HA, HA 1 and HA 2 for 24 h.

4.4.11 Cell adhesion

The cell adhesion study was demonstrated for developed nanofibers (HA 1 to HA 8) in L929 fibroblast cells for 48 h (**Fig. 4.13**). The nanofibers of composition HA 1 and HA 2 showed the highest cell adhesion, which were 76 and 84%, respectively. However, Cur and CDF loaded nanofibers showed ~60 to 70% cell adherence. The Cur and CDF being hydrophobic in nature, the addition of these components showed a decrease in hydrophilicity. As reported hydrophilicity favours cell adhesion accordingly in these studies, too, we observed that cell adhesion was decreased with the addition of hydrophobic components in the nanofibers. The cell adhesion for the respective nanofibers with CDF and Cur being more than 50%, the developed nanofibers are considered suitable for cell proliferation and wound healing application. Finally, from the results of *in vitro* cell culture studies such as, cell

viability, cell adherence, proliferation and scratch assay, we proved that the developed nanofiber support with antibacterial Cur/CDF acts as an extracellular matrix for better cell attachment, faster cell growth and efficient wound healing.
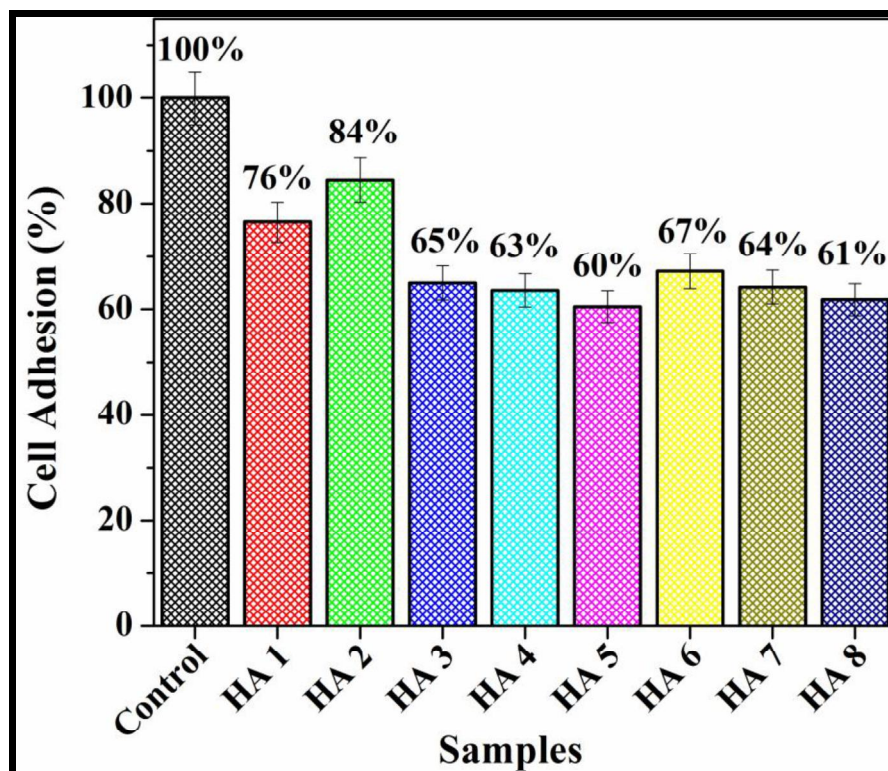
Figure 4. 13 Cell adhesion was studied on L929 fibroblast cell line for 24 h on HA 1 to HA 8 for 24 h**.**

4.4.12 Conclusion

We investigated and compared CDF and Cur loaded nanofibers to demonstrate the antibacterial property of CDF, which is a modified Cur. Blends of HA in combination with   PEO and PHBV were fabricated in the form of nanofiber mats. The surface morphology studies showed smooth and bead-free nanofiber mats. The physicochemical properties revealed the functional interactions and thermal stability of nanofiber mats. The *in vitro* release studies of the respective nanofiber mats demonstrated a decrease in the rate of release of CDF as compared to the rate of Cur release. This significant difference in the release is due to the increased hydrophobicity of CDF when compared with unmodified Cur. The *in vitro* cell culture

studies of nanofiber mats showed hemocompatibility and non-toxicity. In addition, cell proliferation and scratch assay analyses revealed that the fabricated nanofibers are favourable for the proliferation of fibroblast cells. Cur and CDF loaded nanofibers recorded similar antibacterial properties against *S.aureus*. This study indicated that the change in functional groups of Cur did not alter the antibacterial property. Further, the molecular docking experiments on the DHFR protein of *S.aureus* revealed that the CDF too exhibited similar affinity as that of Cur towards the protein of *S.aureus*.. Finally, the overall investigations proved that the developed nanofiber support with antibacterial Cur/CDF acts as an extracellular matrix for better cell attachment, faster cell growth and efficient wound healing. Nevertheless, preclinical studies are necessary to demonstrate its potential as an antibacterial system.

4.6 References

[1] T.K. Beuria, P. Singh, A. Surolia, D. Panda, Promoting assembly and bundling of FtsZ as a strategy to inhibit bacterial cell division: a new approach for developing novel antibacterial drugs, Biochemical Journal 423(1) (2009) 61-69.

[2] G.S. Bbosa, N. Mwebaza, J. Odda, D.B. Kyegombe, M. Ntale, Antibiotics/antibacterial drug use, their marketing and promotion during the post-antibiotic golden age and their role in emergence of bacterial resistance, Health 2014 (2014).

[3] S. Andrei, L. Valeanu, R. Chirvasuta, M.-G. Stefan, New FDA approved antibacterial drugs: 2015-2017, Discoveries 6(1) (2018).

[4] H. Kresse, M.J. Belsey, H. Rovini, The antibacterial drugs market, Nature Publishing Group, 2007.

[5] V. Basile, E. Ferrari, S. Lazzari, S. Belluti, F. Pignedoli, C. Imbriano, Curcumin derivatives: molecular basis of their anti-cancer activity, Biochemical pharmacology 78(10) (2009) 1305-1315.

[6] W. Shi, S. Dolai, S. Rizk, A. Hussain, H. Tariq, S. Averick, W. L'Amoreaux, A. El Idrissi, P. Banerjee, K. Raja, Synthesis of monofunctional curcumin derivatives, clicked curcumin dimer, and a PAMAM dendrimer curcumin conjugate for therapeutic applications, Organic letters 9(26) (2007) 5461-5464.

[7] A.N. Nurfina, M.S. Reksohadiprodjo, H. Timmerman, U.A. Jenie, D. Sugiyanto, H. Van der Goot, Synthesis of some symmetrical curcumin derivatives and their antiinflammatory activity, European journal of medicinal chemistry 32(4) (1997) 321-328.

[8] D.L. Vander Jagt, L.M. Deck, S.F. Abcouwer, R.A. Orlando, R.E. Royer, W.M. Weber, E.V. Bobrovnikova-Marjon, L.A. Hunsaker, Therapeutic curcumin derivatives, Google Patents, 2014.

[9] P. Kesharwani, L. Xie, S. Banerjee, G. Mao, S. Padhye, F.H. Sarkar, A.K. Iyer, Hyaluronic acid-conjugated polyamidoamine dendrimers for targeted delivery of 3, 4-difluorobenzylidene curcumin to CD44 overexpressing pancreatic cancer cells, Colloids and Surfaces B: Biointerfaces 136 (2015) 413-423.

[10] M. Mehanny, R.M. Hathout, A.S. Geneidi, S. Mansour, Exploring the use of nanocarrier systems to deliver the magical molecule; curcumin and its derivatives, Journal of controlled release 225 (2016) 1-30.

[11] F.C. Rodrigues, N.V.A. Kumar, G. Thakur, Developments in the anticancer activity of structurally modified curcumin: An up-to-date review, European journal of medicinal chemistry 177 (2019) 76-104.

[12] X. Chen, L.-Q. Zou, J. Niu, W. Liu, S.-F. Peng, C.-M. Liu, The stability, sustained release and cellular antioxidant activity of curcumin nanoliposomes, Molecules 20(8) (2015) 14293-14311.

[13] R. Arora, A. Kuhad, I.P. Kaur, K. Chopra, Curcumin loaded solid lipid nanoparticles ameliorate adjuvant-induced arthritis in rats, European journal of pain 19(7) (2015) 940-952.

[14] O.M. Koo, I. Rubinstein, H. Onyuksel, Role of nanotechnology in targeted drug delivery and imaging: a concise review, Nanomedicine: Nanotechnology, Biology and Medicine 1(3) (2005) 193-212.

[15] M.S. Cartiera, E.C. Ferreira, C. Caputo, M.E. Egan, M.J. Caplan, W.M. Saltzman, Partial correction of cystic fibrosis defects with PLGA nanoparticles encapsulating curcumin, Molecular pharmaceutics 7(1) (2010) 86-93.

[16] A.V. Jithan, K. Madhavi, M. Madhavi, K. Prabhakar, Preparation and characterization of albumin nanoparticles encapsulating curcumin intended for the treatment of breast cancer, International journal of pharmaceutical investigation 1(2) (2011) 119.

[17] H. Wartlick, B. Spänkuch-Schmitt, K. Strebhardt, J. Kreuter, K. Langer, Tumour cell delivery of antisense oligonuclceotides by human serum albumin nanoparticles, Journal of Controlled Release 96(3) (2004) 483-495.

[18] K.A. Gawde, P. Kesharwani, S. Sau, F.H. Sarkar, S. Padhye, S.K. Kashaw, A.K. Iyer, Synthesis and characterization of folate decorated albumin bio-conjugate nanoparticles loaded with a synthetic curcumin difluorinated analogue, Journal of colloid and interface science 496 (2017) 290-299.

[19] K.A. Gawde, S. Sau, K. Tatiparti, S.K. Kashaw, M. Mehrmohammadi, A.S. Azmi, A.K. Iyer, Paclitaxel and di-fluorinated curcumin loaded in albumin nanoparticles for targeted synergistic combination therapy of ovarian and cervical cancers, Colloids and Surfaces B: Biointerfaces 167 (2018) 8-19.

[20] D. Luong, P. Kesharwani, B.A. Killinger, A. Moszczynska, F.H. Sarkar, S. Padhye, A.K. Rishi, A.K. Iyer, Solubility enhancement and targeted delivery of a potent anticancer flavonoid analogue to cancer cells using ligand decorated dendrimer nano-architectures, Journal of colloid and interface science 484 (2016) 33-43.

[21] P. Kesharwani, S. Banerjee, S. Padhye, F.H. Sarkar, A.K. Iyer, Hyaluronic acid engineered nanomicelles loaded with 3, 4-difluorobenzylidene curcumin for targeted killing of CD44+ stem-like pancreatic cancer cells, Biomacromolecules 16(9) (2015) 3042-3053.

[22] M. Sharma, R. Sharma, D.K. Jain, Nanotechnology based approaches for enhancing oral bioavailability of poorly water soluble antihypertensive drugs, Scientifica 2016 (2016).

[23] P. Kamble, B. Sadarani, A. Majumdar, S. Bhullar, Nanofiber based drug delivery systems for skin: A promising therapeutic approach, Journal of Drug Delivery Science and Technology 41 (2017) 124-133.

[24] P. Sahu, K.K. Sushil, S. Samaresh, K.I. Arun, Stimuli-Responsive Bio-Hybrid Nanogels: An Emerging Platform in Medicinal Arena, J Controlled Release 107(1) (2017) 143-157.

[25] S. Mignani, S. El Kazzouli, M. Bousmina, J.-P. Majoral, Expand classical drug administration ways by emerging routes using dendrimer drug delivery systems: a concise overview, Advanced drug delivery reviews 65(10) (2013) 1316-1330.

[26] H.S. Sofi, R. Ashraf, A.H. Khan, M.A. Beigh, S. Majeed, F.A. Sheikh, Reconstructing nanofibers from natural polymers using surface functionalization approaches for applications in tissue engineering, drug delivery and biosensing devices, Materials Science and Engineering: C 94 (2019) 1102-1124.

[27] D. Kai, G. Jin, M.P. Prabhakaran, S. Ramakrishna, Electrospun synthetic and natural nanofibers for regenerative medicine and stem cells, Biotechnology journal 8(1) (2013) 59-72.

[28] N. Bhattarai, Z. Li, J. Gunn, M. Leung, A. Cooper, D. Edmondson, O. Veiseh, M.H. Chen, Y. Zhang, R.G. Ellenbogen, Natural-synthetic polyblend nanofibers for biomedical applications, Advanced Materials 21(27) (2009) 2792-2797.

[29] T. Uyar, E. Kny, Electrospun materials for tissue engineering and biomedical applications: research, design and commercialization, Woodhead Publishing2017.

[30] B.-S. Kim, I.-S. Kim, Recent nanofiber technologies, Polymer Reviews 51(3) (2011) 235-238.

[31] J. Xue, T. Wu, Y. Dai, Y. Xia, Electrospinning and electrospun nanofibers: methods, materials, and applications, Chemical reviews 119(8) (2019) 5298-5415.

[32] A. Senthamizhan, B. Balusamy, T. Uyar, Recent progress on designing electrospun nanofibers for colorimetric biosensing applications, Current Opinion in Biomedical Engineering 13 (2020) 1-8.

[33] P.R. Patel, K. Pandey, N. Killi, R.V.N. Gundloori, Manipulating hydrophobicity of polyester nanofiber mats with egg albumin to enhance cell interactions, Polymer Engineering & Science 61(10) (2021) 2496-2510.

[34] S.M. Shahriar, J. Mondal, M.N. Hasan, V. Revuri, D.Y. Lee, Y.-K. Lee, Electrospinning nanofibers for therapeutics delivery, Nanomaterials 9(4) (2019) 532.

[35] S.R. King, W.L. Hickerson, K.G. Proctor, Beneficial actions of exogenous hyaluronic acid on wound healing, Surgery 109(1) (1991) 76-84.

[36] J.S. Frenkel, The role of hyaluronan in wound healing, International wound journal 11(2) (2014) 159-163.

[37] Y. Zhao, J. Xiong, X. Shi, F. Ko, Capturing cancer cells using hyaluronic acid-immobilized electrospun random or aligned PLA nanofibers, Colloids and Surfaces A: Physicochemical and Engineering Aspects 583 (2019) 123978.

[38] M.R. El-Aassar, O.M. Ibrahim, M.M.G. Fouda, N.G. El-Beheri, M.M. Agwa, Wound healing of nanofiber comprising Polygalacturonic/Hyaluronic acid embedded silver nanoparticles: In-vitro and in-vivo studies, Carbohydrate Polymers 238 (2020) 116175.

[39] J.J. Ahire, D.D. Robertson, A.J. van Reenen, L.M.T. Dicks, Polyethylene oxide (PEO)-hyaluronic acid (HA) nanofibers with kanamycin inhibits the growth of Listeria monocytogenes, Biomedicine & Pharmacotherapy 86 (2017) 143-148.

[40] A. Zonari, T.M.M. Martins, A.C.C. Paula, J.N. Boeloni, S. Novikoff, A.P. Marques, V.M. Correlo, R.L. Reis, A.M. Goes, Polyhydroxybutyrate-co-hydroxyvalerate structures loaded with adipose stem cells promote skin healing with reduced scarring, Acta biomaterialia 17 (2015) 170-181.

[41] A. Shrivastav, H.-Y. Kim, Y.-R. Kim, Advances in the applications of polyhydroxyalkanoate nanoparticles for novel drug delivery system, BioMed research international 2013 (2013).

[42] S. Padhye, S. Banerjee, D. Chavan, S. Pandye, K.V. Swamy, S. Ali, J. Li, Q.P. Dou, F.H. Sarkar, Fluorocurcumins as cyclooxygenase-2 inhibitor: molecular

docking, pharmacokinetics and tissue distribution in mice, Pharmaceutical research 26(11) (2009) 2438-2445.

[43] A. Singh, J.V. Singh, A. Rana, K. Bhagat, H.K. Gulati, R. Kumar, R. Salwan, K. Bhagat, G. Kaur, N. Singh, Monocarbonyl curcumin-based molecular hybrids as potent antibacterial agents, ACS omega 4(7) (2019) 11673-11684.

[44] A. Vina, Improving the speed and accuracy of docking with a new scoring function, efficient optimization, and multithreading Trott, Oleg; Olson, Arthur J, J. Comput. Chem 31(2) (2010) 455-461.

[45] G.M. Morris, D.S. Goodsell, R.S. Halliday, R. Huey, W.E. Hart, R.K. Belew, A.J. Olson, Automated docking using a Lamarckian genetic algorithm and an empirical binding free energy function, Journal of computational chemistry 19(14) (1998) 1639-1662.

[46] W.L. DeLano, The pymol molecular graphics system (2002), http://www. pymol. org (2002).

[47] M.G. Lerner, H.A. Carlson, APBS plugin for PyMOL, Ann Arbor: University of Michigan (2006).

[48] S.G. Reddy, A.S. Pandit, A. Thakur, Effects of crosslink agents on sodium alginate and lignosulphonic acid blends, 폴리머 40(1) (2016) 63-69.

[49] T.C. Mokhena, M.J. Mochane, A. Mtibe, M.J. John, E.R. Sadiku, J.S. Sefadi, Electrospun alginate nanofibers toward various applications: A review, Materials 13(4) (2020) 934.

[50] N.P. Camacho, P. West, P.A. Torzilli, R. Mendelsohn, FTIR microscopic imaging of collagen and proteoglycan in bovine cartilage, Biopolymers: Original Research on Biomolecules 62(1) (2001) 1-8.

[51] Y. Ke, G. Wu, Y. Wang, PHBV/PAM scaffolds with local oriented structure through UV polymerization for tissue engineering, BioMed research international 2014 (2014).

[52] D.E. Hegazy, G.A. Mahmoud, Radiation Synthesis and Characterization of Polyethylene Oxide/Chitosan-Silver Nanocomposite for Biomedical Applications, Arab Journal of Nuclear Science and Applications 47(2) (2014) 1-14.

[53] S.S. Darandale, P.R. Vavia, Cyclodextrin-based nanosponges of curcumin: formulation and physicochemical characterization, Journal of inclusion phenomena and macrocyclic chemistry 75(3-4) (2013) 315-322.

[54] H. Alsaab, R.M. Alzhrani, P. Kesharwani, S. Sau, S.H.S. Boddu, A.K. Iyer, Folate decorated nanomicelles loaded with a potent curcumin analogue for targeting retinoblastoma, Pharmaceutics 9(2) (2017) 15.

[55] Y. Wang, R. Chen, J. Cai, Z. Liu, Y. Zheng, H. Wang, Q. Li, N. He, Biosynthesis and thermal properties of PHBV produced from levulinic acid by Ralstonia eutropha, PLoS One 8(4) (2013) e60318.

[56] Y. Xu, L. Zou, H. Lu, Y. Wei, J. Hua, S. Chen, Preparation and characterization of electrospun PHBV/PEO mats: The role of solvent and PEO component, Journal of Materials Science 51(12) (2016) 5695-5711.

[57] A.R. Polu, D.K. Kim, H.-W. Rhee, Poly (ethylene oxide)-lithium difluoro (oxalato) borate new solid polymer electrolytes: ion–polymer interaction, structural, thermal, and ionic conductivity studies, Ionics 21(10) (2015) 2771-2780.

[58] M. Chopra, R. Jain, A.K. Dewangan, S. Varkey, S. Mazumder, Design of curcumin loaded polymeric nanoparticles-optimization, formulation and characterization, Journal of Nanoscience and Nanotechnology 16(9) (2016) 9432-9442.

[59] H. Chen, X. Chen, H. Chen, X. Liu, J. Li, J. Luo, A. He, C.C. Han, Y. Liu, S. Xu, Molecular Interaction, Chain Conformation, and Rheological Modification during Electrospinning of Hyaluronic Acid Aqueous Solution, Membranes 10(9) (2020) 217.

[60] S. Agrawal, P.R. Patel, R.V.N. Gundloori, Proteins as Nanocarriers To Regulate Parenteral Delivery of Tramadol, ACS Omega 4(4) (2019) 6301-6310.

[61] T. Mocan, Hemolysis as expression of nanoparticles-induced cytotoxicity in red blood cells, BMBN 1(1) 7-12.

[62] H. Suh, B. Jeong, R. Rathi, S.W. Kim, Regulation of smooth muscle cell proliferation using paclitaxel-loaded poly (ethylene oxide)–poly (lactide/glycolide) nanospheres, Journal of Biomedical Materials Research: An Official Journal of The Society for Biomaterials, The Japanese Society for Biomaterials, and the Australian Society for Biomaterials 42(2) (1998) 331-338.

CHAPTER 5

Blends of oil based polyesteramide as nanofiber mat for dual drug delivery for wound healing application
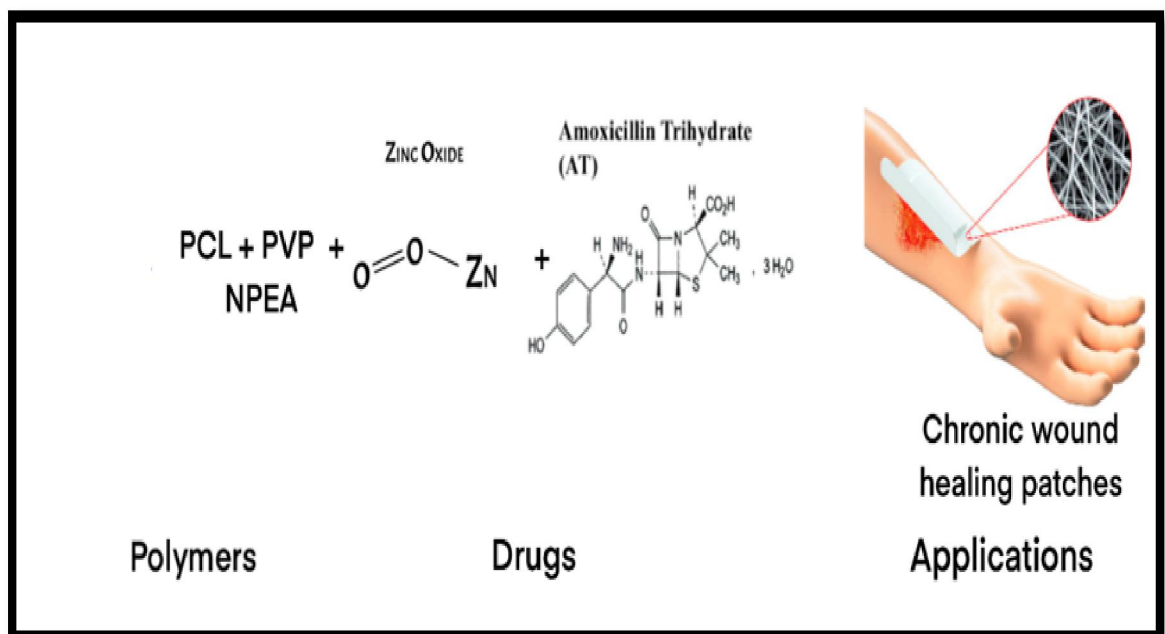
Chapter 5

In this chapter, we developed a dual drug loaded nanofibers system using blends of neem oil based polyesteramide. The dual drugs loaded were zinc oxide and amoxicillin trihydrate. The developed nanofibers were characterized by various analytical tools and evaluated for *in vitro* drug release, cytotoxicity, cell proliferation, and *in vivo* wound healing. The overall investigations concluded that the new nanomaterials may be considered for effective drug release application to enhance chronic wound healing. For practical application, thorough *in vitro* and *in vivo* studies will be performed.

5.1 Introduction

Millions of patients are being affected by chronic and traumatic wounds, skin deprivations conventionally occurred by surgeries, accidents, and burns [1-3]. The loss of the outermost layer of skin (epidermis) will encourage exogenous microbial invasion. Such damages to the physical barrier will be vulnerable to faster bacterial infection[4]. Delay in treatment would lead to amputation, or severity can be life-threatening[5]. Hence, earlier treatment with suitable dressing materials is a primitive step, and such material will further serve as a barrier against the foreign invader. The researchers have innovated various biomaterials like nanofibers[6, 7], hydrogels[8, 9], and films[10] that showed the promising effect that aid in the faster wound healing and effective closing of wounds without leaving any scar on the skin[11, 12].

Amongst all biomaterials, nanofibers are a potential candidate as it provides better characteristic features viz., faster cell proliferation and migration[6, 13], antibacterial activity[13], absorb wound exudates[14], bioactive agent loading[15, 16], favour nutrient and gaseous exchange, and no scar formation[17, 18] as compared to other bulk materials. Furthermore, nanofibers are employed in tissue engineering, as they significantly influence wound healing and skin grafting[19-21]. Nanofibers are fabricated with the electrospinning method, which provides the advantage of nanomaterials, a high surface area to volume ratio, high porosity, three-dimensional structure, high drug loading, and ease of custom-make per prerequisite[22-25]. Besides, the nanofibers mimic the extracellular matrix (ECM), desirable for tissue engineering

and preferably for wound healing application[26]. To date, various natural (collagen, hyaluronic acid, gelatin, chitosan)[27-29], synthetic (polyacrylic acid (PAA)[30], polyvinylpyrrolidone (PVP)[31], polylactic acid (PLA)[32], polycaprolactone (PCL)[33], and semisynthetic for example; chitosan polymers are being exploited for wound healing applications. In the present study, a combination of PVP, neem oil polyesteramide (NPEA), and PCL nanofibers containing two active pharmaceutical ingredients (API), zinc oxide (ZnO) and amoxicillin trihydrate (AT), were examined for wound healing application.

PVP is an FDA approved hydrophilic polymer, having good biocompatibility, potential to enable controlled drug release, blood plasma expander, and supplementary for vitreous humor[34-36]. PCL, which is also an FDA approved polymer, hence, the nanofibers of the blends of hydrophobic PCL and hydrophilic gelatin were used for promoting cell growth.[37]. In these studies, it was understood that manipulating the hydrophiobic PCL enabled a balance of hydrophilic-hydrophobic property, which was crucial for the cell proliferation environment. Besides, PCL can also help in sustained drug release for a longer duration of action and load-bearing ability, and it provides stiffness to the system[38, 39]. Polyesteramide (NPEA) is synthesized by neem oil, widely used for biomedical applications such as antimicrobial[40], antifungal[41], insecticide[42], parasite[43], anti-inflammatory[44]. NPEA was synthesized by our group and showed the application of NPEA nanofibers for tissue regeneration using chlorohexidine digluconate (CH) as an active pharmaceutical ingredient (API)[45].

Zinc oxide (ZnO) is being used for biomedical applications due to its properties such as its potent ability to trigger excess reactive oxygen species (ROS) production, release zinc ions, and induce cell apoptosis, hence being used anticancer and antibacterial fields[46]. Further, it shows distinguish effect in the topical application to reduce super-infection and stimulate the wound re-epithelialization[47, 48]. Some of the studies on ZnO reported its potential to decrease biofilm formation and microbial adhesion due to its antimicrobial activity[49] against various microbes like *Aspergillus niger*[50], *Candida tropicalis*[51], *E.coli*[52], *Salmonella enteritidis*[52]*, Streptococcus pneumoniae*[53] with low toxicity to human cells. Hence it was used for wound healing, where it helped in promoting cell proliferation of endothelial progenitor cells and cell

migration during wound repair[54, 55]. AT, is conventionally used as a broad-spectrum, semisynthetic aminopenicillin antibiotic. AT belongs to the penicillin family group, with a high therapeutic index. World health organization (WHO) enlisted AT as one of the essential drugs for antibiotic and antibacterial applications[34, 56].

The increased burden of wound healing treatment in the health care sector and the intensification of antibiotic resistance against many drugs necessitates developing an advanced system for rapid wound recovery at minimal cost and better patient compliance. Therefore, we propose to develop a new combination of dual drug-loaded nanofibers, which can address antibacterial and antibiotic resistance for faster tissue regeneration without scar formation. Accordingly, we have prepared dual drug-loaded nanofibers using the above mentioned polymers with dual drugs (PCL/PVP/NPEA blends immobilized with ZnO and AT) and studied physicochemical properties by various analytical instruments. The antibacterial activity of developed nanofibers was demonstrated by Gram-positive and Gram-negative (*S.auerus* and *E.coli)* bacteria. Further, cytotoxicity of nanofibers was evaluated on NIH3T3 cells, and *in vitro* wound healing potential was demonstrated. To support the *in vitro* results, we have demonstrated *in vivo* studies using male Swiss albino mice models.

5.2 Materials and methods

5.2.1   Materials

Amoxicillin trihydrate was obtained as a gift sample from Micro labs limited, Bangalore, India. NPEA was synthesized in our lab. Zinc oxide was obtained as a gift sample from the Agarkar Institute, Pune, India. Polyvinylpyrrolidone (M.w~360,000) and polycaprolactone (M.w~70,000- 90,000 were purchased from Sigma-Aldrich Co, St Louis, USA. Chloroform (Alcohol stabilized) analytical grade was obtained from Rankem, Mumbai, India. Methanol HPLC grade was purchased from Fisher Scientific, Mumbai, India.3-(4,5–dimethyl thiazol–2–yl)–5–diphenyltetrazolium bromide (MTT), fetal bovine serum (FBS), phosphate buffered saline (PBS), Dulbecco's modified eagle's medium (DMEM), zein and trypsin were purchased from Sigma-Aldrich Co, St Louis, USA. EDTA (ethylenediaminetetraacetic acid), glucose and antibiotics were procured from Hi-Media Laboratories Ltd., Mumbai, India. Dimethyl sulfoxide

(DMSO), acetone and propanol were bought from Merck Ltd., Mumbai, India. L929 (mouse fibroblast) and MCF-7 (human adenocarcinoma) cell lines were procured from National Centre for Cell Sciences (NCCS), Pune, India. All solvents used were of analytical grade.

5.2.2   Electrospinning of Dual-Drug loaded nanofibers

To prepare polymer solution for electrospinning of PCL 4% (w/v), NPEA 3% (w/v), were dissolved in chloroform and PVP 4% (w/v) was dissolved in dimethylformamide in a separate vial. Later, both the polymer solutions were mixed together on a roller mixer for 12 h to achieve a homogenous solution. ZnO and AT were added in the resultant homogenous solution at various concentrations (as mentioned in **Table 5.1**) and allowed to mix on a roller mixer for another 12 h, this was followed by sonication for 30 min. For fabrication of nanofibers, the resultant homogeneous polymeric blend solution was filled in a 5 mL syringe, which was equipped with a stainless steel hypodermic needle with a blunt end and a fixed pore diameter of ~0.7 mm. This was used as a nozzle for spinning the polymer solution. The filled syringe was mounted on a syringe pump to pump the solution at a controlled flow rate. A high-voltage generator operated in a positive DC mode was connected to the syringe needle, and an aluminum plate was set in a closed chamber to collect the nanofibers. Nanofiber fabrication was carried out as reported earlier [57]. The electrospinning was done at an ambient condition, and all the parameters such as the distance between the tip of the needle and the collector (12 cm), the voltage (15 kV), and the flow rate (0.50 mL/h) were fixed for fabrication of nanofiber mats. The collected nanofibers were kept in a vacuum oven for 4 h to remove any residual solvent. The parameters and procedure remain the same for

fabricating all compositions as shown in **Table 5.1**. A similar method was followed for the development of nanofibers without drugs.

Table 5. 1 Composition of polymer blend for nanofibers (NF) fabrication

Formulations	PCL (w/v%)	PVP (w/v%)	NPEA (w/v%)	AT (w/w%)*	ZnO (w/w%)*
Plain-NF	4	3	3	-	-
ZnO-NF-3%	4	3	3	-	3
AT-NF-3%	4	3	3	3	-
AT-ZnO-NF-3%	4	3	3	3	3
* w.r.t. total polymer weight					

5.3 Characterization of fabricated nanofibers

Environment scanning electron microscopy (E-SEM) [Micro Analysis System, and Model Phoenix, Cambridge, England, UK] was used for evaluating the surface morphology of the fabricated nanofibers. The nanofibers were coated with gold using a coating unit E5000 (Polaron Equipment Ltd., Watford, Hertfordshire, England, and UK). A dual-beam, having electron source of tungsten filament (w) with emission at a resolution of 20 kV in high vacuum was used for the studies. A transmission electron microscope (TEM, FEI model TECNAI G2 F30) was used for analyzing the morphology of fabricated nanofibers. The chemical characterization of nanofibers and raw materials were evaluated by Burker FT-IR spectrometer Tensor II by a pure diamond ATR mode accessory. The thermal properties were evaluated by differential scanning calorimetry (DSC), DSC-TA-Q10, USA. EDX (Micro Analysis System, and

Model Phoenix, Cambridge, England, UK) was used to evaluate the surface elemental analysis of nanofibers. The crystallinity of the pure polymers and nanofiber mats was studied by powder X-ray diffraction (XRD) (PANalytical X'pert Pro diffractometer) and Cu Kα (1.5418 Å) radiation used as an X-ray source. The mechanical strength of the nanofiber mats was estimated by the dynamic mechanical analyzer (RSA3, TA Instruments, USA). The nanofiber mats were cut into strips with dimensions of 20 × 0.5 cm^2 and then mounted onto the tensile grips. The rate of strain and gauge lengths were 10 mm/min and 15 cm, respectively. Mats were subjected to tensile force. Each sample was tested 5 times to authenticate its normal stress-strain curves.

5.3.1 Drug release studies

The release of AT was examined in a phosphate buffer solution (PBS) at 37 °C in bath shaker. Briefly, nanofibers (5 mg) were transferred in PBS (10 mL, pH. 7.4). Intermittently, nanofiber solution (2 mL) was withdrawn from buffer solution and analyzed with UV-Visible spectrophotometer at 272 nm The withdrawn PBS solution was replaced with fresh PBS solution to maintain the constant volume (10 mL) throughout the experiment. The release studies were carried out in duplicates to determine the amount of AT released into the PBS solution with respect to time. A similar protocol was followed for plain-nanofibers. Cumulative drug release was calculated using an Equation 1 as shown below;

Cumulative percent of drug released (%) $= M_t/M_{\infty} \times 100$ Equation 1

Where M_t is the amount of the drug released at time 't' and 'M_{∞}' is the amount of drug present in the nanofiber mat after preparation and estimation.

The acquired percentage of AT released was plotted against time as a cumulative percentage of release.

5.3.2 Cytotoxicity study

MTT assay was carried out to evaluate the cytotoxicity of nanofibers, estimating formazan crystals in terms of colorimetric analysis. NIH3T3 (mouse embryonic fibroblasts) cells (2×10^5 cells/mL) were seeded in 96 well plates and the plate was incubated at 37^0 C in a 5% CO_2 atmosphere for 48 h. After 48 h, the spent medium was discarded and fresh medium (180 µL, supplemented with 1% fetal bovine serum and 1% antibiotic antimycotic solution) was added. Cells were treated with nanofibers alone (control), and nanofibers loaded with zinc oxide nanoparticles without or with antibiotic (AT) (as mentioned in table 1)). Cytotoxicity of different concentrations of zinc oxide nanoparticles (1, 2, 5, 10, 20, 50, 100, 150, and 200 µg/mL) along with PBS alone (control) was analyzed. All treatments were given for 24 h. After 24 h, the spent medium was discarded and washing was done with phosphate buffer saline (pH 7.4). MTT (0.2 mg/mL) was added to each well & the plate was incubated at 37°C, 5% CO_2 for 3 h. After 3 h, the spent medium containing MTT was removed. Purple-coloured formazan crystals were then dissolved using DMSO (dimethyl sulfoxide). Absorbance was recorded at 570 nm using a plate reader (Synergy HT, BioTek Instruments Inc., USA). Cell viability against treatment concentration was plotted.

5.3.3 Antibacterial activity assay

The bactericidal activity of the plain nanofibers, ZnO-NF-3%, and AT-ZnO-NF-3% was tested using growth inhibition studies against representative Gram-positive (*S. aureus*) and Gram-negative (*E. coli*) bacteria. Fresh bacterial colonies on agar slant were cultured on nutrient broth (100 mL). Log phase bacterial growing culture was assessed with the optical density method (CFU corresponding to 1×10^8 cells). The bacterial suspension (1 mL) was then inoculated to fresh broth containing treatment membranes. The treatment groups included a control (without any treatment), ZnO alone (3%) and AT alone (3%). Suspensions were allowed to grow at 37^0 C for 12 h. After 12 h, 10 µL cell suspension from respective treatment was cultured on nutrient agar plates and incubated at 37^0 C for overnight. All the treatment sets were done in triplicates.

5.3.4 *In vitro* wound healing potential studies

The wound healing potential of nanofiber mats was studied with scratch assay and proliferation assay of NIH3T3 cells.

5.3.4.1 Scratch assay

The migration ability of NIH3T3 cells was evaluated with the scratch assay. NIH3T3 cell monolayer was allowed to grow in a petri dish (35 mm) at 37 °C, 5% CO_2 for 24 h. The monolayer was scratched with a sterile pipette tip. Washing was done with PBS to remove scratched cells. Cells were treated with plain NF, ZnO-NF-3%, and AT-ZnO-NF-3%. A wound gap was observed for different time points (3, 6, and 12 h) and images were taken with a digital camera attached to an inverted microscope.

5.3.4.2 Cell Proliferation assay

Ki67 marker was studied for analyzing the proliferative potential of NIH3T3 cells upon treatment with Plain NF, ZnO-NF-3%, AT-NF-3%, and AT-ZnO-NF-3%. For experiments, NIH3T3 (1 X 10^5) cells were seeded on a coverslip and incubated in a Petri dish at 37 °C for 24 h in CO_2 incubator. Cells were washed with PBS and fixed with paraformaldehyde (4%, 15 min/room temperature). Cells were permeabilized with Triton X-100 (0.1% in sodium citrate, 15 min/40 C), followed by blocking using BSA (3% in PBST) for 1 h. Cells were incubated with anti-ki67 antibody (Catalog #PA1-38032, Thermo Fisher Scientific; 1:300, blocking buffer) overnight at 40 C. Hydrogen peroxide (H2O2) treatment (0.3%, 15 min) was given to block endogenous peroxides. Cells were washed with PBST, thrice. For immunofluorescence, cells were incubated with HRP conjugated secondary antibody (Catalog #31635, Thermo Fisher Scientific; 1:1000, 2 h). Brown color was developed by incubating cells with DAB substrate in dark for 10 min. To stain nuclei, cells were counterstained with Haematoxylin (1:1, 3 min/RT). Coverslips were thoroughly washed with PBST and mounted in glycerol (80%). Images were taken at 40X under a bright field inverted microscope. Cell proliferation (%) was estimated by equation 2, counting the number of Ki67 positive cells and a total number of cells.

Proliferating cells (%) = (Ki67 positive cells/ total number of cells) x 100   Equation 2

5.3.5 *In vivo* studies

Experimental animals

The nanofiber mats were studied for wound healing using Male Wistar albino rats, weighing between 150-200 g each. They were purchased from the National Institute of Biosciences, Pune, India. The animals were allowed for acclimatization for 10 days in an animal house approved by CPCSEA (Committee for the Purpose of Control and Supervision of Experiments on Animals). The animals were nourished with the standard diet supplied by Nutrivet Life Sciences, Pune. The experimental study protocol was done as approved by the Institutional Animal Ethics Committee (Ref. No.: MIP/IAEC/2019-20/M1/appr/07).

5.3.5.1 In vivo **wound healing potential studies**

To evaluate the wound healing efficiency of nanofiber mats excision wound rat model was used based on the reported literature[45]. Briefly, thirty-six animals were separated into five groups as Group I, II, III, IV and V (six animals in each), as mentioned in **Table 5.2**.

 Anesthesia was induced in rats with thiopental sodium (40 mg/kg body weight) administration. The rats were depilated on the dorsal side and circular full-thickness wounds of diameter 2.5 cm were created using surgical scissors under aseptic conditions. The nanofiber mats (diameter 2.5 cm) were placed weekly three times on the wounds of groups III, IV and V for treatment. Whereas the Povidone-Iodine ointment was applied on the wound twice a day for the wounds of group II. The area of the wound was calculated and the percentage of wound healing was determined by the following equation 3,

$$\text{Percentage of wound healing (\%)} = \frac{I_a - X_a}{I_a} \times 100$$

Equation 3

Where I_a is the area of the initial wound and X_a is the area of the healed wound at a respective day.

Table 5. 2 Animal grouping for evaluation of wound healing potential.

Name	Treated with
Group I	Control: wound-induced without any treatment
Group II	Standard drug-treated group: treatment with commercially available Povidone-Iodine ointment
Group III	Plain-NF-treated group
Group IV	ZnO-NF-3%-treated group
Group V	AT-ZnO-NF-3%-treated group

5.3.6 Histopathological studies

On the 21st day, the newly formed wound tissue was carefully excised under anesthesia and subjected to histopathological evaluation by two staining methods, namely, hematoxylin and eosin staining (H&E) Masson's trichrome staining method. The stained tissue slides were examined under a light microscope (ten randomly selected fields) for the healing process with the proliferation of granulation tissue comprised of fibroblasts and neo-vascularization process, collagen deposition, the presence of inflammatory cells.

5.4   Results and discussion

Electrospinning enables the production of innovative and effective nanofibers by combining nanoparticles, drugs, and additives to enhance the attributes and performance of nanofibers for specific purposes. To build a composite of active nanofibers, drugs or nanoparticles can be reinforced in a polymer matrix by combining with polymer solution without any chemical treatment. In this study, we developed nanofibers with PVP, PCL, and NPEA by incorporating ZnO and AT, aiming for the development of synergetic nanofibers with dual drugs for rapid wound healing **Fig. 5.1** represents the structures of polymers and amoxicillin.
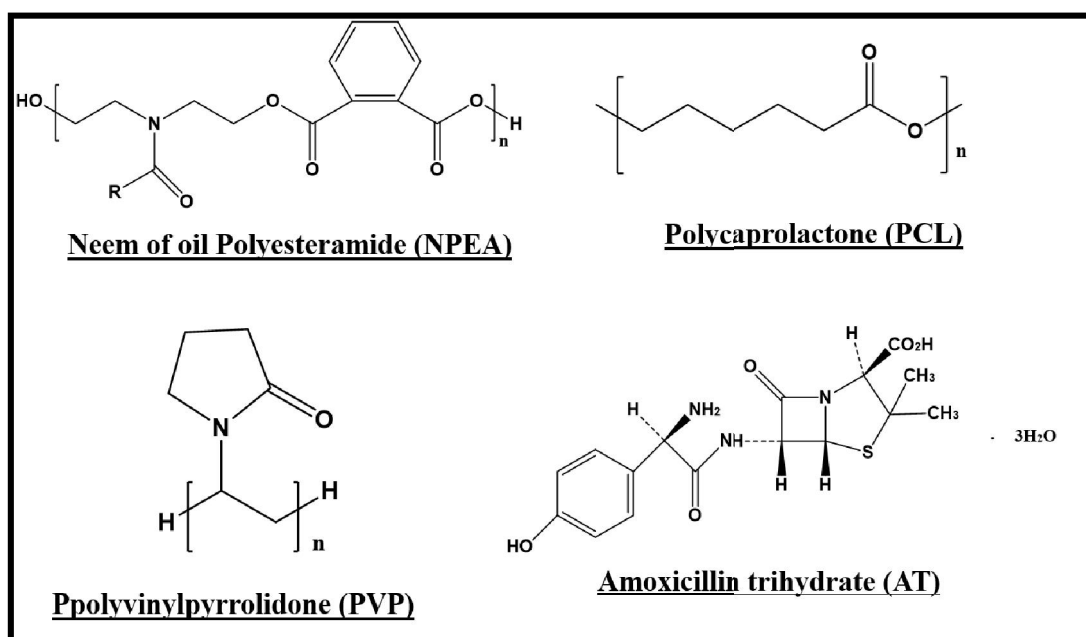
Figure 5. 1 Chemical structures of amoxicillin, PVP, NPEA, and PCL

5.4.1 Characterization of surface morphology of fabricated nanofibers

The surface morphology of Plain-NF, ZnO-NF-3 %, AT-NF-3 %, and AT-ZnO-NF-3 % is shown in **Fig. 5.2** (FE-SEM) and **Fig. 5.3** (TEM). The fabricated nanofibers were validated by FE-SEM and TEM investigation, the diameter of a single nanofiber is ~176nm (TEM). Importantly, the nanofibers produced were smooth and randomly oriented, indicating a homogeneous mixing of polymers and the presence of ZnO was confirmed by TEM analysis.
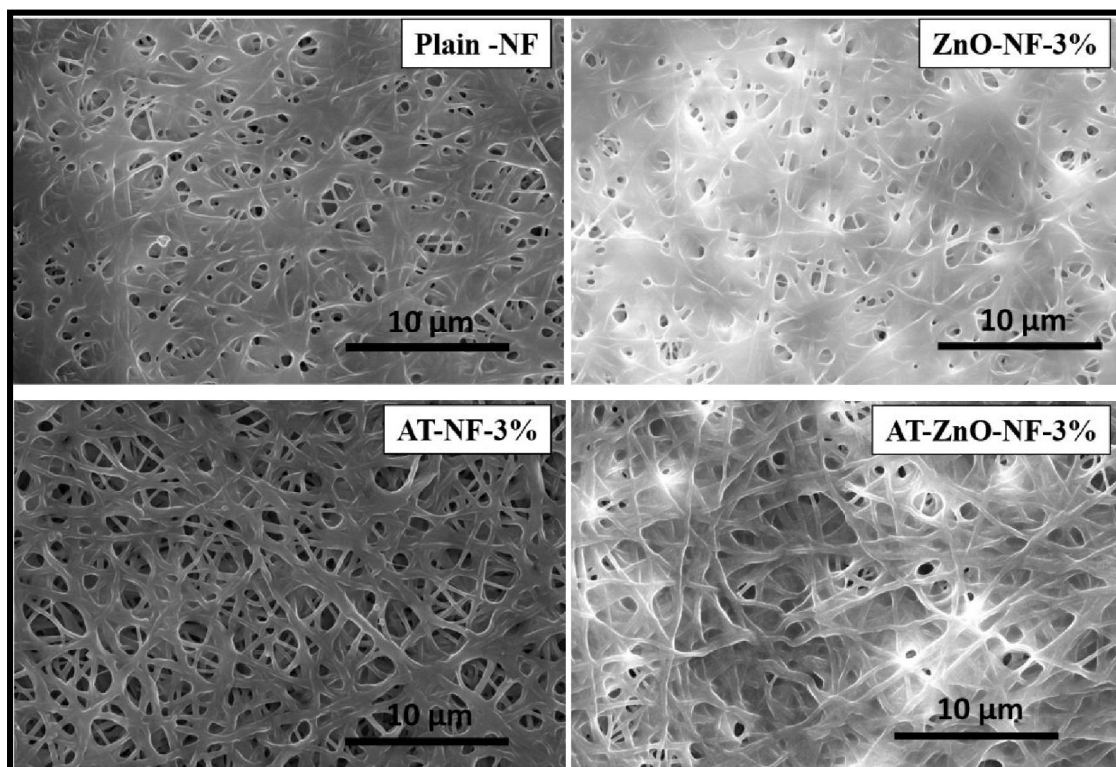
Figure 5. 2 Surface morphology of fabricated nanofibers evaluated by FESEM of Plain-NF, ZnO-NF-3%, AT-NF-3% and AT-ZnO-3%.
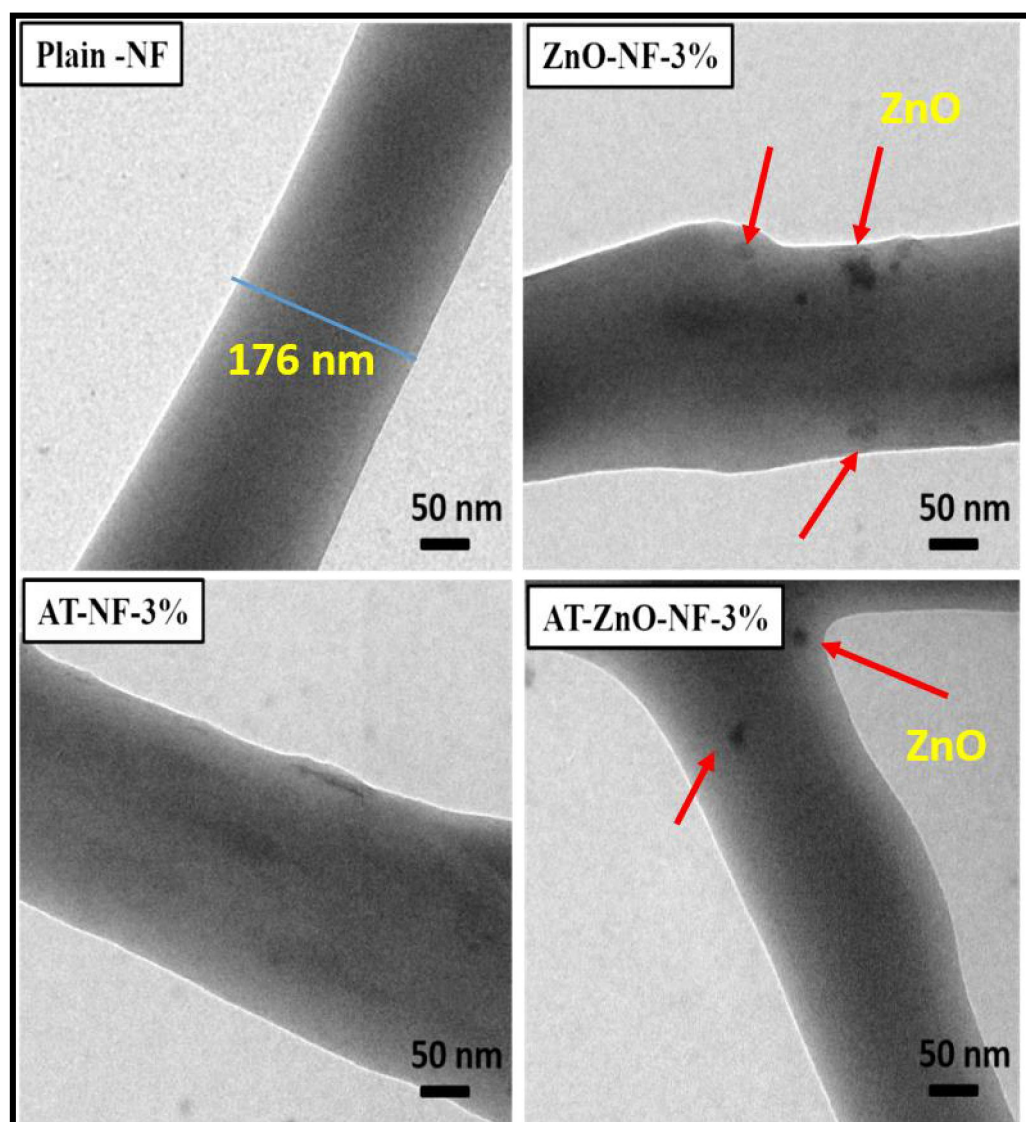
Figure 5. 3 . TEM image of Plain-NF, ZnO-NF-3%, AT-NF-3% and AT-ZnO-3%.

5.4.2 Chemical analyses by FTIR spectrum

The FTIR spectrum was used to examine the presence of active agents after the fabrication of nanofibers. FTIR of raw materials was also analyzed PVP, PCL, NPEA, ZnO, and AT (**Fig. 5.4**). PVP demonstrated O–H stretching at 3425 cm^{-1} as a result of hydrogen-bonded water. The existence of asymmetric stretching of CH$_3$, stretching of –C=O, and stretching of C–N was shown by the typical peaks at 2925, 1665, and 1290 cm^{-1}, respectively[58, 59]. FTIR spectra of PCL recorded peaks for asymmetric –CH$_2$ stretching and symmetric –CH$_2$ stretching were seen at 2943 and 2864 cm^{-1}, respectively. A sharp peak at 1725 cm^{-1} was seen owing to the presence of carbonyl

stretching (–C=O), and a peak at 1186 cm^{-1} was observed due to the presence of –C–C stretching[60]. The FTIR spectra of NPEA measured a peak for –C–H at 2910 cm^{-1}. Additionally, the typical peaks at 1710 cm^{-1} and 1605 cm^{-1} were driven by –C–C=O and –N–C=O (amide) functional groups[45]. FTIR of AT showed the presence of hydrogen-bonded OH stretching, N-H stretching of secondary amine/OH stretching, and CH stretching of aromatic ring was confirmed by absorption bands at 3413 cm^{-1}, 3170 cm^{-1}, and 3033 cm^{-1} respectively. The peak at 2970 cm^{-1} is produced by alkyl group asymmetric CH stretching vibration. The peak at 1789 cm^{-1} corresponds to the C=O stretching vibration and is indicative of the β-Lactum ring of AT. Stretching vibrations (C=O and C-N) of primary amines are designated to absorption peaks at 1693 cm^{-1} and 1249 cm^{-1}, respectively[61] [62, 63]. As reported, several peaks appeared at 3390 cm^{-1}, 2942 cm^{-1}, 1659 cm^{-1}, 1418 cm^{-1}, 1186 cm^{-1}, and 1037 for the ZnO nanoparticles[64]. Further, the peak at 566 cm^{-1} corresponds to metal oxygen (ZnO stretching vibration)[64]. The IR spectra of Plain-NF, ZnO-NF-3%, AT-NF-3%, and AT-ZnO-NF-3% are shown in **Fig. 5.4**, with distinctive peaks such as 3433, 2923, 2855, 1720, and 1660 cm^{-1} indicated the existence of PCL, NPEA, and PVP in the developed nanofibers. Furthermore, the IR of ZnO-NF-3%, AT-NF-3%, and AT- ZnO-NF-3% percent revealed a broad peak about 3433 cm^{-1} due to the NH and hydroxyl groups present in AT. This peak was not seen in the Plain-NF spectra. An intense peak was observed at 1660 cm^{-1}, which was due to the merging of amide I and amide II of AT and as well due to functional interactions with the peaks of the polymer at that range. However, some peaks of ZnO and AT were merged with the peaks of polymers. Nonetheless, the inclusion of ZnO was strongly supported by XRD (**Fig. 5.6**).
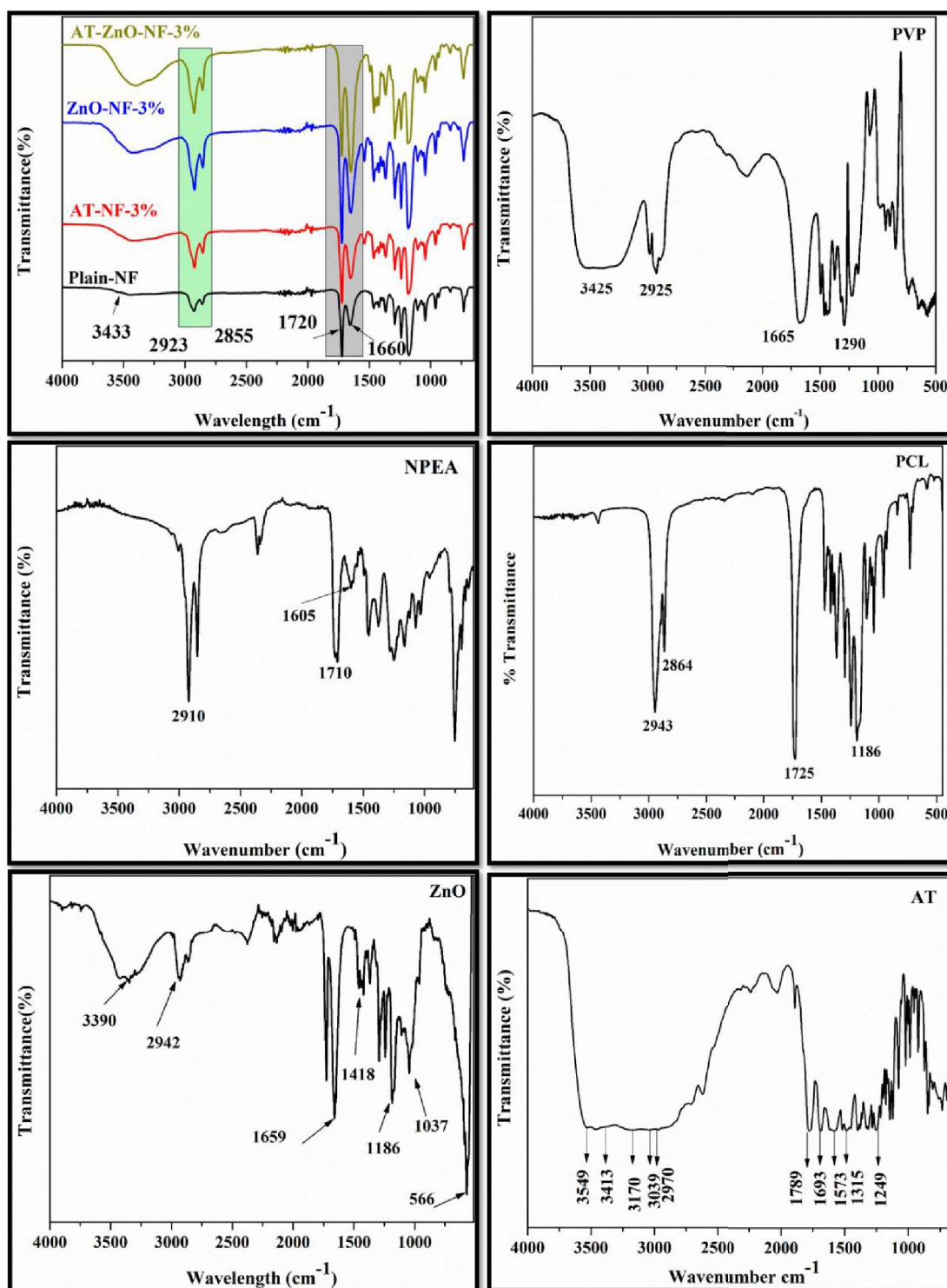
Figure 5. 4 FTIR analysis of Plain-NF, ZnO-NF-3%, AT-NF-3% and AT-ZnO-3% and raw materials, PCL, PVP, NPEA, ZnO and AT.

5.4.3   Differential scanning calorimetry analyses

The thermograms of pure polymers, PCL, PVP, NPEA, and active agents ZnO, and AT was shown in **Fig. 5.5**. Pure ZnO showed an endothermic peak at 130 ºC, which may be due to the dissociation of ZnO molecules and evaporation of water vapors from the surface of ZnO [59, 65]. The thermogram of pure PCL recorded a T_g at -59 ºC and T_m at 56 ºC, suggesting that PCL is semi-crystalline. The obtained values are in accordance with reported literature [57] . NPEA recorded a T_g at -12 ºC. T_m was not recorded hence it is confirmed to be an amorphous polymer[66]. PVP recorded a broad endothermic peak of T_g at 78 ºC and T_m was observed at 184 ºC [67]. The pure AT showed an endothermic peak at 127 ºC, which attributed to T_m. This value is comparable with the reported literature[68]. Plain-NF, ZnO-NF-3%, AT-NF-3%, and ZnO-AT-NF-3% nanofiber mats all exhibited an endothermic peak at 55, 56, 54, and 56 ºC respectively indicating the presence of PCL. There was no significant change in Tm of PCL (**Fig. 5.5**). Since all of the polymers had a similar melting temperature, it suggests that the nanofibers were well blended. The endothermic peaks of ZnO and AT were undetectable, indicating that ZnO and AT were mixed with polymers homogeneous.
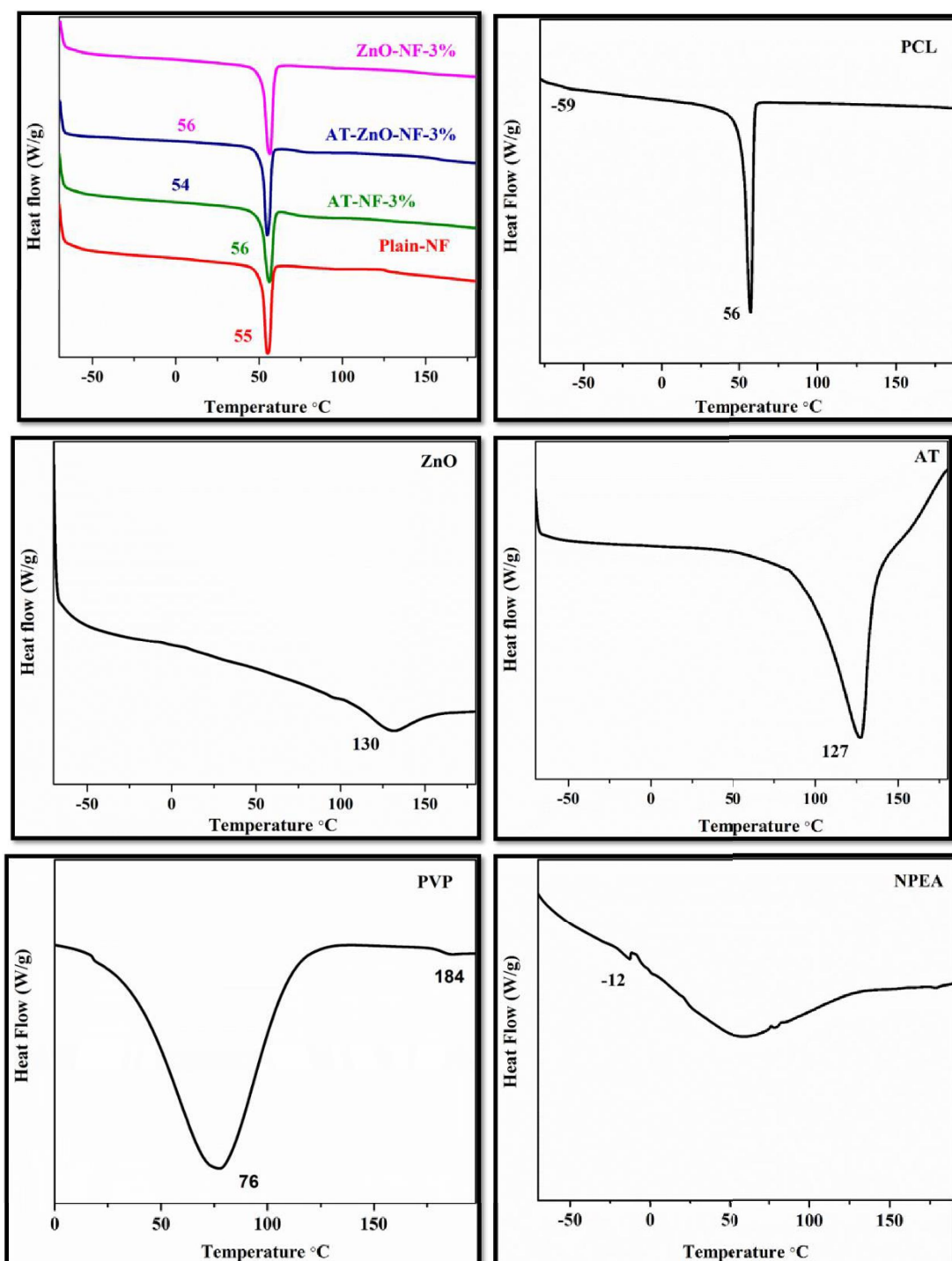
Figure 5. 5 DSC analysis of Plain-NF, ZnO-NF-3%, AT-NF-3% and AT-ZnO-3% and raw materials PCL, NPEA, PVP, ZnO and AT.

5.4.4   XRD analysis

The crystallinity of the fabricated nanofibers and raw materials was investigated using the X-ray diffraction technique (**Fig. 5.6**). As AT is crystalline in nature, the XRD pattern showed many strong peaks at 12, 15, 18, 23, and 28°[69]. The ZnO had a distinct peak at 32, 35, and 36°, which in accordance with reported literature[70]. PVP exhibited a board peak at 11 and 22°, indicating that it is in an amorphous state[71]. PCL has two distinct sharp peaks at 22 and 24°, indicating that it is crystalline in nature[72]. Plain-XRD NF's pattern revealed classic PCL peaks with low intensity at 21 and 23°. PCL is crystalline in nature, whereas PVP is amorphous. After blending the polymers PCL, PVP, and NPEA and fabricating nanofibers, the crystallinity of PCL reduced so the peak intensities decreased. Nevertheless, the crystallinity of nanofibers enhanced after the addition of ZnO (AT- ZnO-- ZnO-NF-3%), which reflected at 8°. Furthermore, AT-ZnO-NF-3% displayed improved peak intensity at 21 and 23° due to the presence of AT. Finally, we conclude that the presence of AT and ZnO impacted the changes in crystalline characteristics due to the systematic structural interactions between polymers and active molecules.
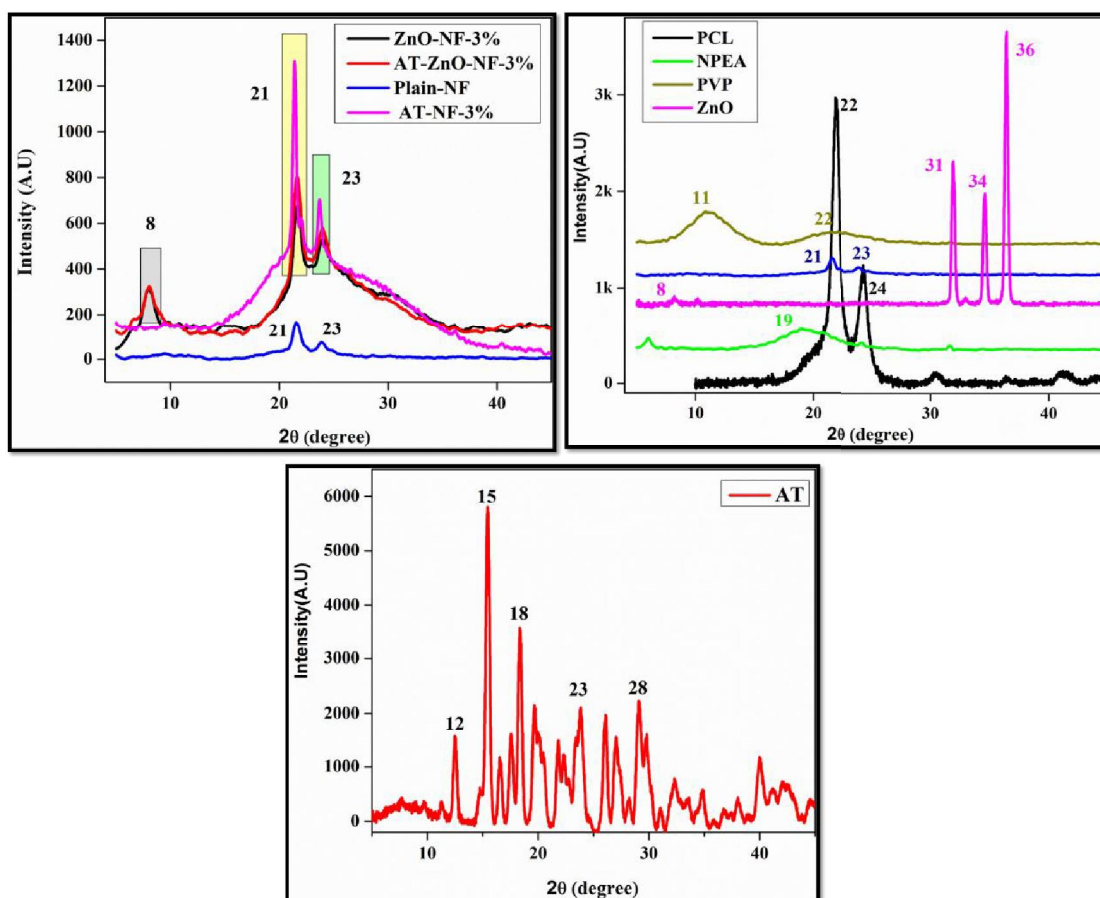
Figure 5. 6 XRD analysis of Plain-NF, ZnO-NF-3%, AT-NF-3% and AT-ZnO-3%.

5.4.5   Drug release studies

Release studies of AT were performed in a water bath shaker for the respective samples loaded with AT (AT-NF-3% and AT-ZnO-NF-3%) in PBS of pH 7.4 at 37℃. AT-NF-3% and AT-ZnO-NF-3% demonstrated a burst release of over 80% in just 120 minutes. About 92% drug release was demonstrated after 480 minutes (**Fig. 5.7**). It was also observed that the presence of ZnO in the nanofiber mat along with AT did not show a significant change in drug release. The results of these studies suggest that the produced nanofibers can be a choice for wound healing, as the first burst release eliminates overgrown bacteria and later with slow release the infection of the wound can be avoided. Similar burst release was also observed when curcumin is loaded in zein–silk fibroin–chitosan nanofibers for wound healing application[73], which proved to be an effective wound healing material. Hence we consider that the developed nanofiber mat can be employed for topical application to treat bacterial infection at a faster rate. A

burst release was observed because of the hydrophilic polymer PVP, which was 3%. To regulate the release, the concentration of PVP can be reduced to either 2 or 1% depending on the requirement.
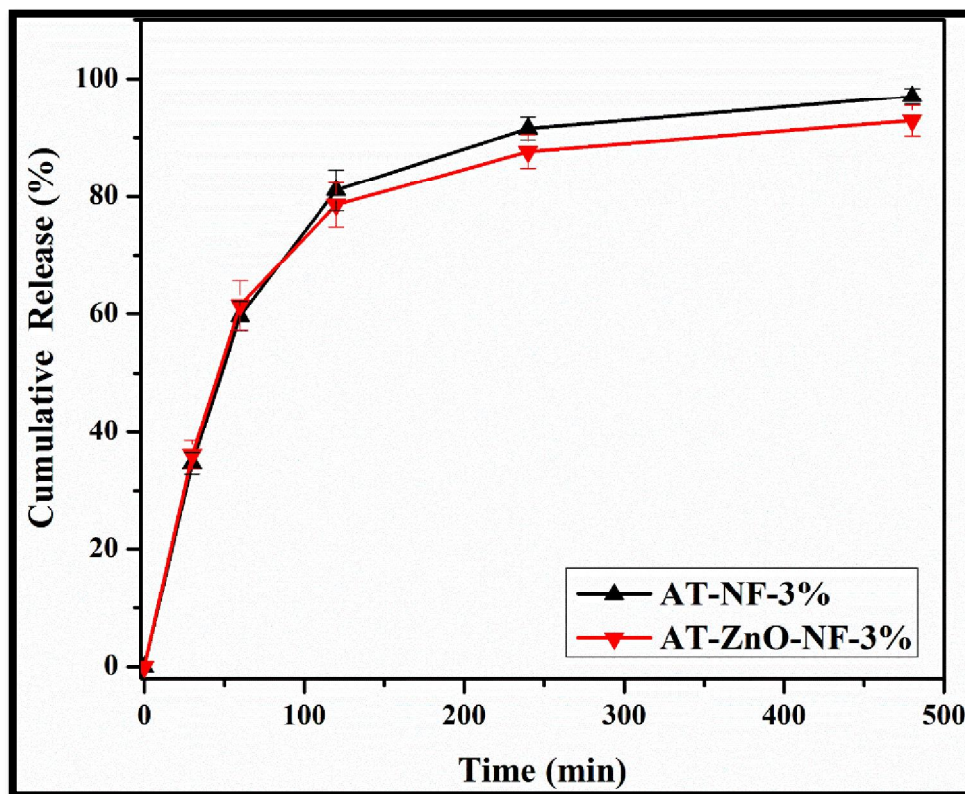
Figure 5. 7 Drug release studies PBS of pH 7.4 at 37oC of AT-NF-3% and AT-ZnO-3%.

5.4.6 Cell viability studies

The developed nanofibers (Plain-NF, ZnO-NF-3%, AT-NF-3% and AT-ZnO-NF-3%.) were studied for cytotoxicity in NIH3T3 (mouse embryonic fibroblasts for 24 h) (**Fig. 5.8**). The developed nanofibers showed more than 70% of cell viability, suggesting safety (ISO 10993-5:2009, E guidelines) of the nanofiber composites for biological application in wound healing. The Plain-NF was used as control, ZnO-NF-3% showed 70±7% of cell viability which is lower in comparison to AT-NF-3% and AT-ZnO-NF-3% as 79±10% and 74±6% respectively. The decrease in cell viability in ZnO loaded nanofibers may be due to ZnO toxicity. However, these results of cell viability studies revealed that the fabricated nanofibers are non-toxic and safe for wound application.
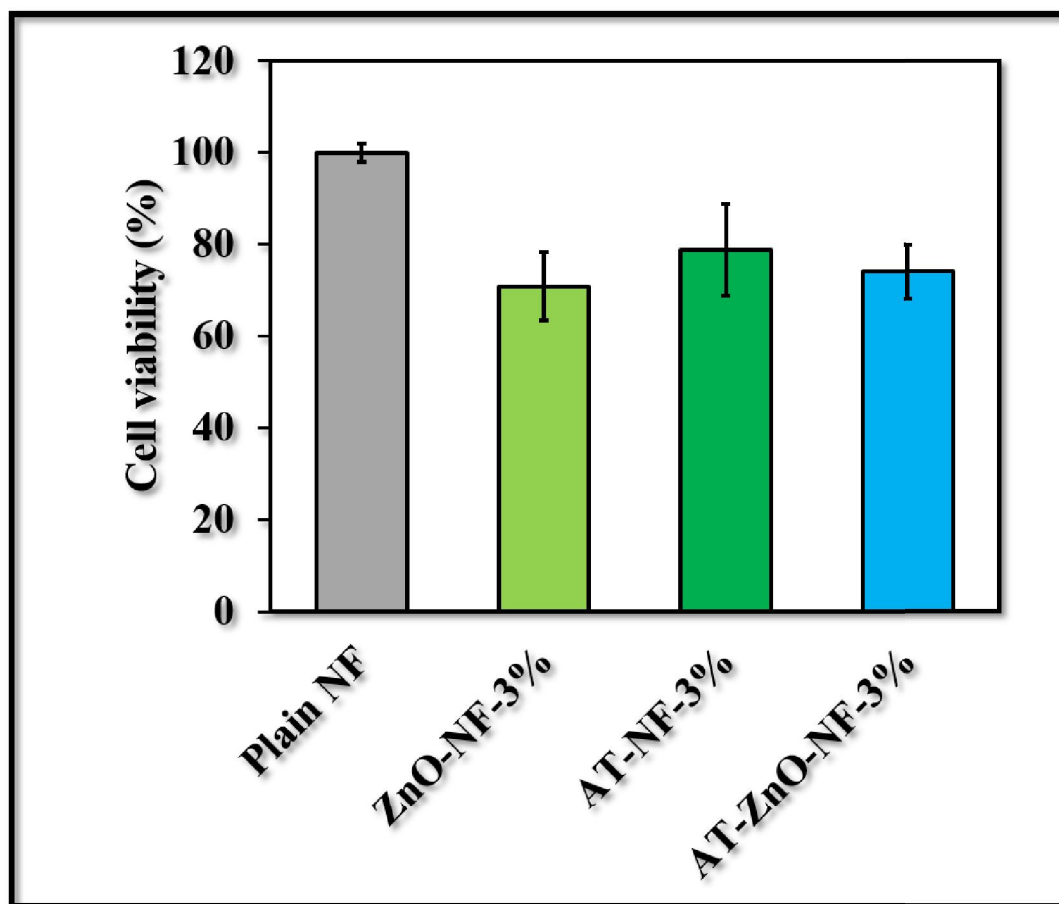
Figure 5. 8 Cytotoxicity was performed using NIH3T3 (mouse embryonic fibroblasts) cells on Plain-NF, ZnO-NF-3%, AT-NF-3% and AT-ZnO-NF-3%.

5.4.7   Antibacterial activity

Control and Plain-NF showed lawn growth of bacterial cultures on nutrient agar. In contrast, AT alone demonstrated complete inhibition of *E. coli* and *S. aureus* (**Fig. 5.9**). Similarly, ZnO alone demonstrated an inhibitory effect on both bacterial cultures. AT-ZnO-NF-3% and AT-NF-3% exhibited more reduced growth of *E. coli* compared to *S. aureus*. Compared to AT alone or ZnO alone reduced inhibitory effect was noted. The reason might be the w/w ratio of AT or ZnO loaded on the NF membrane. Results, suggest that NF mats loaded with standard antibiotic AT and ZnO imparts antibacterial activity to the mat, beneficial for biomedical application.
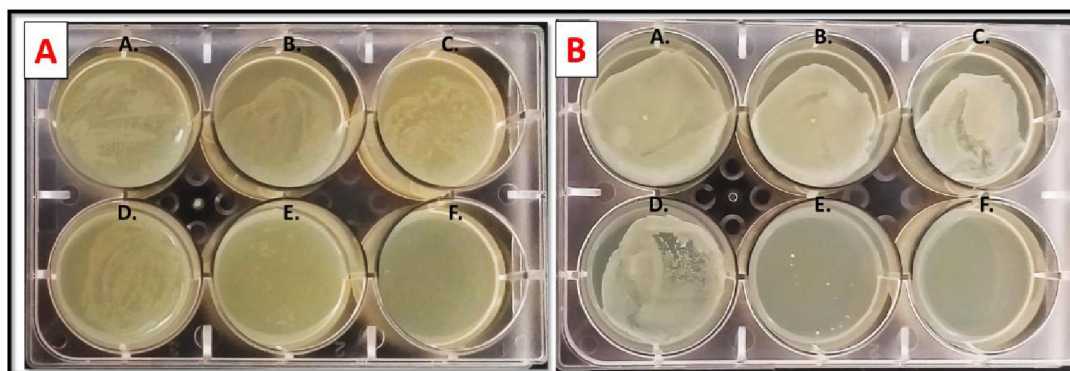
Figure 5. 9 A, Antibacterial activity for Gram-negative bacteria   *E. coli* and **B**, Gram-positive bacteria, *S. aureus*. A. Control (Without any treatment); B. Plain NF; C. AT-ZnO-NF-3%; D. ZnO-NF-3%; E. ZnO alone (3%); F. AT alone (3%).

5.4.8   *In vitro* wound healing potential studies

Scratch assay was performed on NIH3T3 fibroblast cells. Scratch imprinted with the pipette's tip represents the wound to monolayered NIH3T3 cells (**Fig. 5.10**). In control cells (treated with plain NF), the gap was slightly surrounded by cells on 3, 6 or 12 h. Upon 3 h treatment with AT-ZnO-NF-3% demonstrated mobility of cells towards healing the gap in monolayer cells compared to 0 min. Similarly, ZnO-NF-3% treated cells showed slight cell mobility within the scratch. In both, ZnO-NF-3% and AT-ZnO-NF-3%, the scratch was recovered with cell monolayer upon treatment with 6 and 12 h. The scratch healing demonstrated the potential of ZnO loaded NF in healing wound-induced in the NIH3T3 cell monolayer.

As a proliferative indicator, Ki67 staining was carried out to evaluate the wound healing potential of NIH3T3 cells. Except for the G0 phase, the Ki67 marker is actively found in all other cell cycle phases. Representative images showed increased brown-coloured cells, indicating Ki67 markers were found in cells treated with ZnO-NF-3% and AT-ZnO- NF-3% compared to control (**Fig. 5.11**). However, the number of cells and brown stained cells were found to be lower in AT-NF-3% treated cells. Results suggest that the presence of ZnO induces proliferation in NIH3T3 cells. No treatments were found to inhibit cell growth; hence, no statistically significant cell proliferation is observed compared to control. Further, **Fig. 5.11** demonstrated cell proliferation and an average

number of cell count in bar and line graph. However, quantitatively the number of cells was increased with ZnO loaded nanofiber mats. Summarizing, results demonstrate increased proliferative potential due to the presence of ZnO. Additionally, the antibacterial activity of AT and ZnO would benefit the application of AT-ZnO-NF-3% mat in wound healing. Further, **Fig. 5.12** demonstrated cell proliferation and an average number of cell count in bar and line graph.
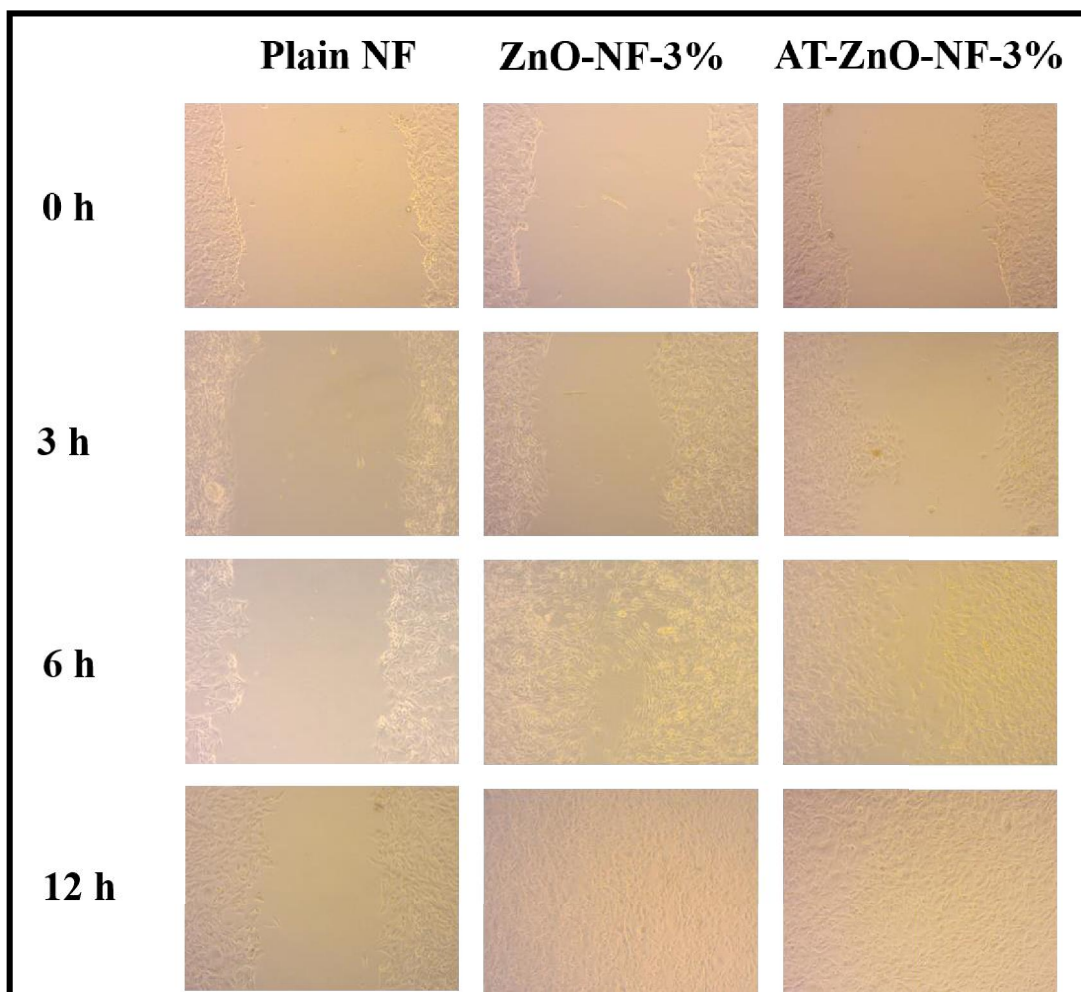
Figure 5. 10 Evaluation of wound healing potential, *in vitro*. Scratch assay demonstrating the wound healing potential of ZnO-NF-3% and AT-ZnO-NF-3% in a time-dependent manner.
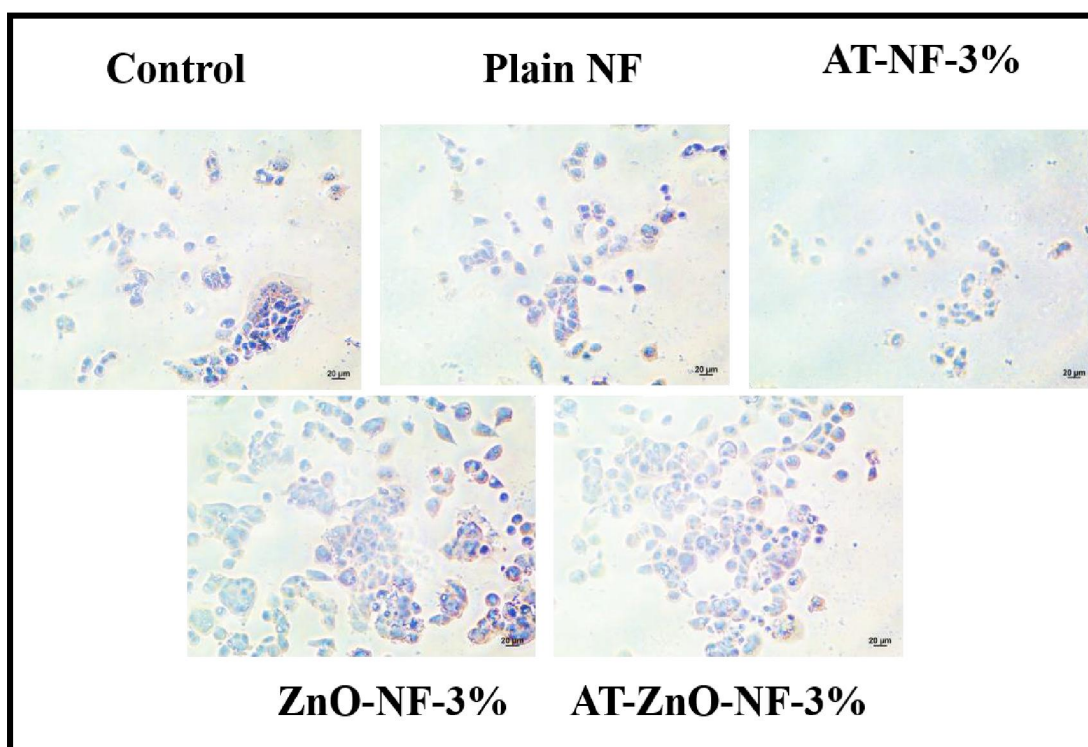
Figure 5. 11 Representative images of Ki67 immunocytohistochemistry demonstrate increased proliferation with ZnO presence. Quantitative estimation of proliferating cells and an average number of cells upon treatment with Plain NF, AT-NF-3%, ZnO-NF-3%, and AT-ZnO-NF-3% after 12 h.
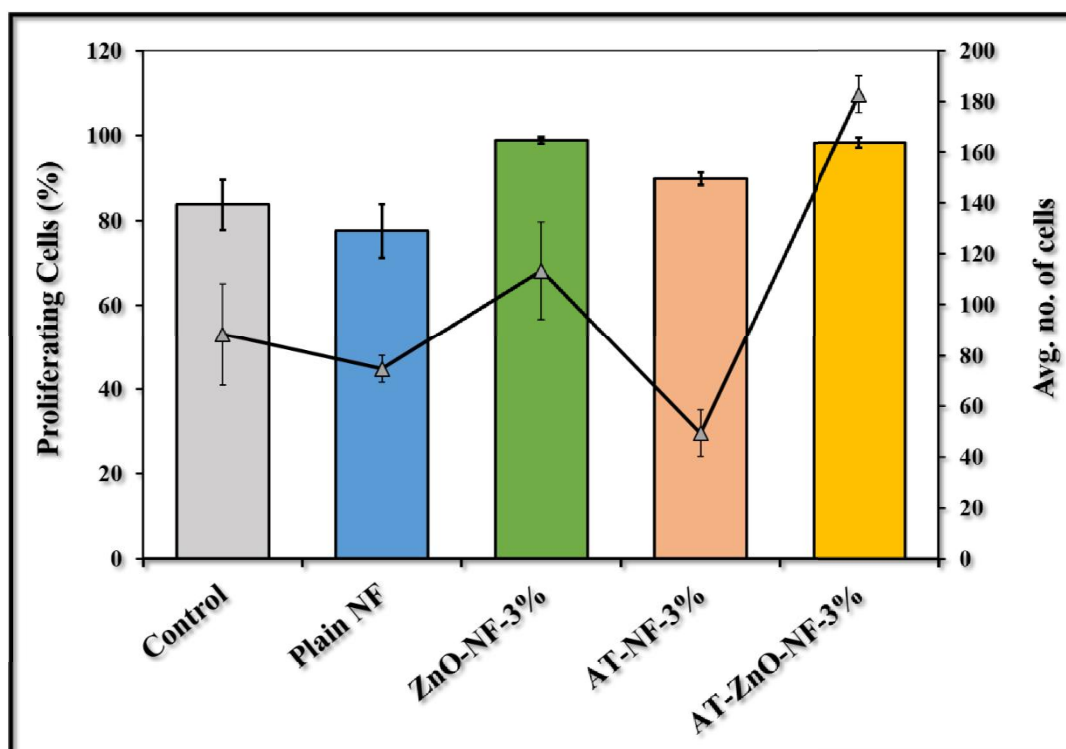
Figure 5. 12 Evaluation of wound healing potential, *in vitro*. Bar diagram of cell proliferation and line graph of average number of cells.

5.4.9 Assessment of wound healing, *in vivo*

Fig. 5.13 demonstrates the representative images of the wound site indicating the progressive decrease in wound area during the treatment period in all groups, except group I. Treatment of animals with nanofiber mats with active agent showed significant wound healing activity compared to the positive and negative control. On the 6th day, the percent of wound healing of rats treated with nanofiber mats plain-NF, ZnO-NF-3%, and AT-ZnO-NF-3% was better than wound-induced control (negative control) and positive control rats. On the 18th day, the rats treated with Plain-NF, ZnO-NF-3% and AT-ZnO-NF-3% recorded more than 90% wound healing whereas, the percent of wound healing treated with the other samples such as Povidone-Iodine ointment and control recorded~82% and~54% respectively as shown in (**Fig. 5.13** and **Table 5.3**).

Table 5. 3 *In vivo* studies showing percentage wound healing on 6th and 18th

Groups	Group details	Wound healing (%)	
		6th day	18th day
Group I	Wound-induced control group	13.33±1.55	54±1.41
Group II	Povidone-Iodine ointment treated	14.66±1.13	82.33±0.78
Group III	Plain-NF-treated group	25.33±2.41	90.66±0.74
Group IV	ZnO-NF-3%-treated group	24±1.65	93.33±0.39
Group V	AT-ZnO-NF-3%-treated group	36.66±1.38	98.66±0.88

Figure 5. 13 Representative images of wound healing development on 6th and 18th day for Wound-induced control group, Povidone-Iodine ointment treated group, Plain-NF-treated group, ZnO-NF-3%-treated group, AT-ZnO-NF-3%-treated group.

5.4.10 Histopathological studies

Histopathological studies of the healed wound tissues were performed on the 21st day of the experimental period to understand the inflammatory response and collagen

formation during the wound healing process. Masson's trichrome stained sections of wound tissues treated and untreated with nanofiber mats are shown in **Fig. 5.14**. Masson's trichrome stain nuclei (dark purple colour) and other basophilic structures selectively stain collagen (blue colour) and muscles (red/pink colour). The wound-induced control animals showed incomplete wound healing with discontinuous deposition of collagen and severe inflammatory response with the presence of neutrophils and basophils (**Fig. 5.14 A**). The wound tissue of Povidone-Iodine (**Fig. 5.14 B**) and Plain-NF (**Fig. 5.14 C**) treated animals showed mild inflammatory response with the presence of few neutrophils macrophages along with fibroblast cells. Further, the ZnO-NF-3% (**Fig. 5.14 D**) and AT-ZnO-NF3% (**Fig. 5.15 E**) showed reformed collagen with thin epidermis and dermis.
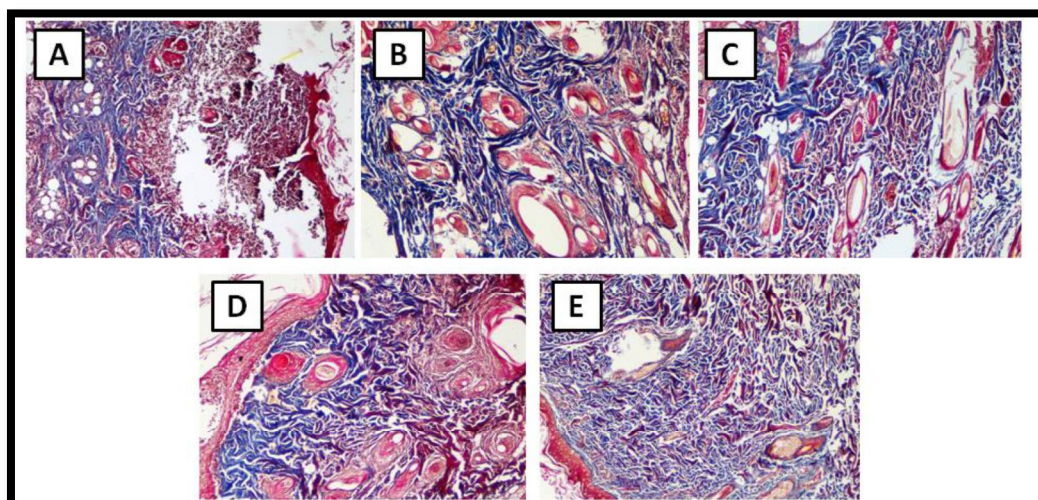
Figure 5. 14 Assessment of wound healing potential, *in vivo* by histopathology studies. Representative images of wound tissue under a light microscope (400X), stained with Masson's trichrome of (A) Group I; (B) Group II, (C) Group III, (D) Group IV, and (E) Group V.

5.5 Conclusion

We used electrospinning technology to create a dual drug (ZnO and AT) loaded nanofibers system for wound healing. The produced nanofibers were smooth and bead-free, TEM analysis confirmed the presence of ZnO. The produced nanofibers were thoroughly mixed, as shown by DSC, XRD, and FTIR, confirming the presence of all

polymers and bioactive agents (ZnO and AT). The drug release studies recorded the burst release of AT. Antibacterial investigations of nanofibers containing the respective ZnO and AT revealed suppression of *E.coli* and *S.aureus* growth. The produced nanofibers reported cell proliferation favoring tissue regeneration. The *in vitro* scratch assay experiment confirmed wound healing as the cells were well grown and got migrated.

Furthermore, *in vivo* wound healing on male Wistar albino rats revealed that nanofibers containing both AT and ZnO drug had a substantial wound healing potential compared to nanofibers having only AT. The histopathology studies showed reformed collagen with thin epidermis and dermis supporting the wound healing studies. Finally, we conclude that the dual drug-loaded nanofibers were considerably favorable for wound healing.

5.6 References

[1] G. FrykbergRobert, Challenges in the treatment of chronic wounds, Advances in wound care (2015).

[2] C.K. Sen, G.M. Gordillo, S. Roy, R. Kirsner, L. Lambert, T.K. Hunt, F. Gottrup, G.C. Gurtner, M.T. Longaker, Human skin wounds: a major and snowballing threat to public health and the economy, Wound repair and regeneration 17(6) (2009) 763-771.

[3] S. Bayat, N. Amiri, E. Pishavar, F. Kalalinia, J. Movaffagh, M. Hashemi, Bromelain-loaded chitosan nanofibers prepared by electrospinning method for burn wound healing in animal models, Life sciences 229 (2019) 57-66.

[4] A.V. Nguyen, A.M. Soulika, The dynamics of the skin's immune system, International journal of molecular sciences 20(8) (2019) 1811.

[5] K.A. Rieger, N.P. Birch, J.D. Schiffman, Designing electrospun nanofiber mats to promote wound healing–a review, Journal of Materials Chemistry B 1(36) (2013) 4531-4541.

[6] A. Memic, T. Abudula, H.S. Mohammed, K. Joshi Navare, T. Colombani, S.A. Bencherif, Latest progress in electrospun nanofibers for wound healing applications, ACS Applied Bio Materials 2(3) (2019) 952-969.

[7] X. Liu, H. Xu, M. Zhang, D.-G. Yu, Electrospun medicated nanofibers for wound healing, Membranes 11(10) (2021) 770.

[8] M.S.B. Husain, A. Gupta, B.Y. Alashwal, S. Sharma, Synthesis of PVA/PVP based hydrogel for biomedical applications: a review, Energy Sources, Part A: Recovery, Utilization, and Environmental Effects 40(20) (2018) 2388-2393.

[9] Y. Liang, J. He, B. Guo, Functional hydrogels as wound dressing to enhance wound healing, ACS nano 15(8) (2021) 12687-12722.

[10] M. Eleroui, A. Feki, A. Hamzaoui, I. Kammoun, M. Bouhamed, O. Boudawara, I.B. Ayed, I.B. Amara, Preparation and characterization of a novel hamada scoparia polysaccharide composite films and evaluation of their effect on cutaneous wound healing in rat, International Journal of Pharmaceutics 608 (2021) 121056.

[11] S. Saghazadeh, C. Rinoldi, M. Schot, S.S. Kashaf, F. Sharifi, E. Jalilian, K. Nuutila, G. Giatsidis, P. Mostafalu, H. Derakhshandeh, Drug delivery systems and materials for wound healing applications, Advanced drug delivery reviews 127 (2018) 138-166.

[12] Y. Dong, Y. Zheng, K. Zhang, Y. Yao, L. Wang, X. Li, J. Yu, B. Ding, Electrospun nanofibrous materials for wound healing, Advanced Fiber Materials 2(4) (2020) 212-227.

[13] I.S. Raja, D.R. Preeth, M. Vedhanayagam, S.-H. Hyon, D. Lim, B. Kim, S. Rajalakshmi, D.-W. Han, Polyphenols-loaded electrospun nanofibers in bone tissue engineering and regeneration, Biomaterials Research 25(1) (2021) 1-16.

[14] E.A. Kamoun, S.A. Loutfy, Y. Hussein, E.-R.S. Kenawy, Recent advances in PVA-polysaccharide based hydrogels and electrospun nanofibers in biomedical applications: A review, International Journal of Biological Macromolecules 187 (2021) 755-768.

[15] K. Kalantari, A.M. Afifi, H. Jahangirian, T.J. Webster, Biomedical applications of chitosan electrospun nanofibers as a green polymer–Review, Carbohydrate polymers 207 (2019) 588-600.

[16] B. Pant, M. Park, S.-J. Park, Drug delivery applications of core-sheath nanofibers prepared by coaxial electrospinning: a review, Pharmaceutics 11(7) (2019) 305.

[17] T.A. Jeckson, Y.P. Neo, S.P. Sisinthy, B. Gorain, Delivery of therapeutics from layer-by-layer electrospun nanofiber matrix for wound healing: An update, Journal of Pharmaceutical Sciences 110(2) (2021) 635-653.

[18] H.S. Sofi, R. Rashid, T. Amna, R. Hamid, F.A. Sheikh, Recent advances in formulating electrospun naofiber membranes: Delivering active phytoconstituents, Journal of Drug Delivery Science and Technology (2020) 102038.

[19] K. Ye, H. Kuang, Z. You, Y. Morsi, X. Mo, Electrospun nanofibers for tissue engineering with drug loading and release, Pharmaceutics 11(4) (2019) 182.

[20] A. Abdal-hay, M. Taha, H.M. Mousa, M. Bartnikowski, M.L. Hassan, M. Dewidar, S. Ivanovski, Engineering of electrically-conductive poly (ε-caprolactone)/multi-walled carbon nanotubes composite nanofibers for tissue engineering applications, Ceramics International 45(12) (2019) 15736-15740.

[21] S. Malik, S. Sundarrajan, T. Hussain, A. Nazir, M. Ayyoob, F. Berto, S. Ramakrishna, Sustainable nanofibers in tissue engineering and biomedical applications, Material Design & Processing Communications 3(6) (2021) e202.

[22] F. Dong, M. Zhang, W.-W. Tang, Y. Wang, Formation and mechanism of superhydrophobic/hydrophobic surfaces made from amphiphiles through droplet-mediated evaporation-induced self-assembly, The Journal of Physical Chemistry B 119(16) (2015) 5321-5327.

[23] Y. Wang, L. Chen, Fabrication and characterization of novel assembled prolamin protein nanofabrics with improved stability, mechanical property and release profiles, Journal of Materials Chemistry 22(40) (2012) 21592-21601.

[24] X. Wang, B. Ding, G. Sun, M. Wang, J. Yu, Electro-spinning/netting: A strategy for the fabrication of three-dimensional polymer nano-fiber/nets, Progress in materials science 58(8) (2013) 1173-1243.

[25] J.A. Bhushani, C. Anandharamakrishnan, Electrospinning and electrospraying techniques: Potential food based applications, Trends in Food Science & Technology 38(1) (2014) 21-33.

[26] P. Karuppuswamy, J.R. Venugopal, B. Navaneethan, A.L. Laiva, S. Sridhar, S. Ramakrishna, Functionalized hybrid nanofibers to mimic native ECM for tissue engineering applications, Applied surface science 322 (2014) 162-168.

[27] J.X. Law, L.L. Liau, A. Saim, Y. Yang, R. Idrus, Electrospun collagen nanofibers and their applications in skin tissue engineering, Tissue engineering and regenerative medicine 14(6) (2017) 699-718.

[28] M. Movahedi, A. Asefnejad, M. Rafienia, M.T. Khorasani, Potential of novel electrospun core-shell structured polyurethane/starch (hyaluronic acid) nanofibers for skin tissue engineering: In vitro and in vivo evaluation, International journal of biological macromolecules 146 (2020) 627-637.

[29] S. Mengistu Lemma, F. Bossard, M. Rinaudo, Preparation of pure and stable chitosan nanofibers by electrospinning in the presence of poly (ethylene oxide), International journal of molecular sciences 17(11) (2016) 1790.

[30] J. Santiago-Morales, G. Amariei, P. Letón, R. Rosal, Antimicrobial activity of poly (vinyl alcohol)-poly (acrylic acid) electrospun nanofibers, Colloids and Surfaces B: Biointerfaces 146 (2016) 144-151.

[31] G. Karayeğen, İ.C. Koçum, D. Çökeliler Serdaroğlu, M. Doğan, Aligned polyvinylpyrrolidone nanofibers with advanced electrospinning for biomedical applications, Bio-medical materials and engineering 29(5) (2018) 685-697.

[32] H.F. Alharbi, M. Luqman, K.A. Khalil, Y.A. Elnakady, O.H. Abd-Elkader, A.M. Rady, N.H. Alharthi, M.R. Karim, Fabrication of core-shell structured nanofibers of poly (lactic acid) and poly (vinyl alcohol) by coaxial electrospinning for tissue engineering, European Polymer Journal 98 (2018) 483-491.

[33] K. Zhang, Y. Wang, T. Sun, B. Wang, H. Zhang, Bioinspired surface functionalization for improving osteogenesis of electrospun polycaprolactone nanofibers, Langmuir 34(50) (2018) 15544-15550.

[34] M.M. Castillo-Ortega, A. Nájera-Luna, D.E. Rodríguez-Félix, J.C. Encinas, F. Rodríguez-Félix, J. Romero, P.J. Herrera-Franco, Preparation, characterization and release of amoxicillin from cellulose acetate and poly (vinyl pyrrolidone) coaxial electrospun fibrous membranes, Materials Science and Engineering: C 31(8) (2011) 1772-1778.

[35] B. Nair, Final report on the safety assessment of polyvinylpyrrolidone (PVP), International journal of toxicology 17(4_suppl) (1998) 95-130.

[36] M.V. Risbud, S.V. Bhat, Properties of polyvinyl pyrrolidone/β-chitosan hydrogel membranes and their biocompatibility evaluation by haemorheological method, Journal of materials science: Materials in medicine 12(1) (2001) 75-79.

[37] M. Heidari, S.H. Bahrami, M. Ranjbar-Mohammadi, P.B. Milan, Smart electrospun nanofibers containing PCL/gelatin/graphene oxide for application in nerve tissue engineering, Materials science and engineering: C 103 (2019) 109768.

[38] S.-F. Chou, K.A. Woodrow, Relationships between mechanical properties and drug release from electrospun fibers of PCL and PLGA blends, Journal of the mechanical behavior of biomedical materials 65 (2017) 724-733.

[39] R. Tavakoli, S. Vakilian, F. Jamshidi-Adegani, S. Sharif, A. Ardeshirylajimi, M. Soleimani, Prolonged drug release using PCL–TMZ nanofibers induce the apoptotic behavior of U87 glioma cells, International Journal of Polymeric Materials and Polymeric Biomaterials 67(15) (2018) 873-878.

[40] J. Jerobin, P. Makwana, R.S.S. Kumar, R. Sundaramoorthy, A. Mukherjee, N. Chandrasekaran, Antibacterial activity of neem nanoemulsion and its toxicity assessment on human lymphocytes in vitro, International journal of nanomedicine 10(Suppl 1) (2015) 77.

[41] J. Wang, J. Li, J. Cao, W. Jiang, Antifungal activities of neem (Azadirachta indica) seed kernel extracts on postharvest diseases in fruits, African Journal of Microbiology Research 4(11) (2010) 1100-1104.

[42] J.D. Stark, J.F. Walter, Neem oil and neem oil components affect the efficacy of commercial neem insecticides, Journal of Agricultural and Food Chemistry 43(2) (1995) 507-512.

[43] T. Musabyimana, R. Saxena, Efficacy of neem seed derivatives against nematodes affecting banana, Phytoparasitica 27(1) (1999) 43-49.

[44] M. Schumacher, C. Cerella, S. Reuter, M. Dicato, M. Diederich, Anti-inflammatory, pro-apoptotic, and anti-proliferative effects of a methanolic neem (Azadirachta indica) leaf extract are mediated via modulation of the nuclear factor-κB pathway, Genes & nutrition 6(2) (2011) 149-160.

[45] N. Killi, A.T. Pawar, R.V.N. Gundloori, Polyesteramide of neem oil and its blends as an active nanomaterial for tissue regeneration, ACS Applied Bio Materials 2(8) (2019) 3341-3351.

[46] J. Jiang, J. Pi, J. Cai, The advancing of zinc oxide nanoparticles for biomedical applications, Bioinorganic chemistry and applications 2018 (2018).

[47] R. Pati, R.K. Mehta, S. Mohanty, A. Padhi, M. Sengupta, B. Vaseeharan, C. Goswami, A. Sonawane, Topical application of zinc oxide nanoparticles reduces bacterial skin infection in mice and exhibits antibacterial activity by inducing oxidative stress response and cell membrane disintegration in macrophages, Nanomedicine: Nanotechnology, Biology and Medicine 10(6) (2014) 1195-1208.

[48] K. Huang, Z. Jinzhong, T. Zhu, Y. Morsi, A. Aldalbahi, M. El-Newehy, X. Yan, X. Mo, Exploration of the antibacterial and wound healing potential of a PLGA/silk fibroin based electrospun membrane loaded with zinc oxide nanoparticles, Journal of Materials Chemistry B 9(5) (2021) 1452-1465.

[49] P.P. Mahamuni-Badiger, P.M. Patil, P.R. Patel, M.J. Dhanavade, M.V. Badiger, Y.N. Marathe, R.A. Bohara, Electrospun poly (3-hydroxybutyrate-co-3-hydroxyvalerate)/polyethylene oxide (PEO) microfibers reinforced with ZnO nanocrystals for antibacterial and antibiofilm wound dressing applications, New Journal of Chemistry 44(23) (2020) 9754-9766.

[50] P. Jamdagni, P. Khatri, J.S. Rana, Green synthesis of zinc oxide nanoparticles using flower extract of Nyctanthes arbor-tristis and their antifungal activity, Journal of King Saud University-Science 30(2) (2018) 168-175.

[51] J.M.T. Souza, A.R. de Araujo, A.M.A. de Carvalho, A.d.G.N. Amorim, T.C. Daboit, J.R.d.S. de Almeida, D.A. da Silva, P. Eaton, Sustainably produced cashew gum-capped zinc oxide nanoparticles show antifungal activity against Candida parapsilosis, Journal of Cleaner Production 247 (2020) 119085.

[52] Y.-j. Liu, L.-l. He, A. Mustapha, H. Li, Z.Q. Hu, M.-s. Lin, Antibacterial activities of zinc oxide nanoparticles against Escherichia coli O157: H7, Journal of applied microbiology 107(4) (2009) 1193-1201.

[53] P. Bhattacharyya, B. Agarwal, M. Goswami, D. Maiti, S. Baruah, P. Tribedi, Zinc oxide nanoparticle inhibits the biofilm formation of Streptococcus pneumoniae, Antonie Van Leeuwenhoek 111(1) (2018) 89-99.

[54] H. Chhabra, R. Deshpande, M. Kanitkar, A. Jaiswal, V.P. Kale, J.R. Bellare, A nano zinc oxide doped electrospun scaffold improves wound healing in a rodent model, RSC Advances 6(2) (2016) 1428-1439.

[55] M.S. Ågren, L. Franzén, M. Chvapil, Effects on wound healing of zinc oxide in a hydrocolloid dressing, Journal of the American Academy of Dermatology 29(2) (1993) 221-227.

[56] F.I.A. El-Ela, A.A. Farghali, R.K. Mahmoud, N.A. Mohamed, S.A.A. Moaty, New approach in ulcer prevention and wound healing treatment using doxycycline and amoxicillin/LDH Nanocomposites, Scientific reports 9(1) (2019) 1-15.

[57] P.R. Patel, K. Pandey, N. Killi, R.V.N. Gundloori, Manipulating hydrophobicity of polyester nanofiber mats with egg albumin to enhance cell interactions, Polymer Engineering & Science 61(10) (2021) 2496-2510.

[58] A. Rahma, M.M. Munir, A. Prasetyo, V. Suendo, H. Rachmawati, Intermolecular interactions and the release pattern of electrospun curcumin-polyvinyl (pyrrolidone) fiber, Biological and Pharmaceutical Bulletin 39(2) (2016) 163-173.

[59] F. Rahmani, H. Ziyadi, M. Baghali, H. Luo, S. Ramakrishna, Electrospun PVP/PVA Nanofiber Mat as a Novel Potential Transdermal Drug-Delivery System for Buprenorphine: A Solution Needed for Pain Management, Applied Sciences 11(6) (2021) 2779.

[60] B. Abderrahim, E. Abderrahman, A. Mohamed, T. Fatima, T. Abdesselam, O. Krim, Kinetic thermal degradation of cellulose, polybutylene succinate and a green composite: comparative study, World J. Environ. Eng 3 (2015) 95-110.

[61] N. Ojah, D. Saikia, D. Gogoi, P. Baishya, G.A. Ahmed, A. Ramteke, A.J. Choudhury, Surface modification of core-shell silk/PVA nanofibers by oxygen dielectric barrier discharge plasma: Studies of physico-chemical properties and drug release behavior, Applied Surface Science 475 (2019) 219-229.

[62] I. Nugrahani, S. Asyarie, S.N. Soewandhi, S. Ibrahim, Solid state interaction between amoxicillin trihydrate and potassium Clavulanate, Malays. J. Pharm. Sci 5(1) (2007) 45-57.

[63] A. Reiss, A. Samide, G. Ciobanu, I. Dabuleanu, Synthesis, spectral characterization and thermal behaviour of new metal (II) complexes with Schiff base derived from amoxicillin, Journal of the Chilean Chemical Society 60(3) (2015) 3074-3079.

[64] N. Jayarambabu, B.S. Kumari, K.V. Rao, Y.T. Prabhu, Germination and growth characteristics of mungbean seeds (Vigna radiata L.) affected by synthesized zinc oxide nanoparticles, International Journal of Current Engineering and Technology 4(5) (2014) 2347-5161.

[65] A.S.K. Heer, Spectral characterization and anti-fungal activity of zinc oxide (zno) nanoparticles synthesized using cynodon dactylon leaf extract, World Journal of Pharmaceutical Research 6 (2017) 16.

[66] N. Killi, R.A. Dhakare, A. Singam, M. Lokanadham, H. Chitikeshi, R.V.N. Gundloori, Design and fabrication of mechanically strong nano-matrices of linseed oil based polyesteramide blends, MedChemComm 7(12) (2016) 2299-2308.

[67] A.M. Abdelghany, E.M. Abdelrazek, S.I. Badr, M.A. Morsi, Effect of gamma-irradiation on (PEO/PVP)/Au nanocomposite: materials for electrochemical and optical applications, Materials & Design 97 (2016) 532-543.

[68] S. Konchada, N. Killi, S. Sayyad, G.B. Gathalkar, R.V.N. Gundloori, Blends of neem oil based polyesteramide as nanofiber mats to control Culicidae, RSC Advances 10(70) (2020) 42827-42837.

[69] M. Narkar, P. Sher, A. Pawar, Stomach-specific controlled release gellan beads of acid-soluble drug prepared by ionotropic gelation method, Aaps Pharmscitech 11(1) (2010) 267-277.

[70] A.K. Zak, R. Razali, W.H. Abd Majid, M. Darroudi, Synthesis and characterization of a narrow size distribution of zinc oxide nanoparticles, International journal of nanomedicine 6 (2011) 1399.

[71] W. El Hotaby, H.H.A. Sherif, B.A. Hemdan, W.A. Khalil, S.K.H. Khalil, Assessment of in situ-Prepared Polyvinylpyrrolidone-Silver Nanocomposite for Antimicrobial Applications, Acta Physica Polonica, A. 131(6) (2017).

[72] R. Balu, T.S. Kumar, M. Ramalingam, S. Ramakrishna, Electrospun Polycaprolactone/Poly (1, 4-butylene adipate-co-polycaprolactam) blends: Potential biodegradable scaffold for bone tissue regeneration, Journal of Biomaterials and Tissue Engineering 1(1) (2011) 30-39.

[73] M. Akrami-Hasan-Kohal, L. Tayebi, M. Ghorbani, Curcumin-loaded naturally-based nanofibers as active wound dressing mats: morphology, drug release, cell proliferation, and cell adhesion studies, New Journal of Chemistry 44(25) (2020) 10343-10351.

CHAPTER 6

Blend of neem oil based polyesteramide as magnetic nanofiber mat for efficient cancer therapy
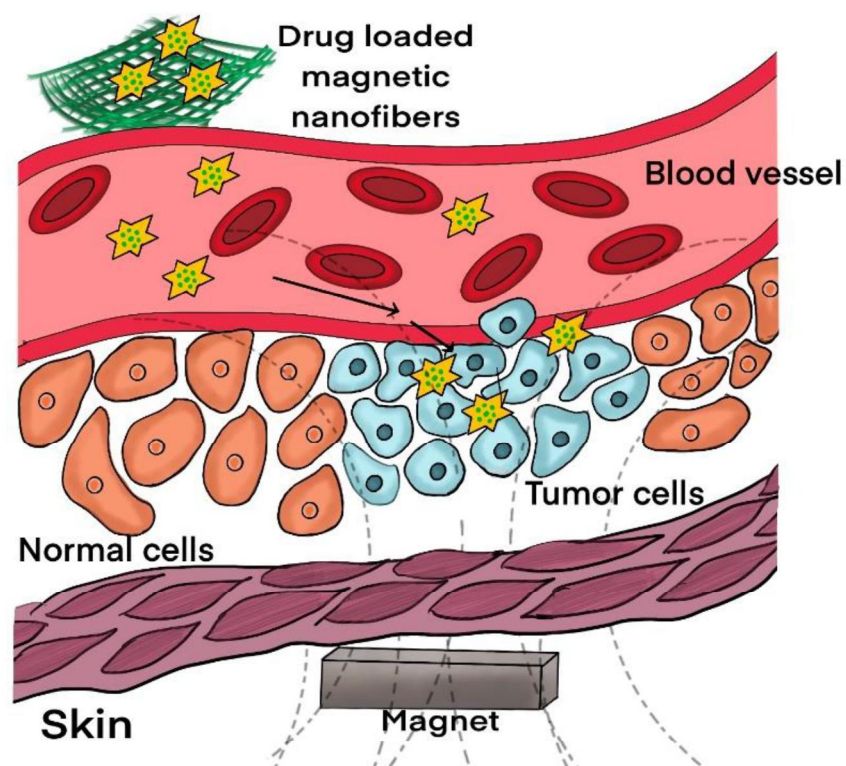
 Chapter 6

This chapter, discusses the fabrication of NPEA, PCL, and PLA embedded nanofibers with SMN by electrospinning method for targeted drug delivery application. The developed SMN nanofibers were evaluated by MTT assay, drug release and SQUID (superconducting quantum interference device).

6.1 Introduction

Advanced nanotechnology is considered to be a promising drug delivery system for cancer treatment for the past few decades. Several drug delivery systems are being studied in the various nanoform such as nanogels[1], nanoparticles[2, 3], micelles[4, 5], emulsion[6], nanofibers[7], etc to treat cancer effectively. Nevertheless, these nanocarriers have no control hence, without discrimination they get deposited in the healthy cells causing many side effects. Currently, the targeted delivery of anticancer agents is considered one of the best methods to minimize the side effects to enhance the patient's compliance[8-10]. Accordingly, to localize the treatment, the nanocarriers functionalized with targeted biomolecules (prodrugs, ex. folic acid, biotin, interferon, etc) that can interact with the receptors of the tumor cells is becoming popular[11-13]. Further advancement in improving the efficacy of the material for the biomedical application led to the development of magnetic nanoparticles housed by polymers in forms designed for magnetic hyperthermia[14], imaging[15], tissue engineering[16], drug delivery[17], sensors[18], purification of cells[19] and separation of biomolecules[20], etc. Recent studies identified magnetic drug targeting nanocarriers as another promising drug delivery approach for treating tumors, which is based on the magnetic movement of the drug delivery carrier and can be manipulated by the magnetic field. The ongoing technology advancement has enabled the development of stronger magnetic properties with sophisticated magnetic probes, for example, theranostic probes, which are associated with diagnostic magnetic resonance imaging (MRI) and therapeutics, wherein it can promote the targeted drug delivery under the influence of magnetic field[21, 22]. As a result, under the influence of the magnetic field, the drug molecules get concentrated at the tumor

site, thereby increasing the efficacy of the treatment and reducing the toxicity to the normal cells.

Iron oxide magnetic particles are widely used for biomedical applications because of their excellent characteristics like biocompatibility, low toxicity to the human body, less sensitivity to oxidation, and high stability under magnetic field[23, 24]. Also, magnetic nanoparticles can behave like paramagnetic material with a decrease in size, and the ease of process to synthesize them along with surface treatment makes it an attractive candidate for biomedical applications. Hence, magnetic nanoparticles are considered an advanced drug delivery system in the field of biomedicine [25, 26]. Among the various magnetic nanoparticles, magnetite (Fe_3O_4)[27] was used extensively for biomedical applications as mentioned above. Nevertheless, the dispersity of the magnetic nanoparticles is the primary concern. Generally, to overcome this hindrance, a two-step process is employed. The first involves the synthesis process of magnetic nanoparticles, and the second is the stabilization of magnetic nanoparticles in a fluid by surface modification by physical or chemical treatment.[28-30]. Accordingly, there are reports on achieving the biocompatibility and dispersibility of the magnetic nanoparticles *via* surface modification by coating with organic[31], inorganic[32], surfactant[33], polymer[34], etc. A long-chain fatty acid surfactant, stearic acid ($C_{17}H_{35}COOH$) was suggested as one of the suitable macromolecules for coating because it is a derivative of 9-hydroxystearic acid, an endogenous cellular lipid responsible for the inhibition of cancer cells. Therefore it is inert, biocompatible, cheap, and possesses low toxicity[35-37][47].

Currently, polymers developed as nanofibers by electrospinning are extensively being used as drug delivery systems, as fabricating a nanofiber system is easy and convenient to modulate and regulate drug release for an extended period. Further, due to its nanosize, the surface-to-volume ratio is high, as a result, the availability of the drug is more for better performance. Moreover, nanofiber permeates exudates, has good mechanical strength, resembles biological tissues, and possesses high porosity[38]. A recent report indicated that piperine was embedded in a nanofibrous patch for the post-surgical treatment of cancer[39]. In another report, 5-fluorouracil (FU) was loaded in chitosan and polycaprolactone nanofibers for cancer

treatment[40]. Such systems have efficacy in the drug delivery domain. In recent advanced studies, the nanofibers immobilized with drugs capped with magnetic nanoparticles are being studied to deliver the drug at the cancer site under the influence of magnetic field for improved therapy for example; NaX zeolite/DOX into the PLA (poly(lactic acid)/chitosan nanofibers were used for targeted cancer treatment[41]. Similar studies showed that the nanofibers with magnetic nanoparticles and a drug, for instance (HPMCP (hydroxypropyl methylcellulose phthalate)/IDN/Fe_3O_4) directed the nanofibers towards the local site for the delivery of drug under the influence of the magnetic field[42]. To implement this concept for targeted drug delivery to treat cancer, we have designed nanofibers using biodegradable and biocompatible polymers immobilized with FU (cancer drug) and magnetic nanoparticles Fe_2O_3 coated with stearic acid.

We are the first one to report stearic acid-coated magnetic nanoparticles embedded in the blends of neem oil based polyesteramide NPEA, PVP (polyvinylpyrrolidone), and PCL (Polycaprolactone) as nanofiber mats for targeted drug delivery application. Neem oil is being used as a bioagent since ancient times to treat inflammation, and treat infections caused due to harmful parasites and microbes[43, 44]. Neem compounds (Azadirachtin and Nimbolide) showed anticancer activity by induction of cellular death, scavenging of free radicals, suppression of the metastasis process, and repression of NF-κB factor[45-48]. Mitogen-activated proteins (MAPKs), protein kinase, and growth-factor-receptor-mediated pathways are all inhibited once NF-κB is suppressed[47]. According to some reports, neem activates the release of cytochrome c and apoptosis-inducing factor (AIF) from mitochondria which is beneficial for cancer therapy[49, 50]. The importance of neem was further expanded by modifying its properties so that neem oil can be used more effectively for biomedical applications. One of the aspects is converting this oil into a polymer like polyesteramide, PEA, where it can be blended with other polymers and fabricated in the form of materials. In doing so, they can impart reasonable physical, thermal, and mechanical properties and shelf-life of it can be increased, such studies were reported from our investigations and demonstrated those for tissue regeneration applications. Nevertheless, there are no reports on cell behavioural responses with the application of NPEA because most of the studies reported are related to material development and

not as a bioactive drug. In the pharmaceutical industry, PVP is widely used for oral drug delivery and topical application[51]. Being amorphous synthetic polymer and possessing a high affinity towards water[52], they are being studied for the immediate release of water-soluble drugs as it also helps increase the dissolution of the poorly water-soluble drugs (acetaminophen and ketoprofen)[53-55]. PCL is a semicrystalline hydrophobic polymer and is approved by FDA (Food and drug administration). It is widely used for biomedical applications [56]. Moreover, PCL has good fiber-forming properties, reproducibility, and mechanical strength[57]. PCL's low degradation rate in physiological conditions helps to release in a sustained manner. The polymeric properties of NPEA, PCL, and PVP complement each other. Hence, our present study aims to fabricate biocompatible nanofibers using NPEA/PCL/PVP with embedded stearic acid-coated magnetic fields nanoparticles (SMN) and loaded with FU for targeted cancer drug delivery. FU is an anti-cancer drug used for various cancer treatments like colon cancer, esophageal cancer, stomach cancer, etc. The drug release was studied in the presence and absence of SMN in the nanofibers. An extensive physicochemical characterization of the nanofibers was also conducted to explore their physical and chemical features. Further, cell viability, cytotoxicity assay, and hemolysis test were also performed. Finally, the potential applications of magnetic nanoparticles have been discussed for targeted drug delivery in cancer treatment.

6.2 Materials and methods

6.2.1 Materials

Polyvinylpyrrolidone (M.w ~ 360,000), Polycaprolactone (M.w ~ 70,000-90,000) and 5- fluorouracil were purchased from Sigma-Aldrich Co, St Louis, USA. Chloroform (alcohol stabilized) analytical grade was obtained from Rankem, Mumbai, India. Methanol HPLC grade was purchased from Fisher Scientific, Mumbai, India. 3-(4,5– dimethyl thiazol–2–yl)–5–diphenyltetrazolium bromide (MTT), fetal bovine serum (FBS), phosphate-buffered saline (PBS), Dulbecco's modified eagle's medium (DMEM), minimum essential medium (MEM), trypsin were purchased from Invitrogen, India. EDTA (ethylenediaminetetraacetic acid), glucose, and antibiotics were procured from Hi-Media Laboratories Ltd., Mumbai, India. Dimethyl sulfoxide (DMSO), acetone, and propanol were bought from Merck Ltd., Mumbai, India. L929

(mouse fibroblast) and MCF-7 (human adenocarcinoma) cell lines were procured from National Centre for Cell Sciences (NCCS), Pune, India.

6.2.2   Stearic acid coating of MNPs

As reported in an earlier publication, the stearic coated magnetite nanoparticles were synthesized [37]. Briefly, the magnetite nanoparticles coated with long-chain stearic acid were synthesized by the co-precipitation method using the iron chloride precursors (FeCl$_3$· 6H$_2$O and FeCl$_2$· 4H$_2$O) and ammonium hydroxide (NH$_4$OH) as the precipitant, in the presence of the corresponding surfactant in the reaction medium. Stearic acid dissolved in 20 mL of 2-propanol (for stearic acid coating) was used. Details of the synthesis are reported previously[58, 59]. After the precipitation reaction, the dispersion obtained was washed with a 1:1, 2-propanol–hexane mixture (in the case of stearic acid). The nanoparticles in the aqueous layer were transferred to the non-aqueous layer (hexane) during the washing process. Later, the non-aqueous layer containing the nanoparticles was separated using a separating funnel and dried at room temperature to obtain nanoparticles in the powder form. The dried powder samples of stearic-acid-coated samples were used for further studies.

6.2.3 Electrospinning of SMN-drug loaded nanofibers

To prepare polymer solution for electrospinning, NPEA 3% (w/v) and PCL 4% (w/v) were dissolved in chloroform and PVP 3% (w/v) was dissolved in methanol separately. Later, both these polymer solutions were mixed on a roller for 12 h to achieve a homogenous solution. The prepared homogenous solution was further used for drug loading. Briefly, modified SMN and a 5% FU with respect to total polymer weight concentration were added into the polymer solution by mixing them on a roller mixer for another 12 h (**Table 6.1**), followed by bath sonication for 30 min. As the drug loading into the nanofibers by active method, due to that negligible amount of drug lost during the electrospinning process. For the fabrication of nanofibers, the prepared homogeneous polymeric blend solution was filled in a 5 mL syringe, equipped with a stainless steel hypodermic needle with a blunt end with a fixed pore. This was used as a nozzle for spinning the polymer solution. The filled syringe was

mounted on a "syringe pump" to pump the solution at a controlled flow rate. A high-voltage generator operated in a positive DC mode was connected to the syringe needle, and an aluminum plate was set in a closed chamber to ground the nanofibers. Electrospinning was done at ambient conditions, and all parameters such as the distance between the tip of the needle and the collector (12 cm), the voltage (15 kV), and the flow rate (0.50 mL/h) were fixed for the fabrication of nanofiber mats. The fabricated nanofibers were collected and were kept in a vacuum oven for 24 h to remove any residual solvents. The parameters and procedure remain the same for fabricating all the compositions.

Table 6. 1 The different compositions used for fabricating nanofibers

Formulation	PVP (w/v%)	NPEA (w/v%)	PCL (w/v%)	SMN (w/w%) w.r.t total polymer weight	FU (w/w%) w.r.t total polymer weight
Plain-NF	3	3	4		
SNM 10%- NF	3	3	4	10	
SNM 20% - NF	3	3	4	20	
SNM 10%-NF-FU 5%	3	3	4	10	5
SNM 20%-NF-FU 5%	3	3	4	20	5
Plain-NF-FU 5%	3	3	4		5

6.3 Characterization of fabricated nanofibers

Environment scanning electron microscopy (Micro Analysis System, and Model Phoenix, Cambridge, England, UK) was used to examine the surface morphology of the fabricated nanofibers. The nanofibers were coated with gold using a coating unit E5000 (Polaron Equipment Ltd., Watford, Hertfordshire, England, UK). A dual-beam, having an electron source of Tungsten filament (W) with emission at a resolution of 20 kV in a high vacuum, was used for the studies. A transmission electron microscope (TEM, FEI model TECNAI G2 F30) was used to analyze the morphology and to evaluate the distribution of SMN by dot mapping of fabricated nanofibers. The functional characteristics of polymers and electrospun nanofibers were recorded using FTIR [Perkins Elmer, spectrometer I, FTIR diffused reflectance (DRIFT) mode, USA]. The spectrum recording was done in the wavelength range from 4000 to 500 cm^{-1} with a resolution of 4 cm^{-1}. Each spectrum is composed of an average of 16 scans. The crystallinity of the pure polymers and nanofiber mats was studied by powder X-ray diffraction (XRD) (PANalytical X'pert Pro diffractometer) and Cu Ka (1.5418 Å) radiation used as an X-ray source. The magnetic measurements of samples were carried out at 300 K using a SQUID (superconducting quantum interference device) magnetometer (Quantum Design SQUID-VSM)[37]. The dynamic mechanical analyser estimated the mechanical strength of nanofiber mats (RSA3, TA Instruments, USA). The nanofiber mats were cut into strips with dimensions of 20 × 0.5 cm^2 and then mounted onto the tensile grips. The rate of strain and gauge lengths were 10 mm/min and 15 cm, respectively. Further, the mats were subjected to a tensile force. Each sample was tested five times to authenticate its normal stress-strain curves. Image J software was used to calculate the average size of nanofibers.

6.3.1 Drug release studies of magnetic and nonmagnetic nanofibers

The respective NM with FU loaded of 10 mg of with and without SMN were placed in a wide-mouth glass bottle containing 5 mL of phosphate buffer saline (PBS) of pH 7.4. The release of FU was monitored at regular intervals by placing the respective container with NM in a temperature-regulated shaker bath of 50 rpm maintained at 37 °C. At each interval of time, 1 mL of buffer solution was removed from the sample

bottle for the estimation of FU and replaced with 1 mL of fresh buffer. The FU containing sample buffer was analyzed by UV visible spectrophotometry (Shimadzu UV-1601PC) at a wavelength of 266 nm to determine the amount released at each interval and extrapolated the quantity using a standard calibration curve of FU. The respective NM without FU was used as a control. The release studies were done in triplicates and all the samples were analyzed in triplicates for reproducibility. The results were presented in terms of cumulative percent release as a function of release time. Equation 1, shows the method for obtaining the cumulative percent of FU released.

$$\text{Cumulative percent of drug released (\%)} = M_t/M_{\infty \times 100} \qquad \text{Equation 1}$$

(where Mt is the amount of drug released at time t and M_∞ is the amount of drug present in the nanofiber mat after preparation and estimation)

6.3.2 Evaluation of percent of hemolytic activity (HP)

Hemolysis assay was executed according to our previously reported procedure[60]. In short, blood was obtained from human volunteers from National Chemical Laboratory, Health center, Pune, India, and the blood samples were stabilized using EDTA. The red blood cells (RBCs) were isolated using density gradient centrifugation from whole blood. Whole blood of volume 5 ml was slowly added on top of 5 mL of PBS saline solution and then centrifuged at 2000 rpm for 30 min. The supernatant was discarded, and red blood cells were collected. Later, the RBCs were washed thrice with phosphate buffer saline of pH 7.4 and were centrifuged at 2000 rpm for 30 min. RBCs' stock solution was prepared without serum at 2% (v/v) in a phosphate buffer of pH 7.4. Later, 2 ml of the diluted RBCs suspension was transferred to each of the 2 ml eppendorf tubes containing native SMN and all the nanofibers' compositions which were classified as shown in **Table 1**. Similarly, negative and positive control of blood samples were prepared. The respective eppendorf tubes were then incubated for 2 h at 37 °C. During the incubation process, the nanoparticles and RBC may settle; therefore, at an interval of every 30 min, the samples were shaken gently to re-suspend samples and were centrifuged at 1500 g for

10 min at room temperature. The supernatant was then placed in another 96-well microtiter plate, and hemoglobin (Hb) release was measured spectrophotometrically at 541 nm using a microtiter plate reader (Tecan) in PBS. The percentage of RBC lysis was calculated based on the assumption that 100% RBC lysis resulted from mixing blood with distilled water at a 1:1 (v/v) ratio. Equation 2 was used for calculating the percent (%) of hemolysis.

HP (%) = Dt – Dnc/ Dpc – Dnc × 100   Equation 2

(Where Dt is the absorbance of the test samples, Dpc and Dnc are the absorbance of the positive and negative controls, respectively)

6.3.3 Cell culture

L929 cell line was maintained at 37°C under 5% CO_2 in a humidified atmosphere and supplemented with DMEM media fortified with 10% FBS. Similarly, the MCF-7 cell line was maintained under similar conditions in MEM media fortified with 10% FBS.

MTT assay: Cytotoxicity assay for test samples with and without FU was done in MCF-7 and L929 cell lines, respectively by the MTT assay. A confluent flask of MCF-7 was harvested by trypsin treatment, and ~10,000 cells per well were seeded in a 96 well plate and incubated at 37 °C under 5% CO_2 for 16 h. NM cut into a round shape of 5 mm diameter were placed in these wells in triplicates and incubated at 37 °C under 5 % CO_2 atmosphere for 24 h. After 24 h the media from the wells was removed, and 110 μL MTT media solution (media containing 10% FBS with filter-sterilized MTT solution (0.45 mg/mL)) was added into each well and incubated in dark at 37 °C under 5% CO_2 atmosphere for 4 h. Later, the media containing MTT was aspirated from the wells, and 100 μL DMSO was added, and the plates were gently shaken to solubilize the formazan crystals, this colored solution was transferred to a fresh plate, and absorbance was measured in a microplate reader at a wavelength of 550 nm. The relative % cell viability was calculated using the following equation 3:

Relative % cell viability = $(A_{test}/A_{control})$ ×100%   Equation 3

(A$_{test}$ is the absorbance of the sample-treated cells, and A$_{control}$ is the absorbance of the untreated cells)

The same procedure was followed for the L929 cell line also in DMEM media.

6.4 Results and discussion

6.4.1   Characterization of surface morphology of fabricated nanofibers

Electrospinning gives enormous scope in fabricating novel and diverse nanofibers because one can manufacture nanofiber with nanoparticles, drugs, and fillers to improve nanofibers' properties and efficacy for the required applications. Drugs or nanoparticles can be reinforced in a polymer matrix by mixing with polymer solution without any chemical modification to fabricate the composite of nanofibers. We have fabricated nanofibers using PVP, PCL, and NPEA by incorporating the SMN and FU for cancer drug delivery applications. Chemical structure of polymers and FU are displayed in **Fig. 6.1**. **Fig. 6.2**, (E-SEM) and **Fig. 6.4** (TEM) show the surface morphology of plain-NF, SMN 10%-NF, and SMN 20%-NF. The diameter of the fabricated nanofibers was between 200 to 300 nm, which E-SEM and TEM analysis confirmed. Moreover, the nanofibers thus formed were smooth and randomly oriented, which validated a homogenous mixing of polymers and a homogenous distribution of FU and SMN. E-SEM images also indicated that with an increase in the concentration of SMN, the diameter of the nanofibers increased. The size distribution of nanofibers was calculated by Image J software (**Fig. 6.5**). Further, TEM, EDX dot mapping revealed that the SMN were uniformly dispersed in the nanofiber system, which can be visualized in **Fig. 6.3**.
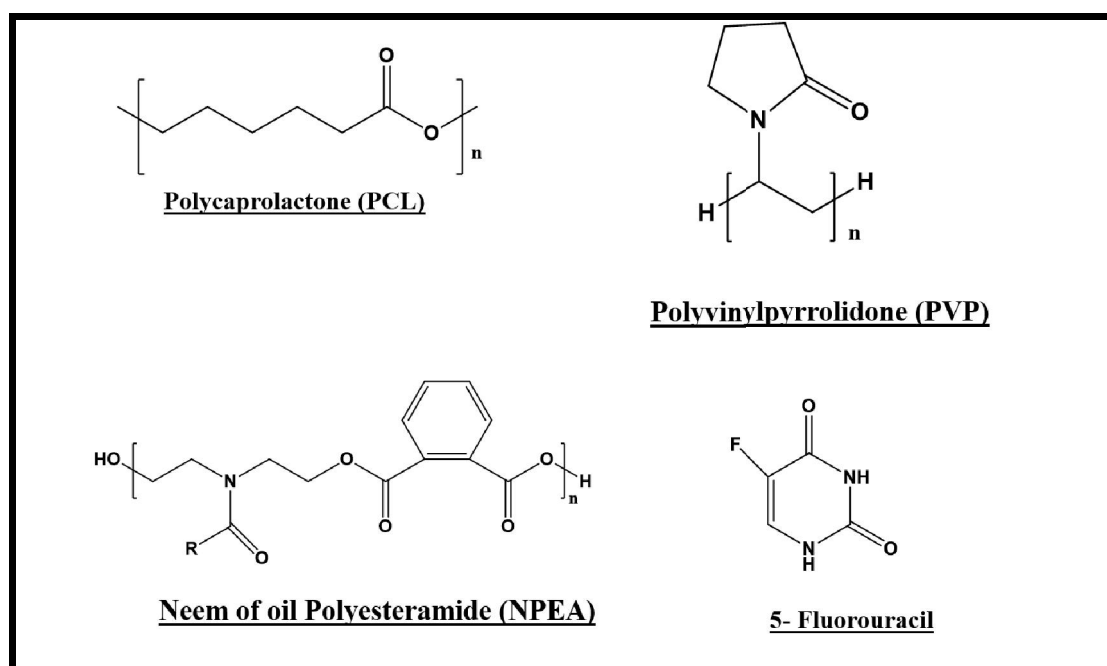
Figure 6. 1 Chemical structures of PCL, PVP, NPEA and FU
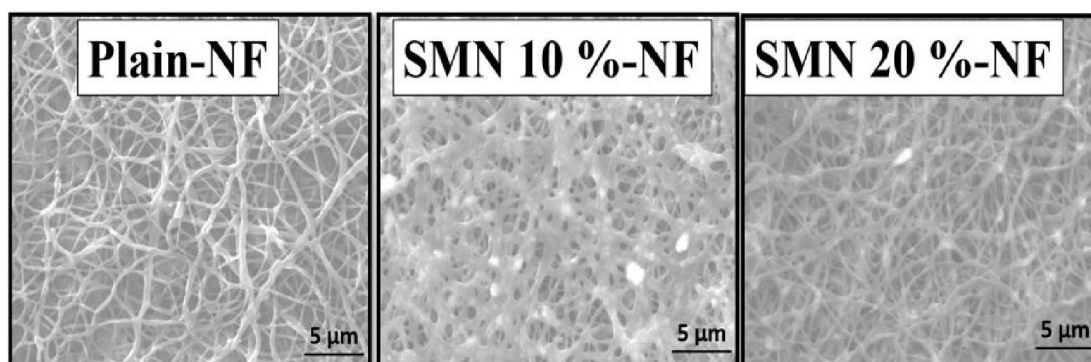
Figure 6. 2 E-SEM image of Plain-NF, SMN 10%-NF SMN 20%-NF.
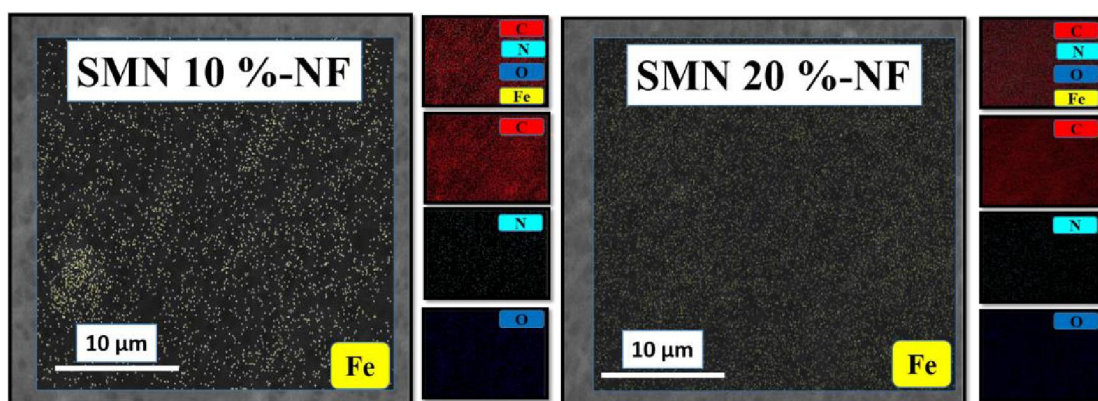
Figure 6. 3 Dot mapping image on TEM instrument: the yellow dots indicate the presence of SMN in SMN 10%-NF and SMN 20%-NF.
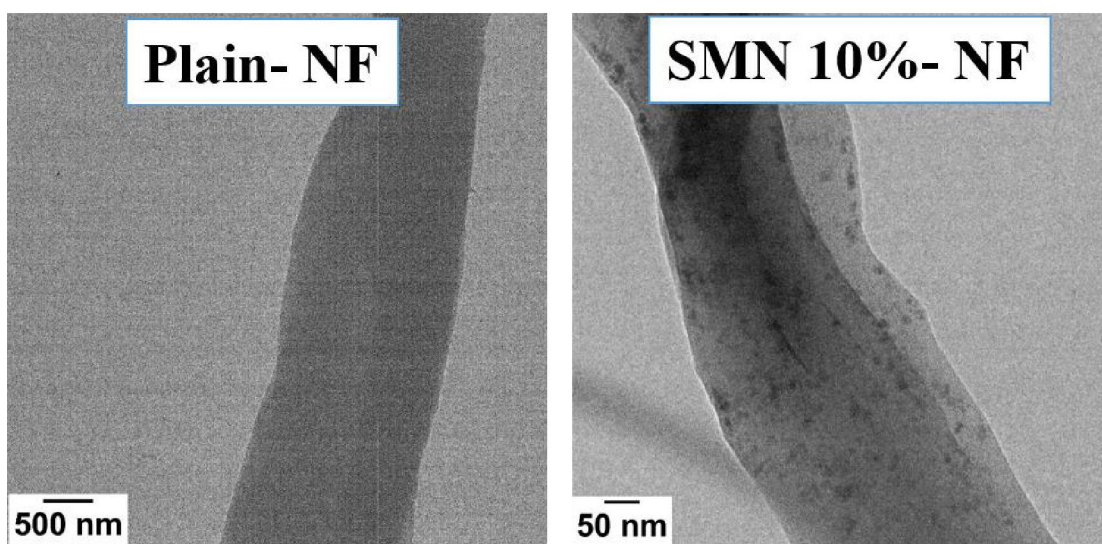
Figure 6. 4 TEM image of Plain-NF and SMN 10%-NF.
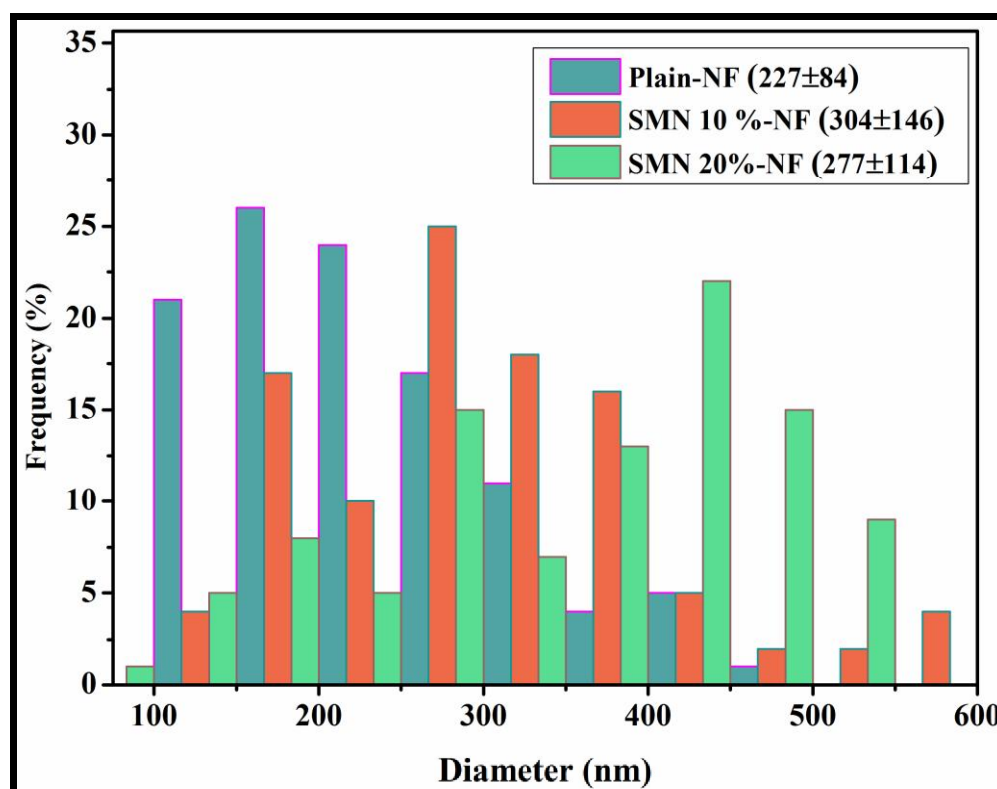
Figure 6. 5 Size distribution by Image J software of Plain-NF, SMN 10%-NF SMN 20%-NF.

6.4.2 Chemical analysis by FTIR

The chemical composition of fabricated nanofibers, PVP, PCL, NPEA, SMN, and FU was analyzed by FTIR spectrum (**Fig. 6.6**). PVP showed O–H stretching at 3425 cm^{-1} due to hydrogen-bonded water[61]. The characteristic peaks at 2925, 1665, and 1290 cm^{-1} indicated the presence of asymmetric stretching of CH_3, stretching of –C=O, and C–N, respectively[62]. PCL spectrum demonstrated peaks at 2943 and 2864 cm^{-1} for the asymmetric –CH_2 stretching and symmetric –CH_2, respectively. A sharp peak at 1725 cm^{-1} was recorded due to the presence of carbonyl stretching (–C=O), and a peak at 1186 cm^{-1} was due to the –C–C stretching[63]. NPEA recorded a peak at 2910 cm^{-1} for –C–H. Further, the characteristic peaks at 1710 cm^{-1} and 1605 cm^{-1} were due to –C–C=O and –N–C=O (amide) functional groups respectively[64]. Pure FU indicated a characteristic peak at 1737 cm^{-1} and 1672 cm^{-1} of –C=O. A peak at 1239 cm^{-1} appeared due to –C–N. The peaks at 3138 cm^{-1} and 1434 cm^{-1} represented N–H (secondary amine group) and –C=F stretching, respectively[65]. IR spectra of SMN that displayed two bands at 2923 and 2852 cm^{-1} for asymmetric and symmetric

stretching vibration of the methylene group ($-CH_2-$) in the fatty acid molecule. A weak band was observed at 1715 cm^{-1} due to carbonyl $-C=O$ stretching vibration, which suggests the presence of free fatty acid molecules on the surface of nanoparticles. A peak at 1525 cm^{-1} was for metal carboxylates due to asymmetrical vibration and a peak at 1441 cm^{-1} was for symmetrical vibration of $-COO^-$ functional group[37]. A peak at 610 cm^{-1} in the spectra indicated Fe–O stretching, frequency of Fe_3O_4, due to the attachment of the fatty acid to the Fe atom on the surface of the nanoparticles through the oxygen atoms of the carboxyl group[66]. The IR spectra of Plain-NF (A), SMN 10%-NF (B), and SMN 10%-NF-FU 5% (C), characteristics peaks such as 2920, 2852, 1713, 1645, and 1174 cm^{-1} confirmed the presence of PCL, NPEA, and PVP in the developed nanofibers. Further, the IR of SMN 10%-NF-FU 5% showed a broad peak around 3343 cm^{-1} due to the N–H group present in the FU, which confirmed the presence of FU in fabricated nanofibers. This peak was not observed in the spectra of Plain-NF, SMN 10%-NF nanofibers. FU's carbonyl peak (-C=O) increased due to its merging with carbonyl peaks of the polymers. However, the peaks of SMN at 2913 and 2845 cm^{-1} were merged with polymers' peaks. Moreover, the peaks at 1542, 1406, and 610 cm^{-1} representing SMN were not observed; previous literature reported similar observations[67]. Nevertheless, the presence of SMN was strongly confirmed in dot mapping and XRD (**Fig. 6.3** and **Fig 6.4**).
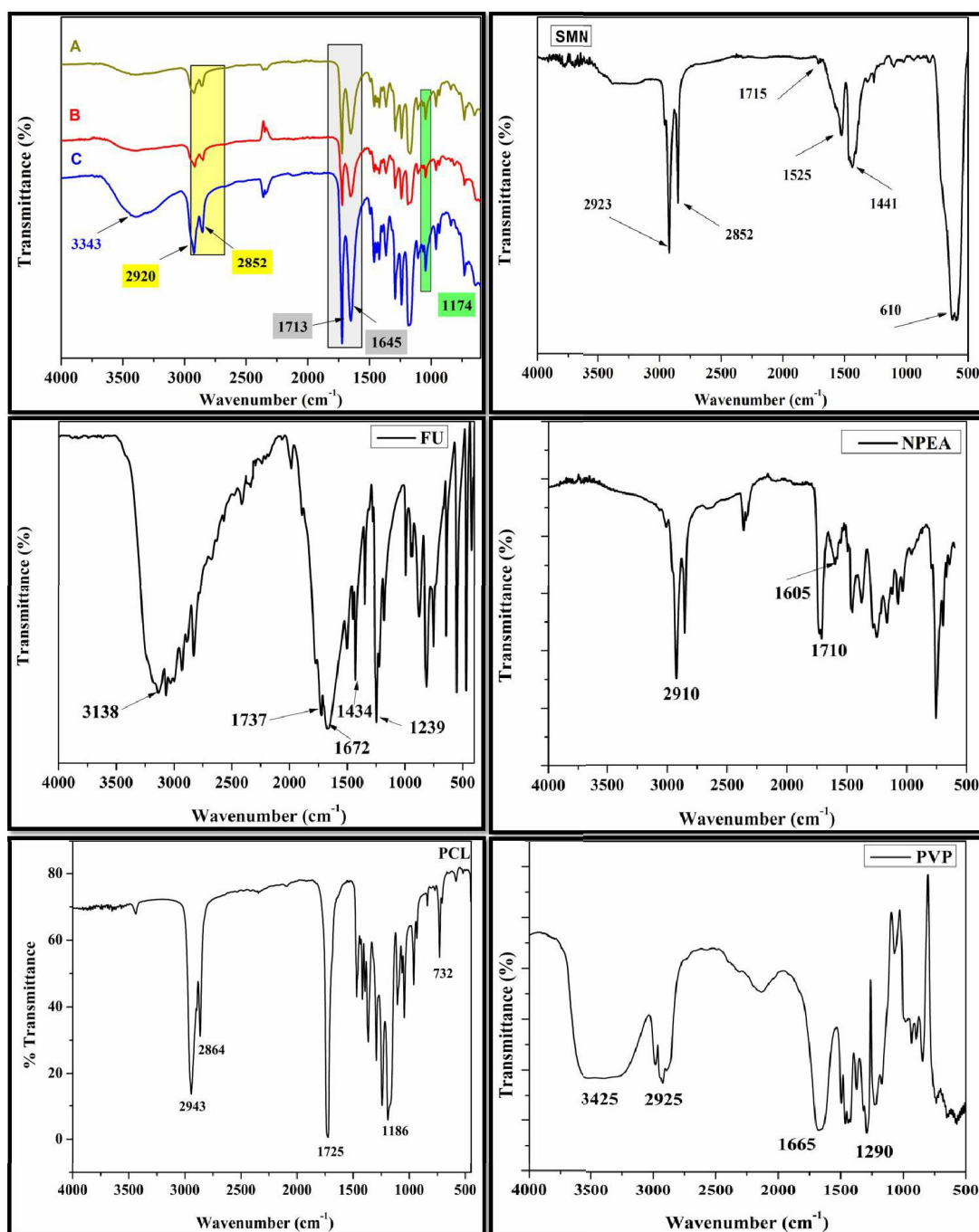
Figure 6. 6 FTIR spectrum of fabricated nanofibers, Plain-NF (A), SMN 10%-NF (B), SMN 10%-NF FU- 5% (C) and raw materials, PVP, PCL, NPEA, FU and SMN.

6.4.3   Thermal analysis of nanofibers

The thermal degradation of developed nanofibers was studied using thermogravimetric analysis (**Fig. 6.7** and **Table 6.2**). In the earlier paper, we have discussed the process of decomposition and the presence of stearic acid-coated

magnetic nanoparticles[37]. **Fig. 6.7**, shows the degradation temperatures of the nanofiber mats with and without SMN. **Fig. 6.7**, shows the Plain-NF decomposition temperature, where the decomposition temperature was initiated from 80 ºC and ended at 309 ºC with a weight loss of ~3%. The loss of weight is attributed to the free water present in the nanofiber mat. Subsequently, a decomposition temperature was recorded from 309 ºC to 403 ºC, where the weight loss was ~8% due to the loss of water molecules coordinated with the nanofibers' polymer network and the residual solvents used for fabrication of nanofibers[68]. And the third decomposition temperature was initiated from 403 ºC and extended up to 473 ºC with a weight loss of 83%. The loss of weight is attributed to PCL, PVP, and NPEA (decomposition of the hydrocarbon chains) as these polymers' decomposition temperature falls between 300 ºC to 460 ºC. In the blends, the decomposition temperatures recorded were not as sharp as observed for the individual polymers because of the blending and fabrication of nanofibers. Further, polymer-polymer interactions shifted the decomposition temperatures of all the polymers used for blending. The plain-NF depicted a total weight loss of 94% with a residue of 6% (approx.) Similarly, the SMN 10%-NF too showed first decomposition temperatures, as observed in the plain nanofiber mat with respect to a weight loss of water, solvent, and free stearic acid molecules (95 to 287 ºC). Following this, the second decomposition temperatures were similar with slight variation in temperatures, and **Table 6.2** shows the various decomposition temperature of the individual polymers and their weight loss. Also, there was a small amount of weight loss in the third decomposition temperature due to the secondary and primary layer of stearic acid, which was coated on magnetic nanoparticles[37]. SMN 10%-NF showed 88% of degradation with 12% of residue, which is higher than Plain-NF, which may be due to the non-degradation of the magnetic nanoparticles. The SMN 10%-NF-FU 5% recorded first decomposition temperature between 85 ºC to 310 ºC and displayed a weight loss of around 14% due to loss of water and stearic acid molecules as mentioned above. Similarly, second and third decomposition temperatures were recorded with 46% and 24% weight loss due to the complete decomposition of PCL, PVP, and NPEA molecules (**Table 6.2**). A slight increase in the degradation was observed which may be due to the interaction of FU with the polymers. The total weight loss was 84% with a residue of 16%. The fabricated

nanofibers possess high heat resistance due to the proper blending of polymer, drug, and SMN.
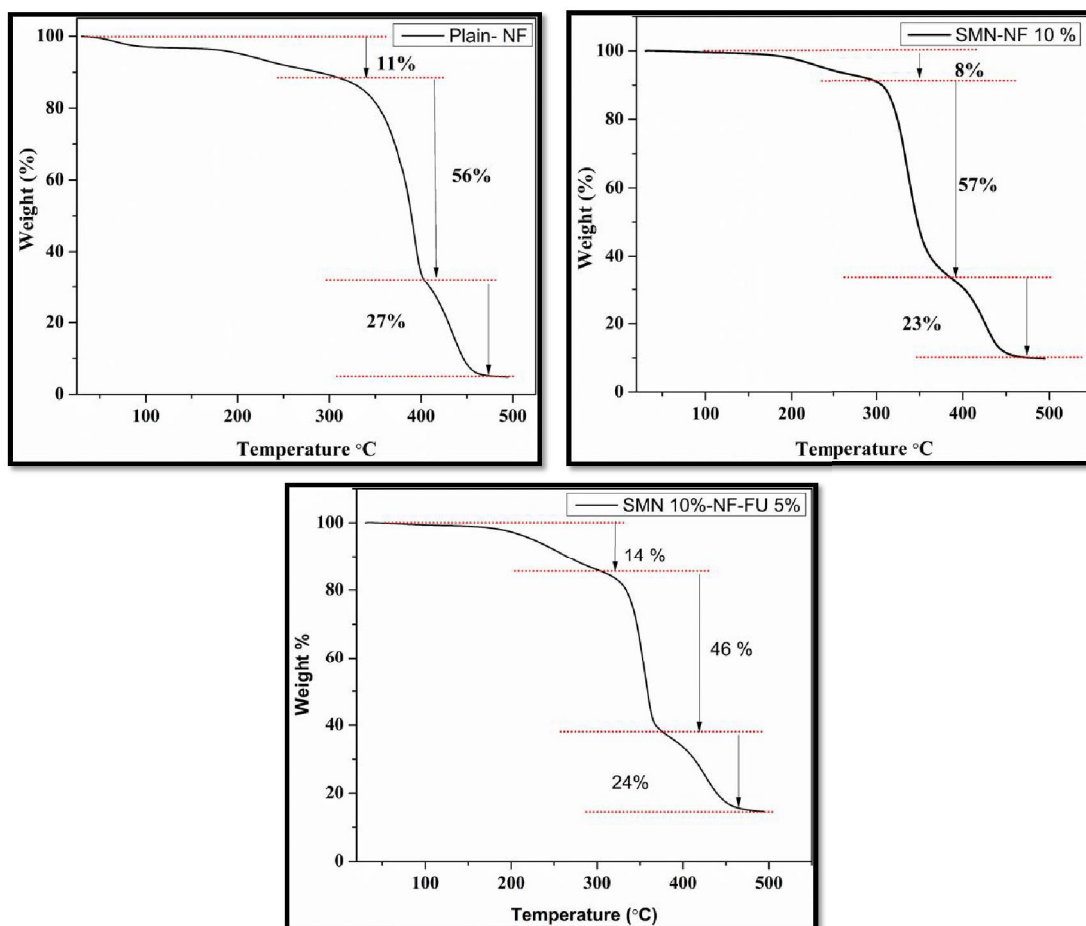
Figure 6. 7 TGA graph of Plain-NF, SMN 10%-NF, and SMN 10%-NF FU- 5%,

Table 6. 2 TGA of Plain-NF, SMN 10%-NF, and SMN 10%-NF FU- 5%.

Formulation	First degradation		Second degradation		Third degradation	
	Start (°C)	End (°C)	Start (°C)	End (°C)	Start (°C)	End (°C)
Plain-NF	80	309	309	403	403	473
Weight loss (%)	**11**		**56**		**27**	

SNM 10%- NF	95	287	287	370	370	474
Weight loss (%)	**8**		**57**		**23**	
SNM 10% - NF-FU 5%	85	370	310	380	380	484
Weight loss (%)	**14**		**46**		**24**	

6.4.4   XRD analysis

X-ray diffraction method was utilized to study the crystallinity of the fabricated magnetic nanofibers and the raw materials (**Figs. 6.8** and **6.9**). XRD pattern of FU demonstrated at a sharp peak at 28° as it is crystalline in nature. The XRD pattern of Plain-NF showed characteristic peaks of PCL peak at 21 and 24°[69]. PCL is crystalline in nature, and PVP is amorphous in nature after blending the polymers PCL, PVP, and NPEA and fabrication of nanofibers, the crystallinity of PCL diminished, and the peak intensity at 21 and 24˚ was reduced. XRD of SMN showed a broad peak at 36° due to the coating of stearic acid coating on magnetic nanoparticles[70]. Similarly, the inclusion of SMN in the SMN 10%-NF also enhanced the crystallinity of PCL as the intensity of the peaks increased when compared with the nanofibers without SMN. Plain-NF. SMN 10%-NF- FU 5% showed an increase in the intensity of the PCL crystalline peaks which could be due to the inclusion of the crystalline drug, FU. The intensity of the PCL peaks was greater than all other nanofiber compositions due to SMN and FU inclusion. The presence of SMN in the nanofibers was confirmed as the peak appeared at 36°. Hence, we conclude that the changes in the crystalline properties were influenced by the presence of FU and SMN and we inferred that all the polymers were well blended.
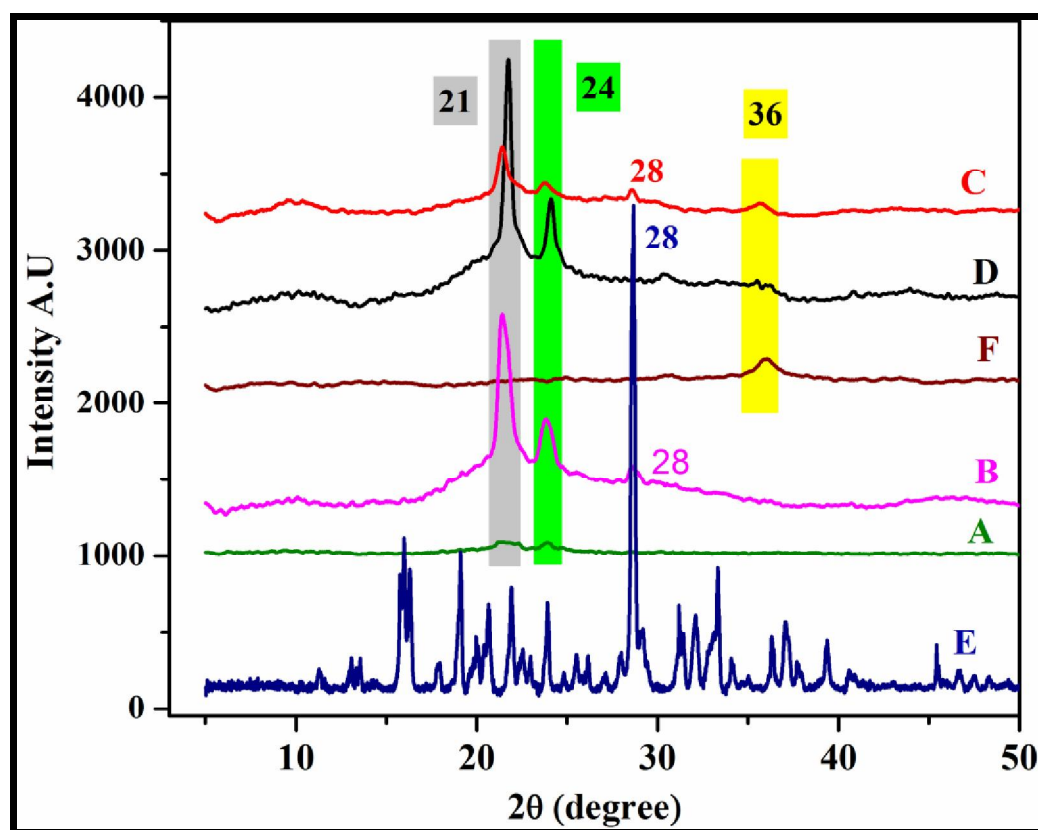
Figure 6. 8 XRD analysis of Plain-NF (A), Plain-NF-FU-5% (B), SMN 10%-NF (C), SMN 10%-NF FU- 5% (D), FU (E) and SMN (F).
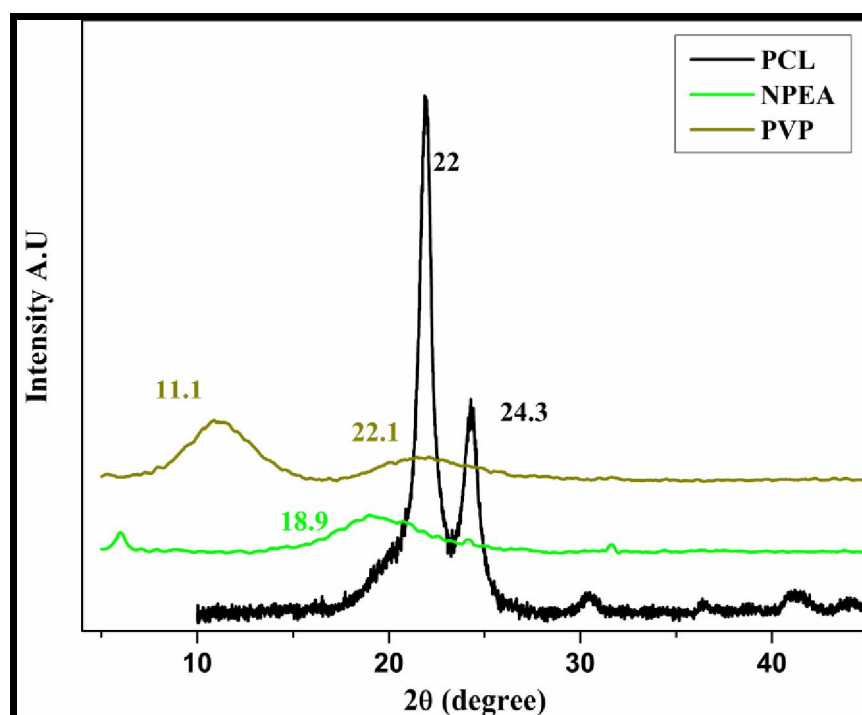
Figure 6. 9 XRD analysis of PVP, PCL and NPEA.

6.4.5 Mechanical studies of nanofibers.

To investigate the mechanical property of SMN 10%-NF, SMN 20%-NF, and Plain-NF, a dynamic mechanical analyzer was used. To demonstrate the mechanical strength in terms of tensile strength, Young's modulus, and breakpoint of nanofibers, stress vs strain graphs were plotted (**Fig. 6.10** and **Table 6.3**). The SMN 10%-NF mat recorded tensile strength of 8.6 MPa, Young's modulus was 0.22 Mpa, and breakpoint at 105%. The SMN 20%-NF mat showed a tensile strength of 6.11 MPa, Young's modulus was 0.15 Mpa, and the breakpoint at 85%. Similarly, Plain-NF indicated tensile of 6.7 MPa, Young's modulus of 0.29 Mpa, and breakpoint at 87%. When we compared the SMN 10%-NF with Plain-NF mat, a rise in tensile strength and a breakpoint was noticed, which was due to SMN acting as support to nanofibers by giving strength to it. When we compared the SMN 10%-NF and SMN 20%-NF there was a significant decrease in tensile strength and the breakpoint due to the further addition of the SMN into the nanofibers. This suggests that up to a particular concentration, SMN can impart mechanical strength, but after optimum concentration, there was a decrease in Young modulus (-31%), breakpoint (-19%), and tensile strength (-28%) of nanofibers. In this context, our result suggests that the SMN 10%-NF possesses good mechanical properties, which are essential to withstand stress during biomedical application.
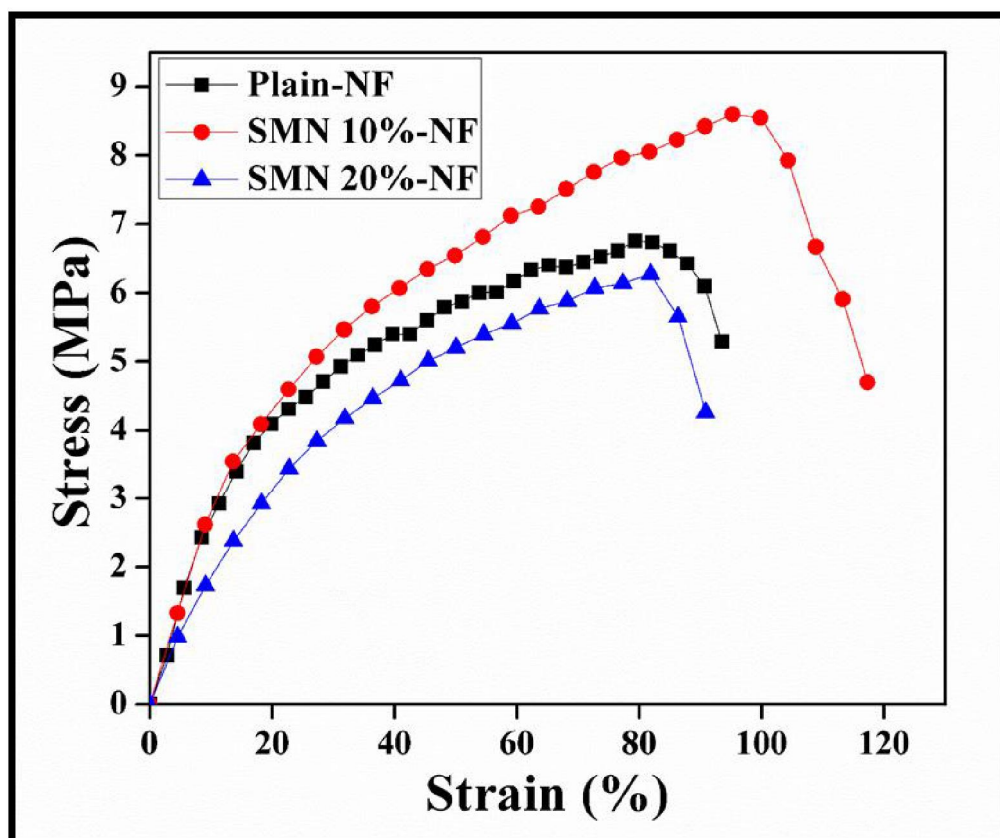
Figure 6. 10 Dynamic mechanical analysis of Plain-NF, SMN 10%-NF, SMN 20%-NF.

Table 6. 3 Dynamic mechanical analysis of Plain-NF, SMN 10%-NF, SMN 20%-NF

Samples	Young's modulus (MPa)	Tensile strength (MPa)	Break point (%)
Plain- NF	0.29	6.7	87
SMN10 %-NF	0.22	8.6	105
SMN20 %-NF	0.15	6.11	85

6.4.6   SQUID analysis of SMN nanofibers

To determine SMN 10%-NF and SMN 20%-NF nanofibers' magnetic properties, field-dependent magnetization studies were carried out at 300K, as shown in **Fig. 6.11**. The absence of a magnetic hysteresis loop, i.e. zero remanence and zero coercivity, shows nanoparticles' superparamagnetic nature [37]. The magnetization of SMN at 30 kOe was 60.7 emu/g, whereas magnetization of SMN 10%-NF at 30 kOe was observed at 4.3 emu/g. The lower value of magnetization in SMN 10%-NF compared to the bulk SMN was attributed to the presence of less content of SMN in the nanofibers. Overall, magnetic studies confirm the magnetic nature of nanofibers[42]. Owing to the magnetic nature, these nanofibers can be moved under the influence of an external magnetic field to deliver the drug to the specific site for controlled release to treat cancer effectively.
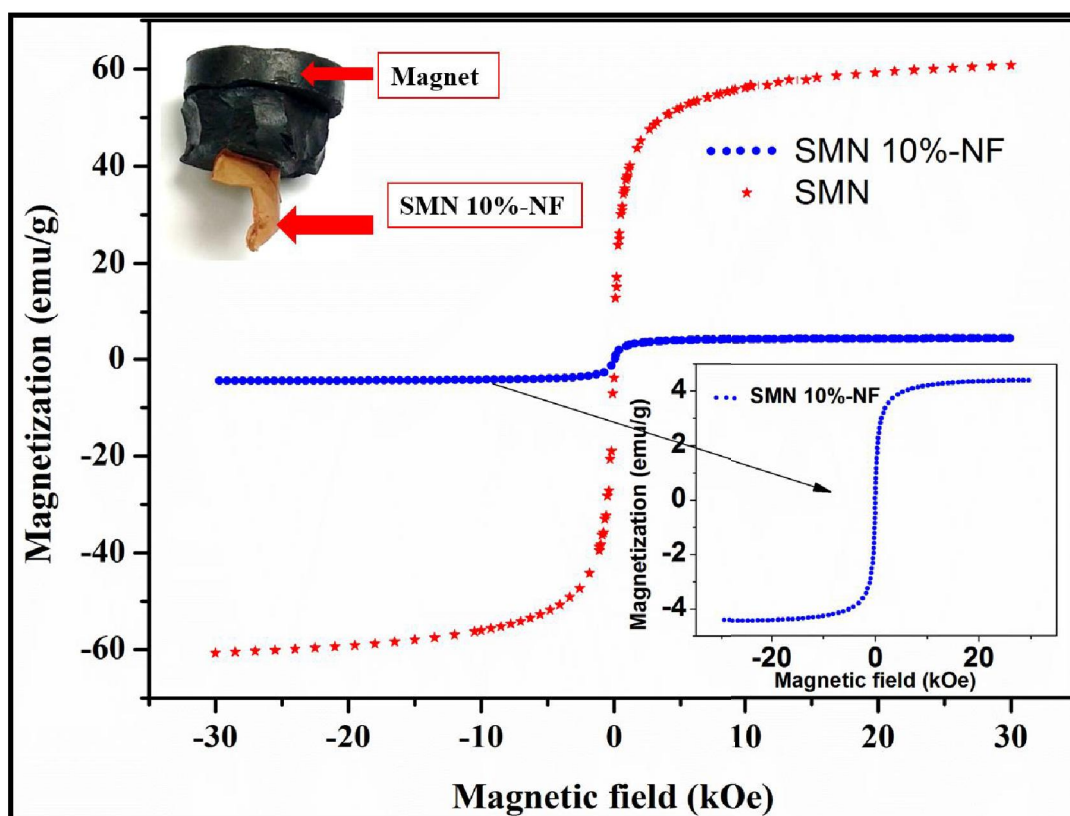
Figure 6. 11 SQUID analysis of SMN 10%-NF and SMN.

6.4.7 Drug release studies of magnetic and nonmagnetic nanofibers

The obtained percent of FU release was plotted as cumulative percent of release against time (**Fig. 6.12**). As anticipated, the SMN loaded nanofibers achieved a higher amount of drug release compared to the Plain-NF in a 2 h of time frame. The Plain-NF-FU 5% demonstrated a 55% of release of FU in the initial 1 h; after 2 h, 65% and after 24 h min, 83% of FU were released. Irrespective of the SMN concentration, the compositions of SMN 10%-NF-FU 5% and SMN 20%-NF-FU 5% recorded ~ 50% release of FU in 0.5 h and 95% release of FU in 4 h. The increase in FU release from the nanofibers of SMN embedded compositions was because of the presence of stearic acid, which induced the drug's solubility and promoted FU's faster diffusion. Similar observations were reported earlier in support of our results[71]. **Fig. 6.12** shows the difference between the cumulative % of FU released over time in existence and the non-existence of SMN in nanofibers. These results demonstrated that SMN loading into nanofibers has a remarkable effect on drug release. Moreover, based on the SQUID analysis, we anticipate that the fabricated SMN nanofibers system with FU can reach the affected area like the digestive tract in the case of bowel diseases, inflammation in arthritis, acute condition sepsis, and range of oncological treatment under the influence of an external magnetic field. Such a system can have a prominent effect on increasing the efficacy by reaching a site of action as well as reducing the side effect of the drug.
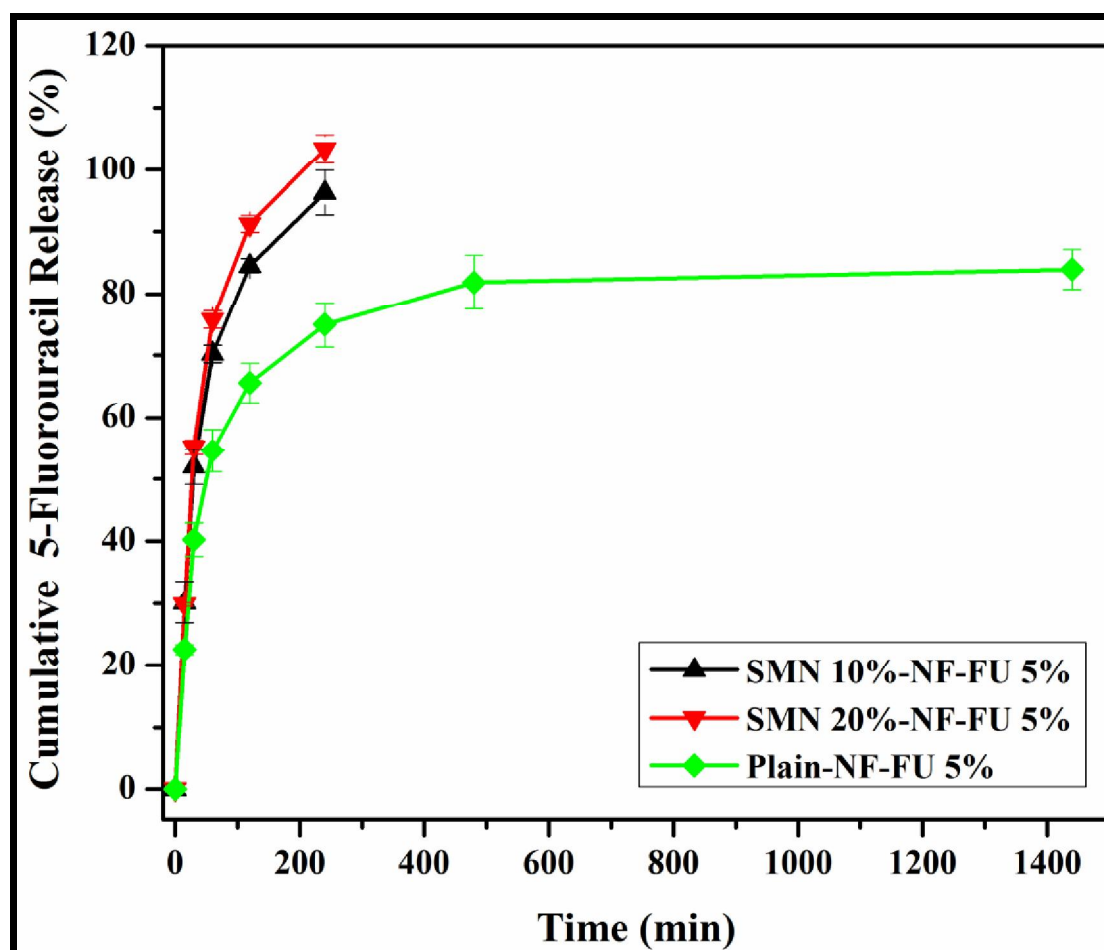
Figure 6. 12 Drug release studies in pH 7.4 PBS at 37±2 °C of Plain-NF-FU-5%,SMN 10%-NF-FU- 5% and SMN 20%-NF-FU- 5%.

6.4.8   Hemolysis assay

Hemolysis test was used to determine the hemolytic activity of fabricated nanofibers. As explained in the materials and methods section, the negative (phosphate buffer of pH 7.4), positive controls (deionized water), and the respective compositions of formulation shown in **Table 1**. were subjected to the hemolysis assay (**Fig. 6.13**). We observed 2.9%, 0.8%, and 1.8% hemolytic activity in Plain-NF, SMN 10%-NF, and SMN 20%-NF respectively (**Fig. 6.14**). The results showed that hemolytic activity decreased in the presence of SMN nanoparticles. The hemolysis data of FU loaded nanofibers, SMN 10%-NF-FU 5% (0.7%) and SMN 20%-NF-FU 5% (1.5%) signified that the hemolytic activity was lower in drug-loaded nanofibers than without drug-loaded nanofibers. In the case of Plain-NF-FU 5%, hemolysis was 2.3%. The hemolysis assay of SMN nanoparticles was only 2.1%. All the results suggested that

the presence of SMN in the nanofibers has reduced the hemolytic activity significantly. According to the reported literature, the material with hemolysis activity below 5%, is considered to be safe for drug delivery application by the invasive method[39]. Therefore, we conclude that the fabricated nanofibers will potentially apply in drug delivery.
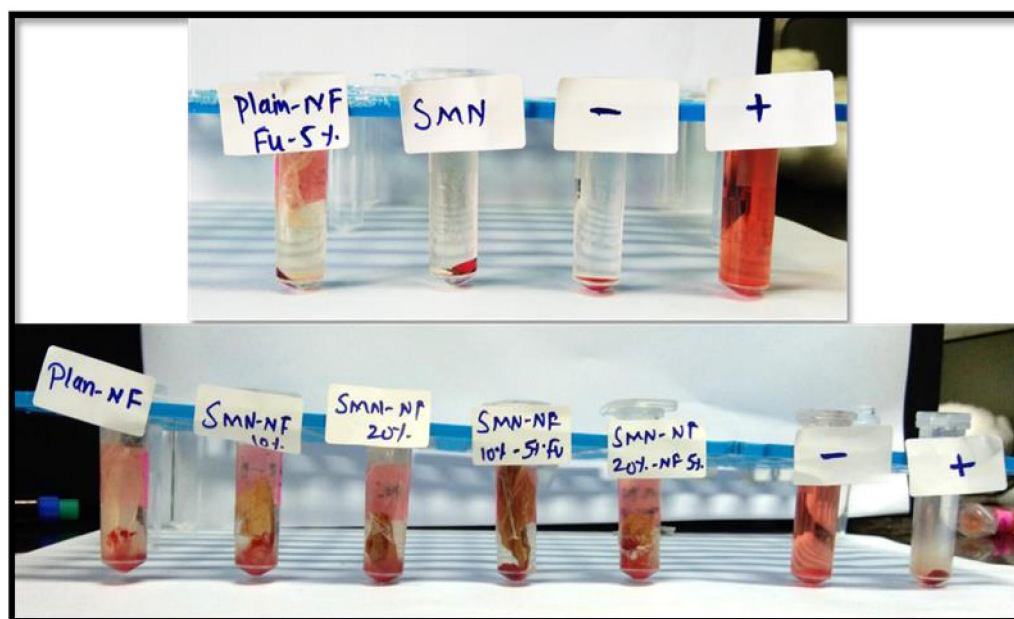
Figure 6. 13 Image of hemolysis assay done in human blood for all the polymeric nanofibers blends.
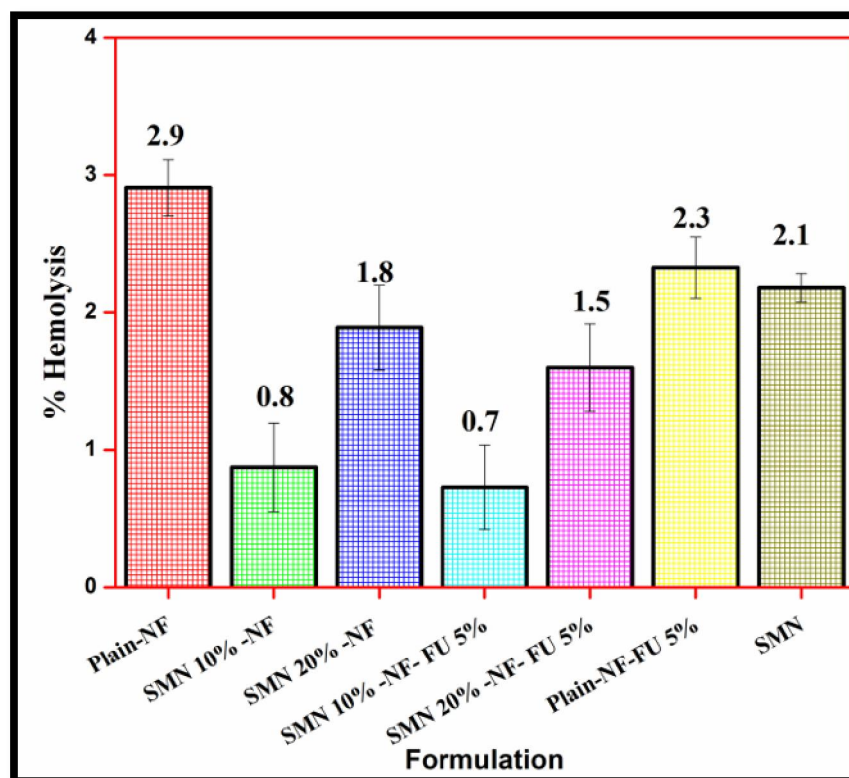
Figure 6. 14 Bar diagram of hemolysis assay of all the compositions which were mentioned in Table 6.1.

6.4.9   Cell viability assay

The developed Plain-NF, SMN 10%-NF, and SMN 20%-NF nanofibers were studied for cytotoxicity studies in the L929 cell line for 24 h. The nanofibers exhibited excellent cell viability of more than 75%, suggesting that the nanofibers system is biocompatible in the L929 cell line. Moreover, it was observed that SMN 20%-NF (87%) has higher cell viability than SMN 10%-NF (84%) and Plain-NF (77%) (**Fig. 6.15 A**). The cell viability increased with an increase in the concentration of SMN in nanofibers. Although, the reason behind such an increase is yet to be studied. Nevertheless, similar observations were reported in some earlier publications[72-74]. Thus cell viability results suggest that SMN are biocompatible and safe to use.

      The cytotoxicity studies were done using MCF-7 breast cancer cell line for Plain NF-FU 5%, SMN 10%-NF-FU 5%, and SMN 10%-NF-FU 5% for 24 h (**Fig. 6.15 B**). The results showed that the developed nanofibers significantly affect MCF-7 cells. As expected, SMN 10%-NF-FU 5% (43%), SMN 20%-NF-FU 5% (42%) and, Plain NF-FU 5% (53%) showed almost half the amount of cell viability towards the

MCF-7 cell line. The increase in cytotoxicity was due to the amount of drug released from the nanofibers, as displayed in the release studies. The Plain NF without FU displayed 74% cell viability after 24 h incubation thus, the nanofiber without FU proved to be non-toxic towards MCF-7 cancer cells. In conclusion, the SMN loaded nanofibers can be a potential candidate for a targeted drug delivery to treat cancer patients.
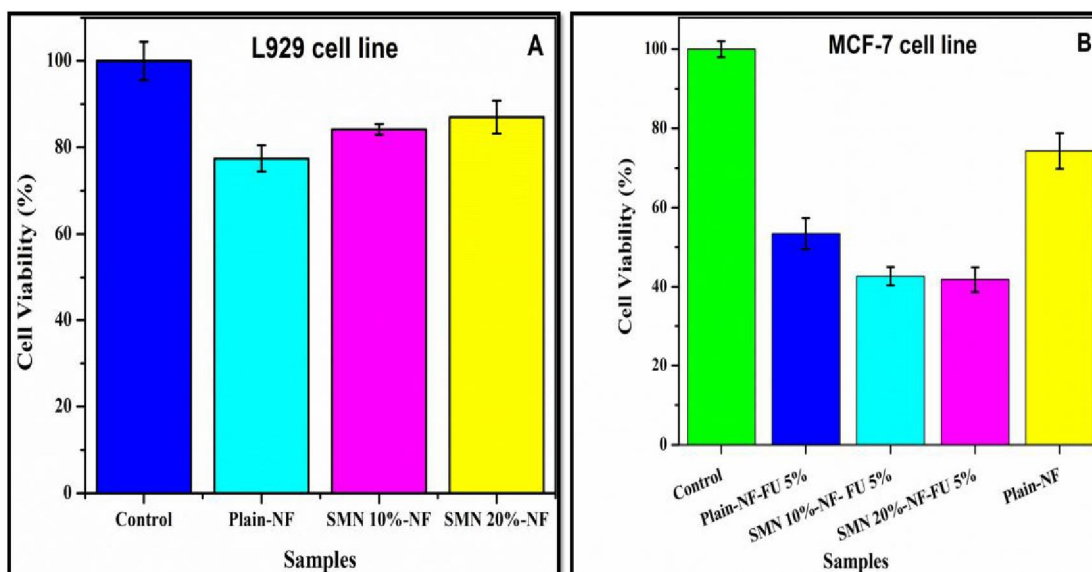
Figure 6. 15 Figure A. Cell viability studies in L929 fibroblast cells for 24 of Plain-NF-FU, SMN 10%-NF FU, and SMN 20%-NF. **Figure B.** Cytotoxicity studies in MCF-7 breast cancer cell line for a period of 24 h of Plain-NF-FU-5%, SMN 10%-NF FU- 5%, and SMN 20%-NF FU- 5%.

6.5 Conclusions

The blends of PVP, PCL, and NPEA containing SMN were successfully fabricated using an easily reproducible electrospinning method. E-SEM and TEM demonstrated that the fabricated nanofibers were smooth and fine without any beads. Further, E-SEM dot mapping confirmed that the SMN was uniformly distributed in nanofibers. FTIR confirmed the presence of all the polymers, SMN, and drug in the nanofibers, and no chemical interactions were observed. The XRD studies showed the changes in the crystalline properties which were influenced by the presence of FU and SMN. Drug release data showed that in the presence of SMN, nanofibers exhibit higher drug release (80% in 120 min) compared to the plain-NF (66% in 120 min). SQUID

analysis demonstrated that the fabricated nanofibers are supraparamagnetic in nature and have zero remanences and zero coercivity. Hemolysis and cell viability assay (in L929 fibroblast cells) indicated that fabricated nanofibers are biocompatible and safe. Moreover, cytotoxicity studies revealed that SMN nanofibers are more toxic to cancer cells than plain- nanofibers, as more than 50% of breast cancer cells were dead within 24 h. Thus, the developed magnetic nanofibers can be an efficient tool for targeted drug delivery applications. The fabrication of nanofibers is easy, cost-effective, reproducible, and can be scaled up, thus opening many opportunities for its use in the biomedical field.

6.6 References

[1] N.K. Preman, R.R. Barki, A. Vijayan, S.G. Sanjeeva, R.P. Johnson, Recent developments in stimuli-responsive polymer nanogels for drug delivery and diagnostics: A Review, European Journal of Pharmaceutics and Biopharmaceutics (2020).

[2] R. Kumari, D. Sunil, R.S. Ningthoujam, Hypoxia-responsive nanoparticle based drug delivery systems in cancer therapy: An up-to-date review, Journal of Controlled Release 319 (2020) 135-156.

[3] A. Kumar, A. Singam, G. Swaminathan, N. Killi, N.K. Tangudu, J. Jose, L.D. Kumar, Combinatorial therapy using RNAi and curcumin nano-architectures regresses tumors in breast and colon cancer models, Nanoscale 14(2) (2022) 492-505.

[4] M. Wang, J. Long, S. Zhang, F. Liu, X. Zhang, X. Zhang, L. Sun, L. Ma, C. Yu, H. Wei, Folate-Targeted Anticancer Drug Delivery via a Combination Strategy of a Micelle Complex and Reducible Conjugation, ACS Biomaterials Science & Engineering 6(3) (2020) 1565-1572.

[5] A. Singam, N. Killi, P.R. Patel, R.V.N. Gundloori, PEGylated ethyl cellulose micelles as a nanocarrier for drug delivery, RSC Advances 11(49) (2021) 30532-30543.

[6] A. Zia, E. Pentzer, S. Thickett, K. Kempe, Advances and opportunities of oil-in-oil emulsions, ACS Applied Materials & Interfaces 12(35) (2020) 38845-38861.

[7] S. Kajdič, O. Planinšek, M. Gašperlin, P. Kocbek, Electrospun nanofibers for customized drug-delivery systems, Journal of Drug Delivery Science and Technology 51 (2019) 672-681.

[8] K.B. Sutradhar, M. Amin, Nanotechnology in cancer drug delivery and selective targeting, International Scholarly Research Notices 2014 (2014).

[9] G.L. Zwicke, G. Ali Mansoori, C.J. Jeffery, Utilizing the folate receptor for active targeting of cancer nanotherapeutics, Nano reviews 3(1) (2012) 18496.

[10] Z. Li, S. Tan, S. Li, Q. Shen, K. Wang, Cancer drug delivery in the nano era: An overview and perspectives, Oncology reports 38(2) (2017) 611-624.

[11] A.R. Shahverdi, F. Shahverdi, E. Faghfuri, F. Mavandadnejad, M.H. Yazdi, M. Amini, Characterization of folic acid surface-coated selenium nanoparticles and corresponding in vitro and in vivo effects against breast cancer, Archives of medical research 49(1) (2018) 10-17.

[12] L. Li, S. He, L. Yu, E.H. Elshazly, H. Wang, K. Chen, S. Zhang, L. Ke, R. Gong, Codelivery of DOX and siRNA by folate-biotin-quaternized starch nanoparticles for promoting synergistic suppression of human lung cancer cells, Drug delivery 26(1) (2019) 499-508.

[13] Y. Yin, Q. Hu, C. Xu, Q. Qiao, X. Qin, Q. Song, Y. Peng, Y. Zhao, Z. Zhang, Co-delivery of doxorubicin and interferon-γ by thermosensitive nanoparticles for cancer immunochemotherapy, Molecular pharmaceutics 15(9) (2018) 4161-4172.

[14] A. Gangwar, S.S. Varghese, S.S. Meena, C.L. Prajapat, N. Gupta, N.K. Prasad, Fe3C nanoparticles for magnetic hyperthermia application, Journal of Magnetism and Magnetic Materials 481 (2019) 251-256.

[15] Y. Deng, A. Xu, Y. Yu, C. Fu, G. Liang, Biomedical Applications of Fluorescent and Magnetic Resonance Imaging Dual-Modality Probes, ChemBioChem 20(4) (2019) 499-510.

[16] Z. Liu, J. Liu, X. Cui, X. Wang, L. Zhang, P. Tang, Recent advances on magnetic sensitive hydrogels in tissue engineering, Frontiers in chemistry 8 (2020) 124.

[17] T. Vangijzegem, D. Stanicki, S. Laurent, Magnetic iron oxide nanoparticles for drug delivery: applications and characteristics, Expert opinion on drug delivery 16(1) (2019) 69-78.

[18] D. Murzin, D.J. Mapps, K. Levada, V. Belyaev, A. Omelyanchik, L. Panina, V. Rodionova, Ultrasensitive magnetic field sensors for biomedical applications, Sensors 20(6) (2020) 1569.

[19] Y. Zhou, D. Yan, S. Yuan, Y. Chen, E.E. Fletcher, H. Shi, B. Han, Selective binding, magnetic separation and purification of histidine-tagged protein using biopolymer magnetic core-shell nanoparticles, Protein expression and purification 144 (2018) 5-11.

[20] S. Tan, K. Saito, M.T.W. Hearn, Stimuli-responsive polymeric materials for separation of biomolecules, Current opinion in biotechnology 53 (2018) 209-223.

[21] Y.-L. Liu, D. Chen, P. Shang, D.-C. Yin, A review of magnet systems for targeted drug delivery, Journal of Controlled Release 302 (2019) 90-104.

[22] S. Sharma, R. Kumar, A. Gaur, A model for magnetic nanoparticles transport in a channel for targeted drug delivery, Procedia Materials Science 10 (2015) 44-49.

[23] E.J. Bealer, K. Kavetsky, S. Dutko, S. Lofland, X. Hu, Protein and polysaccharide-based magnetic composite materials for medical applications, International Journal of Molecular Sciences 21(1) (2020) 186.

[24] O. Hosu, M. Tertis, C. Cristea, Implication of magnetic nanoparticles in cancer detection, screening and treatment, Magnetochemistry 5(4) (2019) 55.

[25] G.M. Ziarani, M. Malmir, N. Lashgari, A. Badiei, The role of hollow magnetic nanoparticles in drug delivery, RSC advances 9(43) (2019) 25094-25106.

[26] Z. Zhang, L. Zhuang, Y. Lin, M. Yan, J. Lv, X. Li, H. Lin, P. Zhu, Q. Lin, Y. Xu, Novel drug delivery system based on hollow mesoporous magnetic nanoparticles for head and neck cancers--targeted therapy in vitro and in vivo, American Journal of Cancer Research 10(1) (2020) 350.

[27] S.E. Minaei, S. Khoei, S. Khoee, F. Vafashoar, V.P. Mahabadi, In vitro anti-cancer efficacy of multi-functionalized magnetite nanoparticles combining alternating magnetic hyperthermia in glioblastoma cancer cells, Materials Science and Engineering: C 101 (2019) 575-587.

[28] M.S.A. Darwish, H. Kim, H. Lee, C. Ryu, J.Y. Lee, J. Yoon, Synthesis of magnetic ferrite nanoparticles with high hyperthermia performance via a controlled co-precipitation method, Nanomaterials 9(8) (2019) 1176.

[29] M.A. Dheyab, A.A. Aziz, M.S. Jameel, O.A. Noqta, P.M. Khaniabadi, B. Mehrdel, Simple rapid stabilization method through citric acid modification for magnetite nanoparticles, Scientific reports 10(1) (2020) 1-8.

[30] I. Khmara, O. Strbak, V. Zavisova, M. Koneracka, M. Kubovcikova, I. Antal, V. Kavecansky, D. Lucanska, D. Dobrota, P. Kopcansky, Chitosan-stabilized iron oxide nanoparticles for magnetic resonance imaging, Journal of Magnetism and Magnetic Materials 474 (2019) 319-325.

[31] E. Katz, Synthesis, properties and applications of magnetic nanoparticles and nanowires—A brief introduction, Magnetochemistry 5(4) (2019) 61.

[32] Y. Jabalera, A. Fernández-Vivas, G.R. Iglesias, Á.V. Delgado, C. Jimenez-Lopez, Magnetoliposomes of mixed biomimetic and inorganic magnetic nanoparticles as enhanced hyperthermia agents, Colloids and Surfaces B: Biointerfaces 183 (2019) 110435.

[33] A. Dadwal, P.A. Joy, Particle size effect in different base fluids on the thermal conductivity of fatty acid coated magnetite nanofluids, Journal of Molecular Liquids 303 (2020) 112650.

[34] A. Gálvez-Vergara, B. Fresco-Cala, S. Cárdenas, Switchable Pickering emulsions stabilized by polystyrene-modified magnetic nanoparticles, Colloids and Surfaces A: Physicochemical and Engineering Aspects 606 (2020) 125462.

[35] D. Ling, T. Hyeon, Chemical design of biocompatible iron oxide nanoparticles for medical applications, Small 9(9-10) (2013) 1450-1466.

[36] Y. Hu, S. Mignani, J.-P. Majoral, M. Shen, X. Shi, Construction of iron oxide nanoparticle-based hybrid platforms for tumor imaging and therapy, Chemical Society Reviews 47(5) (2018) 1874-1900.

[37] A. Dadwal, P.A. Joy, Influence of chain length of long-chain fatty acid surfactant on the thermal conductivity of magnetite nanofluids in a magnetic field, Colloids and Surfaces A: Physicochemical and Engineering Aspects 555 (2018) 525-531.

[38] J. Xue, T. Wu, Y. Dai, Y. Xia, Electrospinning and electrospun nanofibers: methods, materials, and applications, Chemical reviews 119(8) (2019) 5298-5415.

[39] S. Jain, S.R.K. Meka, K. Chatterjee, Engineering a piperine eluting nanofibrous patch for cancer treatment, ACS Biomaterials Science & Engineering 2(8) (2016) 1376-1385.

[40] M. Hadjianfar, D. Semnani, J. Varshosaz, Polycaprolactone/chitosan blend nanofibers loaded by 5-fluorouracil: An approach to anticancer drug delivery system, Polymers for Advanced Technologies 29(12) (2018) 2972-2981.

[41] P. Abasian, M. Radmansouri, M.H. Jouybari, M.V. Ghasemi, A. Mohammadi, M. Irani, F.S. Jazi, Incorporation of magnetic NaX zeolite/DOX into the PLA/chitosan nanofibers for sustained release of doxorubicin against carcinoma cells death in vitro, International journal of biological macromolecules 121 (2019) 398-406.

[42] L. Wang, M. Wang, P.D. Topham, Y. Huang, Fabrication of magnetic drug-loaded polymeric composite nanofibres and their drug release characteristics, Rsc Advances 2(6) (2012) 2433-2438.

[43] J. Jerobin, P. Makwana, R.S.S. Kumar, R. Sundaramoorthy, A. Mukherjee, N. Chandrasekaran, Antibacterial activity of neem nanoemulsion and its toxicity assessment on human lymphocytes in vitro, International journal of nanomedicine 10(Suppl 1) (2015) 77.

[44] J.D. Stark, J.F. Walter, Neem oil and neem oil components affect the efficacy of commercial neem insecticides, Journal of Agricultural and Food Chemistry 43(2) (1995) 507-512.

[45] F. Hao, S. Kumar, N. Yadav, D. Chandra, Neem components as potential agents for cancer prevention and treatment, Biochimica et Biophysica Acta (BBA)-Reviews on Cancer 1846(1) (2014) 247-257.

[46] M.A. Moga, A. Bălan, C.V. Anastasiu, O.G. Dimienescu, C.D. Neculoiu, C. Gavriş, An overview on the anticancer activity of Azadirachta indica (Neem) in gynecological cancers, International journal of molecular sciences 19(12) (2018) 3898.

[47] R.V. Priyadarsini, R.S. Murugan, P. Sripriya, D. Karunagaran, S. Nagini, The neem limonoids azadirachtin and nimbolide induce cell cycle arrest and mitochondria-mediated apoptosis in human cervical cancer (HeLa) cells, Free radical research 44(6) (2010) 624-634.

[48] E. Ahmadian, S.M. Dizaj, S. Sharifi, S. Shahi, R. Khalilov, A. Eftekhari, M. Hasanzadeh, The potential of nanomaterials in theranostics of oral squamous cell carcinoma: Recent progress, TrAC Trends in Analytical Chemistry 116 (2019) 167-176.

[49] P. Srivastava, N. Yadav, R. Lella, A. Schneider, A. Jones, T. Marlowe, G. Lovett, K. O'Loughlin, H. Minderman, R. Gogada, Neem oil limonoids induces p53-independent apoptosis and autophagy, Carcinogenesis 33(11) (2012) 2199-2207.

[50] A. Eftekhari, E. Ahmadian, A. Azami, M. Johari-Ahar, M.A. Eghbal, Protective effects of coenzyme Q10 nanoparticles on dichlorvos-induced hepatotoxicity and mitochondrial/lysosomal injury, Environmental toxicology 33(2) (2018) 167-177.

[51] M. Kurakula, G.S.N.K. Rao, Type of Article: REVIEW Pharmaceutical Assessment of Polyvinylpyrrolidone (PVP): As Excipient from Conventional to Controlled Delivery Systems with a Spotlight on COVID-19 Inhibition, Journal of Drug Delivery Science and Technology (2020) 102046.

[52] C. Wang, C. Ma, Z. Wu, H. Liang, P. Yan, J. Song, N. Ma, Q. Zhao, Enhanced bioavailability and anticancer effect of curcumin-loaded electrospun nanofiber: in vitro and in vivo study, Nanoscale research letters 10(1) (2015) 1-10.

[53] D.-G. Yu, C. Branford-White, K. White, X.-L. Li, L.-M. Zhu, Dissolution improvement of electrospun nanofiber-based solid dispersions for acetaminophen, Aaps Pharmscitech 11(2) (2010) 809-817.

[54] L.-Y. Huang, C. Branford-White, X.-X. Shen, D.-G. Yu, L.-M. Zhu, Time-engineeringed biphasic drug release by electrospun nanofiber meshes, International journal of pharmaceutics 436(1-2) (2012) 88-96.

[55] F. Rahmani, H. Ziyadi, M. Baghali, H. Luo, S. Ramakrishna, Electrospun PVP/PVA Nanofiber Mat as a Novel Potential Transdermal Drug-Delivery System for Buprenorphine: A Solution Needed for Pain Management, Applied Sciences 11(6) (2021) 2779.

[56] F. Liu, Z. Zhao, J. Yang, J. Wei, S. Li, Enzyme-catalyzed degradation of poly (l-lactide)/poly (ε-caprolactone) diblock, triblock and four-armed copolymers, Polymer degradation and stability 94(2) (2009) 227-233.

[57] T. Patr, A. Glória, Mechanical and biological behaviour of PCL and PCL/PLA scaffolds for tissue engineering applications, Chemical engineering transactions 32 (2013) 1645-1650.

[58] H.E. Patel, S.K. Das, T. Sundararajan, a. Sreekumaran Nair, B. George, and T. Pradeep,"Thermal conductivities of naked and monolayer protected metal nanoparticle based nanofluids: Manifestation of anomalous enhancement and chemical effects," Applied Physics Letters 83(14) (2003) 2931.

[59] R. Lenin, P.A. Joy, Role of base fluid on the thermal conductivity of oleic acid coated magnetite nanofluids, Colloids and Surfaces A: Physicochemical and Engineering Aspects 529 (2017) 922-929.

[60] S. Agrawal, P.R. Patel, R.V.N. Gundloori, Proteins as Nanocarriers To Regulate Parenteral Delivery of Tramadol, ACS Omega 4(4) (2019) 6301-6310.

[61] A. Rahma, M.M. Munir, A. Prasetyo, V. Suendo, H. Rachmawati, Intermolecular interactions and the release pattern of electrospun curcumin-polyvinyl (pyrrolidone) fiber, Biological and Pharmaceutical Bulletin 39(2) (2016) 163-173.

[62] V.A. Dhumale, R.K. Gangwar, S.S. Datar, R.B. Sharma, Reversible aggregation control of polyvinylpyrrolidone capped gold nanoparticles as a function of pH, Materials Express 2(4) (2012) 311-318.

[63] A. Benkaddour, K. Jradi, S. Robert, C. Daneault, Grafting of polycaprolactone on oxidized nanocelluloses by click chemistry, Nanomaterials 3(1) (2013) 141-157.

[64] N. Killi, A.T. Pawar, R.V.N. Gundloori, Polyesteramide of Neem Oil and Its Blends as an Active Nanomaterial for Tissue Regeneration, ACS Applied Bio Materials 2(8) (2019) 3341-3351.

[65] D.M. Patel, R.H. Jani, C.N. Patel, Design and evaluation of colon targeted modified pulsincap delivery of 5-fluorouracil according to circadian rhythm, International journal of pharmaceutical investigation 1(3) (2011) 172.

[66] R.D. Waldron, Infrared spectra of ferrites, Physical review 99(6) (1955) 1727.

[67] A.S. Perera, S. Zhang, S. Homer-Vanniasinkam, M.-O. Coppens, M. Edirisinghe, Polymer–magnetic composite fibers for remote-controlled drug release, ACS applied materials & interfaces 10(18) (2018) 15524-15531.

[68] A.B. Chaudhari, P.D. Tatiya, R.K. Hedaoo, R.D. Kulkarni, V.V. Gite, Polyurethane prepared from neem oil polyesteramides for self-healing anticorrosive coatings, Industrial & Engineering Chemistry Research 52(30) (2013) 10189-10197.

[69] R. Balu, T.S. Kumar, M. Ramalingam, S. Ramakrishna, Electrospun Polycaprolactone/Poly (1, 4-butylene adipate-co-polycaprolactam) blends: Potential biodegradable scaffold for bone tissue regeneration, Journal of Biomaterials and Tissue Engineering 1(1) (2011) 30-39.

[70] R. Lenin, A. Dadwal, P.A. Joy, Thermal conductivity studies on magnetite nanofluids coated with short-chain and long-chain fatty acid surfactants, Bulletin of Materials Science 41(5) (2018) 120.

[71] B.U. Killen, O.I. Corrigan, Factors influencing drug release from stearic acid based compacts, International journal of pharmaceutics 228(1-2) (2001) 189-198.

[72] H. Zhang, J. Xia, X. Pang, M. Zhao, B. Wang, L. Yang, H. Wan, J. Wu, S. Fu, Magnetic nanoparticle-loaded electrospun polymeric nanofibers for tissue engineering, Materials Science and Engineering: C 73 (2017) 537-543.

[73] Q. Li, L. Ge, W. Wan, J. Jiang, W. Zhong, J. Ouyang, M. Xing, Magnetically guided fabrication of multilayered iron oxide/polycaprolactone/gelatin nanofibrous structures for tissue engineering and theranostic application, Tissue Engineering Part C: Methods 21(10) (2015) 1015-1024.

[74] S. Tasoglu, C.H. Yu, H.I. Gungordu, S. Guven, T. Vural, U. Demirci, Guided and magnetic self-assembly of tunable magnetoceptive gels, Nature communications 5(1) (2014) 1-11.

CHAPTER 7

Conclusion and Future Prospects
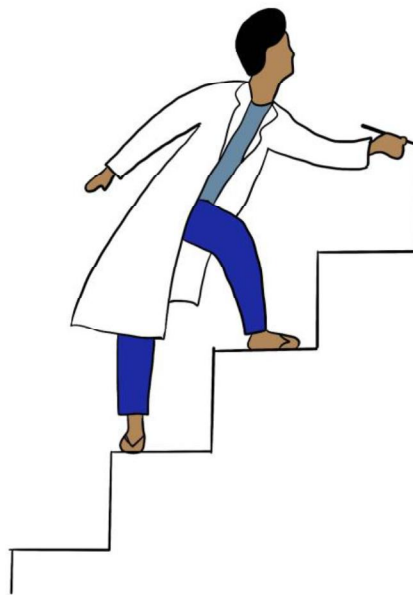
7.1 Conclusion and Future Prospects

The thesis comprises of fabrication and characterization of electrospun nanofibers using biocompatible and biodegradable polymers for wound healing and drug delivery applications. As nanofibers have several advantages like high surface-to-volume ratio, high porosity, ability to mimic with the ECM, and ease of loading the bioactive agents, the developed nanofibers give enormous scope for biomedical application. For the fabrication of nanofibers, electrospinning technique was utilized which is being widely used as it is simple, easy to handle and design and cost effective. The various polymers like HA, PCL, PHBV, PVP, PEO, and NPEA were used to prepare nanofiber. The developed nanofibers system were with and without magnetic nanoparticles, anti-bacterial and anti-cancer drugs were immobilized and studied the respective release profiles to understand scope in biomedical application. Detailed summary and future scope of the thesis were further elaborated in the following paragraphs in chapter wise manner.

Chapter 1 discusses the literature review on nanofibers developed by the electrospinning method. The significance of this technique in developing the nanofiber material as compared to the other techniques was briefed. Also, the application of these nanofibers in various fields was explained. More importantly, the focus was on reviewing the research on biomedical applications of nanofibers. Finally, the research done on the nanofibers for drug delivery and their importance in the controlled release is discussed.

Chapter 2 describes the present research aim and objectives and strategies of the thesis.

Chapter 3, reveals the investigation on the development of nanofibers using a blend of hydrophobic polymers PLA, PCL, and a hydrophilic natural protein, EA. Electrospinning method was followed for the fabrication of the nanofibers. The goal of this work is to use EA to alter the hydrophobicity of PLA and PCL. EA has properties comparable to HSA, which has been authorized by the FDA for biomedical

use. We have also immobilized MTZ for its antibacterial properties. As a result of the investigation, we discovered that the produced nanofibers are smooth and bead-free, which was confirmed by SEM. FTIR, DSC, and XRD for the physicochemical characteristics of nanofibers. Further, fluorescence investigations were done to understand the hydrogen and functional interactions between the polymers and the MTZ. Drug release studies revealed that when the drug concentration in the nanofiber increased, the amount of drug released increased. The cell compatibility of the nanofibers was studied by MTT and hemolysis assays. The results of *in vitro* antibacterial and cell proliferation tests revealed that the nanofibers prepared are suitable for tissue engineering.

Chapter 4 deals with the investigation of Cur and CDF loaded nanofibers for anti-bacterial and wound healing applications. Cur is well recognized due to its wide spectrum of biological activity. But due to its hydrophobic nature, the biological action is not fully utilized. Hence, several forms of curcumin derivatives are being developed to improve the bioavailability for effective application. In this regard, a CDF derivative with an improved anticancer property was synthesized, however, the antibacterial property after derivatizing Cur was not evaluated. Accordingly, we have developed the respective Cur and CDF incorporated electrospun nanofibers to understand the antibacterial property. HA, PEO, and PHBV were blended to fabricate electrospun nanofibers. FESEM confirmed that the fabricated nanofibers were smooth and randomly oriented. Further, DSC and FTIR were used to determine the presence of polymers and drugs, revealing that the polymers and drugs were homogeneously blended and dispersed. From the drug release profile, we observed that 25% of CDF was released within 240 h, while Cur released 37%. Both demonstrated sustained release for a longer period of time. CDF being more hydrophobic, the rate of release was slower than Cur. The cell compatibility studies were validated using hemolysis, MTT, and cell adhesion assays. In addition, we conducted the scratch assay and cell proliferation test to assess the cell proliferation efficacy of the nanofibers. The results being favorable, the developed nanofibers are believed to be suitable for tissue engineering applications. To confirm the sustainability of the antibacterial property of CDF, the antibacterial activity for the respective nanofibers loaded with Cur and CDF

were assessed against *S.aureus* bacteria. The results demonstrated similar antibacterial properties for both CDF and Cur. In addition, molecular docking studies on DHFR, an *S.aureus* protein, for CDF and Cur showed that Cru had a lower affinity than CDF. Based on these findings, we concluded that the CDF sustained its antibacterial property in addition to the improved anticancer property, hence CDF being synergetic, it will have a better scope in cancer therapy.

Chapter 5 analyzes a dual drug loaded nanofibers system for chronic wound healing application. The drug used for wound healing are AT, which is widely used as an antibiotic to fight against various bacteria, and ZnO which is used for topical application to reduce super-infection and stimulate the wound re-epithelialization, and increase cell proliferation. The produced nanofibers were smooth and bead-free as demonstrated by FE-SEM, whereas, TEM confirmed the presence of ZnO into the nanofibers. The *in vitro* drug release showed burst release, in 2 h almost 80% of drug was released and 92% released in 8 h. The anti-bacterial activity of the developed nanofibers was demonstrated by the inhibitory effect against *S.auerus* (Staphylococcus aureus) and *E.coli* (Escherichia coli) bacterial strain. Further, cytotoxicity of nanofibers was evaluated by NHT13 cell and cell proliferation showed that developed nanofibers are suitable for tissue engineering and wound healing applications. In addition, the *in-vivo* studies were carried out in male Swiss albino mice, which showed faster wound healing for developed nanofibers with dual drug compared to Povidone Iodine formulation. Histopathology studies also proved that the developed nanofibers are non-toxic to normal cells and hence showed better reformation of collagen with thin epidermis and dermis as compared to the studies with the control and commercial wound healing material.

Chapter 6 deals with designing and fabrication of non-woven nanofiber mats using NPEA (neem oil Polyesteramide), PCL (polycaprolactone), and PVP (polyvinylpyrrolidone) by incorporation of stearic-acid coated magnetic nanoparticles (SMN) for targeted drug delivery application. The iron oxide magnetic nanoparticles coated with stearic acid were obtained by the co-precipitation method. SMN were embedded into the nanofibers by active loading as SMN are readily dispersible into the organic solvent due to stearic acid coating. SMN nanofibers were fabricated for

the controlled release of FU (5-Flourouracil) to understand the release behaviour in treating cancer. The surface morphology of nanofibers was analyzed by TEM and E-SEM. The dispersivity of SMN was confirmed by mapping in E-SEM. Further, physicochemical properties were characterized by FTIR, XRD, and TGA. The drug, FU was incorporated in the fabricated nanofibers by active loading. *In vitro* drug release studies of the developed nanofibers showed a significant difference in the release of the drug, with and without SMN in PBS at pH 7.4. Later, the biocompatibility of the fabricated SMN nanofibers was analyzed by hemolysis assay and cytotoxicity assay using blood and L929 mouse fibroblast cells, respectively. The efficacy of drug-loaded SMN-NF was analyzed in the MCF-7 cell line, which showed 50% cell death within 24 h. In conclusion, the developed novel magnetic nanofibers may be used as targeted drug delivery systems to treat cancer more efficiently under the influence of a magnetic field.

Future Prospects

Electrospun nanofibers are considered a prominent material in the biomedical field because the high surface area, enhanced porosity, ease of handling and blending of various polymers with immobilized active molecules has enabled these nanofibers as drug delivery systems for improvising patient compliance. The crystalline drugs become amorphous after fabrication of nanofibers hence the solubility and bioavailability of the drug increases, which helps in enhancing the efficiency of the treatment. The investigations on the development of the nanofibers as a drug delivery system enabled us to add knowledge in this area and therefore, the possibility of developing more advanced nanofibers as drug delivery systems shall be proposed.

ABSTRACT

Name of the Student: Patel Pratikshkumar R. **Registration No.:** 10BB15J26033

Faculty of Study: Biological Sciences   **Year of Submission:** 2022

CSIR Lab: NCL, Pune   **Name of the Supervisor:** Dr. GVN Rathna

Title of the Thesis: Design and Development of Non-Woven Nanofibers as Drug Delivery System

The aim of this thesis was to design and develop non-woven nanofibers by electrospinning method for drug delivery application. Accordingly, new underutilised polymers were studied for drug delivery applications by blending with biopolymers, which are safe for the environment. All the nanofibers developed in this research work were subjected to characterization by various physicochemical method and their efficacy were studied by *in vitro* and *in vivo* analysis. In **Chapter 1**, we reviewed the literature on the nanofibers developed by electrospinning method and application in various field was explained. And the effect of parameters on nanofibers were explained briefly. *Chapter 2* investigates the objectives and scope of the work carried out in this thesis. In **Chapter 3**, we prepared a non-woven nanofibers using the combination of hydrophobic polymers (PLA and PCL) and hydrophilic protein (EA) to understand its applicability in tissue engineering. *Chapter 4* deals with the fabrication of hyaluronic acid nanofibers by blending with PHBV, HA and PEO and immobilized Curcumin and CDF to evaluate its anti-bacterial property. In the *chapter 5*, we developed a dual drug loaded nanofibers system using blends of neem oil based polyesteramide for wound healing application and to overcome bacterial resistance. *Chapter 6* developed nanofibers by NPEA, PCL, PLA embedded with SMN by electrospinning method for targeted drug delivery application. *Chapter 7* summarises the overall work done in this thesis and proposes the area of research consideration for drug delivery applications. It also illustrates how the nanofibers might be used to treat wound healing, tissue engineering, and drug delivery while overcoming the limitations of conventional treatments.

List of Publications Emanating from the Thesis Work

1. **Patel Pratikshkumar R,** Komal Pandey**,** Naresh Killi, and Rathna Venkata Naga Gundloori. "Manipulating hydrophobicity of polyester nanofiber mats with egg albumin to enhance cell interactions." Polymer Engineering & Science, **2021**, 61(10), 2496-2510.

2. **Pratikshkumar R. Patel**, Amarnath Singam, Arun K. Iyer, Rathna Venkata Naga Gundloori "Bioinspired Hyaluronic Acid Based Nanofibers Immobilized with 3, 4- Difluorobenzylidene Curcumin for Treating Bacterial Infections." **(Under Revision)**

3. **Pratikshkumar R. Patel**, Amarnath Singam, Rathna Venkata Naga Gundloori "Blend of neem oil based polyesteramide as magnetic nanofiber mat for efficient cancer therapy." **(Under Revision)**

4. **Pratikshkumar R. Patel,** Neha Shashikant Kulkarni, Rathna Venkata Naga Gundloori. "Dual drug loaded Polyesteramide nanofibers for chronic wound healing application" (***Manuscript under preparation***)

List of Publications Non-Emanating from the Thesis Work

1. Agrawal, Shubhang, **Pratikshkumar R. Patel**, and Rathna Venkata Naga Gundloori. "Proteins as Nanocarriers to Regulate Parenteral Delivery of Tramadol." ACS omega 4.4 **(2019)**: 6301-6310.

2. Singam, Amarnath, Naresh Killi, **Pratikshkumar R. Patel**, and Rathna VN Gundloori. "PEGylated ethyl cellulose micelles as a nanocarrier for drug delivery." RSC Advances 11, no. 49 **(2021)**: 30532-30543.

List of Poster presentations and Conferences attended

1. Presented poster in APA, Delhi, November 2017 on "Hydrophilic PLA and PCL Nanofibers Mats for Enhancing Cell Interactions"

2. Presented poster in APA, Delhi, November 2017 on "Hydrophilic PLA and PCL Nanofibers Mats for Enhancing Cell Interactions"

3. Presented poster in MACRO, Thiruvananthapuram, January 2017 on "Dual Drug Loaded Nanoparticles of Human Serum Albumin and PLGA for Treatment of Colorectal Cancer".

4. Presented poster in Science Day Celebration - 2018 held at CSIR-National Chemical Laboratory, Pune

RESEARCH ARTICLE

SPE INSPIRING PLASTICS PROFESSIONALS POLYMER ENGINEERING AND SCIENCE WILEY

Manipulating hydrophobicity of polyester nanofiber mats with egg albumin to enhance cell interactions

Pratikshkumar R. Patel[1,2] | Komal Pandey[1] | Naresh Killi[1,2] |
Rathna Venkata Naga Gundloori[1,2]

[1]Polymer Science and Engineering, CSIR-National Chemical Laboratory, Pune, Maharashtra, India

[2]Academy of Scientific and Innovative Research (AcSIR), Ghaziabad, Uttar Pradesh, India

Correspondence
Rathna Venkata Naga Gundloori, Polymer Science and Engineering, CSIR-National Chemical Laboratory, Homi Bhabha Road, Pune 411008, Maharashtra, India.
Email: rv.gundloori@ncl.res.in

Funding information
CSIR-NCL; AcSIR; CSIR, New Delhi, Grant/Award Numbers: CSC0302, CSC0134

Abstract

A hybrid of poly-L-lactic acid (PLA) and poly-ε-caprolactone (PCL) system was designed using hydrophilic generally regarded as safe (GRAS) protein, egg albumin (EA), and fabricated as nanofiber mats (NM) to facilitate improved cell interactions and functionality. Our studies include, preparation and analysis of physicochemical properties of NM. Surface morphology of NM was smooth with the diameter ranging from 250 to 400 nm. The contact angle of NM decreased from 80 to 45° with the increase in EA concentration. The rate and extent of swelling was increased 3-folds with the addition of EA. Release studies of NM showed maximum amount of MTz was released with the increase in MTz concentration (>85%). The MTz interaction with EA and structure stability of EA was confirmed from fluorescence and circular dichroism studies. NM showed increase in inhibition of bacterial growth of *Staphylococcus aureus* and *Escherichia coli* with the increase in MTz concentration. Cell viability of the NM was >80% and also, the cell proliferation increased as EA content increased. NM hemolytic activity was less than 5% suggesting compatibility. Hence, results concluded that EA had regulated hydrophobicity, promoted cell interactions, and proliferation and therefore, NM is considered safe for tissue regeneration.

KEYWORDS

biocompatibility, biomaterials, drug delivery systems, egg albumin, electrospinning, nanofibers, polyesters

1 | INTRODUCTION

Hydrophobic polymers like poly-ε-caprolactone (PCL) and poly-L-lactic acid (PLA) can form good nanofibers by electrospinning techniques.[1–7] It is reported that the blends of PCL and PLA are being used for various biomedical applications such as scaffolds for bone, tissue regeneration, implants, and sutures as they are biodegradable and biocompatible.[8–18] Several studies have reported that the blends of PCL and PLA complement each other.[19, 20] Because PLA is highly stiff and rigid

due to relatively high glass transition temperature. As a result, it is considered to be brittle and less favorable for biomedical application. Therefore, PCL, being a soft and ductile polymer, with a low melting temperature and glass transition temperature was chosen to blend with PLA to improve the practical application.[21] However, their hydrophobic nature is considered as a limiting factor in modulating desirable biological functions and cell interactions. Accordingly, it is evident that in the field of biomedical application, a hydrophilic polymer (natural or synthetic origin) with biocompatible

properties is considered to be more favorable to interact with cells.[22–24] Hence, blending the PLA and PCL with the hydrophilic polymers of either natural and synthetic origin offers enhanced hydrophilicity of those polymers without being modified chemically. Consequently, a wide variety of blends in the combination of PCL and PLA with hydrophilic polymers were explored for biomedical applications. For instance, the different kinds of polymers such as polyethylene oxide (PEO), poly(2-hydroxyethyl methacrylate), gelatin, collagen, bovine serum albumin and human serum albumin (HSA), and so forth were investigated by designing in various forms such as films, gels, nanomaterials to evaluate their potential for tissue engineering.[25–27] Recently, for tissue engineering application, mimic of extracellular matrix (ECM) is being researched, which comprises versatile nonwoven nanofibrous structures that support cell adhesion and bioactivity. The reported studies showed that the natural polymers, for example, proteins are inherently bioactive with better cell interacting domains (functional groups), facilitating cell adhesion, proliferation, and cell differentiation. In line with these findings, protein blends with PCL, poly lactic-co-glycolic acid (PLGA), and PLA were fabricated in the form of nanofibers to mimic ECM.[28–35] However, the animal proteins such as collagen, gelatin, BSA, and HSA require to pass the stringent regulatory clearances and further, the cost to renew those in their pure form is exorbitant. Further, for the stability of these proteins, chemical cross-linkers may be required, which may lead to cell toxicity. Therefore, protein such as egg albumen (generally regarded as safe [GRAS]) is being explored as it is nontoxic, hydrophilic, easy to renew, cost-effective, and forms a stable structure through physical crosslinks due to the presence of enough sulfhydryl groups to form disulfide linkages. In our earlier studies, we have developed biomaterials in bulk and nanoform using egg albumen blends.[36] The studies were encouraging, so the nano-biomaterials of PCL and PLA blends, which have limited biomedical application due to their hydrophobicity are being studied to improve hydrophilicity. Blending PCL and PLA with egg albumen is anticipated to increase the hydrophilicity of the nano-biomaterial and as explained above, the egg albumen being a protein is inherently bioactive and is suggested to favor cell viability, cell adhesion, and proliferation.

The electrospinning technique is a versatile method for the fabrication of nanofibers. It is the most preferred system because it is easy, simple, economical to use, and can manipulate the diameter of fibers by changing the needle pore diameter as desirable.[37–39] Currently, the electrospinning technique is being extensively studied for biomedical applications, especially in tissue regeneration, because they mimic ECM and provide better cell

interactions.[40–44] The significance of those nanofibers can be further enhanced by immobilizing drugs for controlled release. For instance, immobilization of metronidazole (MTz) in nanofibers can help in preventing the infection from a pathogenic microorganism which is a matter of concern in the healthcare system. MTz belongs to the nitroimidazole class and soluble in aqueous media. The melting temperature is ~ 163°C. It has antibiotic, antifungal, and antiprotozoal activity with a half-life of 8 h. The growth of the microbes is inhibited due to the formation of nitroso radicals, which helps in inhibiting nucleic acid synthesis. As a result, DNA of microbial cells is disrupted. MTz is more active in anaerobic bacteria (primarily Gram-negative bacteria) and protozoans when compared to aerobic bacteria.[45, 46] Figure S5 shows the structure of the MTz.

In this study, we aimed to develop a blend of PCL, and PLA with the hydrophilic egg albumin (EA in the form of nanofiber mats (NM) to enhance the stability and hydrophilicity for cell compatibility and evaluate their potential for tissue regeneration application. Accordingly, EA/PCL/PLA blends of various compositions with the increasing EA content were developed and fabricated NM of various compositions. The surface morphology of the NM was analyzed. The physical and chemical properties of NM using different techniques were studied, the influence of hydrophilicity in cell viability and proliferation were evaluated. Further, the in vitro release of MTz, antibacterial property and interaction of MTz with EA were studied.

2 | MATERIALS AND METHODS

2.1 | Materials

Metronidazole PLA (M_w ~60,000 Da) (PLA) and PCL (M_w ~68,000 Da) (PCL) were purchased from Sigma-Aldrich Co., St. Louis. Egg albumen (EA) acquired from Otto Biochemika Reagent, Mumbai, India. Chloroform and formic acid were of analytical reagent grade, procured from Rankem, Thane, India. Phosphate buffered saline (PBS) 3-(4, 5-Dimethylthiazol-2-yl)-5 diphenyltetrazoliumbromide (MTT), fetal bovine serum (FBS), Dulbecco's modified eagle's medium (DMEM), and trypsin were acquired from Sigma-Aldrich Co., St. Louis. Antibiotics, glucose, 4′, 6-diamidino-2-phenylindole (DAPI), Eosin, and ethylenediaminetetraaceticacid (EDTA) were procured from Hi-Media Laboratories Ltd., Mumbai, India. Propanol, acetone, and dimethyl sulfoxide (DMSO) were bought from Merck Ltd., Mumbai, India. The 3T3L1 (mouse embryonic fibroblast-adipose like cell line) cell line was procured from the National Centre for Cell Sciences (NCCS), Pune, India. All

reagents, solvents, and media for antibacterial studies and components of buffer for drug release studies were of analytical grade and were obtained from the local chemical companies, India.

2.2 | Preparation of solutions for electrospinning

Individual polymer solutions of EA, PCL, PLA, and their blends with and without MTz were prepared in various compositions, as given in Table 1. Chloroform was used as a solvent for the dissolution of PLA and PCL polymers, whereas EA was dissolved in formic acid. The polymers dissolved in respective solvents were mixed and vortexed to obtain homogenous solutions to attain the desired composition of blends. The polymeric blend composition, which can form a good NM, was selected and incorporated with the drug (MTz) at various concentrations of 10%, 20%, and 30%, respectively, to attain drug-loaded polymer blend solutions and fabricated as NM. The 10%, 20%, and 30% was calculated based on the total polymer concentration. For example, 10% of metronidazole is 10 g loaded in 100 g of polymer (wt/wt). Accordingly, the maximum loading was 30%. The various compositions prepared are specified in Table 1. PLA and PCL at 4% each were blended to fabricate nanofiber without EA, which is used as a control (PCE0). To the control, EA was added in different concentrations to PCE0. The concentration of EA was ranged from 1 to 4% (Table 1). The suitable composition, PCE2 with 2% EA was chosen to immobilize the drug, MTz in various concentrations, as given in Table 1.

2.3 | Fabrication of nanofibers of blend solutions by electrospinning method

Polymeric solutions were electrospun using a 10 ml syringe, equipped with a stainless-steel hypodermic needle with the desired pore diameter as a nozzle for spinning the polymer solution. The syringe filled with a polymeric solution was mounted on a syringe pump with a controller to control the flow rate of the solution. The syringe needle was connected to a high-voltage generator operated in positive DC mode. An aluminum plate was set in a closed chamber to collect NM. The electrospinning experiments were done at room temperature. The parameters like the distance between the tip of the needle and the collector was 10 cm; the flow rate and the applied voltage were fixed at 0.50 ml/h and 15 kV, respectively. Typically, most of the polymers were electrospun at the above parameters to attain NM; therefore, all compositions of with and without MTz were

electrospun at those parameters. The developed NM was crosslinked by annealing at 60°C for 2 h in the oven.[36]

2.4 | Characterization

The developed nanofibers with and without MTz were analyzed using various techniques to understand the physical properties of the various nanofibers developed. The morphology and diameter of nanofibers were analyzed by SEM (EDAX, Micro Analysis System, and Model Quanta 200 3D Dual-beam SEM). The sample used for SEM observations was prepared by mounting a small portion of the nonwoven NM on a stub. Later, the mounted stubs were sputtered with gold/palladium using a coating unit; FEI and tungsten filament (W) was used as an electron source and resolution was 3 nm. The functional characteristics of polymers and electrospun nanofibers were recorded using FTIR (Perkins Elmer, spectrometer I, FTIR diffused reflectance [DRIFT] mode). The recording of the spectrum was done in the wavelength range from 4000 to 500 cm^{-1} with a resolution of 4 cm^{-1}. Each spectrum is composed of an average of eight scans.

The crystallinity of MTz polymers and various nanofibers were evaluated using wide-angle X-ray diffraction (WXRD) containing a P-Analytical X-ray diffractometer model X-PERT PRO (Amelo, The Netherlands) with Cu Kα_1 radiation (40 kV, 100 mA, $\lambda = 0.154$). The samples were scanned in the 2θ range of 2–35° to investigate the change in crystal structure before and after the formation of nanofibers with and without MTz. The glass transition temperature (T_g), crystallization temperature (T_c), and melting temperature (T_m) were determined for MTz, pure polymers, and NM with and without MTz using the DSC instrument (Model Q10 DSC, TA Instrument). About 5–6 mg of the sample (polymer/NM) was loaded in a DSC pan, and the pan was sealed by applying pressure. In the first cycle, the sample was equilibrated to −70°C for 2 min and later heated to 100°C at a rate of 10°C/min. In the second cycle, the sample was heated from -70 to 200°C at a rate of 10°C/min. The thermogram was run under the nitrogen atmosphere at a flushing rate, 50 ml/min. The hydrophilicity of the NM was studied using contact angle measurements. Fabricated NM were cut (0.5 × 0.5 cm) and placed on the sample holder. The contact angle was measured by the drop-casting method. A red dye (Rhodamine B, 1 mg in 10 ml of water) was utilized to measure the angle to visualize the water drop. The NM were placed on a glass slide, and a droplet of water was dropped on NM using a pipette. To ensure consistency, the volume of a water droplet at each dispensing was maintained at 30 μl by controlling the speed of the drop and each measurement was taken after

TABLE 1   Compositions used for fabricating NM

Sl. no	PLA (w/vol%)	PCL (w/vol%)	EA (w/vol%)	Drug (wt/wt% w.r.t. to total polymer)
PCE0	4	4	0	0
PCE1	4	4	1	0
PCE2	4	4	2	0
PCE3	4	4	3	0
PCE4	4	4	4	0
PCE2 D10	4	4	2	10
PCE2 D20	4	4	2	20
PCE2 D30	4	4	2	30
PC D20	4	4	0	20

Note: Weight/weight % with respect to total polymer weight (wt/wt% w.r.t to total polymer). P, PLA; C, PCL; E, EA, D, MTz.

5 s of dispensing. For each sample, the contact angle θ, was measured using J image software. Three measurements at different spots were taken and averaged to attain the contact angle.

2.5 | Swelling and weight loss studies

The amount of water absorbed by the NM determines the strength of its hydrophilicity. Swelling studies were done at ambient temperature using 10 mg of NM in duplicates. The respective NM were transferred into a beaker containing 10 ml of distilled water that was maintained at ambient temperature. At successive intervals of time, the swollen weights of NM were taken after removing the surface water gently using the tissue paper. The total amount of water absorbed was calculated using Equation (1).

$$SW = \frac{M - Mi}{Mi} \times 100 \tag{1}$$

where SW is swelling weight in percent, M is the swollen weight of NM in water, Mi is the initial weight of NM.

To study nanofibers' weight loss, the respective NM of various compositions of 1 cm^2 were immersed in a pH 7.4 of PBS solution for 24 h. After 24 h, the NM were removed and dried at room temperature (25°C). Equation (2) was used for calculating the weight loss. All the calculations were done in duplicates.

$$\text{Weight loss}\% = \frac{\text{Final weight} - \text{Initial weight}}{\text{Initial weight}} \times 100 \tag{2}$$

The % of weight loss with dissolution of polymer or protein from NM, Final weight is the weight of NM sample after drying, Initial weight of NM before immersing in PBS.

2.6 | Interaction studies of EA with MTz

The physical interactions between EA and MTz were studied using circular dichroism (CD) and fluorescence spectroscopy. To investigate the changes in the secondary structure of EA in the presence of MTz, CD was used. CD measurements were carried out in the range of 200–250 nm at an interval of 1 nm and the CD spectra were collected with the scan speed of 20 nm/min. An average of 10 scans was done to collect the CD spectrum.

Fluorescence measurements were performed with an LS50B spectrofluorometer (Perkin Elmer). The width of both the excitation and the emission slits were set at 0.625 nm. Fluorescence emission spectra were recorded in the range of wavelengths from 260 to 600 nm using an excitation wavelength of 275 nm. The concentration of 3 μM of EA is kept constant and the respective concentrations of MTz (3, 6, 9, 12, 15, 18, and 21 μM) were added to EA solution for analyzing the interactions between EA and MTz by CD and fluorescence spectrofluorometric.

2.7 | In vitro drug release studies

The respective NM of 5 mg of with and without MTz were placed in a wide-mouth glass bottle containing 2 ml of phosphate buffer saline (PBS) of pH 7.4. The release of MTz was monitored at regular intervals by placing the respective container with NM in a temperature-regulated shaker bath of 50 rpm maintained at 37°C. At each interval of time, 1 ml of buffer solution was removed from the sample bottle for the estimation of MTz and replaced with 1 ml of fresh buffer. The MTz containing sample buffer was analyzed by UV visible spectrophotometry (Shimadzu UV-1601PC) at a wavelength of 320 nm to determine the amount released at each interval and extrapolated the quantity using a standard calibration curve of MTz. The respective NM without MTz was used

as a control. The release studies were done in duplicates and all the samples were analyzed twice for reproducibility. The results were presented in terms of cumulative percent release as a function of release time. Equation (3) shows the method for obtaining the cumulative percent of MTz released.

$$\text{Cumulative amount of MTz released} (\%) \frac{M_t}{M_\infty} \times 100 \quad (3)$$

where M_t is the amount of MTz released at time t, M_∞ is the amount of MTz loaded in NM prior to electrospinning of the respective solution.

2.8 | In vitro antibacterial studies

The bactericidal activity of the nanofibers containing MTz was tested using growth inhibition studies against Gram-positive bacteria *Staphylococcus aureus* and Gram-negative bacteria *Escherichia coli* which are more often found in the wounds.[47, 48] For the antibacterial assay, the bacterial strains were first grown on a solid nutrient agar medium and from the agar plates, fresh colonies were inoculated into 100 ml of nutrient broth medium. Growth was monitored at every 3 h by UV–visible spectrophotometer (Shimadzu, UV-1601) until the optical density (OD) reached 1 at 600 nm (OD of 1 corresponded to a concentration of 10^8 CFU/ml of medium).[49] Subsequently, 1 ml from the above preparation was further added to 100 ml of freshly prepared nutrient broth medium supplemented with the test sample (1 cm × 1 cm). The test samples include NM with and without MTz at concentrations of 10%, 20%, and 30%, respectively. The test samples were compared with the control, where the broth solution (supplemented with bacteria) without NM was used as a control. All the flasks were incubated at 37°C in a rotary shaker at 150 rpm. The growth rates and the bactericidal concentrations were monitored by measuring the OD at 600 nm by UV spectrophotometer at an interval of 0, 1, 2, and 5 h.

2.9 | Evaluation of percent of hemolytic activity

Blood was obtained from human volunteers from National Chemical Laboratory, Health center, Pune, India. The blood sample was stabilized using EDTA. Red blood cells (RBCs) were isolated from whole blood using density gradient centrifugation. The whole blood of 5 ml was slowly added on top of 5 ml of PBS saline solution and then centrifuged at 2000 rpm for 30 min. The

supernatant was discarded and collected the RBCs, which were washed thrice with phosphate buffer saline of pH 7.4 and centrifuged at 2000 rpm for 30 min. A stock solution of the washed RBCs was prepared without serum at 2% (vol/vol) using a phosphate buffer of pH 7.4. Later, 2 ml of the diluted RBCs suspension was transferred to each of the 2 ml Eppendorf tubes containing 10 mg of NM of different compositions of PCE0, PCE1, PCE2, PCE3, and PCE4. Similarly, the negative and positive blood samples were prepared without NM in phosphate buffer and de-ionized water, respectively. The respective Eppendorf tubes were then incubated for 2 h at 37°C. During the incubation, at every 30 min the samples were shaken gently to re-suspend the precipitated RBCs and centrifuged at 1500 g for 10 min at room temperature. The supernatant was then placed in another 96-well microtiter plate, and hemoglobin (Hb) release was measured spectrophotometrically by reading the OD at 541 nm using a micro-titer plate reader (Tecan) in PBS. The percentage of RBC lysis was calculated based on the assumption that 100% RBC lysis resulted by mixing blood with distilled water at a 1:1 (vol/vol) ratio. Equation (4) was used for calculating the percent (%) of HP.

$$\text{HP} (\%) = \frac{Dt - Dnc}{Dpc - Dnc} \times 100 \quad (4)$$

where Dt is the absorbance of the test samples, Dpc and Dnc are the absorbance's of the positive and negative controls, respectively.

2.10 | Cytotoxicity studies

The monolayer cell culture was trypsinized and the cell count was adjusted to 1.0×10^5 cells/ml using DMEM containing 10% FBS. To each well of the 96-well microtiter plate, 0.1 ml of the diluted cell suspension (approximately 10,000 cells) was added. After 24 h, when a partial monolayer was formed, the supernatant was flicked off, and the monolayer was washed once with the medium. About 100 μl of the respective sample concentrations of polymer samples (EA, PCL, PLA, and NM of PCE2) was added to the partial monolayer of microtiter plates. The plates were then incubated at 37°C for 3 days in 5% CO_2 atmosphere, and microscopic examination was carried out and observations were noted after every 24 h interval. After 72 h, the sample solutions in the wells were discarded and 50 μl of MTT in PBS was added to each well. The plates were gently shaken and incubated for 3 h at 37°C in 5% CO_2 atmosphere. The supernatant was removed and 100 μl of propanol was added and the plates

were gently shaken to solubilize the formed formazan. The absorbance was measured using a microplate reader at a wavelength of 540 nm. The percentage growth inhibition was calculated and the concentration of test drug needed to inhibit cell growth by 50% (CTC50) values were generated from the dose–response curves for each cell line.[50] MTT assay was repeated for consistency. Further, to understand the influence of hydrophilicity on cell proliferation, cell culture studies were performed and analyzed by fluorescence microscopy. Briefly, the polymeric blend solutions were prepared in different concentrations, which are shown in Table 1 (PCE0, PCE1, PCE2, PCE3, and PCE4). The prepared solutions were subjected to electrospinning for 10 min to coat a thin layer of NM on the respective glass coverslips. Later on, the individual NM (coverslip) was crosslinked by annealing at 60°C for 2 h. The above-mentioned samples were sterilized by UV irradiation and cultured using HeLa cervical cancer cells. Briefly, cells were seeded at 5000 per well (hemocytometer) on glass coverslips, coated with and without NM. The cells were incubated at 37°C for 24 h in the presence of CO_2 atmosphere and DMEM supplemented with 10% FBS. After the incubation for 24 h, the cells were fixed using 4% paraformaldehyde and washed with PBS. Later, the cells were stained by DAPI (0.5 mg/ml) and eosin (1.0 mg/ml) and then these cells were observed under a fluorescence microscope to understand the cell growth on the NM (Carl Zeiss (Model: Axio Observer.Z1, Oil emersion objective, 20X, Germany). Images of the cells were captured under green and indigo filters.

3 | RESULTS AND DISCUSSION

Although there are several reports on improving hydrophilicity of the PLA- and PCL-based materials, blending these polymers with the economically viable EA to improve stability, compatibility, and hydrophilicity was demonstrated for the first time so as to exploit EA for the application in tissue engineering. As mentioned in Section 1, EA is easy to renew at a lower cost and the structural and functional properties are similar to the FDA-approved HSA. Further EA being a protein, it is suggested to be inherently bioactive and favor cell viability, cell adhesion, and proliferation. Therefore, NM with said properties in addition to hydrophilicty are considered as advanced materials, which mimic ECM for biomedical applications. Therefore, we developed hydrophilic PCL/PLA/EA nanofibers of various compositions (Table 1) and examined hydrophilicity, physicochemical properties, and biocompatibility for analyzing their potential as nanobiomaterial for tissue regeneration.

3.1 | Scanning electron microscopy

The various compositions as given in Table 1 were subjected to electrospinning, where the processing parameters were fixed and the concentrations of the polymers and blend compositions were manipulated to produce the NM. Initially, the respective pure PLA and PCL solutions of different concentrations were tried to optimize the desired concentration to obtain smooth nanofibers. Later, various compositions with EA were developed. Our earlier investigations showed that pure EA could not produce nanofibers at any given concentration because it is less viscoelastic than poly(vinyl alcohol). Therefore, nanofibers of EA were not reported.[36] Figure 1 shows the nanofiber morphology of PLA and PCL with increasing EA concentrations (PCE0, PCE1, PCE2, PCE3, and PCE4). It was observed that the diameter of the NM increased with an increase in EA concentration in the blend composition, from 250 to 400 nm. The diameter of nanofibers was increased with the increasing polymer concentration due to the increased viscoelastic force in the nanofiber jet, which resisted stretching repulsive forces of charges. Therefore, the diameter of the nanofiber was increased.[51] Among the various compositions, PCE2 was chosen for MTz loading as PCE2 recorded a higher percent of swelling (more hydrophilic) when compared to other formulations (Section 3.5). Accordingly, MTz was immobilized in PCE2 at various concentrations (10%, 20%, and 30% of MTz with respect to total polymer concentration) and fabricated in the form of nanofibers, which were designated as PCE2 D10, PCE2 D20, and PCE2 D30. The surface morphology of the nanofibers is shown in Figure 1 and Figure S1 (supporting information of size distribution of NM). The nanofibers appeared to be smooth, and the change in nanofiber diameter was insignificant with the increase in the drug concentration ranging from 10% to 30%. Later, the developed nanofiber mats were stabilized by annealing at 60°C for 2 h to get crosslinked NM, where the sulfhydryl groups of EA were formed as disulfide linkages at 60°C.[36]

3.2 | Fourier transform infrared spectroscopy

The infrared absorption spectra for the pure polymers (EA, PCL, and PLA), MTz, and NM of polymeric blends of EA/PCL/PLA with and without MTz (Figure S2). IR spectrum of pure EA showed characteristic peaks at 3298 cm^{-1}, indicating the presence of –NH stretching of the secondary amide, —C=O stretching at 1650 cm^{-1} (amide-I) and —NH bending at 1542 cm^{-1} (amide II), a weak band at 2880 cm^{-1} due to —SH stretching, —CH stretching at 2965 cm^{-1} and a peak at 1397 cm^{-1} was
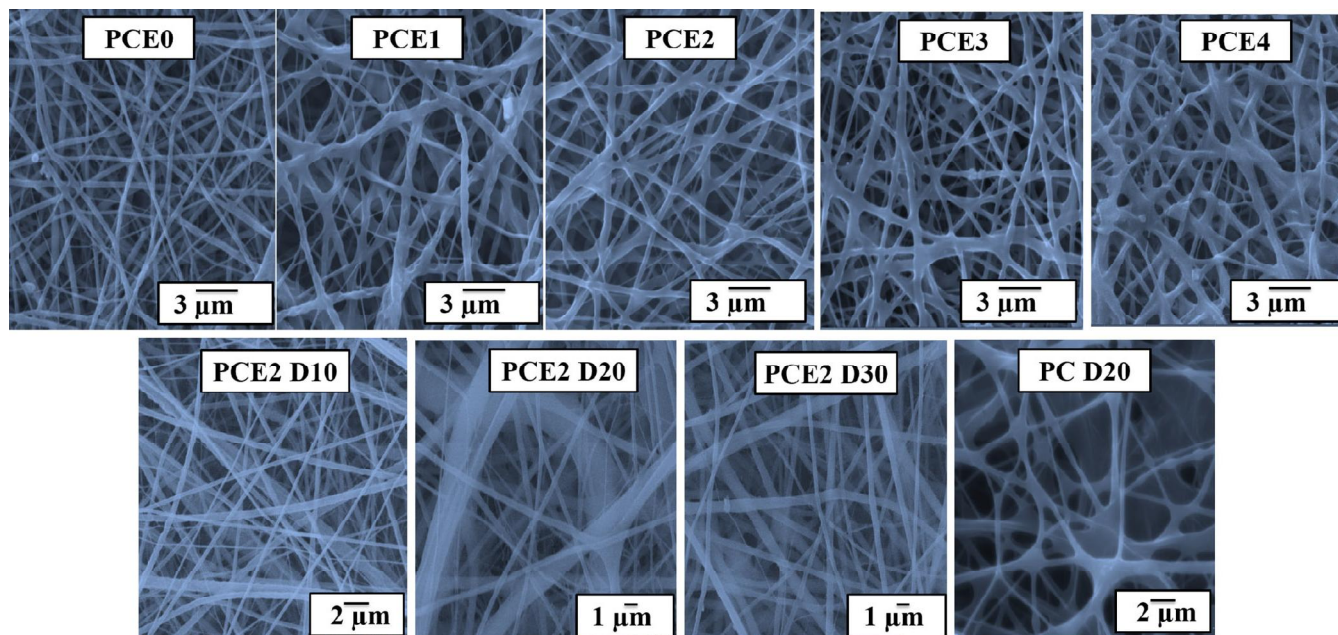
FIGURE 1 SEM image of PCE0, PCE1, PCE2, PCE3, PCE4, PCE2 D10, PCE2 D20, PCE2 D30, and PC D20

observed due to plane wagging. Pure PCL showed a characteristic band at 2943 cm^{-1} which is due to asymmetric stretching of aliphatic —CH$_2$, a peak at 2864 cm^{-1} for symmetric —CH$_2$ stretching and a peak at 1725 cm^{-1} for —C═O stretching. A prominent and sharp peak was recorded at 1186 cm^{-1}, which corresponds to carbonyl stretching of ester bond (—COOC—). IR spectrum of PLA showed a band at 2995 cm^{-1} is due to C—H stretching, 1752 cm^{-1} was recoded due to —C═O, and a band at 1088 cm^{-1} is due to ether C—O—C. The spectrum of the pure MTz showed a broad absorption band at 3233 cm^{-1} due to —OH stretching, 3098 cm^{-1} band due to —CH$_2$ stretching, a band at 1545 cm^{-1} is due to NO$_2$ a band at 1184 cm^{-1} is due to —C—N. The IR spectra of the NM of PCE2 D20 and PCE3 showed the characteristic peaks of all the polymers and MTz, indicating their presence. However, some of the peaks were either merged or shifted to a higher frequency because the corresponding bands of polymers and drug were very close to each other. For example, the carbonyl, amine, and hydroxyl groups. The shifting of bands indicated hydrogen ion interactions between the polymers and MTz (for example the shift of bands from 3248 to 3289 cm^{-1}, 2945 to 2951 cm$^-$1, 1758 to 1763 cm^{-1}, 1656 to 1654 cm^{-1}, 1184 to 1185 cm^{-1}, and 1095 to 1088 cm^{-1}).

3.3 | Wide-angle X-ray diffraction

Figure S3 shows the X-ray diffraction patterns for the pure EA, MTz, the respective nanofibers of pure PCL and PLA, and their blends with EA and MTz. These XRD studies

were done to investigate the degree of crystallinity in the polymers before and after fabrication of nanofibers. As reported, the pure PLA being semicrystalline recorded two peaks at 2Θ of 16° and 19°. Similarly, pure PCL also showed two peaks at 2Θ of 21° and 24°. Pure EA did not show any crystalline peaks as it is amorphous in nature. MTz is crystalline material and its XRD patterns showed a characteristic peak at 12°.[52] MTz became amorphous after immobilizing in NM due to interactions between polymers and MTZ. The XRD of the blend PCE2 NM showed low intense crystalline peaks, at 16°, 21°, and 23° indicating the presence of PCL, PLA. The decrease in the intensity of crystalline peaks of PLA and PCL was due to the blending of the polymers and formation of hydrogen ion interactions between the polymers (PCL/PLA/EA). It may also be understood that the decrease in intensity of the peaks was due to the limited time of reorientation of polymer chains during electrospinning process.[53] Further, in Figure S3, it was observed that due to the addition of MTz (crystalline drug) in NM the intensity of crystalline peak of PLA reduced. However, the crystallinity of PCL was unaltered. Form these observations it is evident that the crystalline MTz was well miscible with PLA and EA (fluorescence studies) than PCL, as a result MTz transformed to amorphous form and the crystalline peak of PLA was reduced

3.4 | Differential scanning calorimetry

Figure 2 shows the thermogram of pure polymers, MTz, and NM of PCE2 and PCE2 20. Pure EA did not record
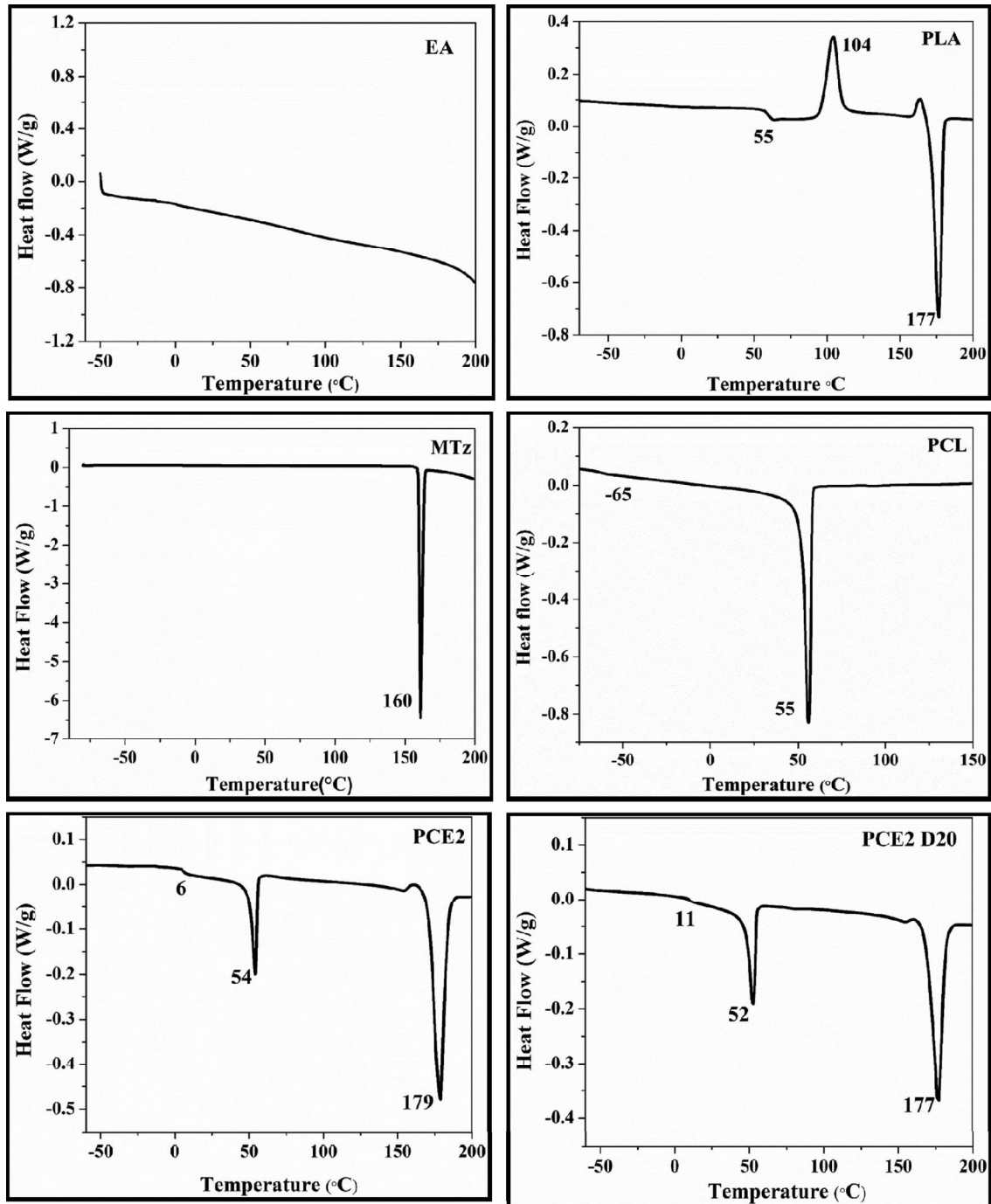
FIGURE 2 DSC thermogram of EA, PCL, PLA, MTz, PCE3, and PCE2 D20

any glass transition temperature (T_g) or melting temperature (T_m) as it is a natural protein. PCL being crystalline in nature, the thermogram of pure PCL recorded T_g at $-65°C$ and the T_m at $55°C$.[54] The (T_g) of pure PLA was recorded at $55°C$ while T_m recorded at $177°C$ and crystalline temperature (T_c) of pure PLA was observed at $104°C$.[55] The pure MTz depicted an endothermic peak due to T_m at $160°C$, which is similar to the reported literature.[56] The nanofibers blend of PCE2 showed T_m of

both PLA and PCL at 179 and $54°C$ respectively, however, a new T_g was recorded at $6°C$. This T_g appeared between the T_g of PCL and PLA, which indicates a homogenous blending of polymers. Further, the increase in T_m of PLA was due to the incorporation of PCL as PCL promoted the crystallization of PLA[21] as a result of interactions between them. The MTz-loaded nanofibers of PCE2 D20 blend represented all the peaks of the polymers except the T_m of MTz, because it had lost its

crystallinity due to the interactions between functional molecules of polymers and MTz. The XRD patterns of PCE2 D20 also indicated the same (Figure S3). The T_g increased with the immobilization of MT$_Z$ in PCE2, indicating interactions of MTZ with polymers and hence NM of PCE2 D20 is considered to be rigid.

3.5 | Measurements of hydrophilicity

Hydrophilicity is one of the important aspects for the biomaterials to be used in tissue regeneration because it was well understood that the materials with hydrophilicity show better cell interactions than the materials that are hydrophobic.[57] In these investigations, the hydrophilicity of the NM was determined by qualitative and quantitative methods such as contact angle measurements and swelling behavior.

3.5.1 | Contact angle

The contact angle was defined as the angle formed by the intersection of two tangent lines to the liquid and solid surfaces at the perimeter of contact between the two phases and the third surrounding phase. It is understood that the water contact angle will decrease with increasing surface hydrophilicity. In these studies, to understand the water contact angle, the concentration of PLA and PCL were kept constant and the concentration of EA was changed from 1% to 4%. The contact angles of NM were recorded for PCE0 (80.8°), PCE1 (62.7°), PCE2 (57.3°),

PCE3 (51.9°), and PCE4 (45.0°). The decrease in contact angle from 80.87° to 45.0° indicated an increase in hydrophilicity of NM, which is due to an increase in EA concentration in NM (Figure 3).

3.5.2 | Swelling and weight loss studies

The hydrophilicity of NM was also determined by the quantitative method in aqueous media following Equation (1). Figure 4 shows the swelling behavior of NM of various compositions at different time intervals, such as 5, 15, and 60 min. It was observed that there was a
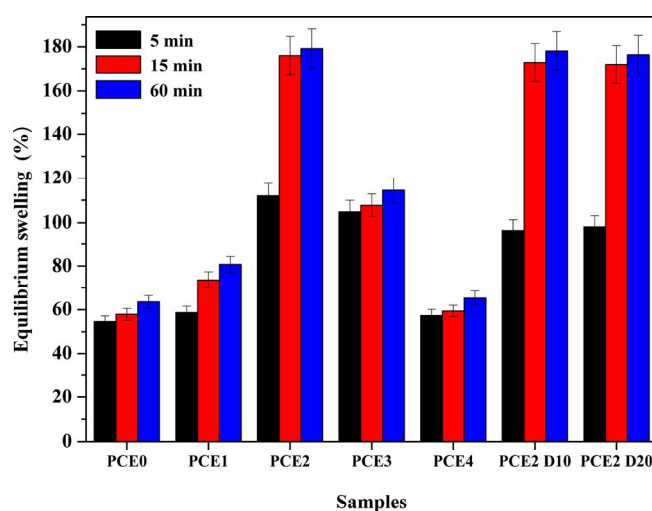
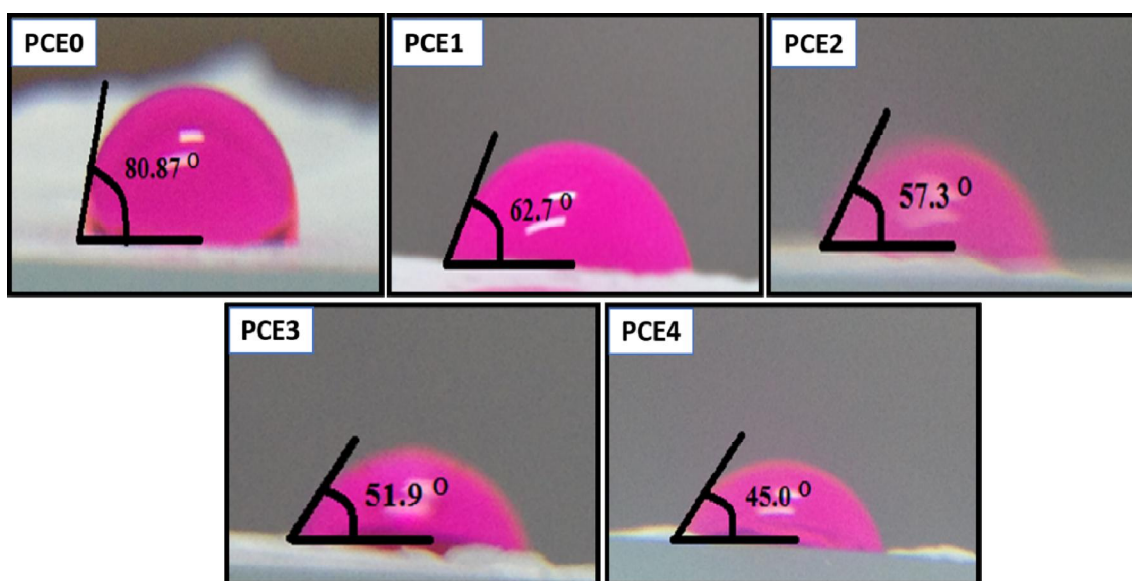FIGURE 4   Percent of swelling for PCE0, PCE1, PCE2, PCE3, PCE4, PCE2 D10, and PCE2 D20 NM

FIGURE 3   Contact angle measurement of PCE0, PCE1, PCE2, PCE3, and PCE4

marginal increase in swelling for the NM composition of PCE0 because PCL and PLA are hydrophobic. In the case of PCE1, the swelling of the NM was higher when compared to PCE0 due to the presence of EA. Likewise, there was a gradual increase in swelling with the increase in the concentration of EA in the blend compositions PCE2. However, a decrease in swelling was observed for the compositions PCE3 and PCE4 which attributes due to an increase in crosslinking density with an increase in the concentration of EA. PEC2 being ideal for drug release studies, MTz was loaded in PEC2. It was noticed that the percent of swelling for the MTz-loaded PCE2 was insignificant because of the increased interactions between EA and MTz (Figure 4).

The weight loss of PCE0, PCE1, PCE2, PCE3, and PCE4 was investigated in the pH 7.4 of PBS solution for 24 h and the results are depicted in Figure S4. The PCE0 composition did not record weight loss as PCL and PLA are hydrophobic in nature. The hydrophilic compositions, PCE1 and PCE2 had not shown any weight loss, which indicated that EA at 1% and 2% resulted in homogenous blending with PLA-PCL and therefore well entrapped and crosslinked. Whereas 3% and 4% of EA were excess and was present on the surface of the nanofiber mat, hence prone for easy dissolution and therefore recorded weight loss, which was 2.08% and 2.87% for PCE3 and PCE4, respectively.

3.6 | Interaction study of EA and MTz

The binding interaction of EA and MTz was studied by fluorescence spectroscopy and CD method. The studies were done by keeping the concentration of EA constant and varying MTz. The native tryptophan of EA (3 μM) was excited at 285 nm and emission was seen at 331 nm. Quenching of EA increased as the concentration of MTz increased from 3 to 21 μM. Quenching was observed due to the interactions between EA and MTz. The increasing in quenching shows the strong binding property of MTz with EA. MTz does not show any peak in fluorescence spectroscopy. Further, there was no shift of emission peak with the addition of MTz in EA; Figure 5 depicts an increase in quenching intensity with an increase in MTz concentration.

CD is one of the efficient and reliable methods to determine the changes in the secondary structure of the protein. CD was used to verify changes in the secondary structure of EA in the presence of MTz. CD plot of EA showed two-bands at 208 and 222 nm, which is a characteristic property of α- helix of protein. Our studies observed that there was no change in the secondary structure even after increasing the concentration of MTz from 3 to 21 μM. This indicated that the interactions are physical (Figure 6).
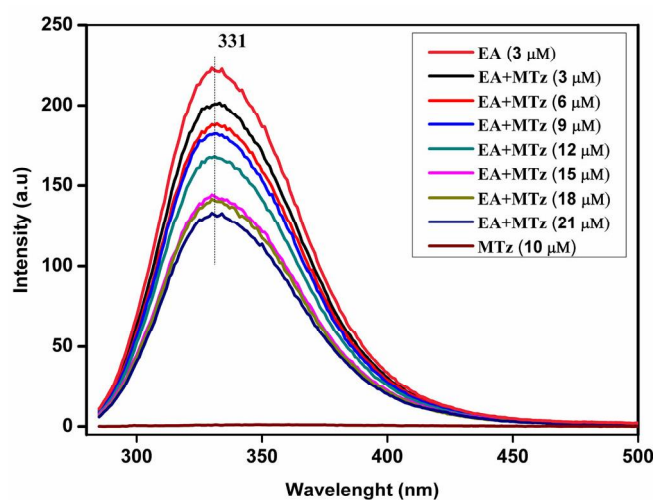

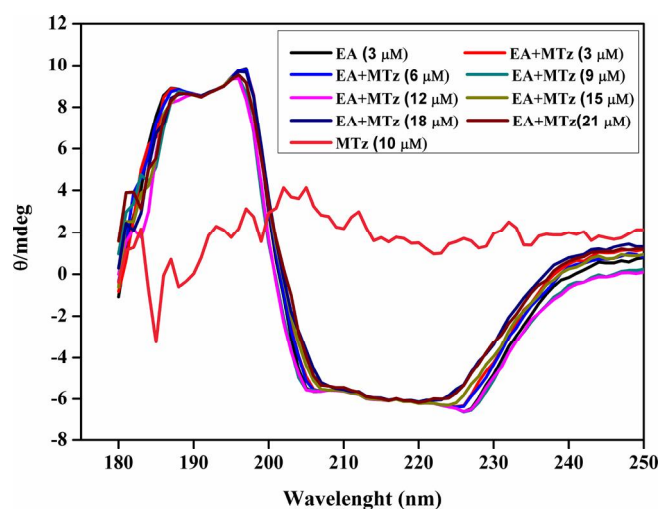**FIGURE 5** Fluorescence spectroscopy of EA and MTz (3–21 μM)

FIGURE 6 Circular dichroism of EA and MTz (3–21 μM)

3.7 | Drug release study

To understand the release profile of MTz-loaded nanofibers, in vitro release studies were done for the NM of PCE2 D10, PCE2 D20, and PCE2 D30 in phosphate buffer of pH 7.4 at 37 ± 0.5°C in a water bath shaker as a function of time. The obtained release data were compared with the MTz-loaded NM of PC D20 to understand the rate and extent of MTz released in the presence and absence of the hydrophilic component, EA. Figure 7, depicts the release profiles of all the compositions. It was observed that 52% of the drug was released in 3 h for the NM loaded with 30% of MTz wherein burst release followed by slow and sustained release was recorded up to 79 h, where a total of 85% of MTz was released. While in 20% MTz-loaded NM, 42% of the drug was released in 3 h and later 28% of MTz was released in 79 h, indicating slow

and sustained release. In 10% of MTz-loaded NM, 74% was released in 79 h. More percent of drug was released in case of 30% drug-loaded NM than 20% because of the excess of the drug present on the surface of the nanofibers. From the overall results, it was observed that initial burst release followed by slow and sustained release was recorded for all the compositions. Also, the amount and the rate of the MTz released increased as the concentration of the MTz increased in the NM because of the concentration gradient of MTz and the process of dissolution and diffusion of MTz.[58] Further, as expected, the NM of PC D20 (without EA) recorded only 40% of MTz after 79 h of release studies, which practically indicated that in the absence of hydrophilic component (EA), the rate and the extent of release was significantly less than the NM with EA. Similar, observations were reported for the nanofibers of PLA,
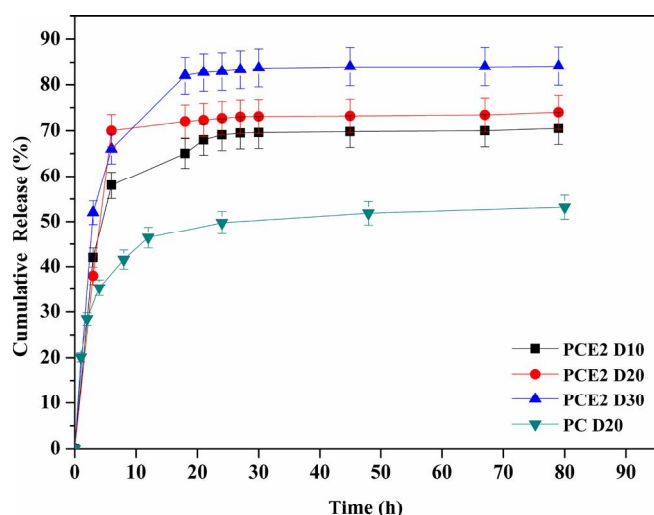
poly(ethylene-co-vinyl acetate) (PEVA), or a blend of the two polymers, which was loaded tetracycline hydrochloride.[59]

3.8 | Antibacterial study

The OD method was used to determine the antibacterial activity of NM with and without MTz at different concentrations on the growth of *S. aureus and E. coli*. The bacterial medium without NM was used as a control. *S. aureus and E. coli* were used to study antibacterial activity because mostly Gram-positive and Gram-negative bacteria are found in the wounds. The OD was measured at 600 nm at regular intervals from 0 to 5 h to determine the number of bacteria present in the medium. It was evident that as the OD is greater, the lesser the antibacterial activity. From Figure 8, it was observed that the OD was maximum for both control and the NM of PCE2, as there was no bacterial inhibition. However, OD decreased with the increasing MTz concentration in NM (PCE2 D10, PCE2 D20, and PCE2 D30) as it had inhibited *S. aureus* and *E. coli*. Accordingly, NM with 30% drug loaded (PCE2 D30) showed maximum antibacterial activity. Similar studies were reported, which confirmed that MTz is effective against *S. aureus* and *E. coli* bacterial strain.[60, 61]

3.9 | Hemolysis assay

In order to study the compatibility of the developed material with human blood, hemolysis studies are considered one of the most reliable methods. For our studies, we collected blood samples from the volunteers of CSIR-National Chemical Laboratory, at NCL-dispensary, Pune,
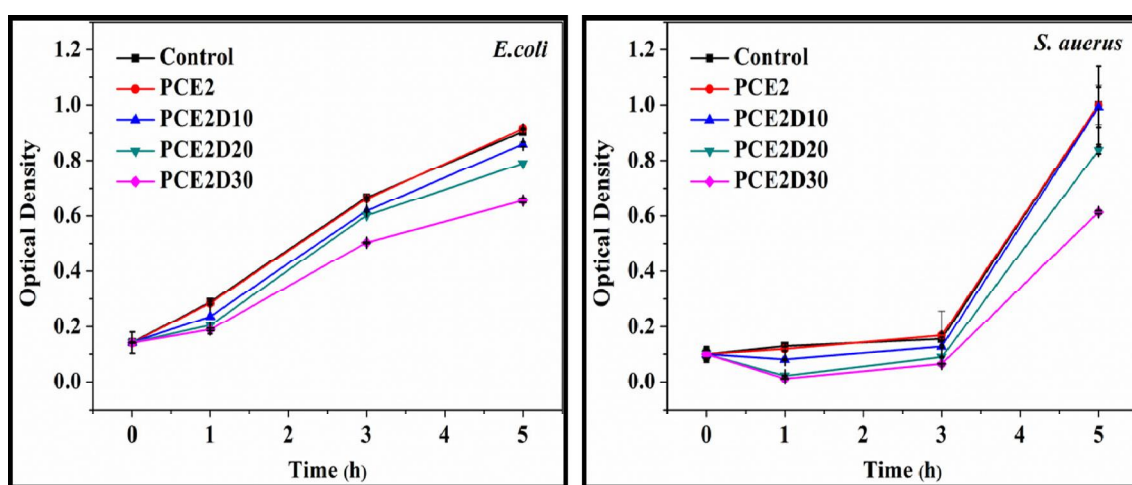

FIGURE 7 Release studies of MTz from NM in pH 7.4 phosphate buffer solution

FIGURE 8 Antibacterial studies were done in *Staphylococcus aureus* and *Escherichia coli* of PCE2, PCE2 D10, PCE2 D20, and PCE2 D30
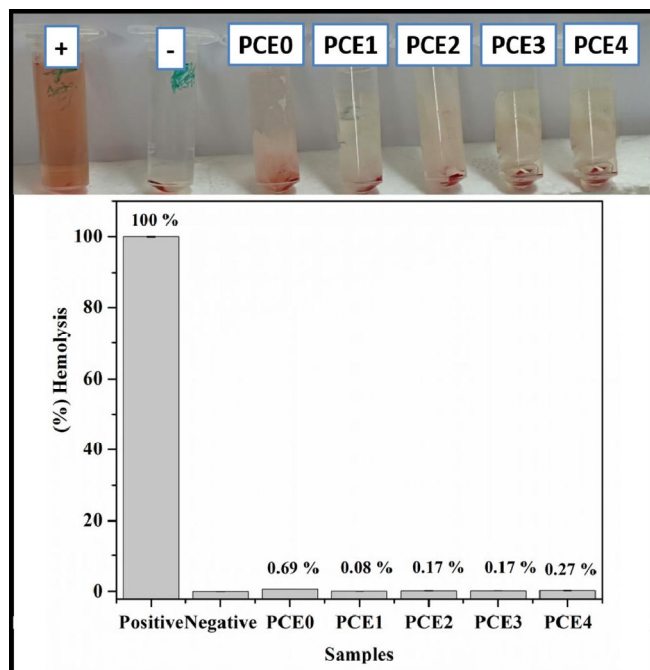
after obtaining ethical clearance. As described in the experimental Section 2.9, the negative and positive control and compositions of PCE0, PCE1, PCE2, PCE3, and PCE3 were subjected to hemolysis test (Figure 9). The results showed 0% hemolytic activity for the negative control (phosphate buffer, pH 7.4) whereas the positive control (de-ionized water) showed 100% hemolytic activity. The nanofibers without EA PCE0 showed 0.69% of hemolytic activity, the nanofibers with EA, at various compositions recorded less than 0.3% (PCE1 [0.08%], PCE2 [0.17%], PCE3 [0.17%], and PCE4 [0.27%]). According to the reported literature,[62] the materials that showed hemolytic activity below 5% are considered safe for drug delivery by an invasive method. From our studies, we observed that NM of all the compositions showed hemolytic activity less than 5% and therefore, these can be used for biomedical application.

3.10 | Cytotoxicity studies

Cell viability studies were done using MTT assay for the test samples of pure polymers such as EA, PCL, PLA, and the nanofibers of PCE2. The percent of cytotoxicity of pure polymer and nanofibers were studied on cells of 3 T3-L1. Figure 10 represents the relative cell viability of the pure polymers of EA, PCL, PLA, and NM of PCE2 (Table 1) at a concentration of 1000 μg/ml. Earlier studies reported that the pure PCL and PLA are biocompatible

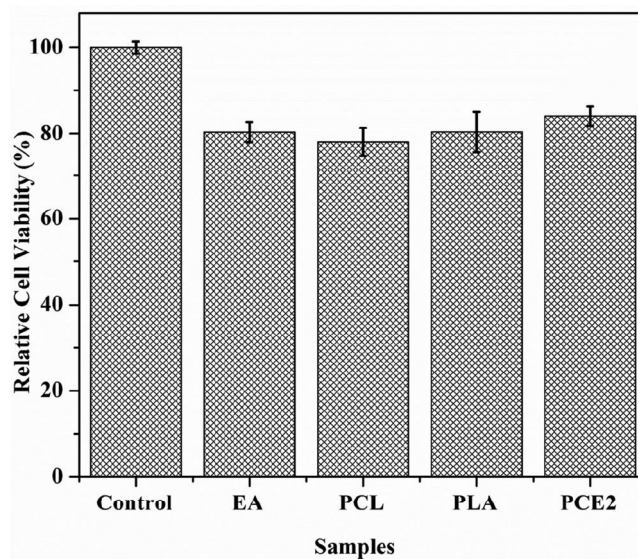and FDA approved and EA being an edible protein, is GRAS. In our studies, the respective cell viability of EA, PCL, PLA, and PCE2 was recorded at 80%, 78%, 80%, and 84% respectively. So, it was considered that all these polymers showed cell viability at ~80% to 85%. PCE2 showed maximum cell viability because of increased hydrophilicity, indicating that hydrophilicity enhances cell interactions, favoring cell viability. The remaining 15%–20% of cytotoxicity could be due to the extensive period of cell culture for 72 h instead of 24–48 h because of which, the cells might have got exhausted. Similar observations were reported in earlier studies.[63] Hence, we concluded that pure polymers and the fabricated nanofibers are nontoxic and compatible with 3 T3-L1. Therefore, we consider that these will be suitable as a scaffold for tissue regeneration.

Further, the effect of hydrophilicity on cell growth was studied by fluorescence microscopy for NM with and without EA (PCE0, PCE1, PCE2, PCE3, and PCE4) against HeLa cells by culturing these samples for 24 h. Figure 11 show the fluorescence images of the tested sample (control (A), PCE0 (B), PCE1 (C), PCE2 (D), PCE3 (E), and PCE4 (F)), where image A was used as a control (glass coverslips which are without nanofibers). Images from B–F showed a gradual increase in the number of cells due to an increase in hydrophilicity with the increase in the concentration of EA in the NM. The low density of cells was observed in images A and B as compared to the images of C, D, E, and F because EA is absent in samples A and B. Further, the density of the cells was ploddingly enhanced in images C, D, E, and F as the concentration of EA was increasing. The Figure 11 suggested that EA has a significant effect on the growth of cells without EA. From this data, we concluded that EA can be utilized in tissue engineering or drug

FIGURE 11 Fluorescence microscopy images of (A) control, (B) PCE0, (C) PCE1, (D) PCE2, (E) PCE3, (F) PCE4, and (1) bright field, (2) DAPI, (3) eosin, (4) merged
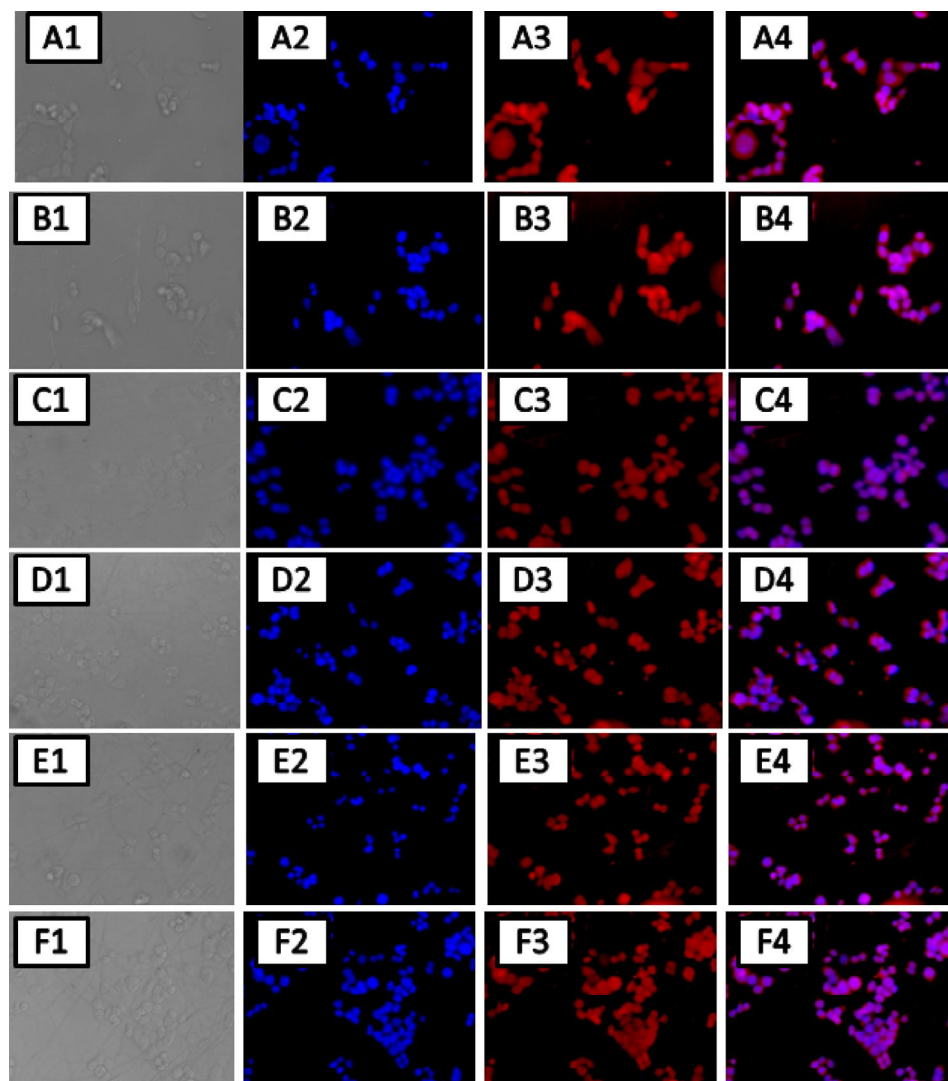
delivery system as it is more favorable for cells to multiply and hence anticipate better patient compliance with the application.

The overall results of the various analysis suggested that hydrophilicity is considered one of the main factors for better interactions with the cells to promote cell division and cell proliferation.

4 | CONCLUSION

In this study, we developed NM using hydrophobic polymers PCL, PLA blended with hydrophilic natural protein, EA as it is less exploited for biomedical application though the properties are similar to that of FDA-approved HSA. The motive behind this study is to replace the very expensive proteins with the affordable EA as it would be cost-effective in renewing and application. The developed nanomaterials with EA showed an increase in hydrophilicity with the increase in EA concentration, which was confirmed by the swelling and contact angle studies. Physicochemical properties such as FTIR, DSC, XRD, and fluorescence studies were analyzed to understand the hydrogen and functional interactions between the polymers and the MTZ. After fabrication of NM with MTz, the crystalline peak of MTz disappeared, indicating strong functional interactions between EA and MTz and hence became amorphous after fabrication. The drug release studies showed the release of MTz was proportional to the concentration of MTz and hydrophilicity of the NM. As anticipated, the positive results of the MTT assay, cell proliferation, hemolysis, and in vitro antibacterial studies revealed that the developed NM with EA are suitable for tissue regeneration and therefore recommended for next level studies for the application.

ORCID

Pratikshkumar R. Patel https://orcid.org/0000-0002-2893-3721

Komal Pandey https://orcid.org/0000-0001-9864-4944

Naresh Killi https://orcid.org/0000-0001-8772-6848

Rathna Venkata Naga Gundloori https://orcid.org/0000-0002-8084-2296

REFERENCES

[1] H. Li, C. Zhu, J. Xue, Q. Ke, Y. Xia, *Macromol. Rapid Commun.*, **2017**, *38*(9), 723.

[2] S. K. Bhullar, D. Rana, H. Lekesiz, A. C. Bedeloglu, J. Ko, Y. Cho, Z. Aytac, T. Uyar, M. Jun, M. Ramalingam, *Mater. Sci. Eng. A*, **2017**, *81*, 334.

[3] R. P. Shadamarshan, H. Balaji, H. S. Rao, K. Balagangadharan, S. V. Chandran, N. Selvamurugan, *Colloids Surf. B. Biointerfaces* **2018**, *171*, 698.

[4] Mohandesnezhad, S.; Alizadeh, E.; Pilehvar-Soltanahmadi, Y.; Davaran, S.; Goodarzi, A.; Khatamian, M.; Zarghami, N.; Samiei, M.; Aghazadeh, M., In vitro evaluation of novel Zeolite-hydroxyapatite blended scaffold for dental tissue engineering. **2020**.

[5] N. Eselini, S. Tirkes, A. O. Akar, U. Tayfun, *J. Elastomers Plast.* **2020**, *52*(8), 701.

[6] L. Huang, J. Tan, W. Li, L. Zhou, Z. Liu, B. Luo, L. Lu, C. Zhou, *J. Mech. Behav. Biomed. Mater.* **2019**, *90*, 604.

[7] S. Afshar, S. Rashedi, H. Nazockdast, M. Ghazalian, *Int. J. Biol. Macromol.* **2019**, *138*, 1130.

[8] S. Pisani, R. Dorati, B. Conti, T. Modena, G. Bruni, I. Genta, *React. Funct. Polym.*, **2018**, *124*, 77.

[9] S. F. Hashemi, M. Mehrabi, A. Ehterami, A. M. Gharravi, F. S. Bitaraf, M. Salehi, *J. Drug Deliv. Sci. Technol.* **2021**, *61*, 2077.

[10] F. S. Fattahi, A. Khoddami, O. Avinc, *J. Text. Polym.* **2019**, *7*, 47.

[11] T. V. Shah, D. V. Vasava, *e-Polymers* **2019**, *19*(1), 385.

[12] S. Liu, Y.-Y. Xie, B. Wang, *Neural Regen. Res.* **2019**, *14*(8), 1352.

[13] M. Ojaghi, F. Soleimanifar, A. Kazemi, M. Ghollasi, M. Soleimani, N. Nasoohi, S. E. Enderami, *J. Cell. Biochem.* **2019**, *120*(6), 9917.

[14] M. Salehi, A. Ai, A. Ehterami, M. Einabadi, A. Taslimi, A. Ai, H. Akbarzadeh, G. J. Ameli, S. Farzamfar, S. Shirian, *Nanomed. J.* **2020**, *7*(2), 115.

[15] W. Nie, Y. Gao, D. J. McCoul, G. J. Gillispie, Y. Zhang, L. Liang, C. He, *Int. J. Nanomedicine* **2019**, *14*, 3929.

[16] M. Nofar, D. Sacligil, P. J. Carreau, M. R. Kamal, M.-C. Heuzey, *Int. J. Biol. Macromol.* **2019**, *125*, 307.

[17] T. Xu, J. M. Miszuk, Q. Yao, Z. Liang, H. Sun, H. Fong, Electrospun three-dimensional nanofibrous scaffolds based on polycaprolactone for stem cells differentiation and bone regeneration. in *Electrospun Polymers and Composites*, Elsevier, Cambridge **2021**, p. 179.

[18] S. M. Espinoza, H. I. Patil, E. San Martin Martinez, R. Casañas Pimentel, P. P. IGE, *Int. J. Polym. Mater. Polym. Biomater.* **2020**, *69*(2), 85.

[19] K. K. Sankaran, U. M. Krishnan, S. Sethuraman, *J. Biomater. Sci. Polym. Ed.* **2014**, *25*(16), 1791.

[20] H. J. Haroosh, Y. Dong, D. S. Chaudhary, G. D. Ingram, *Appl. Phys. A* **2013**, *110*(2), 433.

[21] R. T. Zhu, M. H. Tan, P. Zhang, L. Zhang, X. M. Chen, F. W. Yang, *Morphological Structure and Thermal Property of PLA/PCL Nanofiber by Electrospinning*, Trans Tech Publications, Switzerland **2014**, p. 418.

[22] A. Sadeghi, F. Moztarzadeh, J. A. Mohandesi, *Int. J. Biol. Macromol.* **2019**, *121*, 625.

[23] G. K. Arbade, J. Srivastava, V. Tripathi, N. Lenka, T. U. Patro, *J. Biomater. Sci. Polym. Ed.* **2020**, *31*(13), 1648.

[24] C. Lei, H. Zhu, J. Li, J. Li, X. Feng, J. Chen, *Polym. Eng. Sci.* **2015**, *55*(4), 907.

[25] H.-J. Jin, J. Park, R. Valluzzi, P. Cebe, D. L. Kaplan, *Biomacromolecules* **2004**, *5*(3), 711.

[26] J. B. Rose, S. Pacelli, A. J. E. Haj, H. S. Dua, A. Hopkinson, L. J. White, F. R. A. J. Rose, *Materials* **2014**, *7*(4), 3106.

[27] Z. Gün Gök, M. İnal, O. Bozkaya, M. Yiğitoğlu, İ. Vargel, *J. Appl. Polym. Sci.* **2020**, *137*(41), 49257.

[28] T. Li, L. Wang, Y. Huang, B. Xin, S. Liu, *J. Biomater. Sci. Polym. Ed.* **2020**, *31*(9), 1223.

[29] A. Prabhath, V. N. Vernekar, V. Vasu, M. Badon, J. E. Avochinou, A. D. Asandei, S. G. Kumbar, E. Weber, C. T. Laurencin, *J. Biomed. Mater. Res. A* **2021**, *109*, 1.

[30] J. Hu, M. P. Prabhakaran, X. Ding, S. Ramakrishna, *J. Biomater. Sci. Polym. Ed.* **2015**, *26*(1), 57.

[31] C. Martins, F. Sousa, F. Araujo, B. Sarmento, *Adv. Healthc. Mater.* **2018**, *7*(1), 1035.

[32] M. İnal, Z. Gün Gök, G. Elif Kartal, N. Banu Verim, S. Murat, T. Apaydın, M. Yiğitoğlu, *J. Nanosci. Nanotechnol.* **2021**, *21*(5), 3041.

[33] Y. Zheng, D. Su, J. Yuan, J. Zha, Y. Xiao, J. Che, *Polym. Eng. Sci.* **2020**, *60*(4), 802.

[34] W. Kalaithong, R. Molloy, T. Theerathanagorn, W. Janvikul, *Polym. Eng. Sci.* **2017**, *57*(8), 875.

[35] V. Švachová, V. Khunová, D. Pavliňák, Z. Fohlerová, L. Vojtová, *Polym. Eng. Sci.* **2017**, *57*(6), 506.

[36] G. V. N. Rathna, J. P. Jog, A. B. Gaikwad, *Polym. J.* **2011**, *43*(7), 654.

[37] X. Xie, Y. Chen, X. Wang, X. Xu, Y. Shen, A. Aldalbahi, A. E. Fetz, G. L. Bowlin, M. El-Newehy, X. Mo, *J. Mater. Sci. Technol.* **2020**, *59*, 243.

[38] J. Wang, J. A. Jansen, F. Yang, *Front. Chem.* **2019**, *7*, 258.

[39] S. Nagam Hanumantharao, S. Rao, *Fibers* **2019**, *7*(7), 66.

[40] Z. Bao, C. Xian, Q. Yuan, G. Liu, J. Wu, *Adv. Healthc. Mater.* **2019**, *8*(17), 670.

[41] H. S. Sofi, R. Ashraf, A. H. Khan, M. A. Beigh, S. Majeed, F. A. Sheikh, *Mater. Sci. Eng. C* **2019**, *94*, 1102.

[42] A. Haider, S. Haider, M. R. Kummara, T. Kamal, A.-A. A. Alghyamah, F. J. Iftikhar, B. Bano, N. Khan, M. A. Afridi, S. S. Han, *J. Saudi Chem. Soc.* **2020**, *24*(2), 186.

[43] I. R. Calori, G. Braga, P. D. C. C. de Jesus, H. Bi, A. C. Tedesco, *Eur. Polym. J.* **2020**, *129*, 621.

[44] F. Tuğcu-Demiröz, S. Saar, F. Tort, F. Acartürk, *Drug Dev. Ind. Pharm.* **2020**, *46*(6), 1015.

[45] F. Cd, K. Ne, K. C. Lamp, *Drugs* **1997**, *54*(5), 679.

[46] N. Dione, S. Khelaifia, J.-C. Lagier, D. Raoult, *Int. J. Antimicrob. Agents* **2015**, *45*(5), 537.

[47] E. Fulkerson, C. J. Della Valle, B. Wise, M. Walsh, C. Preston, P. E. Di Cesare, *J. Bone Joint Surg. Am.* **2006**, *88*(6), 1231.

[48] T. Amna, M. S. Hassan, N. A. M. Barakat, D. R. Pandeya, S. T. Hong, M.-S. Khil, H. Y. Kim, *Appl. Microbiol. Biotechnol.*, **2012**, *93*(2), 743.

[49] F. P. Tally, B. R. Goldin, N. Sullivan, J. Johnston, S. L. Gorbach, *Antimicrob. Agents Chemother.* **1978**, *13*(3), 460.

[50] Obaleye, J. A.; Lawal, A., Synthesis, characterization and anti-fungal studies of some metronidazole complexes. **2009**.

[51] B. Tarus, N. Fadel, A. Al-Oufy, M. El-Messiry, *Alex. Eng. J.* **2016**, *55*(3), 2975.

[52] M. Budai-Szűcs, A. Léber, L. Cui, M. Józó, P. Vályi, K. Burián, B. Kirschweng, E. Csányi, B. Pukánszky, P. L. A. Electrospun, *Drug Des. Devel. Ther.* **2020**, *14*, 233.

[53] D. W. Hutmacher, T. Schantz, I. Zein, K. W. Ng, S. H. Teoh, K. C. Tan, *J. Biomed. Mater. Res. A* **2001**, *55*(2), 203.

[54] Ceylan, M.; Yang, S.-Y.; Asmatulu, R., Effects of gentamicin-loaded PCL nanofibers on growth of Gram positive and Gram negative bacteria. **2017**.

[55] A. K. Matta, R. U. Rao, K. N. S. Suman, V. Rambabu, *Procedia Mater. Sci.* **2014**, *6*, 1266.

[56] U. Hani, R. S. Bhat, H. G. Shivakumar, *Lat. Am. J. Pharm.* **2011**, *30*(1), 161.

[57] W. Wang, G. Caetano, W. S. Ambler, J. J. Blaker, M. A. Frade, P. Mandal, C. Diver, P. BÃ¡rtolo, *Materials*, **2016**, *9*(12), 992.

[58] Y. L. Patel, P. Sher, A. P. Pawar, *AAPS PharmSciTech* **2006**, *7*(4), 24.

[59] E.-R. Kenawy, G. L. Bowlin, K. Mansfield, J. Layman, D. G. Simpson, E. H. Sanders, G. E. Wnek, *J. Control. Release* **2002**, *81*(1–2), 57.

[60] N. Killi, R. A. Dhakare, A. Singam, M. Lokanadham, H. Chitikeshi, R. V. N. Gundloori, *Med. Chem. Commun.* **2016**, *7*(12), 2299.

[61] M. H. El-Newehy, S. S. Al-Deyab, E.-R. Kenawy, A. Abdel-Megeed, *Fib. Polym.* **2012**, *13*(6), 709.

[62] A. A. Shitole, P. W. Raut, N. Sharma, P. Giram, A. P. Khandwekar, B. Garnaik, *J. Mater. Sci. Mater. Med.* **2019**, *30*(5), 1.

[63] S. Agrawal, P. R. Patel, R. V. N. Gundloori, *ACS Omega* **2019**, *4*(4), 6301.

SUPPORTING INFORMATION

Additional supporting information may be found online in the Supporting Information section at the end of this article.